Cellular tropism and cell-to-cell fusion properties of the infectious bronchitis virus spike glycoprotein.

Erica Jane Bickerton

A thesis submitted for the degree of Doctor of Philosophy

Department of Biological Sciences, University of Warwick

Institute for Animal Health

September 2010

Table of Contents

List of figures and tables.

Acknowledgements

Heartfelt thanks go to Prof. Paul Britton and Dr. Maria Armesto for all their support and guidance as my PhD supervisors at IAH. Thank you to Prof. Andrew Easton for being my supervisor at the University of Warwick and to BBSRC and IAH for funding. Many thanks also go to all the members of the Coronavirus group, past and present, for keeping me sane whilst working in the lab. I would like to express my gratitude to the members of IAH Microbiological Services, especially Ruth Hennion and Gillian Hill, for their invaluable assistance in preparing cell cultures and media. I am grateful to my parents for their encouragement and proof-reading skills, my dogs, Poppy and Alfie, for keeping me company while I wrote my thesis and to Christopher for everything.

Declaration

I declare that the work in this thesis is original, except where stated by special reference, and that it has not been presented previously to support another degree. The work performed is the author's sole efforts.

The thesis was prepared according to the Guide to Examinations for Higher Degrees by Research, September 2009.

Summary

There are numerous vaccines available for the control of infectious bronchitis virus (IBV) in poultry, however protection is short-lived and poorly cross-protective between strains. The vaccines must currently be grown in embryonated eggs, a cumbersome and expensive process. The ability to grow vaccines on a cell-line such as Vero cells would be highly advantageous.

The spike (S) glycoprotein of IBV is comprised of two subunits, S1 and S2, has a vital role in virulence *in vivo* and is responsible for cellular tropism *in vitro*. This project aims to identify the amino acids present in the S glycoprotein involved in determination of cellular tropism and cell-to-cell fusion.

The IBV Beaudette strain is able to replicate in both primary chick kidney (CK) cells and Vero cells, whereas the IBV M41 strain replicates in primary cells only. Recombinant IBVs with chimaeric S genes were generated using a reverse genetics system with the genomic background of Beaudette and part of the S gene from M41. Their growth characteristics and cellular tropism were investigated. The S2 subunit of Beaudette was found to be sufficient to confer the ability to grow on Vero cells and swapping just three amino acids with corresponding ones from M41 was sufficient to remove the ability of the Beaudette S glycoprotein for growth on Vero cells.

Beaudette was further adapted to syncytia formation on Vero cells by serial passage and isolates were sequenced to identify amino acid changes between parent and Vero-adapted viruses that are potentially involved in cell-to-cell fusion.

Understanding the way in which IBV infects host cells is vital in order to rationally design better vaccination and treatment strategies and help to reduce the prevalence of IBV infection in poultry worldwide. Using the IBV reverse genetics system, we now have the potential to grow IBV vaccines on Vero cells.

Table of Abbreviations

ACE2	Angiotensin-converting enzyme 2
ADP	Adenosine diphosphate
ALV	Avian leukosis virus
ASLV	Avian sarcoma-leukosis virus
BCoV	Bovine coronavirus
BeCoV	Beluga whale coronavirus
BES	N,N-bis[2-hydroxethyl]-2-Aminoethanesulfonic acid
BHK-21	Baby hamster kidney cell line
BSA	Bovine serum albumen
BuCoV	Bulbul coronavirus
CCoV	Canine coronavirus
CDC	Centres for disease control and prevention
cDNA	Copy DNA
CEACAM	Carcinoembryonic antigen-related cell adhesion molecule
CKC	Chick kidney cells
cpe	Cytopathic effect
Cyto	Cytoplasmic tail
DEAE	Diethylaminoethyl
DEFRA	Department for environment, food and rural affairs
DNA	Deoxyribose nucleic acid
dNTP	Deoxy nucleotide triphosphate
dsRNA	Double stranded RNA
DTT	Dithiothreitol

E	Envelope protein
E. coli	Escherichia coli
EDTA	Ethylenediaminetetraacetic acid
ER	Endoplasmic reticulum
ERGIC	ER-Golgi intermediate compartment
FCoV	Feline coronavirus
FCS	Foetal calf serum
GAG	Glycosaminoglycan
GMP	Guanosine 5'-monophosphate
gpt	Xanthine-guanine phosphoribosyltransferease gene
gRNA	Genomic RNA
GTP	Guanosine 5'-triphosphate
HA	Haemagglutinin protein
HCoV-229E	Human coronavirus 229E
HCoV-HKU1	Human coronavirus HKU1
HCoV-OC43	Human coronavirus OC43
HE	Haemagglutinin esterase protein
HECoV	Human enteric coronavirus
HEV	Porcine haemagglutinating encephalomyelitis virus
HIV	Human immunodeficiency virus
hpi	Hours post-infection
HR1 and 2	Heptad repeats 1 and 2
HS	Heparan sulfate
HSBS	Heparan sulphate-binding site
I	Internal ORF

IAH	Institute for animal health
IBV	Infectious bronchitis virus
IRES	Internal ribosome entry site
kb	Kilo bases
kDa	Kilo Dalton
LB	Luria-Bertani broth or agar
M	Membrane protein
MEM	Minimum essential medium
MHV	Murine hepatitis virus
moi	Multiplicity of infection
MPA	Mycophenolic acid
mRNA	Messenger RNA
MunCoV	Munia coronavirus
MXH	Solution containing MPA, xanthine and hypoxanthine
N	Nucleocapsid protein
nsp	Non-structural protein
ORF	Open reading frame
PBS	Phosphate buffered saline
P_3	Passage 3 virus
PCoV	Puffinosis coronavirus
PCR	Polymerase chain reaction
PDI	Protein disulphide isomerase
PEDV	Porcine epidemic diarrhoea virus
PFGE	Pulsed field gel electrophoresis
pGPT	Plasmid containing GPT

PhCoV	Pheasant coronavirus
pp1a and pp1ab	Replicase polyproteins 1a and 1ab
RBD	Receptor-binding domain
RdRp	RNA-dependent RNA polymerase
rFPV-T7	Recombinant fowlpox virus expressing T7 RNA polymerase
rIBV	Recombinant IBV
RNA	Ribonucleic acid
rpm	revolutions per minute
RSV	Rous sarcoma virus
RT	Room temperature
RTC	Replication-transcription complex
RtCoV	Rat coronavirus
RT-PCR	Reverse transcription-PCR
rVV	Recombinant vaccinia virus
S	Spike glycoprotein
SARS-CoV	Severe acute respiratory syndrome coronavirus
SDS	Sodium dodecyl sulphate
SOB	Super optimal broth
SOC	Super optimal broth with catabolite repression
SPF	Specific pathogen free
SS	Signal peptide
ssDNA	Single-stranded DNA
ssRNA	Single-stranded RNA
TBE	Tris borate EDTA buffer
TCoV	Turkey coronavirus

TDS	Transient dominant selection system
TE	Tris/HCl EDTA buffer
TGEV	Porcine transmissible gastroenteritis virus
ThCoV	Thrush coronavirus
TM	Transmembrane domain
TOCs	Tracheal organ cultures
TPB	Tryptose phosphate broth
tRNA	Transfer RNA
TRS	Transcription regulation sequence
UTR	Untranslated regions
UV	Ultraviolet
VV	Vaccinia virus
XMP	Xanthosine 5’-monophosphate

Chapter 1: Introduction

The *Nidovirales*

The *Coronaviridae* are members of the order *Nidovirales*, and comprise two subfamilies, the *Coronavirinae* and *Torovirinae*, which share a similar morphology. There are three genera of coronaviruses, *alpha-*, *beta-* and *gammacoronaviruses* (Figure 1.1; Carstens, 2010), which were so named for their visual resemblance to the corona of the sun in negatively stained preparations (Figure 1.2; Tynell, 1968).

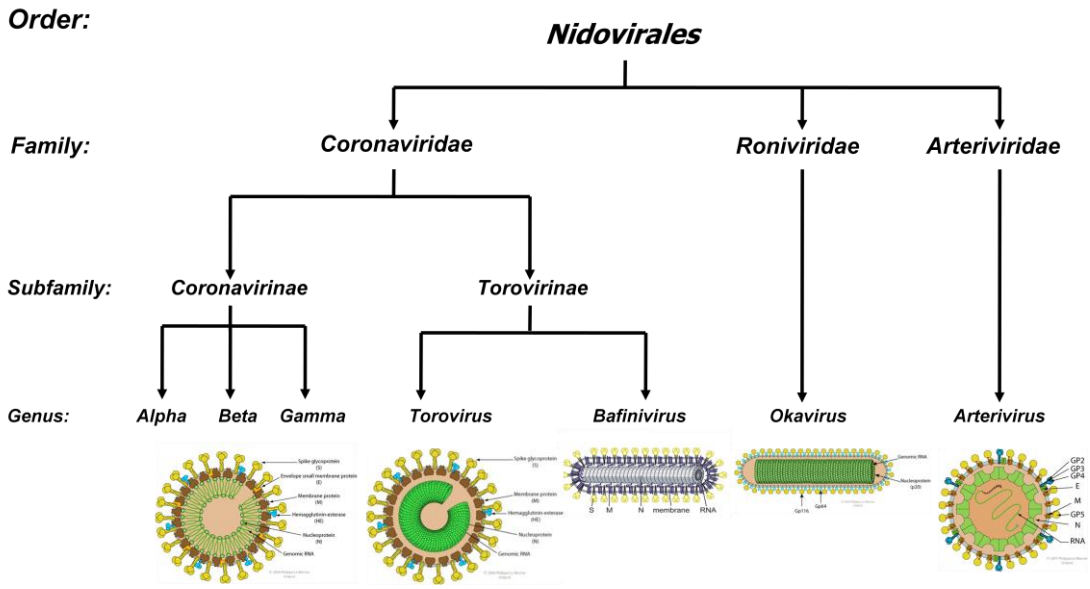

Figure 1.1. The *Nidovirales*. Three families comprise the *Nidovirales*, the *Coronaviridae*, *Roniviridae* and *Arteriviridae*. The *Coronaviridae* is split into two subfamilies, the *Coronavirinae* and the *Torovirinae*. There are three genera in the *Coronavirinae*, *alpha-*, *beta-* and *gammacoronavirus*. Representative virion diagrams of each of the *Nidovirales* genera are shown underneath (virion diagrams from ViralZone, Swiss Institute of Bioinformatics).

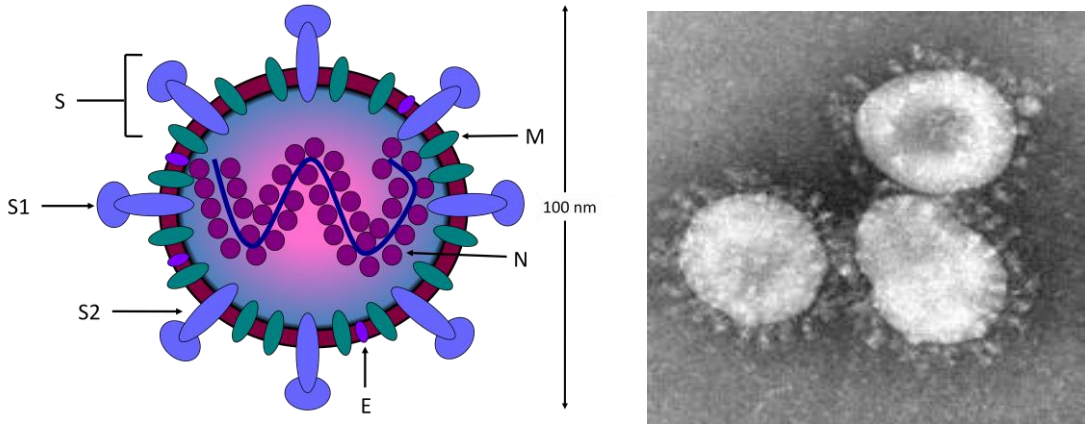

Figure 1.2. Coronavirus structure and electron micrograph of Coronavirus particles. Coronaviruses are surrounded by spike glycoproteins (S), which are comprised of S1 and S2 subunits, membrane proteins (M) and a small number of envelope proteins (E), all of which are embedded in a lipid membrane. The core structure is comprised of the nucleocapsid (N) protein and the RNA genome, which form a helical nucleocapsid. Micrograph obtained from the CDC Public Health Image Library, ID number 4814.

The *Coronavirinae*

Representative members of each of the coronavirus genera are shown in Table 1.1. Coronaviruses are enveloped viruses with a single-stranded positive-sense RNA genome of 26 – 32kb, the largest genomes of all RNA viruses currently known. The genome of infectious bronchitis virus (IBV) is 27.6kb (Boursnell *et al.*, 1987).

In addition to their large genomes, coronaviruses have a number of features that separate them from other positive-sense RNA viruses. The genome is capped and polyadenylated and is associated with the N protein forming a helical nucleocapsid within the virus particles. Although common among negative-sense RNA viruses, coronaviruses are the only positive-sense RNA viruses to possess helical nucleocapsids.

Table 1.1. Coronavirus genera and species

Genus	Species	
alphacoronavirus	Canine coronavirus (CCoV)	
	Feline coronavirus (FCoV)	
	Human coronavirus 229E (HCoV-229E)	
	Porcine epidemic diarrhoea virus (PEDV)	
	Porcine transmissible gastroenteritis virus (TGEV)	
betacoronavirus	Bovine coronavirus (BCoV)	
	Human coronavirus HKU1 (HCoV-HKU1)	
	Human coronavirus OC43 (HCoV-OC43)	
	Human enteric coronavirus (HECoV)	
	Murine hepatitis virus (MHV)	
	Porcine haemagglutinating encephalomyelitis virus (HEV)	
	Puffinosis coronavirus (PCoV)	
	Rat coronavirus (RtCoV)	
	Severe acute respiratory syndrome coronavirus (SARS-CoV)	
gammacoronavirus	IBV-like avian	Infectious bronchitis virus (IBV)
		Turkey coronavirus (TCoV)
		Pheasant coronavirus (PhCoV)
	Non-IBV-like avian	Munia coronavirus (MunCoV)
		Bulbul coronavirus (BuCoV)
		Thrush coronavirus (ThCoV)
	Mammalian	Beluga whale coronavirus SW1 (BeCoV)
		Asian leopard cat coronavirus
	Others*	Goose coronavirus
		Pigeon coronavirus
		Duck coronavirus

* The derivation of these species of *gammacoronavirus* has yet to be determined.

From the International Committee on Taxonomy of Viruses, Index of Viruses – Coronaviridae, (2008).

The helical nucleocapsids are enclosed within lipid envelopes containing the S glycoprotein, M protein and E protein (Figure 1.2). Some *betacoronaviruses* such as MHV and HCoV-OC43 also contain haemagglutinin esterase (HE) proteins in their envelopes.

Coronavirus genome organisation

The genomic RNA has a 5' m7GpppN-cap and a 3' polyA tail. Untranslated regions (UTRs) are found at the 5' and the 3' ends that have been shown to be involved in replication and translation (Senanayake and Brian, 1999). The same general genome organisation is shared within the genus: 5' UTR – replicase gene – structural protein genes – UTR 3' (Figure 1.3). Gene 1 encompasses the first two-thirds of the entire genome and consists of two large open reading frames, ORF 1a and 1b (Boursnell *et al.*, 1987). ORF 1a and 1b overlap slightly and are translated by a -1 frameshift mechanism (Brierley *et al.*, 1987), the signal for which lies in the overlapping region, using a pseudoknot structure and a slippery sequence located between ORF1a and 1b. The two overlapping ORFs result in two large replicase proteins, pp1a and 1ab, the latter being a fusion protein of the first ORF as a result of the -1 frameshift. Both proteins are proteolytically cleaved by two or three virus-encoded proteases. Autoproteolytic processing of pp1a and 1ab polyproteins produces the fifteen (IBV) or sixteen (other coronaviruses) replicase proteins. Two domains found within the ORF1b region are unique to the Nidovirales. These are the zinc-binding domain and the uridylate-specific endoribonuclease (Gorbalenya *et al.*, 2006).

Coronaviruses produce a nested set of sub-genomic mRNAs during the replication cycle (Sawicki and Sawicki, 1995), which are, apart from the last mRNA,

structurally polycistronic but functionally monocistronic as only the translation initiation site closest to the 5' terminus is utilised. Each mRNA has the same 3' terminus and short 5' leader sequence, which is identical to the 5' end of the genome (Lai *et al.*, 1983).

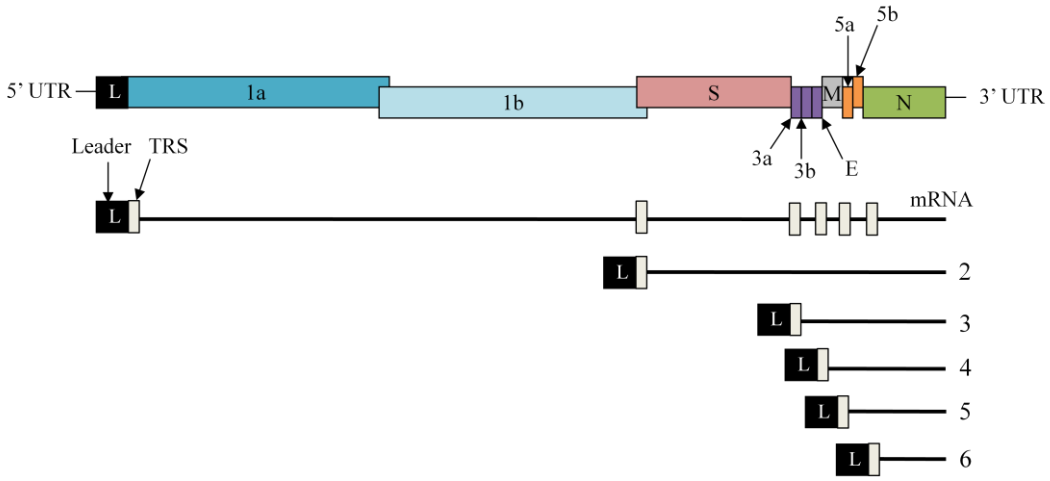

Figure 1.3. IBV genome structure and subgenomic mRNAs. Gene 1 is comprised of ORFs 1a and 1b, which are located proximal to the 5' untranslated region (UTR) and the leader sequence. These encode proteins associated with RNA replication and transcription. The S, E, M and N genes are located proximal to the 3' UTR and encode the proteins found in virus particles. Interspersed between these structural protein genes are accessory genes encoding non-structural proteins 3a, 3b, 5a and 5b, which are not essential for replication. The nested set of IBV mRNAs (genome and subgenomic mRNAs 2 – 6) is shown below. The genome-length mRNA shows the location of the transcription regulation sequences (TRS). Gene lengths are not to scale.

The 3'-proximal ORFs encode the structural proteins genes in the order S – E – M – N, with some *betacoronaviruses* also having an HE protein, the gene of which is situated upstream of the S gene in the genome. In addition to the polymerase gene and structural protein genes, coronaviruses also have several polycistronic genes

encoding non-structural or accessory proteins. IBV encodes four accessory proteins, 3a, 3b, 5a and 5b (Figure 1.3), the functions of which are as yet unknown. Some *betacoronaviruses* contain an internal ORF (I) within the N gene, which is expressed in a +1 frameshift to the N protein sequence (Fischer *et al.,* 1997).

Coronavirus replication cycle (Figure 1.4)

The coronavirus S glycoprotein mediates attachment to host cell receptors and fusion of the virion membrane to the host cell membrane (Koch *et al.,* 1990; Luo and Weiss, 1998). Binding of the S1 subunit to the host cell receptor induces conformational changes in the spike (Zelus *et al.,* 2003), leading to virus-cell fusion and release of the nucleocapsid into the cytoplasm (Risco *et al.,* 1996).

The entry mechanisms for the *coronavirinae* have not been fully elucidated. The SARS coronavirus has been shown to utilise the clathrin-dependent endocytosis pathway before being transported to early endosomes (Inoue *et al.,* 2007) where entry is pH-dependent (Yang *et al.,* 2004). The MHV strain A59 has also been shown to enter host cells via clathrin-dependent endocytosis (Eifart *et al.,* 2007), however another variant of MHV, JHMV, is able to enter host cells directly from the cell-surface (Nash and Buchmeier, 1997).

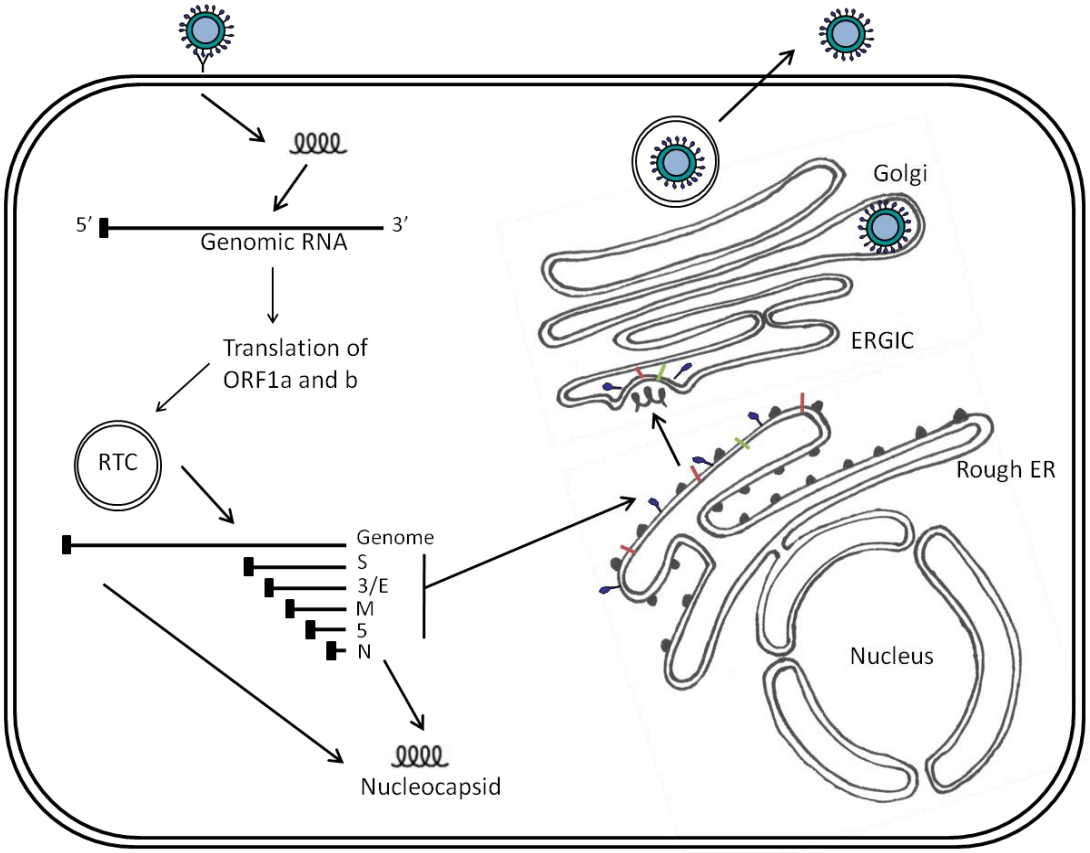

Figure 1.4. The replication cycle of IBV. The virus particle attaches to the host cell receptor (as yet unknown) and fuses with the cell membrane via the S glycoprotein. Genomic RNA is released from the N protein and acts as an mRNA for the translation of the replicase proteins. A –1 frame shift from ORF1a to ORF1b in the replicase gene generates the replicase polyproteins, pp1a and pp1ab, in differing amounts. Virus-encoded proteinases proteolytically cleave replicase polyproteins and they assemble in double membrane replication-transcription complexes (RTC). Sub-genomic mRNAs are produced from the rest of the genomic RNA and express the structural and other non-structural viral proteins at the rough endoplasmic reticulum (ER) and assemble at the ER-Golgi intermediate compartment (ERGIC). The N protein associates with the genomic RNA to form the nucleocapsid and is incorporated into the forming virions at the ERGIC. Complete virus particles bud off from the Golgi apparatus and exit the cell by exocytosis.

Conformational changes in the spike leading to virus-cell fusion may be caused by low pH within endosomes, as in the case of IBV. Chu *et al.,* (2006) used fluorescence-dequenching assays to determine that IBV undergoes direct low-pH-dependent fusion activation within acidic endosomes. Fusion was unaffected by the presence of protease inhibitors and did not occur at neutral pH. Pre-treatment of virions at low pH did not affect virus entry, indicating that conformational changes in the IBV S glycoprotein are reversible (Chu *et al.,* 2006). In contrast, studies of MHV-A59 have indicated that low pH-triggered conformational changes of the spike are irreversible (Eifart *et al.,* 2007).

While it appears that entry of IBV and MHV both depend on low pH, proteases may be involved in entry of HCoV-229E and SARS-CoV. The spike of HCoV-229E has been shown to be activated by the endosomal protease cathepsin L (Kawase *et al.,* 2009), as has that of SARS-CoV (Simmons *et al.,* 2005), which has also been demonstrated to be activated by the transmembrane protease TMPRSS2 in the lung (Matsuyama *et al.,* 2010). The S subunits of HCoV-229E and SARS-CoV are not cleaved during biosynthesis, whereas the S subunits of MHV and IBV are cleaved during biosynthesis.

A model for coronavirus transcription and translation (Figure 1.5) has been described by Sawicki and Sawicki (1995). It is hypothesised that upon virus entry and uncoating, ORF1 of genomic RNA is directly translated, producing pp1a and pp1ab. The replicase polyproteins are cleaved by virus-encoded proteinases (Ziebuhr *et al.,* 2000) and form replication-transcription complexes (RTC), which copy the genome. Minus strand templates are synthesised from the genome; genome-length templates

are produced by continuous transcription, subgenome-length templates are produced by discontinuous transcription.

A transcription regulation sequence (TRS) is found at the 5' end of each gene and at the 3' end of the leader sequence. RNA synthesis of the negative-sense transcripts is thought to begin at the 3' end of the genome and continue until a TRS is reached. The RTC either pauses and then continues on to the next TRS or switches to the TRS at the leader sequence and continues transcription to form the negative-sense sub-genomic RNA with an anti-leader sequence at the 3' end. The method by which the 3' end of the nascent negative strand may relocate to the 5' end of the genomic template is as yet unknown. The negative sense genome-length and sub-genomic RNAs are used as templates for genomic and sub-genomic mRNA synthesis. It is thought that the RTCs age, releasing the minus strand templates for degradation (reviewed by Sawicki *et al.,* 2007). Newly synthesised viral RNA is found associated with convoluted membranes and double-membrane vesicles (Gosert *et al.,* 2002) thought to originate from the endoplasmic reticulum (Knoops *et al.*, 2008), although autophagy may also be involved (Prentice *et al.,* 2004). These membranes may serve to protect viral RNA from degradation and may provide an optimal environment for viral RNA synthesis (van Hemert *et al.*, 2008).

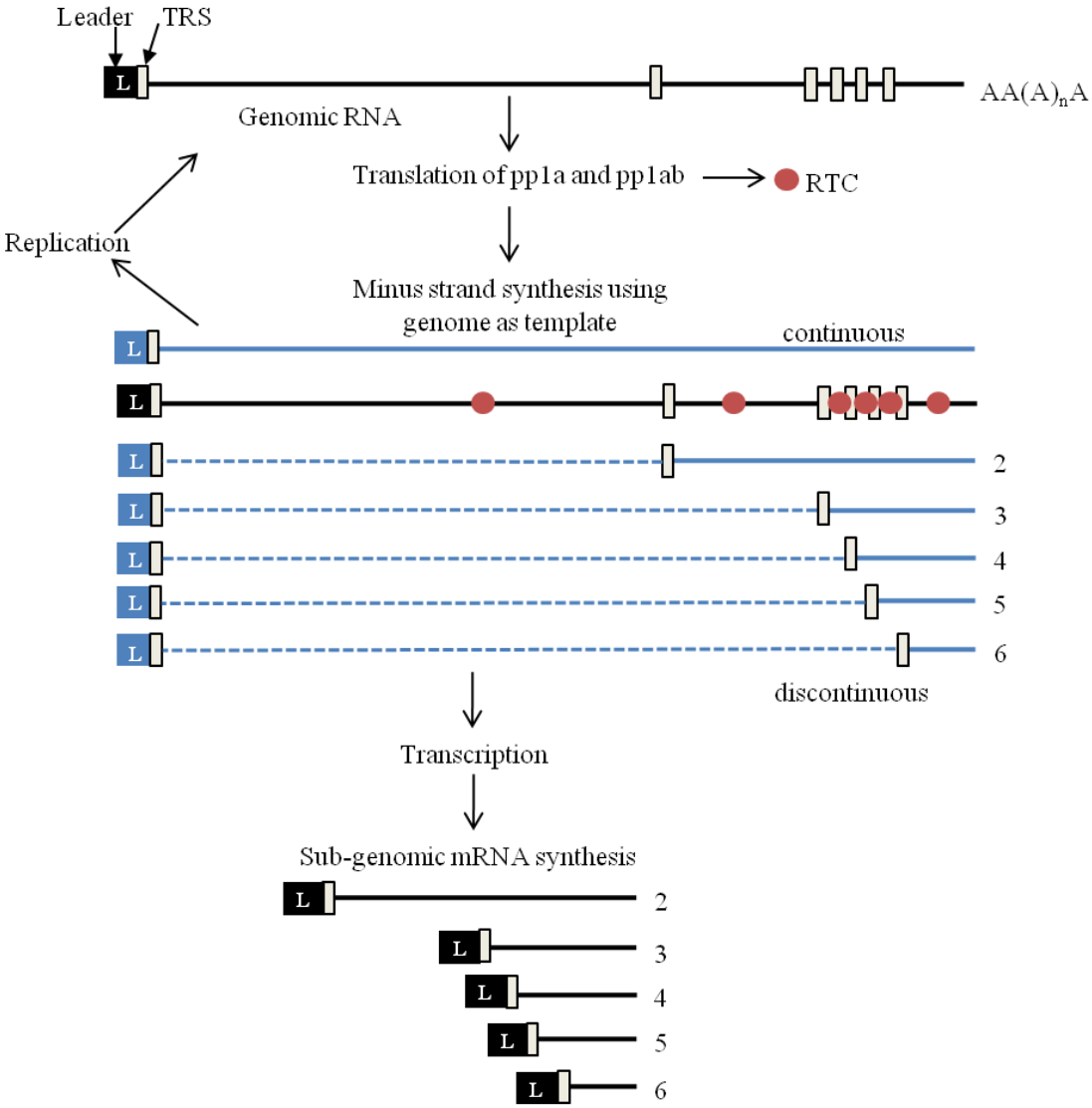

Figure 1.5. Coronavirus replication-transcription model. Genomic RNA is translated, producing pp1a and pp1ab, which form RTCs. The RTCs recognise *cis*-acting elements at the 5' and 3' ends of the genome and copy the genome continuously into a genome-length negative-strand template or discontinuously into the sub-genomic negative-strand templates. Negative strands are shown in blue and are used as templates for genomic and sub-genomic mRNA synthesis (shown in black). TRSs are shown as grey boxes either 5' to each mRNA or at the 5' end of the genome corresponding to the leader junction site. Anti-leader sequences are also shown in blue. The RTCs age, releasing the minus strand templates for degradation. Adapted from Sawicki *et al.*, (2007).

A nested set of sub-genomic mRNAs are produced, which express the structural and accessory viral proteins at the endoplasmic reticulum (ER). Most sub-genomic mRNAs are functionally monocistronic and only the ORF at the 5' end is translated by a cap-dependent mechanism. Bi- or tricistronic sub-genomic mRNAs are translated via a leaky-scanning mechanism or by internal ribosome entry (Liu and Inglis, 1992; Le *et al.,* 1994). The nucleocapsid associates with the M protein (Sturman *et al.,* 1980) and structural proteins assemble at the ER-Golgi intermediate compartment (ERGIC; Klumperman *et al.,* 1994). Complete virus particles bud off from the Golgi apparatus and exit the cell by exocytosis (Tooze *et al.,* 1987).

Replicase proteins

Two large non-structural precursor polyproteins are produced from gene 1, pp1a and pp1ab, comprising 70 – 80 % and 20 – 30 % respectively (Ziebuhr *et al.,* 2000). Proteolytic processing of pp1a and pp1ab by several ORF1a-encoded proteinases including a 3C-like cysteine proteinase results in ~ 16 non-structural proteins (nsp), which are involved in replication. IBV does not have the equivalent to nsp1, however nsp2 to nsp16 correspond to those of the other coronaviruses. ORF1a encodes nsp1 to nsp11 and ORF1b encodes nsp12 to nsp16.

Gorbalenya *et al.* (1989) used comparative sequence analysis to identify several functions of the polyproteins encoded by gene 1 including an RNA-dependent RNA polymerase (RdRp), nucleic acid binding domain, two proteases and an RNA helicase. The RNA helicase (nsp13) and RdRp (nsp12) are encoded by ORF1b (Gorbalenya *et al.,* 1989) and are produced in less amounts than the ORF1a-encoded proteins, which are involved in proteolytic activity and membrane association (van

der Meer *et al.,* 1999). The replicase proteins assemble into RTCs, forming double-membrane vesicles (DMV), the sites of viral RNA synthesis (Gosert *et al.,* 2002).

Nsp1 inhibits host protein synthesis by degrading host mRNAs (Kamitani *et al.,* 2006). Nsp3 is involved in ADP ribosylation (Eckerle *et al.,* 2006) and contains 1 or 2 papain-like proteinase sites depending on the coronavirus group, which are involved in processing nsp1 and 2 (Graham and Denison, 2006). Nsp5 encodes a 3C-like proteinase, which processes the remaining nsps (Lu *et al*., 1996) and cleaves pp1a and pp1ab at conserved central and C-terminal regions (reviewed by Ziebuhr *et al.,* 2000). Nsp7 and nsp8 form a super-complex shaped like a hollow cylinder consisting of eight molecules of each that may act as a cofactor to RdRp (Zhai *et al.,* 2005). The nsp7-nsp8 super-complex interacts with nsp9, an ssRNA and ssDNA binding protein (Sutton *et al.,* 2004; Egloff *et al.,* 2004). Nsp8 and nsp9 bind tRNA, possibly suggesting an ability to interfere with host-cell translation (Ponnusamy *et al.,* 2006). Nsp 10 is involved in RNA synthesis (Donaldson *et al.,* 2006). Nsp14 has 3' – 5' exonuclease activity, nsp15 is an endoribonuclease and nsp16 is an RNA methyltransferase (Eckerle *et al.,* 2006).

The functions of some replicase nsps remain to be elucidated. Several nsps may be involved in the formation of the replication complex, which associates with host cell membranes, in particular the late endosomal membranes. Membrane association of the replication complex is mediated by the replicase protein subunits (van der Meer *et al.,* 1999). Nsps 3, 4 and 6 have transmembrane domains and may be involved in anchoring the RTCs to host membranes (Oostra *et al.,* 2007; Oostra *et al.,* 2008). Nsp2 has been shown to be recruited to RTCs and no exchange of nsp2 between the

cytoplasm or other DMVs occurs (Hagemeijer *et al.,* 2010). Other nsps interact to mediate viral RNA synthesis in the host cell.

Accessory proteins

All coronaviruses encode a number of non-structural proteins not derived from gene 1, which are interspersed between the structural genes and vary between different coronaviruses. IBV has four accessory proteins, 3a, 3b, 5a and 5b that are not essential for virus replication (Casais *et al.,* 2005; Hodgson *et al.,* 2006). The numbers indicate the relative location of the ORF within the genome.

Gene 3 is well conserved between IBV-like avian *gammacoronaviruses* (Jia and Naqi, 1997) and is tricistronic, encoding two accessory proteins, 3a and 3b, and the structural envelope protein (E) corresponding to ORF 3c (Smith *et al*., 1990). Translation of ORF 3c is independent of the translation of ORFs 3a and 3b, the latter of which is translated via leaky ribosomal scanning (Liu and Inglis, 1992). Ribosomes bind to the cap structure at the 5' end of the RNA and scan until they reach the initiation codon for ORF 3a, AUG, where translation starts (Kozak, 1981). Sometimes the first initiation codon is missed by the ribosome and it continues scanning until it reaches the initiation codon for ORF3b. This is not the case for the initiation of ORF3c, however. ORFs 3a and 3b form a unique folding region containing a sequence complementary to the 18s ribosome subunit situated 3' from two pseudoknot structures prior to the 3c initiation codon (Le *et al.,* 1994). This acts as an internal ribosomal entry site (IRES) for the initiation of translation of 3c. Hodgson *et al.* (2006) showed that 3a and 3b are not essential for replication of IBV

in vitro, however the titres of recombinant IBVs lacking 3a declined earlier than the parent virus in tracheal organ cultures (TOCs).

Gene 5 of IBV is bicistronic and contains ORFs 5a and 5b. Casais *et al.* (2005) produced a series of recombinant IBVs in which the complete expression of gene 5 products was prevented. These recombinants were able to replicate to a similar titre to the parent virus, indicating that 5a and 5b are not essential for IBV replication *in vitro*.

Although the role of IBV accessory proteins is unclear, the accessory proteins of MHV may be determinants of pathogenicity. A study was carried out by de Haan *et al.* (2002) in which a series of recombinant viruses were produced with deleted accessory genes. Replication of recombinant viruses was similar to parent virus *in vitro* however recombinants were attenuated *in vivo*. A recent study has indicated that MHV 5a is able to confer resistance to interferon (Koetzner *et al.,* 2010).

Structural proteins

The M glycoprotein

Most abundant of the structural proteins is the 25 kDa M glycoprotein (formerly known as the E1 protein), which spans the viral envelope three times (Godeke *et al.,* 2000). The first membrane-spanning domain targets the M protein to the cis Golgi (Machamer *et al.,* 1990) and is sufficient for membrane binding, retention in the Golgi and formation of multimers (Tseng *et al.,* 2010). The M protein has a short N-terminal ectodomain and a large C-terminal cytoplasmic domain that interacts with

the nucleocapsid and is involved in assembly of virus particles (Narayanan *et al.,* 2003). Interaction of the M protein with the S glycoprotein retains the spike in the ERGIC (McBride *et al.,* 2007). A single tyrosine residue at amino acid position 195 in the M protein of the SARS-CoV has been identified as being necessary for interaction of the S and M proteins and assembly of virions (McBride and Machamer, 2010).

The E protein

The E protein is membrane-associated and contains a transmembrane region of a hydrophobic domain flanked by two hydrophilic domains. The cytoplasmic tail of the E protein contains Golgi targeting information (Corse and Machamer, 2002). The E protein is a minor component of the virus envelope and is the least abundant structural protein. It is thought that interaction of the E and M proteins may cause membrane curvature (Fischer *et al.,* 1998), promoting budding of virus particles and is fundamental for the assembly of virus particles (Lim and Liu, 2001). The E protein forms cation-selective ion channels in the lipid envelope, enhancing membrane permeability (Wilson *et al.,* 2004).

The N protein

The N protein is a phosphorylated, highly basic structural protein that forms a helical nucleocapsid when bound to the coronavirus RNA genome within the virus particles. The carboxy-terminal domain interacts with the M protein (Hurst *et al.,* 2005) and is packaged into viral particles by the M protein when bound to genomic RNA (Narayanan *et al.,* 2003). The N protein does not have a transmembrane domain but

is dynamically associated with membrane-associated viral RTCs (Sims *et al.,* 2000; Verheije *et al.,* 2010).

The S glycoprotein

The spike glycoprotein is a 180 kDa membrane glycoprotein projecting 20 nm from the virus surface (Figure 1.6; Delmas and Laude, 1990). Cellular tropism of IBV is determined by the S glycoprotein (Casais *et al.,* 2003), which has two subunits, the N-terminal S1 subunit responsible for binding to host cell receptors (Koch *et al.,* 1990) and the C-terminal S2 subunit responsible for cell-cell and virus-cell fusion (Luo and Weiss, 1998). The subunits are both approximately 80 kDa in size.

The coronavirus S glycoprotein is synthesised as a single polypeptide chain, which oligomerises into homotrimers in the ER of the host cell and are processed in the Golgi apparatus (Delmas and Laude, 1990). Oligosaccharides are added to the spikes co-translationally. Studies with tunicamycin by Rottier *et al.,* (1981) indicated that the S glycoprotein of MHV has N-glycosidically linked oligosaccharides while the M protein has O-linked oligosaccharides. The S and M glycoproteins of IBV however were found to both have N-linked high-mannose type oligosaccharides (Cavanagh *et al.,* 1983). Sequence analysis has predicted that the SARS-CoV S glycoprotein has 23 potential N-linked glycosylation sites (Rota *et al.,* 2003), one of which (N330) was found to interact with mannose-binding lectin (Zhou *et al.,* 2010). A number of N-linked glycosylation sites were found to be critical for DC/L-SIGN-mediated virus entry and also to have facilitated zoonotic transmission (Han *et al.,* 2007).

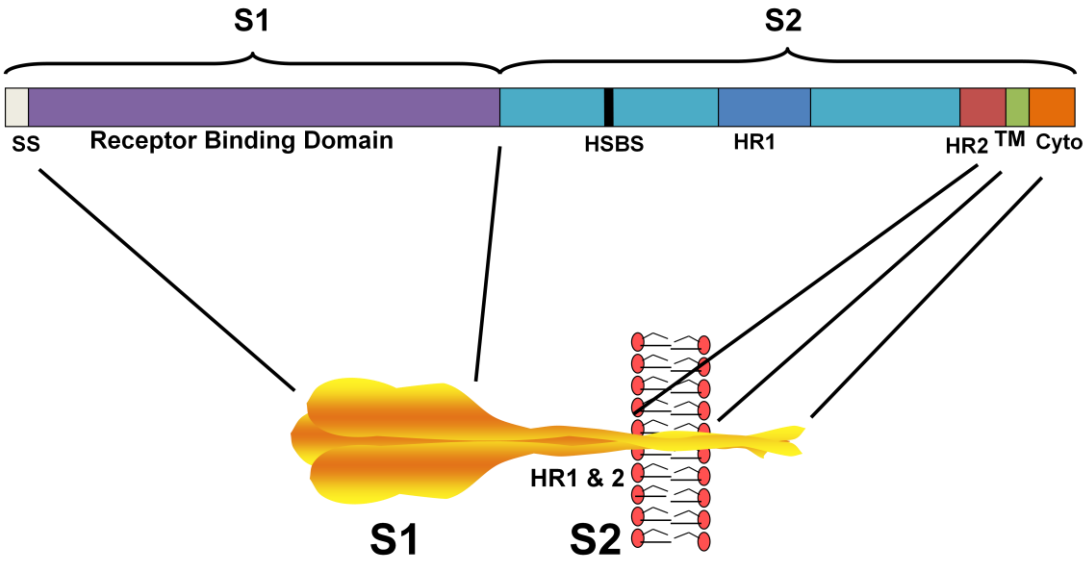

Figure 1.6. IBV S glycoprotein structure. The IBV S glycoprotein domains are organized with the S1 domain at the N-terminus and the S2 domain at the C-terminus. A signal peptide (SS) is located within S1 along with the receptor-binding domain. Within the S2 subunit are two heptad repeats (HR1 and 2), a transmembrane domain (TM) and a cytoplasmic tail (Cyto). The IBV S glycoprotein is cleaved by host cell proteases between the S1 and S2 subunits. The Beaudette strain of IBV contains a putative heparan sulphate-binding site (HSBS) within the S2 subunit.

The spike of MHV is thought to regulate the transport of the viral genome from the cell surface to the ER (Zhu *et al.*, 2009), from where the spike is transported to the ERGIC (Lontok *et al.*, 2004). The spike interacts with the M protein on pre-Golgi membranes forming multimeric complexes (Opstelten *et al.*, 1995) and is incorporated into forming virions (de Haan *et al.*, 1999). Unlike the other membrane-bound proteins, however, the coronavirus S glycoprotein is not required for the assembly of virions (Baudoux *et al.*, 1998). Excess S protein can be transported to the plasma membrane where it may participate in cell-cell fusion,

although transport of spikes not incorporated into virions through the Golgi is very slow (Vennema *et al.,* 1990). The IBV S protein contains a canonical dilysine ER retrieval signal (-KKXX-COOH) (Youn *et al.,* 2005) and a tyrosine-based endocytosis signal in its cytoplasmic tail (Lontok *et al.,* 2004).

There is no clear consensus of the role of S glycoprotein cleavage in fusion. The two S subunits of some coronaviruses including IBV, MHV and HCoV-OC43, are cleaved during biosynthesis by a furin-like protease in the Golgi apparatus (de Haan *et al.,* 2004) but remain non-covalently linked. The S1/S2 junction in IBV strains Beaudette and M41 is situated at the amino acid sequence RRFRR at amino acid position 552 (Cavanagh *et al.,* 1986). Cleavage of the MHV S glycoprotein differs between strains and host cells (Frana *et al.,* 1985) and is not required for infectivity (Bos *et al.,* 1995) or for binding to cellular receptors (Zelus *et al.,* 2003). Cleavage inhibition of the MHV S glycoprotein affects cell-cell fusion but not virus-cell fusion, indicating that cell-cell and virus-cell fusion are distinct processes (de Haan *et al.,* 2004). Entry of IBV and MHV has been shown to be pH-dependent (Chu *et al.,* 2006; Eifart *et al.,* 2007).

The S subunits of HCoV-229E and SARS-CoV are not cleaved during biosynthesis; however the S glycoprotein of SARS-CoV is susceptible to protease cleavage within the human airway, enhancing virus entry (Kam *et al.,* 2009). The HCov-229E and SARS-CoV S glycoproteins are both activated by proteases during viral entry (Kawase *et al.,* 2009; Simmons *et al.,* 2005). Cleavage of the SARS-CoV S glycoprotein by furin enhances cell-cell fusion not virus-cell fusion (Follis *et al.,* 2006).

The receptor-binding domain (RBD) is an independently folded region of the spike responsible for interfacing with the viral receptor, usually 180 – 130 amino acids in length. Although all coronavirus RBDs are found within the S1 subunit, they are virus-specific and vary in position throughout the S1 domain. The RBD of MHV is located at the N-terminus of S1 (Kubo *et al.*, 1994) and the HCoV-229E RBD is located at the C-terminus of S1 (Bonavia *et al.*, 2003). The RBD of SARS-CoV is located at the C-terminus of the S1 subunit between residues 270 – 510 (Babcock *et al.*, 2004), however the residues 217 – 234 are also critical for virus entry (Guo *et al.*, 2009). The specific location of the RBD of IBV has yet to be elucidated, although studies by Cavanagh *et al.* (1986) have determined that it is present in the S1 subunit.

The coronavirus S glycoprotein is a type I fusion protein (Bosch *et al.*, 2003), which is characterised by the presence of a number of domains including a pair of extended α-helices, also known as heptad repeats (HR; Figure 1.6). The two helical domains, HR1 and HR2, form a trimer of hairpins or six-helix bundle, creating a stalk structure anchored to the virion membrane by a transmembrane domain. The heptad repeats draw the host cell and viral membranes together upon receptor binding. This causes destabilisation of the membranes and may allow the entry of the viral nucleocapsid (Sainz *et al.*, 2005).

A fusion peptide consisting of around twenty hydrophobic amino acids is located at the amino-terminal end of the first HR and a cluster of aromatic amino acids is situated near a hydrophobic transmembrane domain (Chambers *et al.*, 1990; Sainz *et al.*, 2005). Binding of the S1 subunit to the receptor is thought to induce a

conformational change, activating the fusion peptide (Matsuyama and Taguchi, 2002b).

The position of the SARS-CoV fusion peptide has been sought by several groups, however the exact location is still unknown. Putative locations of the fusion peptide include the N-terminal region of HR1, a region C-terminal to an S2 cleavage site and the N-terminal region of S2 (Petit *et al.,* 2005; Sainz *et al.,* 2005; Madu *et al.*, 2009). Putative fusion peptides for MHV have been identified within HR1 or immediately upstream of HR1 (Luo and Weiss, 1998; Xu *et al.,* 2004). The fusion peptide of IBV has yet to be elucidated.

Class I fusion proteins of other viruses

Whilst relatively little is currently known about the S glycoproteins of coronaviruses, the fusion proteins of some other viruses have been more widely studied and may offer insight into the fusion properties of coronaviruses. Class I fusion proteins are produced by paramyxoviruses, orthomyxoviruses, retroviruses, filoviruses and arenaviruses. There are three common modes of entry of enveloped viruses. The fusion proteins of some, such as HIV, undergo conformational changes upon binding to cellular receptors which induce fusion of viral and cellular membranes. Fusion may be activated by acidic pH, as in the case of influenza virus, or by proteolytic cleavage of the fusion protein like Ebola virus.

The best studied of the viral fusion proteins is the haemagglutinin (HA) protein of influenza A and B viruses, which, like the coronavirus S glycoprotein, is responsible for both receptor binding and fusion (Gamblin *et al.*, 2004). The HA precursor

protein is cleaved into two subunits, HA1 and HA2, which form a homotrimer. The HA1 subunits form the globular heads of the homotrimer and HA2 forms a triple-stranded coiled-coil containing the fusion peptide. Conformational changes in HA1 and HA2 are triggered by low pH within endosomes mediating fusion of the viral envelope with the endosomal membrane. The HA conformational changes are irreversible, unlike those of the IBV S glycoprotein, which is able to revert to its original form after exposure to low pH (Chu *et al.,* 2006). The fusion peptide is inserted into the endosomal membrane, bringing the viral envelope close. It is thought that the membranes fuse by hemifusion, in which the outer layers of the viral and cellular membranes fuse followed by the inner layers, forming a pore (Melikyan *et al.,* 1995).

Entry of HIV occurs via the plasma membrane. Similar to Influenza virus and coronaviruses, the HIV glycoprotein, gp160, is responsible for both receptor binding and fusion. Gp160 is proteolytically cleaved into two subunits, gp120 and gp41, by cellular proteases. Binding of gp120 to the receptor/coreceptor induces conformational changes and fusion activation of gp41, facilitating the fusion of the viral and cellular membranes by insertion of the fusion peptide into the host cell membrane (reviewed by Chan and Kim, 1998).

Ebola virus enters host cells via endosomes, where cysteine proteases, cathepsin B and L, cleave the GP1 subunit of the glycoprotein (GP) and activate it for fusion (Chandran *et al.,* 2005). Cathepsin L is also involved in the fusogenic activation of the SARS-CoV and HCoV-229E S glycoproteins (Simmons *et al.,* 2005; Kawase *et*

al., 2009), indicating the possibility that these coronaviruses may employ a similar manner of cellular entry to Ebola virus.

Paramyxoviruses differ from coronaviruses in that they contain two glycoproteins within their envelopes, a fusion protein and an attachment protein. The fusion protein has a globular head attached to a trimeric coiled-coil stalk (Yin *et al.*, 2006). The homotrimeric fusion protein is proteolytically cleaved and undergoes a conformational change at neutral pH to promote fusion of the viral and host cell envelopes by inserting the fusion peptide into the host cell membrane and rearranging to form a six-helix bundle, bringing the fusion peptide and transmembrane domains close together.

Class II fusion proteins are produced by members of the Flaviviridae, including flaviviruses, hepaciviruses and pestiviruses, and contain an internal fusion peptide and three parallel β-sheet domains (Garry and Dash, 2003).

Coronavirus tropism and receptors

Coronaviruses generally exhibit restricted cell and tissue tropism, which is dependent upon the S glycoprotein of individual coronavirus strains (Casais *et al.*, 2003; Sanchez *et al.*, 1999; Tekes *et al.*, 2010). Some strains of IBV, following adaptation, are able to replicate in primary chicken cells such as chick kidney (CK) cells, however the Beaudette strain exhibits an extended host range and can replicate in Vero and baby hamster kidney (BHK-21) cell lines (Casais *et al.*, 2003; Otsuki *et al.*, 1979). This is determined by the S glycoprotein (Casais *et al.*, 2003).

The host-cell receptors for several coronaviruses have been identified. The *alphacoronaviruses* HCoV-229E and TGEV both use aminopeptidase N as host cell receptor (Delmas *et al.,* 1992; Yeager *et al.,* 1992), although binding of TGEV to sialic acid is required for enteropathogenicity. This is not required for *in vitro* replication (Schwegmann-Wessels *et al.,* 2002).

The *betacoronaviruses* have been found to utilise a variety of different receptors. Major histocompatibility complex class I C has been identified as an attachment factor for HCoV-HKU1 (Chan *et al.,* 2009). SARS-CoV has been shown to use angiotensin-converting enzyme 2 (ACE2) as a receptor (Li *et al.,* 2003) along with CD209L (Jeffers *et al.,* 2004) and is also thought to use the C-type lectins DC-SIGN and L-SIGN as alternative receptors independent of ACE2 (Han *et al.,* 2007). Bovine coronavirus utilises *N*-acetyl-9-O-acetylneuraminic acid as a receptor (Schultze and Herrler, 1992). The principal receptor for MHV is murine carcinoembryonic antigen-related cell adhesion molecule (CEACAM; Williams *et al.,* 1991) although the virus also attaches to O-acetylated sialic acid. Surprisingly however, this is mediated by the HE protein rather than the S glycoprotein (Langereis *et al.,* 2010).

The most widely studied *gammacoronavirus* is IBV, the receptor for which has not yet been elucidated. It was suggested by Miguel *et al.,* (2002) that the Arkansas 99 strain of IBV may use feline aminopeptidase N as an entry receptor on feline cells, however this has been disputed (Chu *et al.,* 2007). A recent study has shown that two strains of IBV, M41 and Beaudette-US, use sialic acid as an attachment factor (Winter *et al.,* 2006) and infection of the tracheal epithelium is dependent upon sialic

acid (Winter *et al.,* 2008). This has been confirmed by Madu *et al.,* (2007), who have also identified a heparan sulfate (HS) binding site between amino acid residues 686 – 691 within the S2 subunit of the Beaudette S glycoprotein and shown that HS may be involved as a cofactor in Beaudette virus entry to host cells. Yamada and Liu, (2009) also identified a potential furin cleavage motif within the putative heparan sulphate binding site studied by Madu *et al.,* (2007).

Heparan sulphate is a glycosaminoglycan (GAG) found on the surface of mammalian cells (reviewed by Liu and Thorp, 2002). The consensus sequence for a heparin-binding site is XBBXBX, where B is a basic amino acid and X is a hydropathic amino acid (Cardin and Weintraub, 1989). The sequence identified in the Beaudette S glycoprotein was SRRKRS or SRRRRS (Madu *et al.,* 2007). This sequence was not found in the S glycoprotein of any other strains of IBV, which is a possible explanation for the extended host range of Beaudette in comparison to M41. A number of other viruses are able to use HS as an adhesion receptor, including foot and mouth disease virus and herpes simplex virus (Liu and Thorp, 2002).

A variant of the *betacoronavirus* MHV derived from persistently infected murine cells was found to have the ability to infect baby hamster kidney-21 cells (BHK-21; Schickli *et al.,* 1997). The extended host range was mapped to the N-terminal region of the spike (Schickli *et al.,* 2004; Thackray and Holmes, 2004). This strain, MHV/BHK, has been identified as using heparan sulphate as an entry receptor (de Haan *et al.,* 2005). A cell-culture adapted strain of the *alphacoronavirus* FCoV, FCoV UCD1, has traded its ability to be cleaved at the S1/S2 junction by a furin-like

protease for the capacity to bind heparan sulphate and has gained an extended host range (de Haan *et al.*, 2008).

Infectious bronchitis

Infectious bronchitis virus is the aetiological agent of the disease infectious bronchitis that affects poultry. IBV replicates primarily in the respiratory tract but also in many other epithelial surfaces including enteric surfaces, oviducts and kidneys (Ambali and Jones, 1990) causing a highly contagious respiratory disease characterised by nasal discharge, snicking, tracheal ciliostasis and rales in chickens (Hodgson *et al.,* 2004). Egg production and quality may be impaired in layers and weight gain in broilers is reduced. Infected birds are predisposed to secondary bacterial infections and mortality in young chicks is not uncommon. Faecal excretion of the virus is a consequence of replication in the intestinal tract, however, this does not normally result in clinical disease.

Infectious bronchitis was first described in the US in the 1930s and is prevalent in poultry farming across the world due to its intensive nature. In a study carried out by DEFRA (2005), infectious bronchitis was found to cost the UK economy nearly £19 million per year, mainly due to loss of egg production, and has serious implications for animal welfare, second only to skeletal problems. The cost of control is approximately £5 million per year in the UK.

IBV vaccines

The most common vaccines against IBV are live attenuated vaccines, although other types of vaccines against IBV exist including inactivated virus and subunit vaccines

and some promising vector vaccines are under development (reviewed by Cavanagh, 2007). There are many different serotypes of IBV that are poorly cross-protective; however the S glycoprotein alone is sufficient to confer protective immunity (Koch *et al.,* 1990; Tomley *et al.,* 1987). Since the advent of a reverse genetics system for IBV (Britton *et al.,* 2005; Casais *et al.,* 2001), there has been the possibility for rational design of recombinant IBV strains for vaccine development.

Live attenuated IBV vaccines are currently produced by blind repeated passages of IBV field strains through embryonated eggs. As serial passage reduces the immunogenicity of the virus, a balance between virus attenuation and loss of immunogenicity must be achieved by trial and error, as the molecular basis of attenuation is as yet unknown.

The most commonly used current IBV vaccines include those based on H52 and H120, which were derived from the Massachusetts strain of IBV after 52 and 120 passages in embryonated eggs respectively. Protection is short-lived and both layers and broilers may be vaccinated more than once during their short life spans.

IBV infection may predispose laying hens to secondary bacterial infections thus reducing egg production further. In fact, inoculation of broilers with IBV vaccine strain H52 increased the susceptibility of the birds to colibacillosis even more so than infection with virulent IBV field strains M41 and D387 (Matthijs *et al.,* 2003). Some strains of IBV are nephropathogenic and are not protected against by current vaccination procedures (Cook *et al.,* 2001).

A study by Huang and Wang (2007) investigated amino acid changes in three strains of IBV after attenuation in embryonated eggs. The majority of changes occurred within the S glycoprotein. Between 2 and 6 changes were observed in the S1 amino acid sequence, 2 – 3 changes were observed in the S2 amino acid sequence and 0 – 3 changes were observed in the rest of the genome, excluding the replicase gene. The S glycoprotein alone is sufficient to induce good protective immunity; however differences of just a few amino acids have a detrimental impact on cross-protection. It is thought, however, that it is the replicase that confers pathogenicity rather than the structural or accessory genes in IBV (Armesto *et al.,* 2009).

Each batch of attenuated virus is different and efficacy *in vivo* will not be identical. Virus growth on embryonated eggs is expensive and cumbersome, each egg only producing a small volume of allantoic fluid from which the virus is isolated. The supply of embryonated eggs is not guaranteed to be reliable, which may affect production of large quantities of vaccine. As demand for seasonal and pandemic influenza vaccines rises, the supply of embryonated eggs for the production of other vaccines may be reduced.

Another concern about the use of embryonated eggs is the possible presence of adventitious viruses, which may compromise the vaccine stocks or cause pathology in the vaccinated chickens. One such adventitious virus of chicken eggs is the retrovirus, avian leukosis virus (ALV; Harris *et al.,* 1966). Retroviruses are able to insert their genome into the host cell genome and some can induce oncogenic transformation (reviewed by Maeda *et al.,* 2008). Integration of the ALV genome

into the host cell genome can incorporate host genes into the viral genome, forming several related oncogenic viruses, including Rous sarcoma virus (RSV).

In light of the numerous disadvantages of egg-based vaccine production, the ability to produce live vaccines on a cell line would be beneficial to the vaccine industry as well as the poultry industry. Vaccine production on cell lines is faster and more efficient than on eggs and large volumes of vaccine can be produced using cell lines. Vero cells were isolated in 1962 from kidney epithelial cells extracted from an African green monkey (*Cercopithecus aethiops*). They have already been validated for virus growth and diagnostic purposes and are licensed for use in human vaccine manufacture. Vero cells are currently used in the production of polio and rabies vaccines (Frazatti-Gallina *et al.,* 2004; Montagnon *et al.,* 1981) and several influenza virus vaccines have been developed for growth on Vero cells (Govorkova *et al.,* 1995; Kistner *et al.,* 1998). Vero cells have been extensively tested for tumorigenic properties, can be grown in suspension or flat bed and it is possible to achieve consistent virus yields.

Aims

Infectious bronchitis remains a major problem in the poultry industry, despite the existence of many different vaccines. The advent of a reverse genetics system for IBV (Britton *et al.,* 2005; Casais *et al.,* 2001) will allow the rational design of more effective vaccines, however, these must still currently be grown on embryonated eggs, a cumbersome and expensive system.

The IBV S glycoprotein has two roles during the course of infection. The first is to attach to the host cells via host cell receptors and the second is to fuse the virus envelope with the host cell membrane, releasing the viral genome into the host cell cytoplasm. The S glycoprotein is also involved in fusion of infected cells to form syncytia. These steps are critical to the initiation of infection. The aim of this thesis is to identify the amino acids involved in each of these steps, thus explaining the cellular tropism of IBV at a molecular level and enabling the rational design of IBV vaccines that may be grown on Vero cells. In order to carry out these aims, two objectives were investigated:

Objective 1

To establish which subunit or domain of the S glycoprotein from the rIBV Beau-R strain is responsible for its ability to grow in Vero cells, an African green monkey kidney cell line.

Objective 2

To identify which amino acids on the S glycoprotein are involved in cell-cell fusion by cell culture adaptation of rIBV Beau-R for syncytia formation on Vero cells.

Chapter 2: Materials and Methods

Animal cell culture and virus stocks

All primary cells and continuous cell lines were prepared by the Institute for Animal Health media and tissue culture department:

Chick kidney (CK) cells are primary cells prepared by the trypsinisation of kidneys from two- to three-week-old, specific pathogen free (SPF), Rhode Island Red chicks.

Vero cells are a continuous cell line originating from African green monkey epithelial and fibroblast kidney cells.

BHK-21 cells are a continuous cell-line originating from baby hamster kidney fibroblasts.

Viruses

Beau-R is a molecular clone of Beaudette-CK (Beau-CK), a CK cell-adapted Beaudette virus derived by multiple passages in embryonated chicken eggs and CK cells. There are two nucleotide substitutions in Beau-R when compared to Beau-CK, C19666 → U and A27087 → G in the ORF 1b and N genes respectively. Beau-R is apathogenic in adult birds and has an extended host range in cell culture. Like Beau-CK, Beau-R is able to grow on Vero and BHK-21 cells in addition to the ability to grow on primary chicken cells such as CK cells, but does not form syncytia.

M41-CK is a pathogenic strain of IBV that has been passaged in CK cells. This strain is only able to grow in primary chicken cells, not Vero cells.

BeauR-M41(S) has the genetic background of Beau-R but the S gene from M41.

Like M41-CK, this strain is also unable to grow in Vero cells and can only grow in primary chicken cells.

Beau-US was adapted from Beau-CK and like Beau-CK, also has an extended host range in cell culture, growing in Vero and BHK-21 cells as well as primary chicken cells. Unlike Beau-R, Beau-US forms syncytia in cell culture.

Cell culture medium

Table 2.1. BES medium (1x) for cell culture of IBV on CK or Vero cells. Sterile water was added to a final volume of 100 ml.

Ingredient	**Volume**	**Final concentration**
10x Eagles's MEM (Sigma)	10 ml	1x
TPB	10 ml	10%
Bovine serum albumen (BSA) fraction V (10% w/v filter sterilised; Sigma)	2 ml	1%
N,N-bis[2-hydroxethyl]-2-Aminoethanesulfonic acid (BES, 1 M filter sterilised; Sigma)	2 ml	20 mM
Sodium bicarbonate (7.5%)	2.8 ml	0.2%
L-glutamine (100x; Gibco)	1 ml	2 mM
Nystatin (100,000 U/ml; Sigma)	0.25 ml	250,000 U/l
Penicillin and streptomycin (100,000 U/ml; Sigma)	0.1 ml	100,000 U/l each

Table 2.2. BES medium (2x) for plaque assay of IBV on CK or Vero cells. Sterile water was added to a final volume of 100 ml.

Ingredient	Volume	Final concentration
10x Eagles's MEM (Sigma)	20 ml	2x
TPB	20 ml	20%
BSA fraction V (10% w/v filter sterilised; Sigma)	4 ml	2%
BES (1 M filter sterilised Sigma)	4 ml	40 mM
Sodium bicarbonate (7.5%)	5.6 ml	0.4%
L-glutamine (100x; Gibco)	2 ml	4 mM
Nystatin (100,000 U/ml; Sigma)	0.5 ml	500,000 U/l
Penicillin and streptomycin (100,000 U/ml; Sigma)	0.2 ml	200000U/l each

Table 2.3. Eagle's MEM (1x) for cell culture of VV on Vero cells. Sterile water was added to a final volume of 100 ml.

Ingredient	Volume	Final concentration
10x Eagles's MEM (Sigma)	10 ml	1 x
Foetal Calf Serum (FCS, Sigma)	5 ml	5 %
Sodium bicarbonate (7.5%)	2.3 ml	0.175 %
L-glutamine (100x; Gibco)	1 ml	1 x
Nystatin (100,000 U/ml; Sigma)	0.25 ml	250,000 U/l
Penicillin and streptomycin (100,000 U/ml; Sigma)	0.1 ml	100,000 U/l each

Table 2.4. Eagle's MEM (2x) for plaque assay of VV on Vero cells. Sterile water was added to a final volume of 100 ml.

Ingredient	Volume	Final concentration
10x Eagles's MEM (Sigma)	20 ml	2 x
FCS (Sigma)	10 ml	10 %
Sodium bicarbonate (7.5%)	4.6 ml	0.35 %
L-glutamine (100x; Gibco)	2 ml	2 x
Nystatin (100,000 U/ml; Sigma)	0.5 ml	500,000 U/l
Penicillin and streptomycin (100,000 U/ml; Sigma)	0.2 ml	200,000 U/l each

Table 2.5. Glasgow MEM (1x) for cell culture of IBV or VV on BHK-21 cells.

Ingredient	Volume	Final concentration
G-MEM	360 ml	1x
FCS (Sigma)	4 ml	1 %
TPB	40 ml	0.29 %
Nystatin (100,000 U/ml; Sigma)	2 ml	0.5 %
Penicillin and streptomycin (100,000 U/ml; Sigma)	0.4 ml	0.1 %

Cells were washed with phosphate buffered saline a (PBSa) prepared by IAH media services. PBSa Powder (119.4 g, BioWhittaker) was added to 10 litres SuperQ water and adjusted to pH 7.2 with 1M hydrochloric acid. Solutions were autoclaved at 115°C for 20 minutes.

Bacterial cultures

SOC medium was used for culturing *Escherichia coli* (*E. coli*) following transformation with each plasmid.

Table 2.6. SOC medium for transformation of *E. coli*. Medium was prepared by IAH media services and autoclaved at 115°C for 20 minutes.

Ingredients	Quantity	Final concentration
SOB powder (Q-BIOgene)	31 g	1x
1 M Glucose (Fisher)	20 ml	20 mM
Water	1 L	

Luria-Bertani (LB) broth was used for culturing *E. coli.* Broth was prepared by IAH media services by addition of LB Broth Base (Miller) to 1 L water then autoclaving at 115^{o}C for 15 minutes. Ampicillin (Sigma-Aldrich) was added to the broth to a final concentration of 100 μg/ml to culture *E. coli* transformed with plasmids encoding β-lactamase for ampicillin resistance. LB-agar plates were prepared with LB-broth containing 1.5 % Bacto agar plus 100 μg/ml ampicillin.

DNA-based methods

Small-scale plasmid DNA purification

Escherichia coli, transformed with the required plasmid, was grown overnight in 5 ml of LB broth containing ampicillin (100 μg/ml). The Qiaprep Spin Miniprep Kit (Qiagen) was used for the DNA purification following the manufacturer's protocol. Bacterial cells were lysed under alkaline conditions then plasmid DNA was adsorbed

onto silica-gel columns in the presence of high salt, which was subsequently removed with wash buffer. DNA was eluted with nuclease-free water (Sigma).

Large-scale plasmid DNA purification

Escherichia coli, transformed with the required plasmid, was grown overnight in 200 ml of LB broth containing ampicillin (100 μg/ml). Cultures were centrifuged at 2,000g for 25 minutes to pellet the bacteria. DNA was isolated and purified using the Qiafilter plasmid maxi kit (Qiagen) according to manufacturer's instructions. DNA was bound to DEAE contained on a silica-based resin. Contaminants were removed with increased salt concentration; DNA was concentrated and salt removed by isopropanol precipitation. DNA was eluted into water.

PCR amplification of DNA fragments

Polymerase chain reaction (PCR) was used to amplify specific IBV cDNA or VV DNA sequences.

Table 2.7. PCR recipe

Ingredients	Volume	Final concentration
10 x Taq DNA polymerase buffer	5 μl	1 x
50 mM $MgCl_2$	2 μl	2 mM
10 mM dNTP mix	1 μl	0.2 mM
10 pmol forward oligonucleotide	1 μl	0.2 pmol
10 pmol reverse oligonucleotide	1 μl	0.2 pmol
template DNA	2 μl	
nuclease-free water (sigma)	37.5 μl	
Taq polymerase	0.5 μl	

PCRs were performed using a Px2 thermal cycler with hotlid (Thermo Electron Corporation) with the following cycles:

95°C	2 minutes	
95°C	30 seconds	30 cycles
X°C	30 seconds*	
72°C	1 minute per kb of DNA to be amplified	
72°C	5 minutes	

*Annealing temperature was dependent upon the melting temperature of the primers.

Agarose gel electrophoresis

DNA was separated and visualised by agarose gel electrophoresis in 0.8 – 1.2 % agarose and 1 x Tris borate EDTA (TBE) buffer (Invitrogen) with 0.1 µg ethidium bromide per ml of agarose gel. Gels were run using a Galileo bioscience 9 x 11 cm horizontal submarine gel apparatus in 1 x TBE buffer at ~5 V/cm gel length. DNA was visualised by exposure of the gel to 260 nm UV light. A 1 µg 1kb+ DNA ladder (Invitrogen) was used to establish DNA band sizes.

Table 2.8. DNA loading buffer recipe

Ingredient	Amount
Glycerol (BDH)	2 ml
Ficoll 400 (Sigma)	50 mg
Bromphenol blue (Sigma)	25 mg
Water	3 ml

Purification of DNA from PCR

Prior to sequencing or ligation of the PCR products into the pGPT vectors, DNA was purified using the QIAquick PCR purification kit (Qiagen) according to manufacturer's instructions. DNA adsorbs to the QIAquick silica membrane in the

presence of high salt concentration, is washed by an ethanol-containing buffer during centrifugation and eluted into water.

DNA restriction enzyme digestion

Restriction enzyme digestions were performed at 37°C according to manufacturer's protocol.

DNA dephosphorylation for cloning

Plasmid DNA was dephosphorylated using shrimp alkaline phosphatase (Promega) after restriction enzyme digestion to prevent self-ligation according to the manufacturer's instructions.

DNA ligation

The quantities of vector DNA and PCR product were determined using a NanoDrop 1000. A 3:1 ratio of insert to vector was used. Assuming vector and insert DNA solutions are of equimolar concentration:

T4 DNA ligase (Invitrogen)	1 μl
10x DNA ligase buffer (Invitrogen)	3 μl
Vector DNA	1 μl
PCR DNA	3 μl
Nuclease-free water	22 μl

Transformation of *E. coli* and plasmid screening

One Shot® MAX Efficiency™ DH5α-T1R *E. coli* were transformed with the ligation mixture according to manufacturer's instructions. Transformed *E. coli* were plated out on LB-agar plates containing ampicillin (100 μg/ml) and incubated overnight at 37^{o}C. Individual *E. coli* colonies were picked and cultured in 5 ml LB

broth containing ampicillin (100 μg/ml) overnight at 37°C then DNA was extracted and sequenced to check the insert was correct.

RNA-based methods

Purification of RNA from cells

Cellular and viral RNA was purified from cell culture supernatant using an RNeasy mini kit (Qiagen) according to the manufacturer's protocol. Guanidine isothiocyanate lysis buffer was used to lyse cells. RNA was bound to the column in the presence of ethanol then washed and eluted with RNase-free water.

Reverse transcription

IBV cDNA was generated from isolated cellular RNA and specific regions were amplified by PCR.

1 μl	10 mM dNTPs	
1 μl	10 pmol random primer	65°C, 5 minutes
6 μl	sterile H_2O (Sigma)	ice
5 μl	RNA	
	+	
4 μl	First strand buffer	
1 μl	DTT	25°C, 10 minutes
1 μl	RNase Out (Invitrogen)	50°C, 1 hour
1 μl	Superscript III (Invitrogen)	70°C, 15 minutes

One-step RT-PCR

In order to detect IBV in cell culture supernatant, isolated RNA was analysed for the presence of IBV RNA by one-step reverse transcription-PCR (RT-PCR) using Ready-to-Go RT-PCR beads from GE Healthcare, manufacturer's protocol followed. Each bead contains M-MuLV Reverse Transcriptase, RNase Inhibitor, buffer, nucleotides and *Taq* DNA polymerase. The primers used were BG-69 (GCTTTTGCCACTATTATCTTC) and BG-142 (AGGGATCAAATACTTCTGTG) located across the 3' end of the S gene. The PCR product spanned nucleotides 23666 – 24137, and was 471bp in length.

Table 2.9. RT-PCR recipe. Reagents were added to the RT-PCR bead on ice.

Ingredients	**Volume**	**Final concentration**
0.5 µg/µl pd$(N)_6$ random cDNA primer	2 µl	0.02 µg/µl
10 pmol forward oligonucleotide	1 µl	0.2 pmol
10 pmol reverse oligonucleotide	1 µl	0.2 pmol
template RNA	5 µl	
nuclease-free water (Sigma)	41 µl	

RT-PCRs were performed using a Px2 thermal cycler with hotlid (Thermo Electron Corporation) with the following cycles:

42°C 30 minutes
95°C 5 minutes
95°C 1 minute
X°C 1 minute*
72°C 1 minute per kb of DNA to be amplified
} 35 cycles
72°C 5 minutes
4°C hold

*Annealing temperature was dependent upon the melting temperature of the primers.

Reverse genetics system

Plasmids containing the chimaeric S gene, either whole or just the part being altered, and the xanthine-guanine phosphoribosyltransferase (gpt) gene from *E. coli* were constructed. The plasmids were used to insert the chimaeric S gene into a recombinant vaccinia virus (rVV) containing either the entire full-length IBV cDNA genome or the full-length IBV cDNA genome minus the S gene. Vaccinia virus was used as a vector for the IBV cDNA because it has the capacity to accept a large amount of foreign DNA into its genome without loss of stability (Thiel and Siddell, 2005).

The gpt gene from *E. coli* is used in the selection of recombinant viruses with the correct insert as it confers resistance to mycophenolic acid (MPA) in the presence of xanthine and hypoxanthine under the control of the vaccinia virus P7.5 promoter. MPA inhibits purine metabolism, preventing the formation of rVV plaques. This is overcome by incorporating the gpt gene into the rVV genome and the addition of xanthine and hypoxanthine to cell culture medium (Figure 2.1).

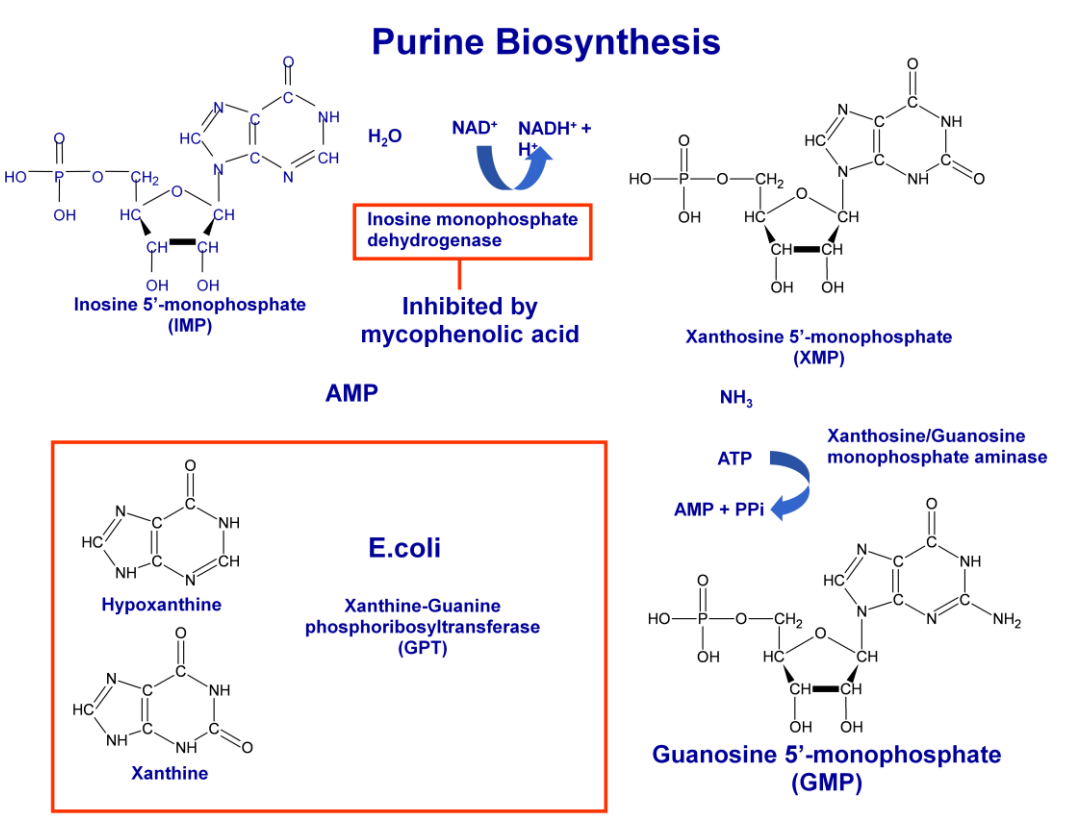

Figure 2.1. Diagram of purine biosynthesis in a eukaryotic cell. MPA inhibits inosine monophosphate dehydrogenase, thereby preventing the formation of xanthosine 5'-monophosphate (XMP) and ultimately preventing the synthesis of guanosine 5'-triphosphate (GTP) via guanosine 5'-monophosphate (GMP). This results in intracellular depletion of purine nucleotides and inhibition of cell growth (Mulligan and Berg, 1981). The gpt gene is able to synthesise GMP from hypoxanthine and xanthine. Recombinant VV expressing gpt can grow in presence of MPA, xanthine and hypoxanthine, however those lacking gpt cannot.

MXH solutions

MPA (mycophenolic acid): 10 mg/ml in 0.1N NaOH (30 mM); 400X concentrated.

Xanthine: 10 mg/ml in 0.1N NaOH (66 mM); 40x concentrated.

Hypoxanthine: 10 mg/ml in 0.1N NaOH (73 mM); 667x concentrated.

Table 2.10. MXH (gpt selection) medium for TDS.

Ingredient	Volume	Final concentration
2x E-MEM	50 ml	1x
2 % agar	50 ml	1 %
30 mM MPA	250 µl	75 µM
66 mM Xanthine	2.5 ml	165 µM
73 mM Hypoxanthine	149 µl	184 µM

Generation of rVV by homologous recombination

A general outline of the generation of rVVs containing IBV cDNA with chimaeric S genes is as follows (Figure 2.2). Plasmids containing the chimaeric S genes were transfected into vaccinia virus infected-Vero cells using lipofectin from Invitrogen and gpt selection components were added to select for vaccinia viruses that have integrated the whole plasmid DNA into their genome. Homologous recombination between the plasmids and the rVV genome inserted the chimaeric S gene into the rest of the IBV cDNA. The gpt gene was also inserted.

Vero cells were grown in six-well plates to approximately 70% confluency and infected with recombinant vaccinia virus at an moi of 0.2. Cells were incubated at 37°C in a CO_2 incubator for 2 hours to allow the virus to adsorb to the cells. The inoculum was removed and cells were washed with OPTIMEM 1 with GLUTAMAX-1 (GIBCO). Each well was then transfected with 5 µg of the plasmid containing the gpt gene and the chimaeric S gene with 12 µl of Lipofectin (Invitrogen) in 3 ml OPTIMEM. Cells were incubated for 60 – 90 minutes at 37°C then the transfection medium was replaced with 5ml of fresh cell culture medium. MXH components, 12.5 µl of MPA, 125 µl of Xanthine and 7.4 µl of Hypoxanthine, were added to each well after overnight incubation at 37°C and cells were further

incubated at 37°C until extensive VV cpe was observed. Cells were scraped into the supernatant and pelleted by centrifugation at 13k rpm for 2 minutes. Cell pellet was resuspended in 400 µl cell culture medium and stored at -80°C.

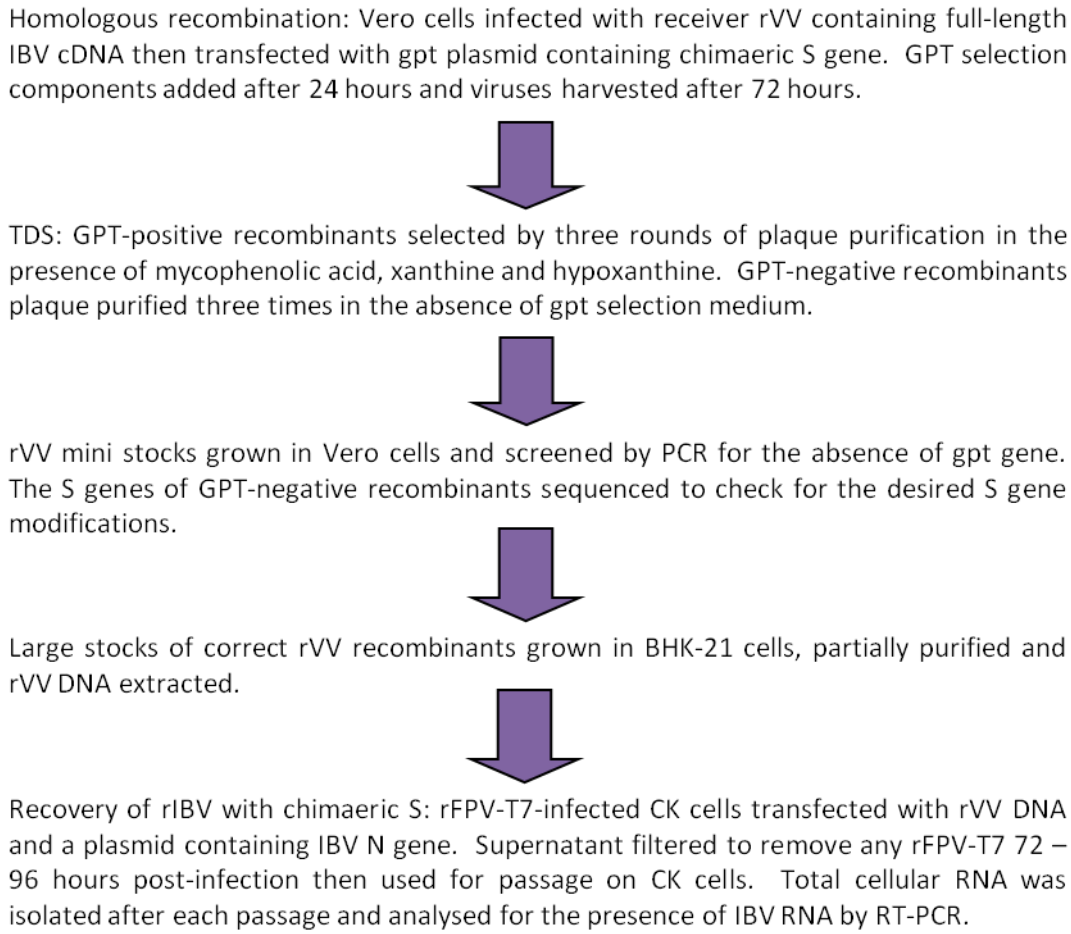

Figure 2.2. Flow chart of recombinant virus isolation protocol. Homologous recombination between plasmids containing the modified S gene sequence and the rVV genome inserts the chimaeric S gene into the rest of the IBV cDNA along with the gpt gene. Gpt-positive recombinants are selected by plaque purification in the presence of MXH components then gpt-negative recombinants are selected by plaque purification in the absence of MXH components. Recombinants are screened by PCR and sequencing then large stocks grown in BHK-21 cells, partially purified and rVV DNA extracted. Recombinant IBVs are recovered in CK cells using rFPV-T7 and a plasmid containing the IBV N gene.

Transient dominant selection (TDS)

TDS was used to generate rVVs which have integrated the plasmid DNA containing the chimaeric S gene (Figure 2.3; Britton *et al.,* 2005). The TDS involved integration of modified sequences and a dominant selectable marker, the *E. coli* gpt gene under the expression of a VV promoter, into defined sequences by homologous recombination. Recombinant VV with a gpt+ phenotype were selected using MPA during three rounds of plaque purification. Integration resulted in unstable tandem repeat sequences that were only maintained by presence of MPA in cell culture media.

Three rounds of plaque purification were then carried out in the absence of gpt selection components to select rVVs that have recombined to lose the plasmid DNA but kept the chimaeric S gene. The gpt+ rVV were intrinsically unstable due to the presence of direct repeat sequences and were subject to two potential double crossover recombination events. One event resulted in the generation of the original IBV sequence and the second in the generation of IBV with chimaeric S gene. The gpt gene is spontaneously lost in the absence of selection medium. Both events should occur with the same frequency, resulting in 50% of the gpt- rVVs containing the chimaeric S gene. Selective pressure was exerted on the IBV cDNA to recombine to form the full-length genome containing the chimaeric S gene sequences by removing MPA.

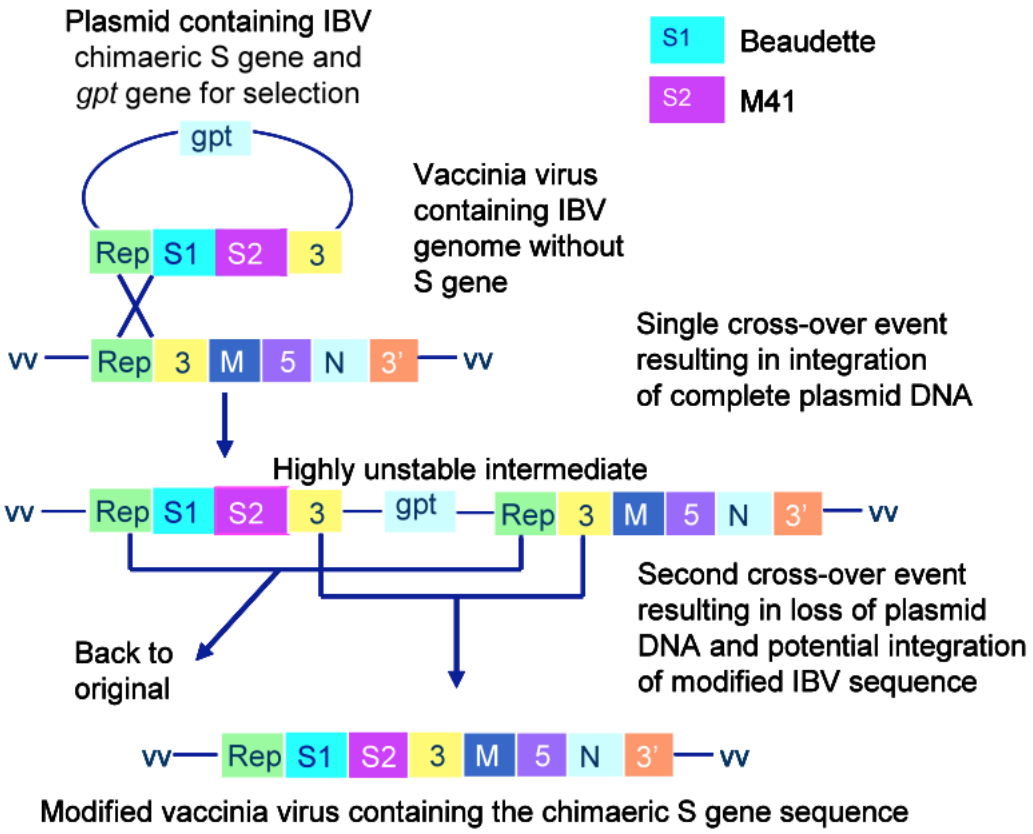

Figure 2.3. The transient dominant selection system. A plasmid vector containing gpt is constructed from the altered S gene and parts of the neighbouring genes in the IBV genome. The plasmid is transfected into Vero cells infected with rVV containing the IBV genome minus the S gene. A single cross-over event results in the integration of the complete plasmid DNA and a highly unstable intermediate is produced due to the presence of repeat sequences. A second cross-over event results in the loss of the plasmid DNA and the integration of the modified IBV cDNA into the vaccinia virus genome. Three rounds of plaque purification in the presence of gpt selection components and three rounds in absence are carried out to select for rVV containing the altered S gene. Large virus stocks are prepared in BHK-21 cells from which virus is purified and DNA extracted.

Virus stocks from the homologous recombination steps were freeze-thawed three times and sonicated for 2 minutes. Virus dilutions were prepared 10^{-1} – 10^{-3} in cell culture medium. Confluent Vero cells in six-well plates were washed with PBS then inoculated in duplicate with 500 µl of each virus dilution per well. Cells were incubated for 1 – 2 hours at 37°C. The inoculum was replaced with 3 ml cell culture medium overlay containing 1x MXH gpt selection medium and 1 % agar and further incubated for 4 days at 37°C. Cells were stained with 0.01 % neutral red in 2 ml cell culture medium containing 1 % agar. Approximately six well-isolated plaques were picked for each recombinant into 400 µl of cell culture media.

Three plaque purifications were carried out in the presence of selection medium, taking 2 – 3 plaques forward from each recombinant at each stage. Then three rounds of plaque purification were carried out in the absence of selection medium. The 10^{-1} virus dilution was grown in the presence of selection media and the 10^{-2} and 10^{-3} dilutions were grown in the absence. When no plaques form in the positive-selection wells, it means that the rVV has lost the gpt gene.

Growth of small rVV stocks

After the third round of plaque purification in absence of gpt selection components, mini stocks of rVV were grown in Vero cells. Confluent Vero cells in six-well plates were inoculated with 150 µl rVV plaque (freeze-thawed 3 times and sonicated for 2 minutes) and 350 µl cell culture medium per well. Cells were incubated at 37°C for 1 hour then cell culture medium was topped up to 3 ml. Cells were incubated at 37°C until rVV cytopathic effect (cpe) reached 70 – 80 %. Cells were scraped into the supernatant and centrifuged for 1 minute at 13K rpm. The supernatant was

discarded and the cell pellet was resuspended in 500 µl of cell culture medium. Virus stocks were stored at -20°C.

Small-scale DNA extraction

DNA was extracted from rVV mini-stocks to ascertain whether the viruses still contained the gpt gene using the QIAamp DNA mini kit from Qiagen, manufacturer's protocol followed. The cells were scraped into the supernatant, centrifuged at 13k rpm for 3 minutes then the pellets were resuspended in cell culture medium. The cell pellets were lysed using proteinase K then the DNA was adsorbed onto the QIAamp silica membrane during centrifugation. Bound DNA was washed in buffers containing guanidine hydrochloride during subsequent centrifugation steps then eluted in water. Further PCRs were carried out on the gpt negative viruses across the S gene and sequenced to check that the desired mutations were present.

Growth of large rVV stocks

Large stocks of rVV were grown in BHK-21 cells. Vaccinia virus has a wide host range in cell culture but grows particularly well in BHK-21 cells so a large amount of viral DNA can be extracted in this way. Ten T150 flasks of confluent BHK-21 cells were each inoculated with 2 ml rVV mini-stock at an moi of 0.1 – 1. Cells were incubated for 1 hour at 37°C then 20 ml of cell culture medium was added to each flask. Cells were further incubated until all cells showed cpe, then the flasks were smacked to detach the cells from the plastic. The cells and supernatant were transferred to 50 ml Falcon tubes and pelleted by centrifugation for 15 minutes at 1200 rpm in a refrigerated centrifuge (4°C) using sealed buckets. The supernatant was discarded and the cell pellets were resuspended in 2 ml of 10mM Tris/HCl pH

9.0, 1 mM EDTA (TE; pH 9) per falcon and mixed well. Resuspended cell pellets were pooled and stored at -80°C until virus purification was carried out.

Vaccinia virus purification

Large stocks of rVV were partially purified through a 30% (w/v) sucrose cushion prior to DNA extraction. Cells were lysed by freeze-thaw three times (dry ice/37°C) and sonication for 2 minutes (cup form sonicator; continuous pulse at 70% duty cycle). Cells were immediately placed on ice then centrifuged for 10 minutes at 2.5k rpm at 4°C to remove the nuclei. The supernatant was made up to 13 ml with TE pH 9 buffer then layered on 16 ml 30% sucrose (1 mM tris/HCl pH 9.0, filtered) in a Beckman ultra-clear (25 x 89mm) ultracentrifuge tube and centrifuged using a Superspin 630 rotor in a Sorvall OTD65B ultracentrifuge at 14k rpm for 60 minutes at 4°C. All of the sucrose solution was removed and the pellet was resuspended in 5 ml of 10 mM TE buffer pH 9 and stored at -80°C.

Large-scale DNA extraction

Stock Proteinase K solution (100X) was prepared in water to a concentration of 20 mg/ml. The final concentration of Proteinase K in the reaction was 0.2 mg/ml.

Table 2.11. Proteinase K digestion buffer (x2)

Ingredient	Volume	Final concentration
NaCl 5 M	16 ml	200 mM
Tris/HCl pH 7.5 1 M	40 ml	10 mM
EDTA 0.5 M	4 ml	0.4%
SDS 10%	8 ml	400 mM
H_2O	132 ml	

Recombinant vaccinia virus DNA was extracted by phenol-chloroform. An equal volume of pre-warmed (50°C) 2x proteinase K buffer and 200 µl 20 mg/ml solution of proteinase K was added to the partially purified virus in a 50 ml Falcon tube and incubated for 2.5 hours at 50°C. The vaccinia virus DNA solution was divided into two equal volumes in 15 ml Falcon tubes. An equal volume of phenol-chloroform containing 8-hydroxy-quinoline was added to each tube and mixed carefully by inversion 5 – 10 times. Samples were centrifuged at 2.5k rpm for 15 minutes in a refrigerated (4°C) centrifuge. The upper phase was removed, without disturbing the interphase, to a clean 15 ml Falcon tube. A second phenol-chloroform extraction was carried out followed by one chloroform extraction. DNA was precipitated by the addition of 0.1 volumes of 3 M sodium acetate and 2.5 volumes of -20°C absolute ethanol to each tube. Tubes were centrifuged at 3.5k rpm for 45 minutes. The supernatant was discarded then 10 ml of -20°C 70% ethanol was added to the DNA pellets, left on ice for 5 minutes for the ethanol to dissolve any salts and centrifuged at 3.5k rpm for 30 minutes. The ethanol was removed and the tubes were placed at an angle in a fume cupboard for 20 – 30 minutes to allow any remaining ethanol to evaporate off. Pellets were resuspended in 100 µl of water (Sigma) and left to re-dissolve overnight at 4°C then quantified using a NanoDrop 1000 (Thermo Scientific).

Pulsed field gel electrophoresis (PFGE)

Extracted vaccinia virus DNA, 1 µg, was digested with Sal1 in a 20 µl reaction volume, to check the amount and quality of the DNA. A SalI restriction site is located either side of the rIBV cDNA, digestion results in an unique 28kb SalI restriction fragment in which the IBV genomic full-length cDNA is present (Figure

2.4). A 0.8 % Bio-Rad pulsed field certified ultra pure DNA grade agarose gel was prepared with 0.5x TBE buffer (GIBCO). Digested DNA was run with Bio-Rad CHEF DNA size standard ladder, 8 – 48 kb, to check that the rIBV cDNA was intact. This is shown by a band of ~34 kb (Figure 2.5). Gel was run on CHEF-DR II PFGE apparatus (Bio-Rad). Initial pulse time was set at 0.1 second and final pulse time was set at 1.0 second. The gel was run for 12 hours at 6.0 V/cm then stained with ethidium bromide.

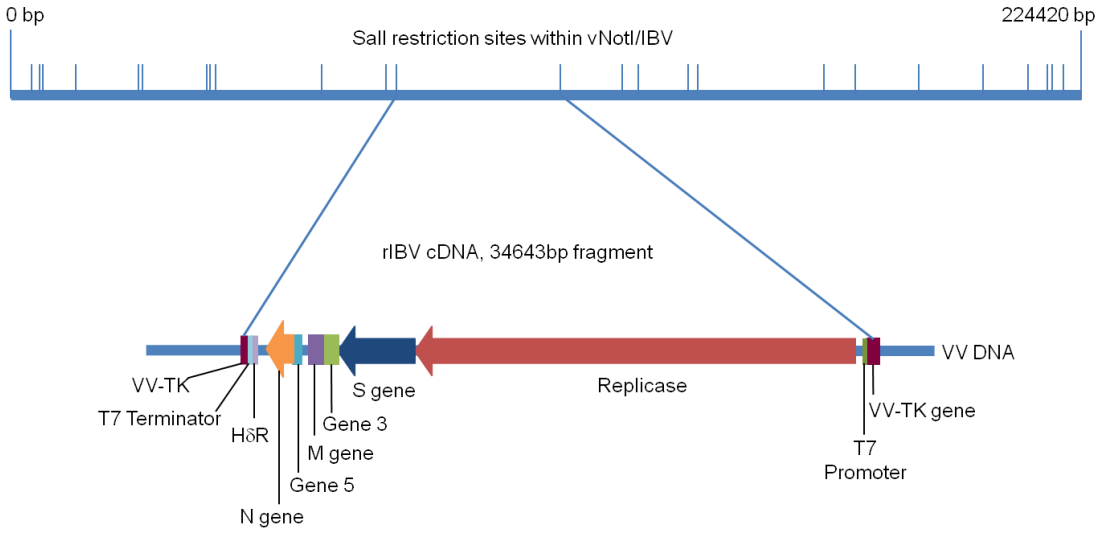

Figure 2.4. Restriction map of vaccinia virus DNA digested with SalI. There are 26 SalI restriction sites within the vNotI/IBV genome producing fragments between 213 – 34643 bp, the largest of which contains the complete rIBV cDNA inserted within the vaccinia virus thymidine kinase (TK) gene.

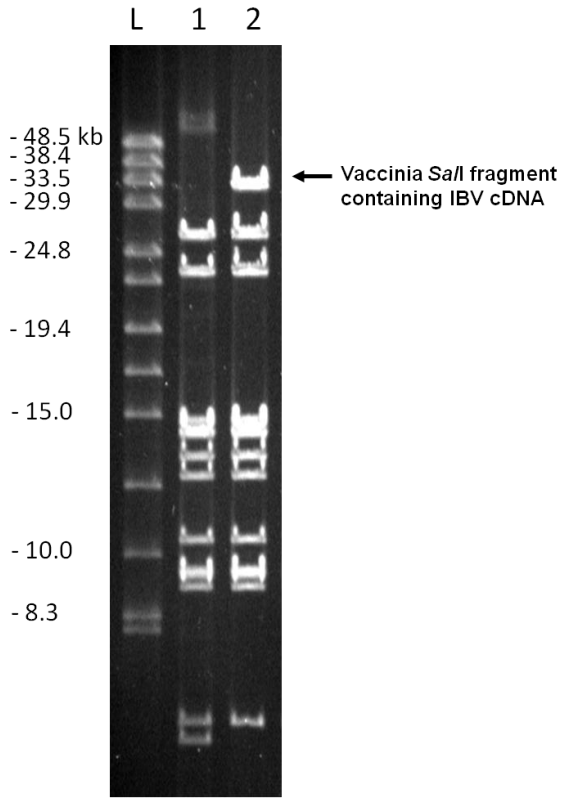

Figure 2.5. Agarose pulsed field gel analysis of extracted vaccinia virus DNA. DNA was extracted from large stocks of (1) vNotI/tk and (2) vNotI/IBV, vaccinia virus containing Beau-R cDNA, then digested with SalI and run on an agarose pulsed field gel overnight. The band at around 34 kb shows the intact whole rIBV cDNA. DNA ladder is indicated by L. Gel was stained with ethidium bromide.

Rescue of recombinant IBV

Following the isolation of a recombinant vaccinia virus containing the complete cDNA of the IBV genome including the correct S gene, the infectious rIBV was recovered from the rVV DNA. Recombinant fowlpox virus (rFPV-T7) was used for the production of T7 RNA polymerase to generate infectious IBV RNA from the rVV DNA. A plasmid containing the IBV N protein, pCi-Nuc, was used to aid the recovery of rIBVs (Figure 2.6).

CK cells at 30 – 40 % confluency in six-well plates were infected with rFPV-T7 at an moi of 10 and incubated for 1 hour at 37°C. The inoculum was removed and each well of CK cells was then transfected with 10 µg rVV DNA, 5 µg of pCi-Nuc, a plasmid containing the IBV nucleocapsid protein directed by CMV/T7 promoters, and 30 µl lipofectin (Invitrogen) in 3 ml OPTIMEM 1 with GLUTAMAX-1 (GIBCO). Cells were incubated at 37°C overnight then the transfection media was replaced with fresh cell culture media. Once cpe was observed, cell culture medium was filtered through 0.22 microns to remove any rFPV-T7. This was either used directly for passage on CK cells (see below) or stored at -80°C until use.

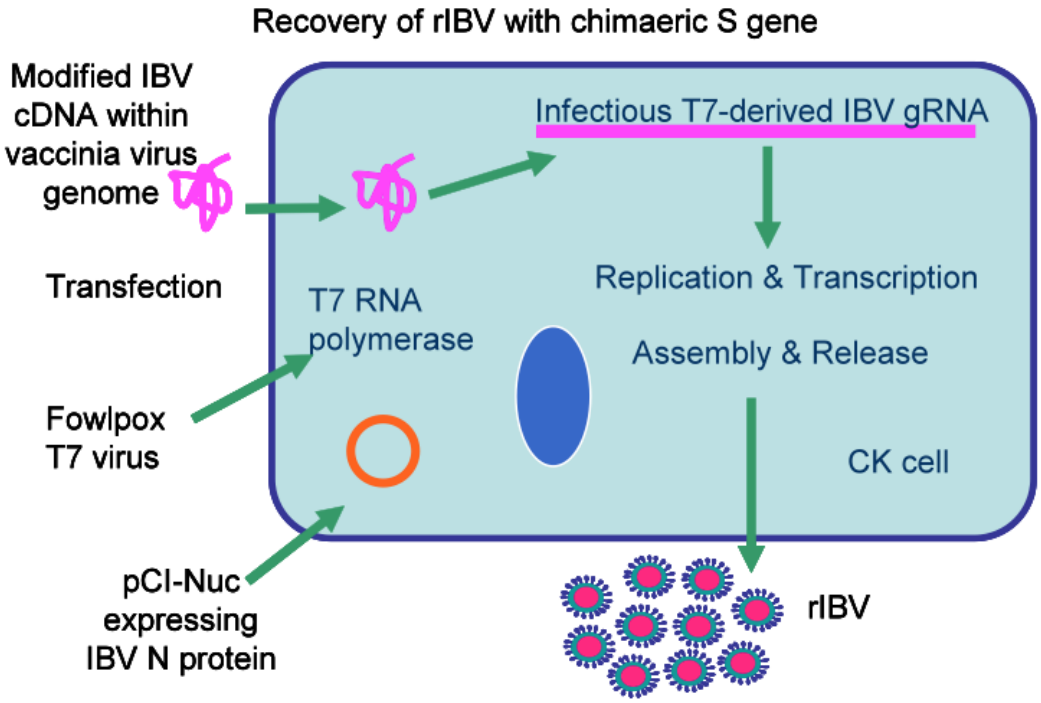

Figure 2.6. Recovery of rIBVs. CK cells were infected with recombinant fowlpox virus, rFPV-T7, then transfected with rIBV cDNA within the rVV genome and a plasmid expressing the IBV N protein, pCi-Nuc. Recombinant IBVs were released into the cell culture supernatant, which was then filtered and used for passage on CK cells.

Passage of rescued rIBV on CK cells

CK cells were grown to confluency in T25 flasks then washed with PBS. Cells were inoculated with 1 ml of the filtered medium and incubated at 37°C for 1 hour. The medium was topped up to 5 ml with fresh cell culture medium. Cells were incubated until cpe was observed or for up to 72 hours, whichever came sooner, then supernatant was harvested and stored at -80°C until the next passage. After two passages on CK cells, one replicate was chosen from each rIBV isolate and a large stock was grown in CK cells. This comprised the third passage (P_3) in CK cells.

The P_3 viruses were then used for three passages on confluent Vero cells, a continuous cell line originating from African green monkey epithelial and fibroblast kidney cells, grown in six-well plates. Two wells were used per isolate for each passage. The cells were inoculated with 500 µl supernatant per well and topped up to 3 ml with cell culture medium after incubating at 37°C for one hour. The supernatants from both wells per isolate were pooled when harvested at 48 – 72 hours post-infection.

Bright-field microscopy

Photographs of Vero, CK and BHK-21 cells infected with rIBV were taken by bright-field microscopy using a Leica DM IRB inverted light microscope with a camera attached to a PC.

Titrations

Recombinant IBVs were titrated on CK cells and the number of plaque forming units per ml was calculated. Virus supernatant was serially diluted 1:10 in cell culture medium. Confluent CK cells in six-well plates were washed with PBS then inoculated with 500 µl diluted supernatant and incubated at 37°C for 1 hour.

Inoculum was replaced with 3 ml medium containing 1% agar and plates were incubated at 37°C for 48 – 72 hours. Living cells were stained with 0.01% neutral red and plaques counted several hours later.

Growth curves

Vero, CK and BHK-21 cells were grown to confluency in 6-well plates then three wells per virus per time point were inoculated with Beau-R, M41-CK, BeauR-M41(S), BeauR-M41(S1), BeauR-M41(S2), BeauR-S-M41-Hep and M41-S-BeauR-Hep at a multiplicity of infection of 0.1. Cells were incubated with the inoculum for 1 hour then the inoculum was replaced with cell culture medium. The supernatant from three wells per virus was harvested at each time point, 1, 12, 24, 48 and 72 hours post-infection. The samples from each time point were titrated separately on CK cells and the titres averaged.

Indirect immunofluorescence

Infection

CK, Vero or BHK-21 cells were grown on coverslips in 24-well plates. Cells at approximately 50% confluency were inoculated with 150 µl IBV per well and incubated for 1 hour at 37^{o}C then the cell culture medium was topped up to 500 µl.

Fixing, permeabilisation and blocking

Infected cells were fixed with 4% paraformaldehyde in PBS for 20 minutes then permeabilised with 0.5% Triton-X100 (PBS) for 10 minutes and blocked with 0.5% BSA (PBS) for 1 hour at RT or overnight at 4°C.

Antibodies

Primary antibodies used were rabbit anti-IBV polyclonal antibody, produced at IAH and thought to mainly label the IBV N protein, diluted 1:400. Mouse anti-dsRNA J2 IgG2a monoclonal antibody from English and Scientific Consulting Bt. recognizes dsRNA independent of the sequence and nucleotide composition, diluted 1:1000. Endoplasmic reticulum was labelled with mouse anti-PDI (protein disulphide isomerase) 1D3 monoclonal antibody from MBL International, diluted 1:400.

Secondary antibodies used were AlexaFluor goat anti-mouse 488, goat anti-mouse 568 and goat anti-rabbit 488, all diluted 1:200 (Invitrogen).

Immunolabelling

Primary antibodies were diluted in 0.5% BSA (PBS) to a final volume of 200 µl then added to fixed and permeabilised cells and incubated on an orbital shaker at room temperature (RT) for 1 hour. Cells were washed twice with PBS then three times with PBS on an orbital shaker for five minutes. Diluted secondary antibody (0.5% BSA (PBS), 200 µl) was added and cells were incubated on an orbital shaker at RT for 1 hour with the same wash procedure. The nuclei were stained with DAPI (Invitrogen) according to the manufacturer's recommendations. Cells on the cover slips were mounted onto glass slides using Vectashield mounting medium for Fluorescence (Vector Laboratories) and sealed with nail varnish. Immunolabelled cells were examined using a Leica TCS SP5 DM6000 confocal microscope with the Leica Microsystems LAS AF software.

Chapter 3: Investigation into the cellular tropism of the Beau-R strain of IBV determined by the S glycoprotein

Summary

The IBV Beaudette strain is able to replicate in both primary CK cells and Vero cells, whereas the IBV M41 strain is able to replicate in CK cells only. This is believed to be due to the S gene as BeauR-M41(S), a recombinant IBV with the S gene from M41 in the background of Beaudette, has the cellular tropism of M41, not Beaudette (Casais *et al.,* 2003). Two rIBVs with the genomic background of Beaudette and either the S1 or S2 subunit from M41 were generated using a vaccinia virus reverse genetics system and their growth characteristics and cellular tropism were investigated. The Beaudette S2 subunit of the S glycoprotein was found to be sufficient to confer the ability to grow on Vero cells.

Introduction

The IBV spike glycoprotein, a 180-kDa membrane glycoprotein, is found as a homo-trimeric structure in the virion membrane (Delmas and Laude, 1990) and is comprised of two subunits. The N-terminal S1 subunit is responsible for binding to host cell receptors (Koch *et al.,* 1990) and the C-terminal S2 subunit is responsible for cell-cell and virus-cell fusion (Luo and Weiss, 1998). The two S subunits are cleaved during biosynthesis by a furin-like protease in the Golgi apparatus (de Haan *et al.,* 2004) but remain non-covalently linked.

Beau-R is a molecular clone derived from the Beaudette-CK strain of IBV, which in turn was derived by multiple passage of the Beaudette isolate in embryonated eggs followed by passage on primary CK cells. Beau-R is an apathogenic virus in adult birds that exhibits an ability to grow in an extended host range in cell culture including the ability to grow on Vero cells, an African green monkey kidney cell line. M41 is a pathogenic strain of IBV, which only has the ability to grow on primary chicken cells such as CK cells and replicates well when inoculated into the allantoic cavity of developing chicken embryos. Unlike Beau-R, M41 does not have the ability to grow on Vero cells.

The S glycoproteins of the M41 and Beaudette strains share 96% amino acid identity (Figure 3.1) and it has been shown that it is the S glycoprotein only that confers tissue tropism as BeauR-M41(S), an rIBV containing the M41 S gene within a Beaudette background, was unable to grow in Vero cells (Casais *et al.*, 2003).

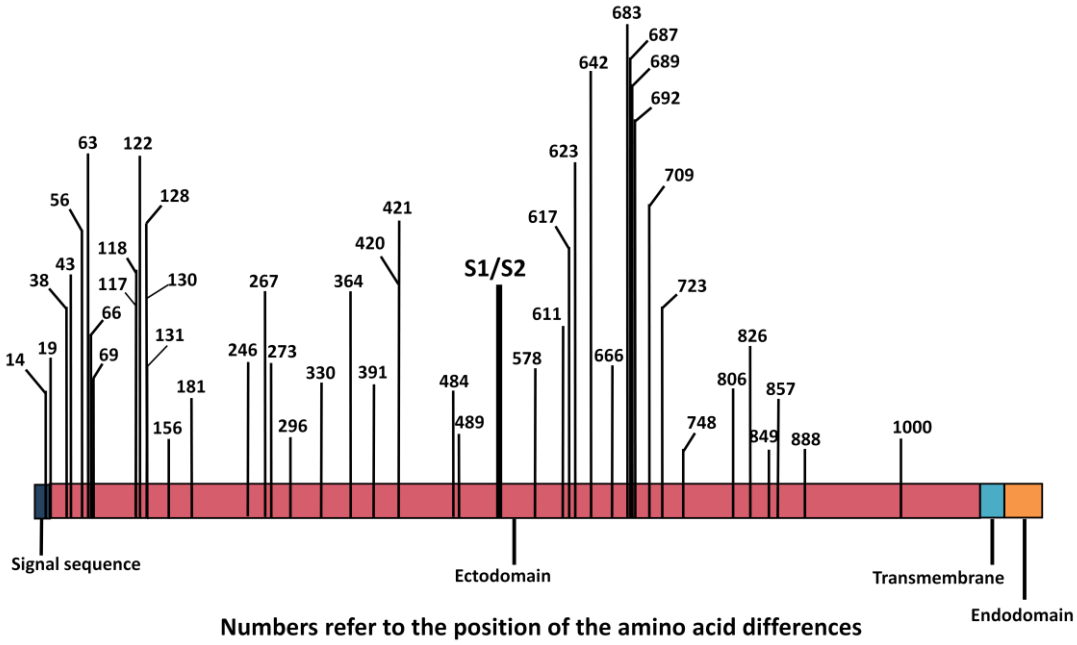

Figure 3.1. Locations of the amino acid differences between the S glycoproteins of Beau-R and M41-CK. There are 46 amino acid differences between the S glycoproteins of Beau-R and M41-CK. The differences are fairly evenly distributed between the S1 and S2 subunits, with S1 containing 27 amino acid differences and S2 containing 19.

In order to determine which subunit of the S glycoprotein from the IBV Beau-R strain is responsible for its ability to grow in Vero cells, two chimaeric rIBVs have been made (Figure 3.2). As the amino acid differences between the S glycoproteins of Beau-R and M41-CK are fairly evenly spread between the S1 and S2 subunits, it was decided to swap the subunits between the two strains within the background of Beau-R. Each recombinant has one subunit of the Beau-R S glycoprotein substituted for the equivalent subunit from the S glycoprotein of the M41 strain of IBV. All other genes are from Beau-R. The growth characteristics of the two rIBVs carrying the chimaeric S glycoproteins on different cell types have been investigated using growth kinetics and confocal microscopy with indirect immunofluorescence.

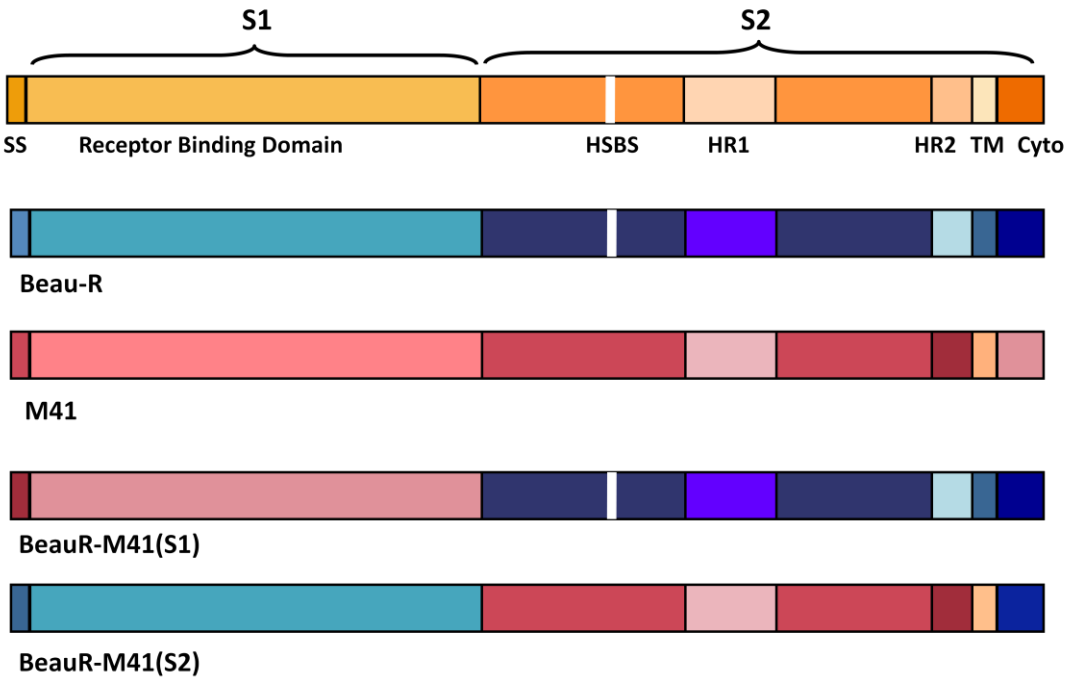

Figure 3.2. Schematic diagram of the S genes of different strains of IBV. The S1 domain contains the receptor binding domain and the cleaved signal sequence (SS). The S2 domain contains two heptad repeats, HR1 and 2, a transmembrane (TM) domain and a cytoplasmic (Cyto) domain. Beau-R also contains a putative heparan sulphate binding sequence (HSBS) not found in M41. The S1 and S2 subunits of Beau-R and M41-CK were swapped to create two chimaeras, BeauR-M41(S1) and BeauR-M41(S2).

Methods

Overlapping PCR

The S genes of Beaudette and M41 are contained within the plasmids pGPT-IBV-StuI-BamHI and pGPT-M41S respectively (Figure 3.3). The overlapping PCR strategy (Figure 3.4) was carried out to generate plasmids carrying the chimaeric S genes, pGPT-BeauR-S1-M41-S2 and pGPT-M41-S1-BeauR-S2 (Figure 3.5). Primers were designed within the replicase gene and gene 3 close to restriction sites already contained within the IBV genome. The S1/S2 junction in IBV strains Beaudette and M41 is situated at the amino acid sequence RRFRR at amino acid position 552 (Cavanagh *et al.*, 1986). The S gene sequence is identical between Beau-R and M41 at the S1/S2 cleavage site so primers were also designed across this location. Around 500 nucleotides were left either side of the S gene to allow for subsequent manipulations. The S gene sequences in plasmids pGPT-BeauR-S1-M41-S2 and pGPT-M41-S1-BeauR-S2 were sequenced to show that they contain the correct M41- and Beaudette-derived sequences.

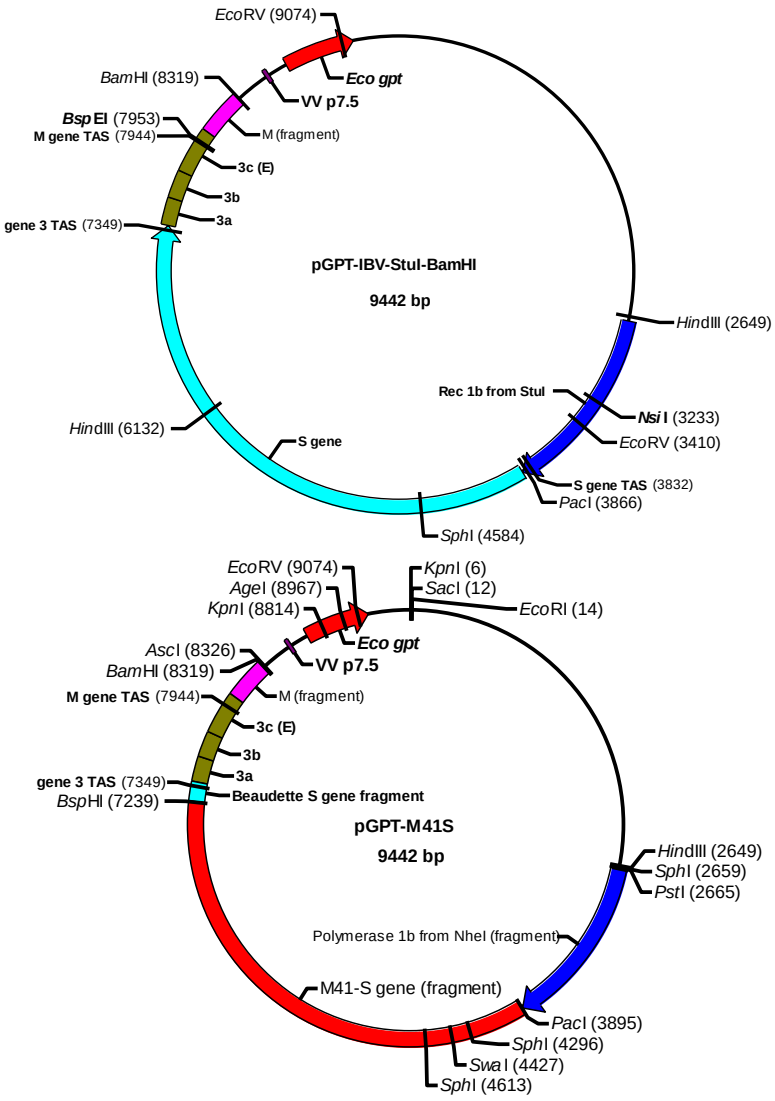

Figure 3.3. Diagrams of pGPT-IBV-StuI-BamHI and pGPT-M41S. The plasmids pGPT-IBV-StuI-BamHI and pGPT-M41S were used to amplify the Beau-R and M41 S1 and S2 subunits by PCR. The replicase gene and gene 3 surrounding both S genes are derived from Beaudette. The C-terminus of the M41 S gene in pGPT-M41S has been exchanged for the Beau-R S gene C-terminus because this is the region of the S glycoprotein that interacts with the M protein. The C-terminal ends of the M41 and Beau-R S proteins are different to each other, so to enable interaction of the chimaeric S protein with the other structural proteins from Beau-R, it was decided to keep the Beau-R S gene C-terminus. The Beau-R S gene was removed from pGPT-IBV-StuI-BamHI using restriction sites NsiI (located within the replicase gene) and BspEI (located within gene 3). The chimaeric S genes were ligated to the remainder of pGPT-IBV-StuI-BamHI to create the plasmids pGPT-BeauR-S1-M41-S2 and pGPT-M41-S1-BeauR-S2 (Figure 3.5).

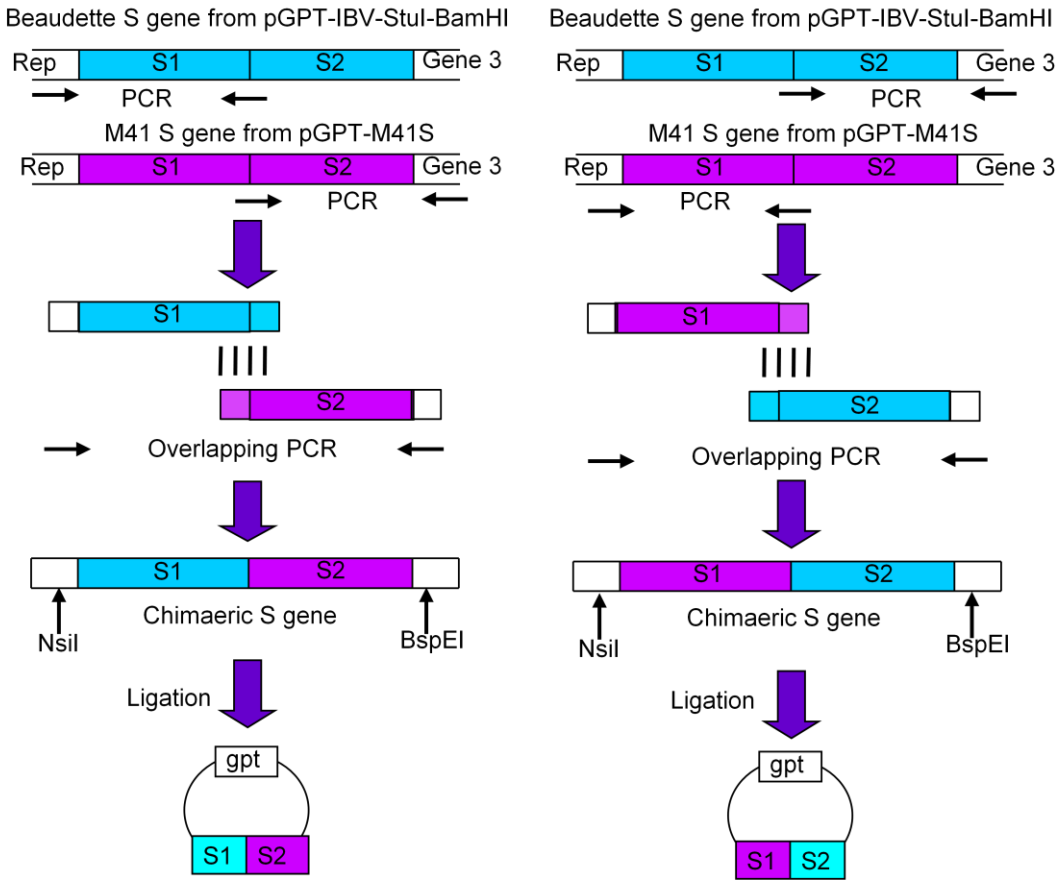

Figure 3.4. Generation of plasmids containing chimaeric S glycoprotein genes. The S1 and S2 subunits of Beau-R and M41 were amplified from two plasmids, pGPT-M41S and pGPT-IBV-StuI-BamHI (Figure 3.3), by PCR using primers located in the replicase gene, across the S1/S2 junction and gene 3. Overlapping PCR was used to combine the subunits, forming the chimaeric S genes, which were then cut with NsiI (restriction site located in the replicase gene) and BspEI (restriction site located in gene 3). The receiver plasmid, pGPT-IBV-StuI-BamHI, was also cut with NsiI and BspEI and the Beaudette S gene was separated by agarose gel electrophoresis and extracted using QIAquick gel extraction kit (Qiagen). The chimaeric S genes were ligated into the remaining pGPT-IBV-StuI-BamHI backbone containing the *E. coli* guanine xanthine phosphoribosyltransferase (gpt) gene.

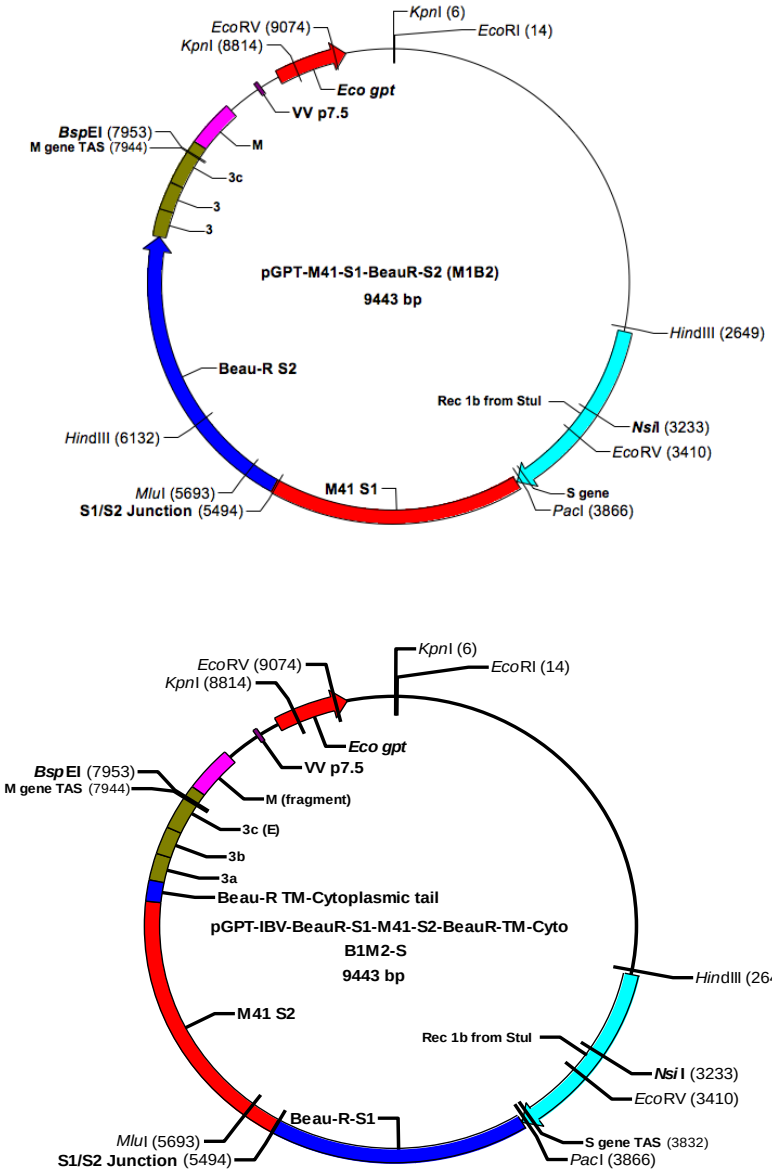

Figure 3.5. Diagrams of pGPT-BeauR-S1-M41-S2 and pGPT-M41-S1-BeauR-S2. pGPT-BeauR-S1-M41-S2 contains the S1 subunit from Beau-R and the S2 subunit from M41. pGPT-M41-S1-BeauR-S2 contains the S1 subunit from M41 and the S2 subunit from Beau-R. The M41 subunits were derived by PCR from pGPT-M41S and the Beau-R subunits were derived from pGPT-IBV-StuI-BamHI. The replicase gene and gene 3 surrounding the S genes are derived from Beaudette. As in pGPT-M41S (Figure 3.3), the C-terminus of the M41 S gene in pGPT-B1M2 has been exchanged for the Beau-R S gene C-terminus because this is the area that interacts with the M protein.

Reverse genetics system and recovery of rIBV

The plasmids pGPT-BeauR-S1-M41-S2 and pGPT-M41-S1-BeauR-S2 (Figure 3.5) were used to insert the chimaeric S gene into vNotI/IBV_{FL}-ΔS, a recombinant vaccinia virus containing the full-length IBV cDNA genome minus the S gene. After the third round of plaque purification in absence of gpt selection components, mini stocks of rVV were grown in Vero cells, the DNA extracted and PCRs carried out to identify whether the viruses still contained the gpt gene. Further PCRs were carried out on the gpt negative viruses to check for the presence of the S gene, which is absent in the parent rVV. Viruses that were both gpt negative and S gene positive were sequenced across the S gene and neighbouring genes to check that the internal sequences were correct. Two lineages of rVVs for each type of modified S gene were identified as having the chimaeric S gene sequence correctly inserted into the IBV genome and were used for the recovery of rIBVs BeauR-M41(S1) and BeauR-M41(S2) in CK cells. After three passages in CK cells the rIBVs were then passaged three times in Vero cells.

Results

Recovery and passage of rIBVs

Rescue of rIBV BeauR-M41(S1) and BeauR-M41(S2) in CK cells

DNA was extracted from two isolates of each rVV containing the full-length IBV cDNA with chimaeric S genes, digested with SalI and analysed by pulsed field gel electrophoresis to check that the full-length cDNA genomes were intact (Figure 3.6). This is indicated by the presence of a 30kb SalI fragment. The chimaeric S gene sequences were verified by sequencing. Two isolates of each rIBV BeauR-M41(S1), isolates 2 and 3, and BeauR-M41(S2), isolates 4 and 15, were rescued from CK cells.

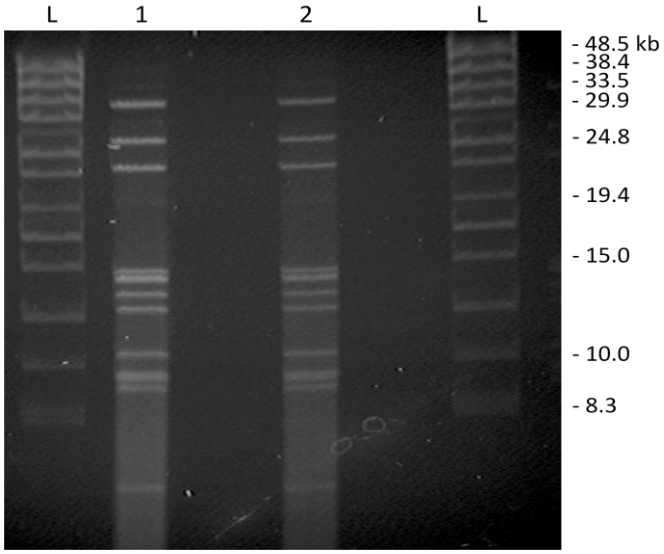

Figure 3.6. Example agarose pulsed field gel analysis of extracted vaccinia virus DNA containing rIBV cDNA. DNA was extracted from large stocks of two isolates each of vaccinia virus containing rIBV BeauR-M41(S1) (2 and 3) or BeauR-M41(S2) (4 and 15) cDNA then digested with SalI and run on an agarose pulsed field gel overnight. The band at around 30 kb shows the intact whole rIBV cDNA. Lanes 1 and 2 contain vaccinia virus DNA. DNA ladders are indicated by L. Gel was stained with ethidium bromide.

Sequencing of P_3-CKC rIBVs

The rescued viruses were passaged three times on CK cells. At each passage on CK cells, RNA was extracted from the infected cell supernatant and RT-PCRs were carried out across the end of the S genes to confirm virus presence. The entire S gene sequences of the P_3-CKC viruses were checked (example areas shown in Figures 3.7 – 3.10). The BeauR-M41(S1) sequences corresponded to that of the M41 sequence within the S1 subunit and the Beau-R sequence within the S2 subunit. The BeauR-M41(S2) sequences corresponded to that of the Beau-R sequence within the S1 subunit and the M41 sequence within the S2 subunit.

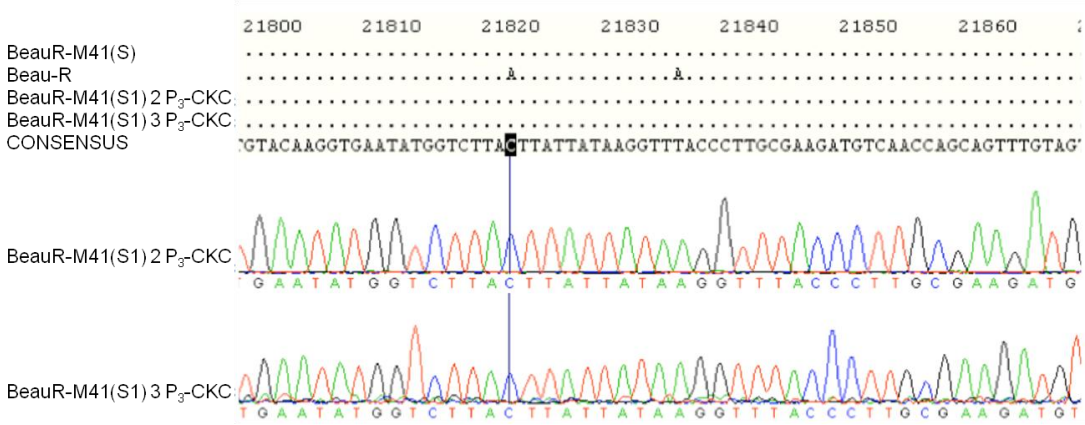

Figure 3.7. Sequencing to check the S1 subunit of BeauR-M41(S1) P_3-CKC isolates. RNA was extracted from BeauR-M41(S1) P_3-CKC cell culture supernatant, RT-PCRs were carried out across the S gene, purified and sequenced in positive and negative directions. The BeauR-M41(S1) sequences correspond to that of the M41 sequence within the S1 subunit. The nucleotide positions are shown above each section of sequencing. Nucleotides corresponding to the consensus sequence are shown by dots, differing nucleotides are shown by letter. The highlighted nucleotide is indicated by a blue line on the sequence trace.

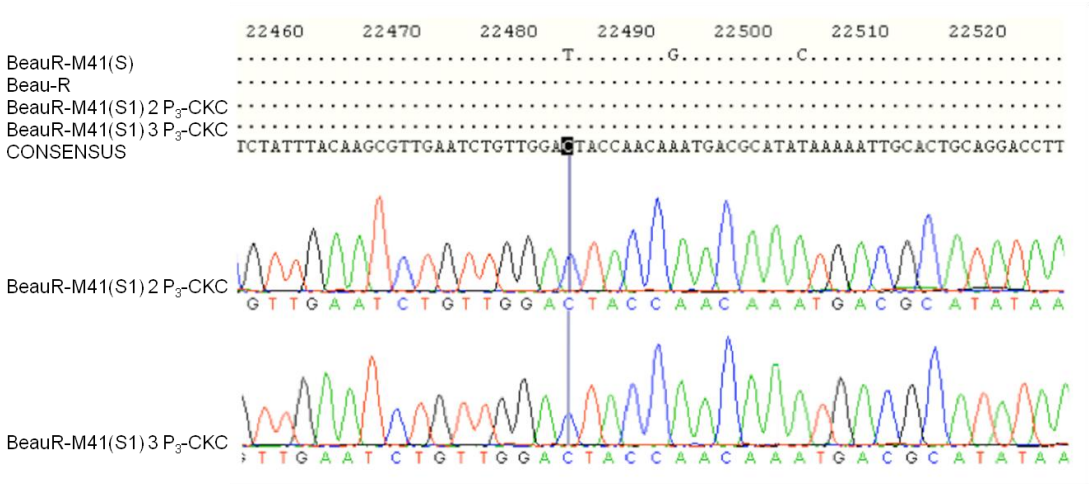

Figure 3.8. Sequencing to check the S2 subunit of BeauR-M41(S1) P_3-CKC isolates. RNA was extracted from BeauR-M41(S1) P_3-CKC cell culture supernatant, RT-PCRs were carried out across the S gene, purified and sequenced in positive and negative directions. The BeauR-M41(S1) sequences correspond to that of the Beau-R sequence within the S2 subunit. The nucleotide positions are shown above each section of sequencing. Nucleotides corresponding to the consensus sequence are shown by dots, differing nucleotides are shown by letter. The highlighted nucleotide is indicated by a blue line on the sequence trace.

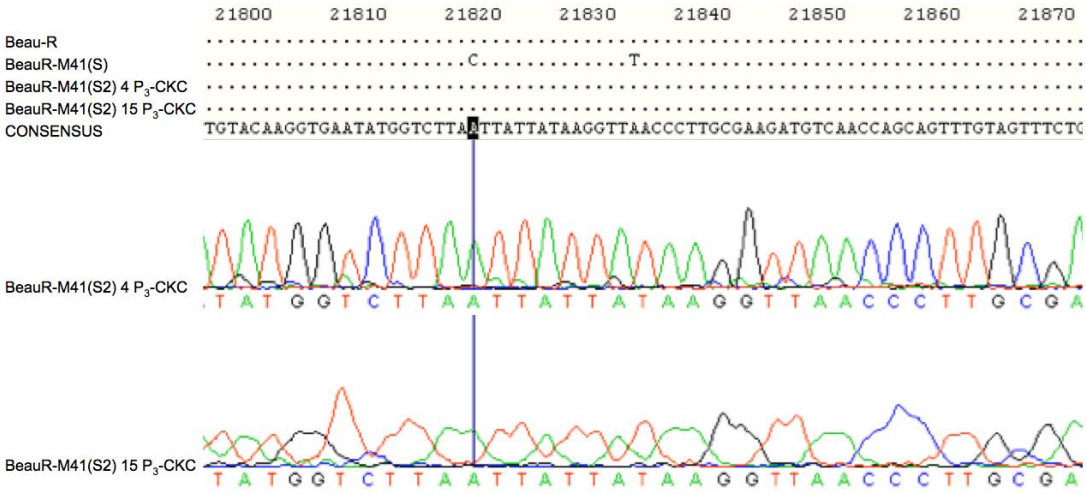

Figure 3.9. Sequencing to check the S1 subunit of BeauR-M41(S2) P_3-CKC isolates. RNA was extracted from BeauR-M41(S2) P_3-CKC cell culture supernatant, RT-PCRs were carried out across the S gene, purified and sequenced in positive and negative directions. The BeauR-M41(S2) sequences correspond to that of the Beau-R sequence within the S1 subunit. The nucleotide positions are shown above each section of sequencing. Nucleotides corresponding to the consensus sequence are shown by dots, differing nucleotides are shown by letter. The highlighted nucleotide is indicated by a blue line on the sequence trace.

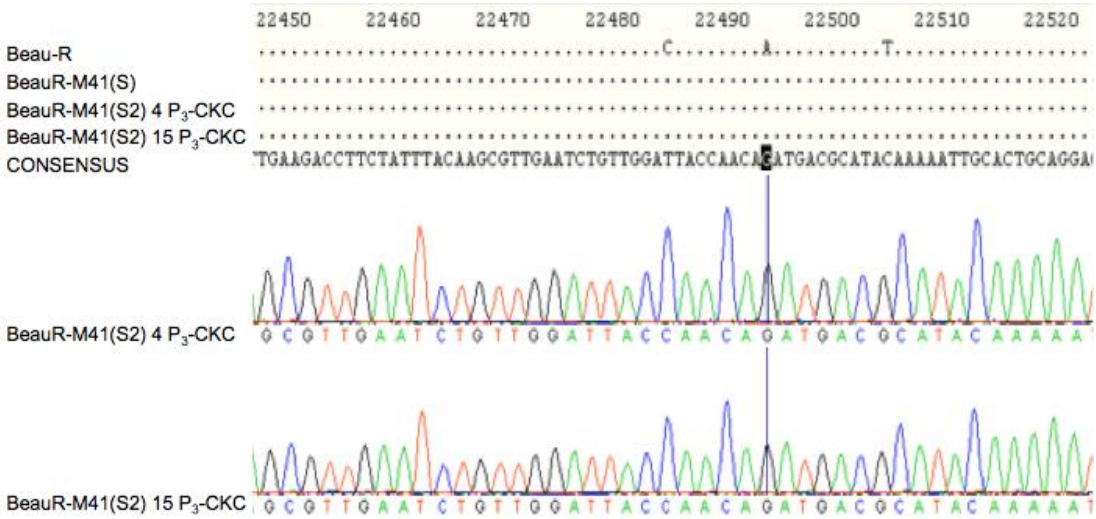

Figure 3.10. Sequencing to check the S2 subunit of BeauR-M41(S2) P_3-CKC isolates. RNA was extracted from BeauR-M41(S2) P_3-CKC cell culture supernatant, RT-PCRs were carried out across the S gene, purified and sequenced in positive and negative directions. The BeauR-M41(S2) sequences correspond to that of the M41 sequence within the S2 subunit. The nucleotide positions are shown above each section of sequencing. Nucleotides corresponding to the consensus sequence are shown by dots, differing nucleotides are shown by letter. The highlighted nucleotide is indicated by a blue line on the sequence trace.

Passage of P_3-CKC rIBVs on Vero cells

The P_3-CKC rIBVs were passaged three times on Vero cells to determine whether virus replication could be maintained on this mammalian cell line. At each passage, RNA was extracted and RT-PCRs were carried out across the end of the S genes to confirm virus presence (Figure 3.11). RT-PCR results showed that both BeauR-M41(S1) isolates grew on Vero cells at each passage. Cytopathic effect in the form of rounded and floating cells were observed from around 24 hours post-infection and all PCRs were positive for virus presence. In contrast, the RT-PCRs for the presence of BeauR-M41(S2) isolates were either very faint (isolate 4) or negative (isolate 15) by passage 3 when visualised by agarose gel electrophoresis.

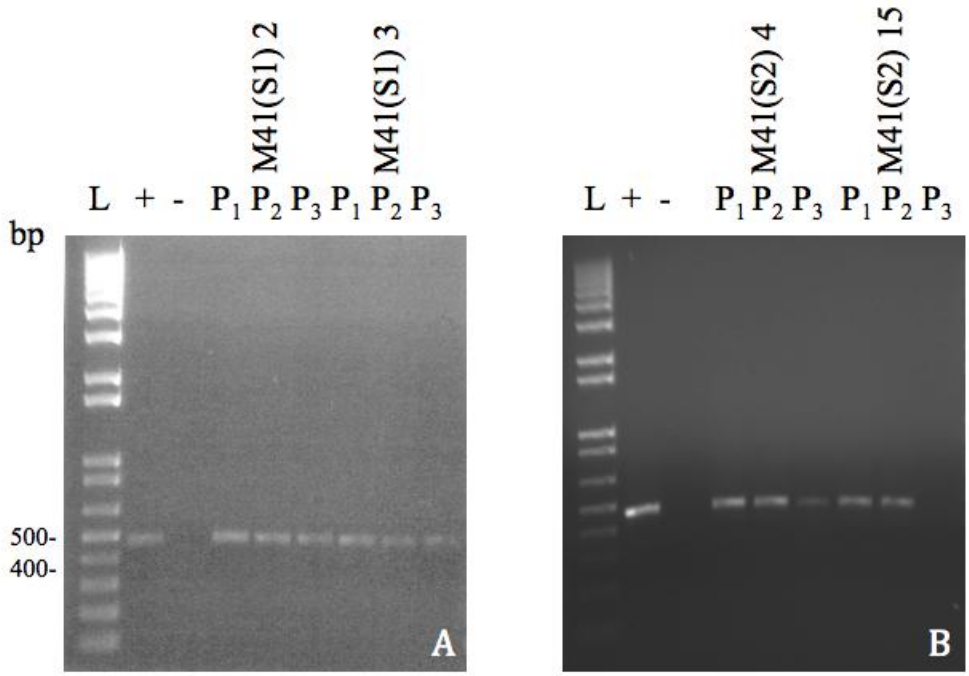

Figure 3.11. Agarose gel analysis of RT-PCR products from rIBV BeauR-M41(S1) and BeauR-M41(S2) P_{1-3}-Vero isolates. RNA was extracted from Vero cell culture supernatants of (A) rIBV BeauR-M41(S1) 2 and 3 and (B) rIBV BeauR-M41(S2) 4 and 15 P_{1-3}-Vero, RT-PCRs were carried out on each sample. A molecular size ladder (L) is shown to compare the sizes of DNA fragments. Positive control (+) shows a band between 400-500 bp. Negative control (-) shows no band. All passages of BeauR-M41(S1) have bands of correct sizes. Band intensity decreases from P_{1-3} of BeauR-M41(S2) and P_3 of isolate 15 can no longer be seen.

The BeauR-M41(S2) isolates caused no cytopathic effect (cpe) when grown on Vero cells (Figure 3.12). BeauR-M41(S1) isolates were further passaged on Vero cells in order to establish whether this virus could further adapt to growth on Vero cells. Syncytia began to form in Vero cell culture from P_5 (Figure 3.12). It was determined that BeauR-M41(S1) replication on Vero cells was stable so no further passages were carried out after passage 7. The S genes of the BeauR-M41(S1) P_7-Vero isolates were sequenced to ascertain whether any nucleotide or amino acid changes had occurred (Figure 3.13).

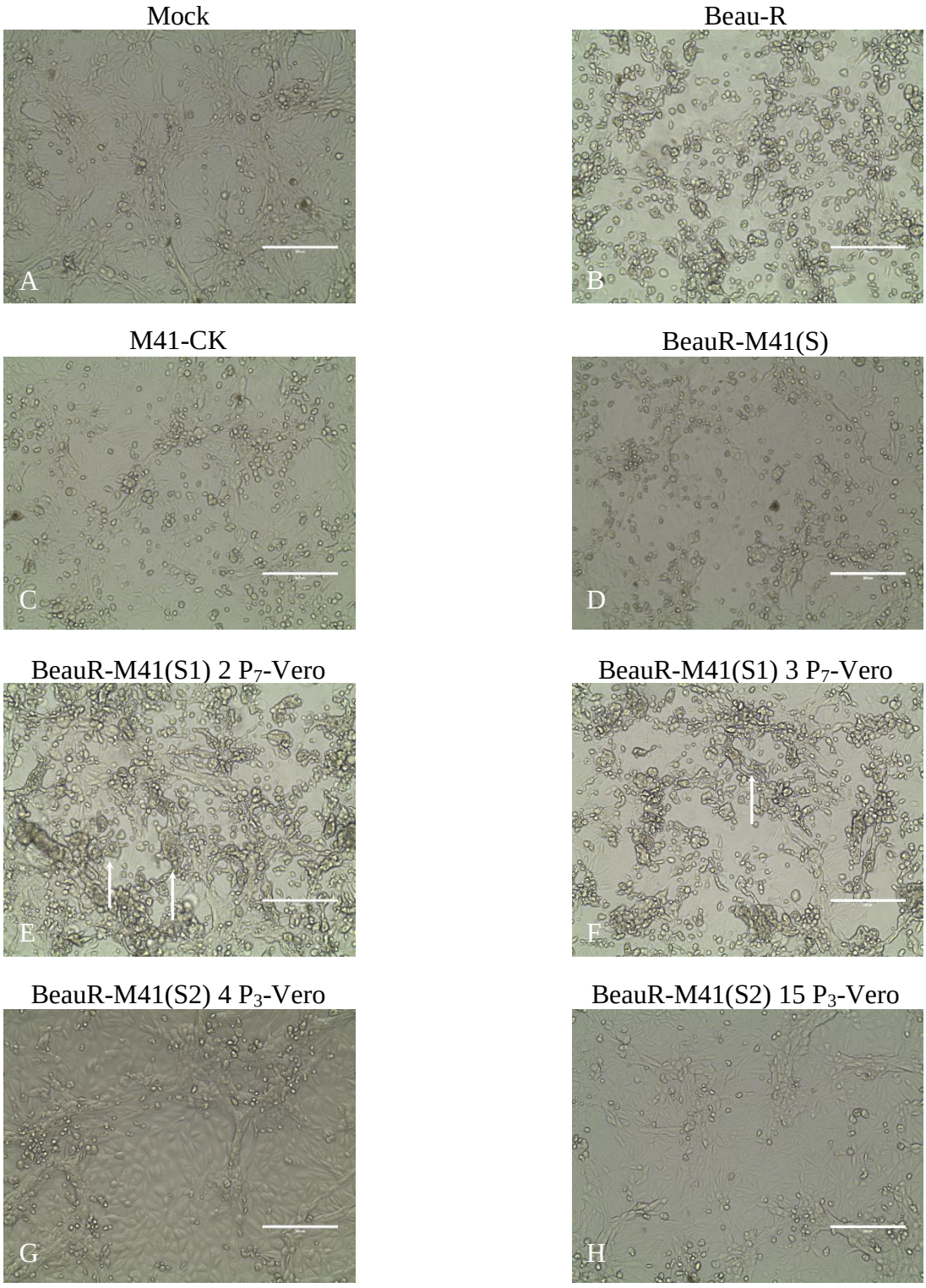

Figure 3.12. Brightfield microscopy of rIBV growth on Vero cells. Vero cells infected with A. mock, B. Beau-R, C. M41-CK, D. BeauR-M41(S), E. BeauR-M41(S1) 2 P_7-Vero, F. BeauR-M41(S1) 3 P_7-Vero, G. BeauR-M41(S2) 4 P_3-Vero, H. BeauR-M41(S2) 15 P_3-Vero. Syncytia indicated by arrows. Photographs taken 48 hours post-infection.

Sequencing of BeauR-M41(S1) P_7-Vero S genes

RNA was extracted from infected cell supernatant and RT-PCRs were carried out across the S gene. These were then sequenced and compared to Beau-R and BeauR-M41(S) sequences (Figure 3.13). Five nucleotide differences were identified between the BeauR-M41(S1) P_7-Vero isolates and the parent viruses, Beau-R and BeauR-M41(S), all of which are located within the S2 subunit.

The first three changes are located at nucleotide positions 22243 – 5, GTT – AAC, and were identified in isolate 2, although isolate 3 appears to have a mixed population between AAC and GTT (Figure 3.13A). These nucleotide changes result in an amino acid change of phenylalanine – threonine. It also appears that there is a mixed population of several nucleotides downstream between AATATGG – TTTAAGT.

The fourth nucleotide change occurs at position 23022 and was identified in isolate 3 only (Figure 3.13B). This results in an amino acid change of alanine – valine. The fifth nucleotide change was identified in isolate 2 only and occurs at position 23387, resulting in an amino acid change of threonine – isoleucine (Figure 3.13C). It is possible that these changes could contribute to the further adaptation of BeauR-M41(S1) to growth on Vero cells and may be involved in syncytium formation.

Figure 3.13. Sequencing of BeauR-M41(S1) P_7-Vero S genes. RNA was extracted from BeauR-M41(S1) P_7-Vero cell culture supernatant, RT-PCRs were carried out across the S gene, purified and sequenced in positive and negative directions. Five nucleotide differences were observed in the S genes of BeauR-M41(S1) P_7-Vero isolates when compared to Beau-R and BeauR-M41(S), all of which occurred within the S2 subunit. The sequences otherwise corresponded to M41 in the S1 subunit and Beau-R in the S2 subunit. The nucleotide positions are shown above each section of sequencing. Nucleotides corresponding to the consensus sequence are shown by dots, differing nucleotides are shown by letter. The highlighted nucleotide is indicated by a blue line on the sequence trace.

A

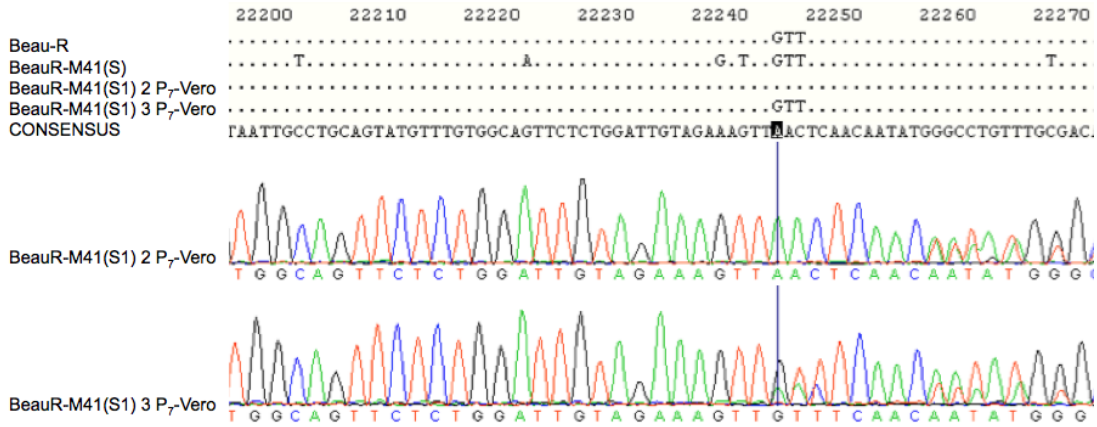
22200 22210 22220 22230 22240 22250 22260 22270
Beau-R
BeauR-M41(S)
BeauR-M41(S1) 2 P7-Vero
BeauR-M41(S1) 3 P7-Vero
CONSENSUS
BeauR-M41(S1) 2 P7-Vero
BeauR-M41(S1) 3 P7-Vero

B

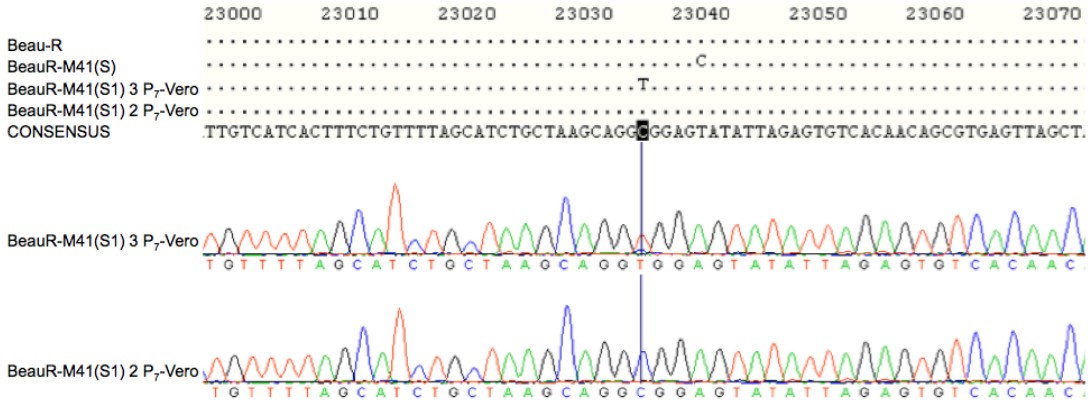
23000 23010 23020 23030 23040 23050 23060 23070
Beau-R
BeauR-M41(S)
BeauR-M41(S1) 3 P7-Vero
BeauR-M41(S1) 2 P7-Vero
CONSENSUS
BeauR-M41(S1) 3 P7-Vero
BeauR-M41(S1) 2 P7-Vero

C

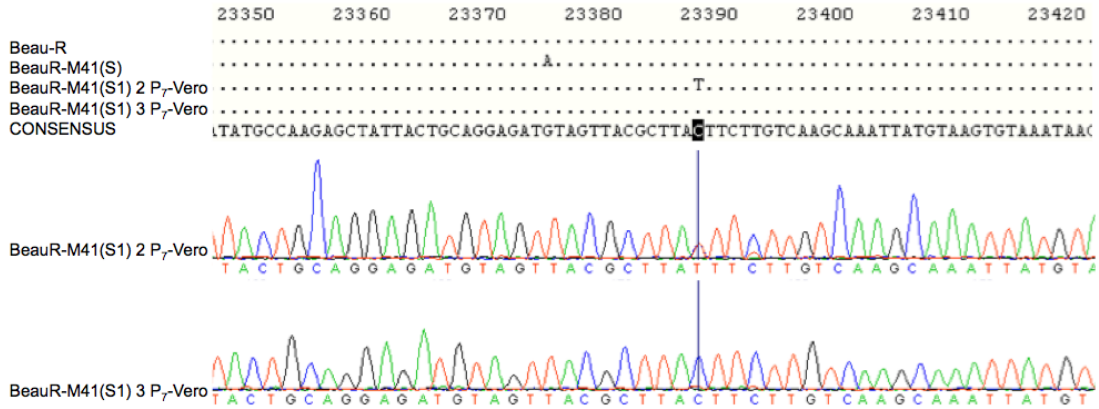
23350 23360 23370 23380 23390 23400 23410 23420
Beau-R
BeauR-M41(S)
BeauR-M41(S1) 2 P7-Vero
BeauR-M41(S1) 3 P7-Vero
CONSENSUS
BeauR-M41(S1) 2 P7-Vero
BeauR-M41(S1) 3 P7-Vero

Titration of rIBVs on CK cells

Isolates 2 and 3 of rIBV BeauR-M41(S1) P_3-CKC, P_3-Vero and P_7-Vero and isolates 4 and 15 of rIBV BeauR-M41(S2) P_3-CKC and P_3-Vero were titrated on CK cells and compared to parent strains of IBV, Beau-R, M41-CK and BeauR-M41(S) (Table 3.1). Beau-R and BeauR-M41(S) are recombinant strains of IBV, M41-CK is not. The titres for the P_3-CKC recombinant viruses were comparable to those of laboratory strains Beau-R and M41-CK. BeauR-M41(S) titre was lower than the others, as was BeauR-M41(S1) isolate 3. It is possible that these titres could be increased by further passage in CK cells.

The titres of all P_3-Vero rIBV were lower than those of the P_3-CKC rIBV, however further passage on Vero cells increased the titres of BeauR-M41(S1) isolates and by P_7-Vero, titres were closer to the original P_3-CKC and Beau-R titres. In fact, the BeauR-M41(S1) 3 P_7-Vero titre was actually greater than that of BeauR-M41(S1) 3 P_3-CKC. The titres of the BeauR-M41(S2) P_3-Vero isolates were dramatically lower than the P_3-CKC isolates, isolate 15 was undetectable.

Table 3.1. Comparison of rIBV titres on CK cells. Virus supernatant was serially diluted 1:10 in cell culture medium. Confluent CK cells in six-well plates were infected with 500 µl diluted supernatant in duplicate and incubated at 37°C for 1 hour. Inoculum was replaced with 3 ml medium containing 1% agar and plates were incubated at 37°C for 48 – 72 hours. Living cells were stained with 0.01% neutral red and plaques counted several hours later. The number of plaque forming units (pfu) per ml was calculated. The titres are an average of three separate experiments.

Virus	**Titre (pfu/ml)**
Beau-R	9×10^9
M41-CK	3×10^9
BeauR-M41(S)	3×10^4
BeauR-M41(S1) 2 P_3-CKC	1×10^{10}
BeauR-M41(S1) 2 P_3-Vero	3×10^7
BeauR-M41(S1) 2 P_7-Vero	4×10^8
BeauR-M41(S1) 3 P_3-CKC	3×10^4
BeauR-M41(S1) 3 P_3-Vero	2×10^4
BeauR-M41(S1) 3 P_7-Vero	5×10^7
BeauR-M41(S2) 4 P_3-CKC	5×10^9
BeauR-M41(S2) 4 P_3-Vero	4×10^2
BeauR-M41(S2) 15 P_3-CKC	4×10^9
BeauR-M41(S2) 15 P_3-Vero	0

Analysis of rIBV growth phenotypes by confocal microscopy

Chick kidney, Vero and BHK-21 cells on coverslips were infected with isolates 2 and 3 of rIBV BeauR-M41(S1) P_3-CKC, P_3-Vero and P_7-Vero and isolates 4 and 15 of rIBV BeauR-M41(S2) P_3-CKC and P_3-Vero. Cells were also infected with Beau-R, M41-CK and BeauR-M41(S) for comparison (Figure 3.14). Infected cells were immunolabelled with mouse anti-dsRNA, secondary antibody AlexaFluor 488 goat anti-mouse (green). Nuclei were labelled with DAPI (blue).

Many infected CK cells were observed in wells inoculated with the parent virus controls, Beau-R, M41-CK and BeauR-M41(S) (Figure 3.14). Infected cells were often found clustered in infectious centres but some individual infected cells, presumably as a result of a second cycle of infection, were also seen.

Many infected Vero and BHK-21 cells were observed in wells inoculated with Beau-R. As with CK cells, infected Vero cells were mainly found clustered in infectious centres but individual infected cells were also seen. However infected BHK-21 cells were discrete from each other and no infectious centres were observed. This growth pattern is different to that observed on CK and Vero cells.

Only small numbers of infected Vero or BHK-21 cells were observed with M41-CK or BeauR-M41(S), many of which had low levels of immunofluorescence, and no infectious centres were observed. Although it appears that M41-CK and BeauR-M41(S) are able to replicate within Vero and BHK-21 cells, infectious progeny virus

does not infect neighbouring cells and there is no virus spread. It is possible that progeny virus is unable to be released from the host cells or it may not be infectious.

No fluorescent cells were observed in the mock-infected wells using an anti-dsRNA antibody.

Figure 3.14. Confocal microscopy of rIBV growth on CK, Vero and BHK-21 cells. Chick kidney cells were infected with A. mock, B. Beau-R, G. M41-CK and H. BeauR-M41(S). Vero cells were infected with C. mock, D. Beau-R, I. M41-CK and J. BeauR-M41(S). Baby hamster kidney-21 cells were infected with E. mock, F. Beau-R, K. M41-CK and L. BeauR-M41(S). Infected cells were fixed 24 hours post-infection and immunolabelled with mouse anti-dsRNA, secondary antibody AlexaFluor 488 goat anti-mouse (green, Invitrogen). Nuclei were labelled with DAPI (blue). Images have been brightened for printing.

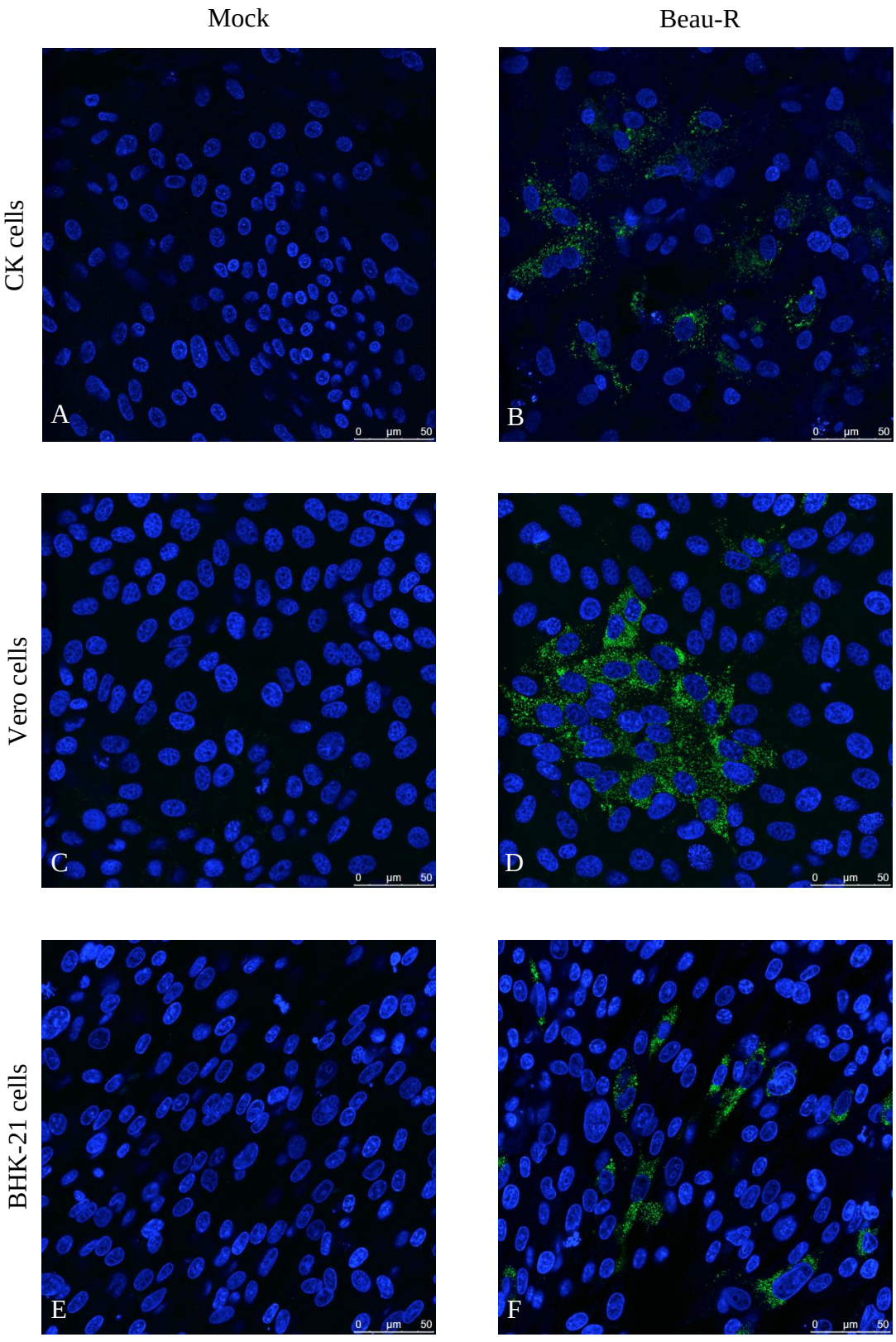
Mock
Beau-R
CK cells
Vero cells
BHK-21 cells
A
B
C
D
E
F
0 µm 50

Figure 3.14. Confocal microscopy of rIBV growth on CK, Vero and BHK-21 cells. Chick kidney cells were infected with A. mock, B. Beau-R, G. M41-CK and H. BeauR-M41(S). Vero cells were infected with C. mock, D. Beau-R, I. M41-CK and J. BeauR-M41(S). Baby hamster kidney-21 cells were infected with E. mock, F. Beau-R, K. M41-CK and L. BeauR-M41(S). Infected cells were fixed 24 hours post-infection and immunolabelled with mouse anti-dsRNA, secondary antibody AlexaFluor 488 goat anti-mouse (green, Invitrogen). Nuclei were labelled with DAPI (blue). Images have been brightened for printing.

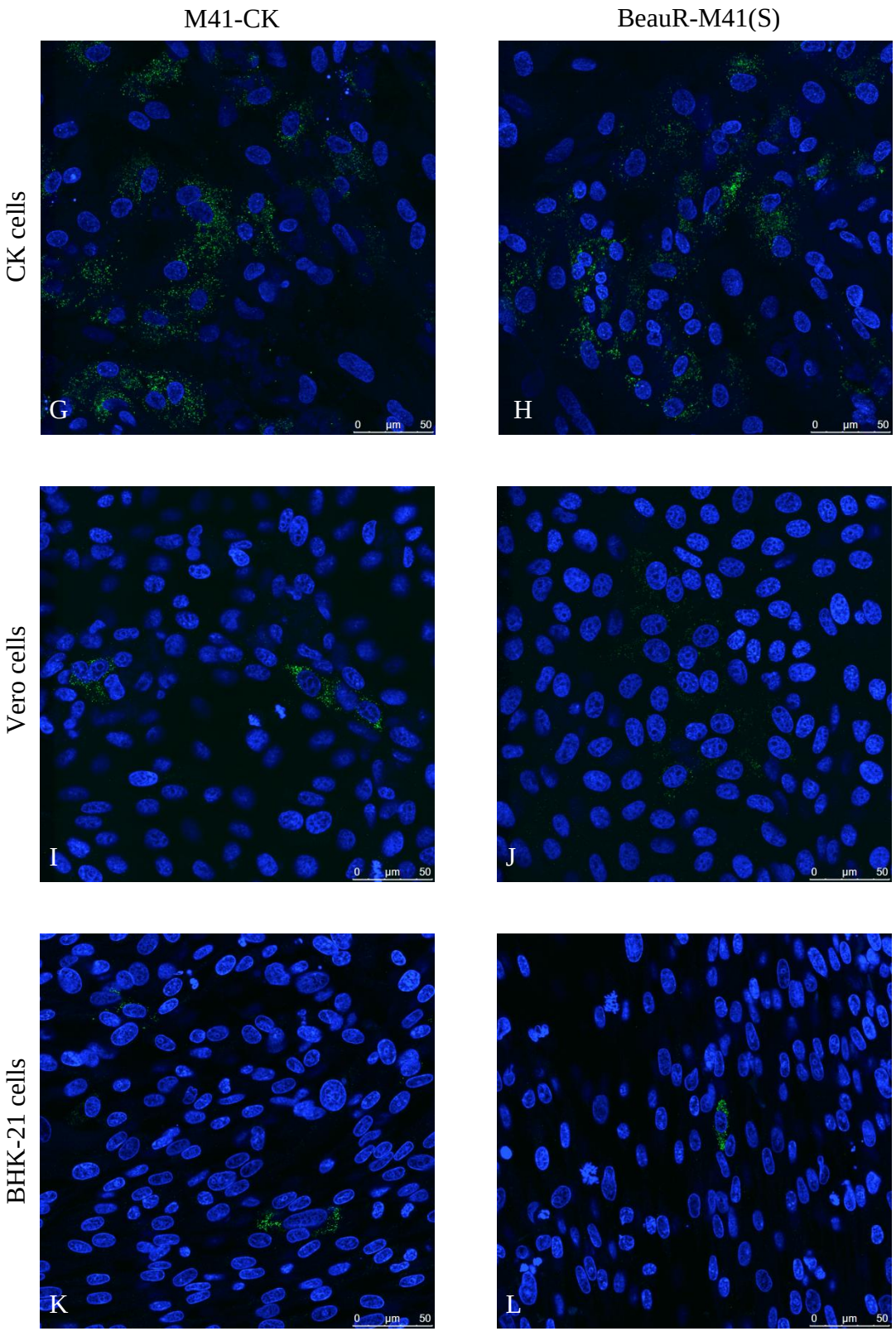
M41-CK
BeauR-M41(S)
CK cells
Vero cells
BHK-21 cells
G
H
I
J
K
L
0 μm 50

Infectious centres were observed in CK and Vero cells infected with both BeauR-M41(S1) P_3-CKC isolates. The rIBV also replicated in BHK-21 cells although as with Beau-R, single infected cells were mainly observed rather than infectious foci (Figure 3.15).

BeauR-M41(S1) P_3-Vero isolates also replicated in CK and Vero cells and infected cells were mainly observed in infectious centres. Only a small number of infected BHK-21 cells were observed however, and none were observed in infectious centres (Figure 3.16).

Many infectious centres were observed in CK and Vero cells infected with BeauR-M41(S1) P_7-Vero isolates. As with the P_3-CKC and P_3-Vero isolates, infected BHK-21 cells were observed singly rather than in infectious foci, although groups of infected cells did occur in the same field of vision (Figure 3.17).

There appears to be no difference between the growth phenotypes of the different BeauR-M41(S1) isolates and Beau-R on CK, Vero and BHK-21 cells. All isolates grew well on CK and Vero cells, forming infectious centres. The isolates grew less well on BHK-21 cells and infected cells were not observed in infectious foci, rather singly. Progeny virus from BHK-21 cells may be less infectious or less progeny virus may be released from BHK-21 cells.

Figure 3.15. Confocal microscopy of rIBV BeauR-M41(S1) P_3-CKC growth on CK, Vero and BHK-21 cells. Chick kidney cells were infected with A. BeauR-M41(S1) 2 P_3-CKC, B. BeauR-M41(S1) 3 P_3-CKC. Vero cells were infected with C. BeauR-M41(S1) 2 P_3-CKC, D. BeauR-M41(S1) 3 P_3-CKC. Baby hamster kidney-21 cells were infected with E. BeauR-M41(S1) 2 P_3-CKC, F. BeauR-M41(S1) 3 P_3-CKC. Infected cells were fixed 24 hours post-infection and immunolabelled with mouse anti-dsRNA, secondary antibody AlexaFluor 488 goat anti-mouse (green, Invitrogen). Nuclei were labelled with DAPI (blue). Images have been brightened for printing.

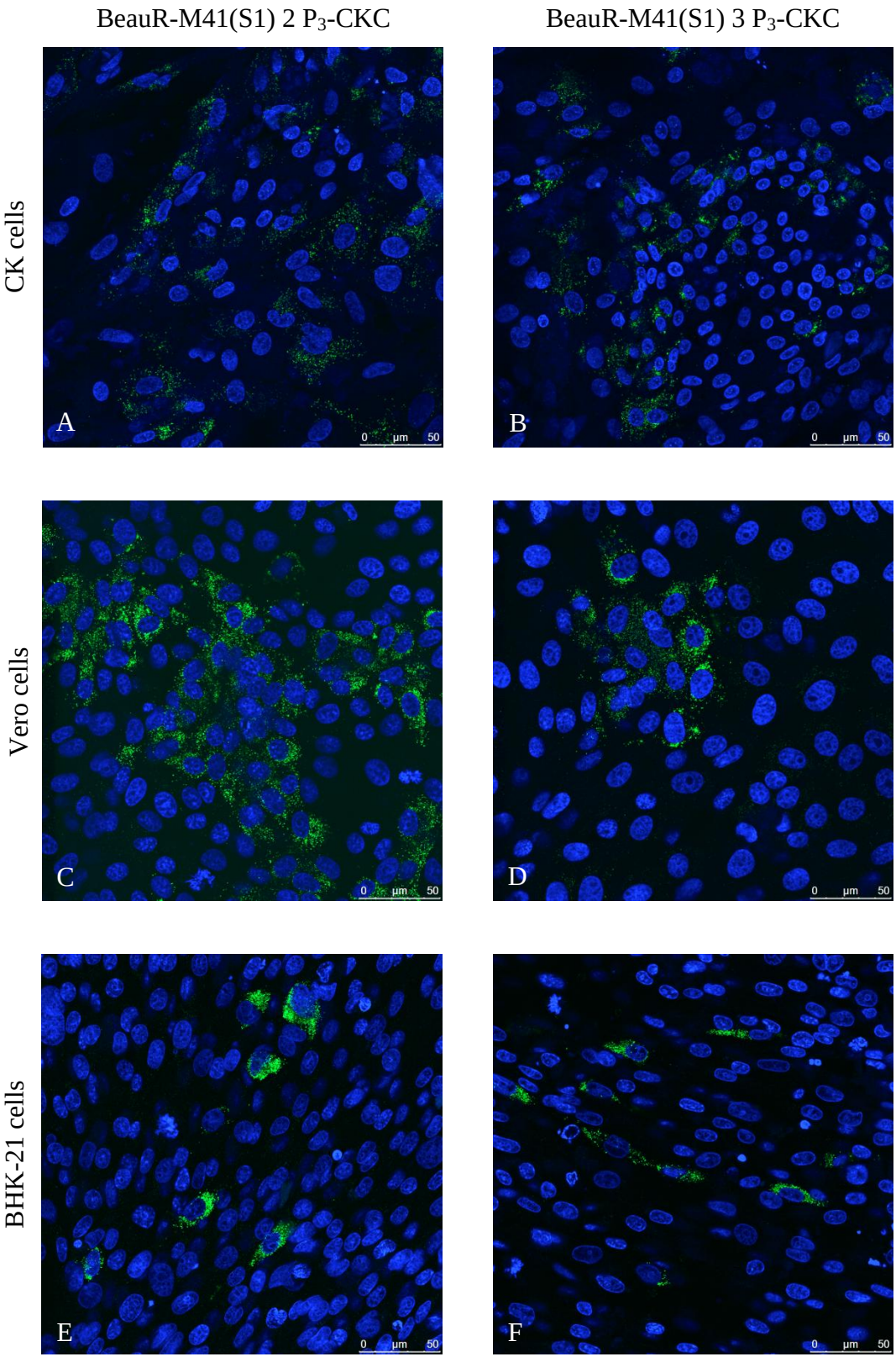
BeauR-M41(S1) 2 P3-CKC
BeauR-M41(S1) 3 P3-CKC
CK cells
Vero cells
BHK-21 cells
A
B
C
D
E
F
0 µm 50

Figure 3.16. Confocal microscopy of rIBV BeauR-M41(S1) P_3-Vero growth on CK, Vero and BHK-21 cells. Chick kidney cells were infected with A. BeauR-M41(S1) 2 P_3-Vero, B. BeauR-M41(S1) 3 P_3-Vero. Vero cells were infected with C. BeauR-M41(S1) 2 P_3-Vero, D. BeauR-M41(S1) 3 P_3-Vero. Baby hamster kidney-21 cells were infected with E. BeauR-M41(S1) 2 P_3-Vero, F. BeauR-M41(S1) 3 P_3-Vero. Infected cells were fixed 24 hours post-infection and immunolabelled with mouse anti-dsRNA, secondary antibody AlexaFluor 488 goat anti-mouse (green, Invitrogen). Nuclei were labelled with DAPI (blue). Images have been brightened for printing.

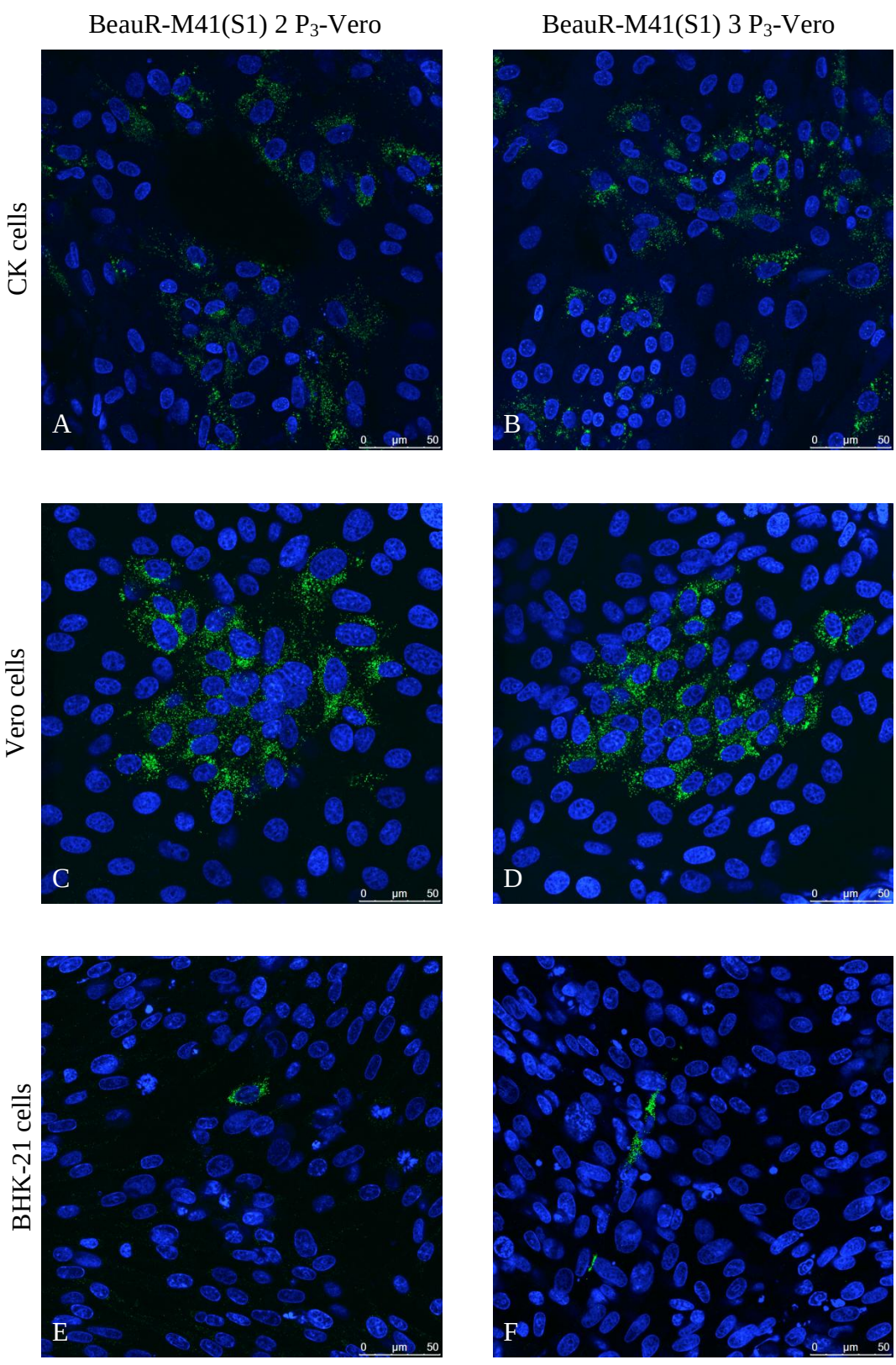
BeauR-M41(S1) 2 P3-Vero
BeauR-M41(S1) 3 P3-Vero
CK cells
Vero cells
BHK-21 cells
A
B
C
D
E
F
0 μm 50

Figure 3.17. Confocal microscopy of rIBV BeauR-M41(S1) P_7-Vero growth on CK, Vero and BHK-21 cells. Chick kidney cells were infected with A. BeauR-M41(S1) 2 P_7-Vero, B. BeauR-M41(S1) 3 P_7-Vero. Vero cells were infected with C. BeauR-M41(S1) 2 P_7-Vero, D. BeauR-M41(S1) 3 P_7-Vero. Baby hamster kidney-21 cells were infected with E. BeauR-M41(S1) 2 P_7-Vero, F. BeauR-M41(S1) 3 P_7-Vero. Infected cells were fixed 24 hours post-infection and immunolabelled with mouse anti-dsRNA, secondary antibody AlexaFluor 488 goat anti-mouse (green, Invitrogen). Nuclei were labelled with DAPI (blue). Images have been brightened for printing.

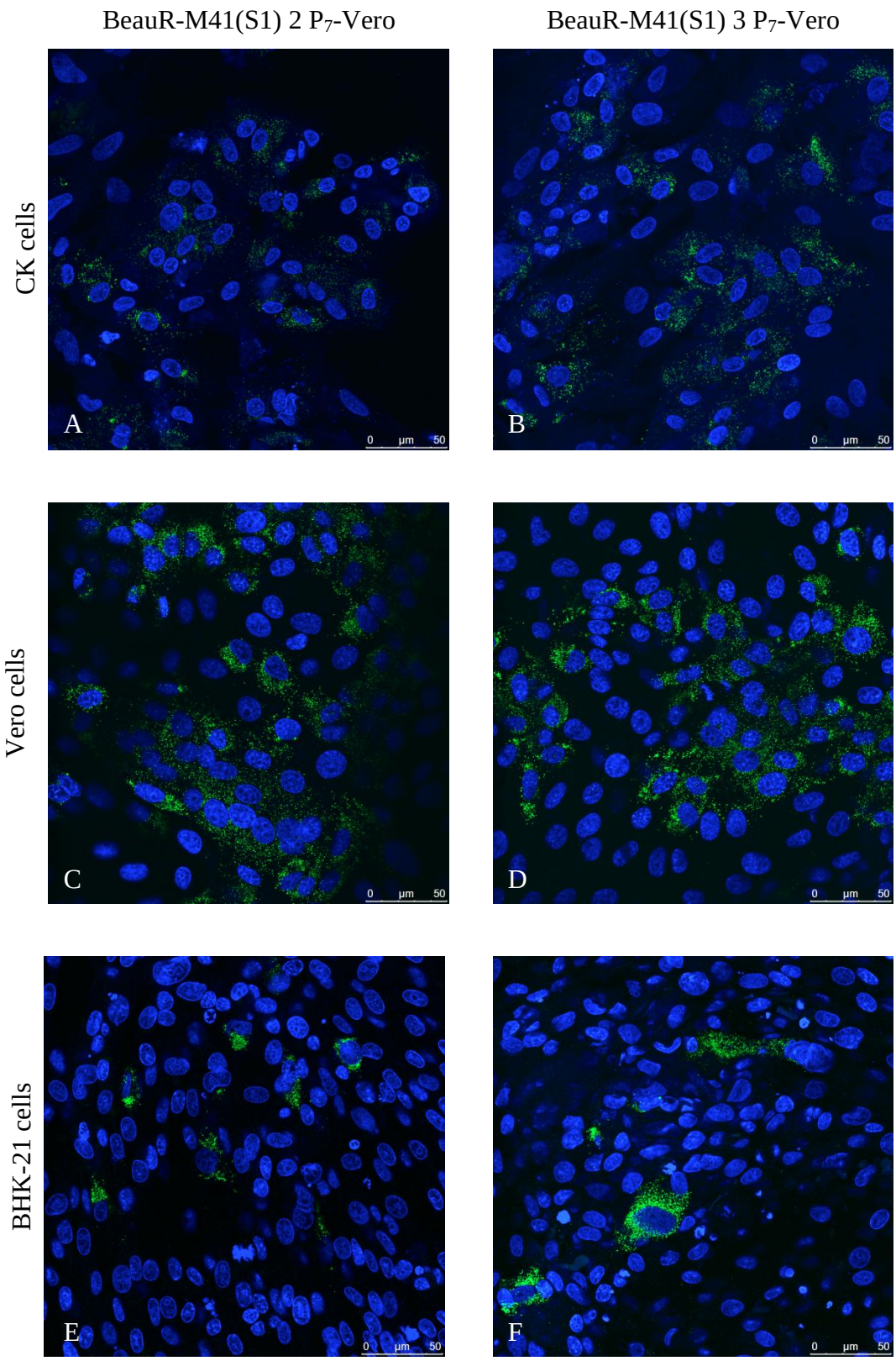
BeauR-M41(S1) 2 P7-Vero
BeauR-M41(S1) 3 P7-Vero
CK cells
Vero cells
BHK-21 cells
A
B
C
D
E
F
0 µm 50

Both BeauR-M41(S2) P_3-CKC isolates grew well on CK cells, forming infectious centres. Only a small number of infected Vero cells were observed, none of which were in infectious centres. Groups of infected BHK-21 cells were seen in wells inoculated with BeauR-M41(S2) P_3-CKC isolates. All infected cells observed were singular, not clustered in infectious centres. More infected BHK-21 cells were observed than infected Vero cells, although there did not appear to be any virus spread in either cell type (Figure 3.18).

Infectious centres were observed in CK cells infected with BeauR-M41(S2) 4 P_3-Vero but no infected cells were observed in wells inoculated with BeauR-M41(S2) 15 P_3-Vero. No infected Vero cells were observed in wells inoculated with BeauR-M41(S2) P_3-Vero isolates. Only a small number of infected BHK-21 cells were observed following infection with BeauR-M41(S2) 4 P_3-Vero and only infected cells with faint immunofluorescence were observed with BeauR-M41(S2)15 P_3-Vero. Infected cells were all single, not in infectious centres (Figure 3.19).

While BeauR-M41(S2) P_3-CKC isolates grew well on CK cells and infected small numbers of Vero and BHK-21 cells, P_3-Vero isolate 4 was only able to infect CK cells, forming infectious centres. No infected cells were observed in wells infected with BeauR-M41(S2) 15 P_3-Vero. As indicated in Figure 3.7 and Table 3.1, passage of BeauR-M41(S2) on Vero cells significantly decreased the virus titre, in fact no BeauR-M41(S2) isolate 15 remained after three passages. This is confirmed by confocal microscopy with indirect immunofluorescence as no infected cells of any type investigated were observed.

Figure 3.18. Confocal microscopy of rIBV BeauR-M41(S2) P_3-CKC growth on CK, Vero and BHK-21 cells. Chick kidney cells were infected with A. BeauR-M41(S2) 4 P_3-CKC, B. BeauR-M41(S2) 15 P_3-CKC. Vero cells were infected with C. BeauR-M41(S2) 4 P_3-CKC, D. BeauR-M41(S2) 15 P_3-CKC. Baby hamster kidney-21 cells were infected with E. BeauR-M41(S2) 4 P_3-CKC, F. BeauR-M41(S2) 15 P_3-CKC. Infected cells were fixed 24 hours post-infection and immunolabelled with mouse anti-dsRNA, secondary antibody AlexaFluor 488 goat anti-mouse (green, Invitrogen). Nuclei were labelled with DAPI (blue). Images have been brightened for printing.

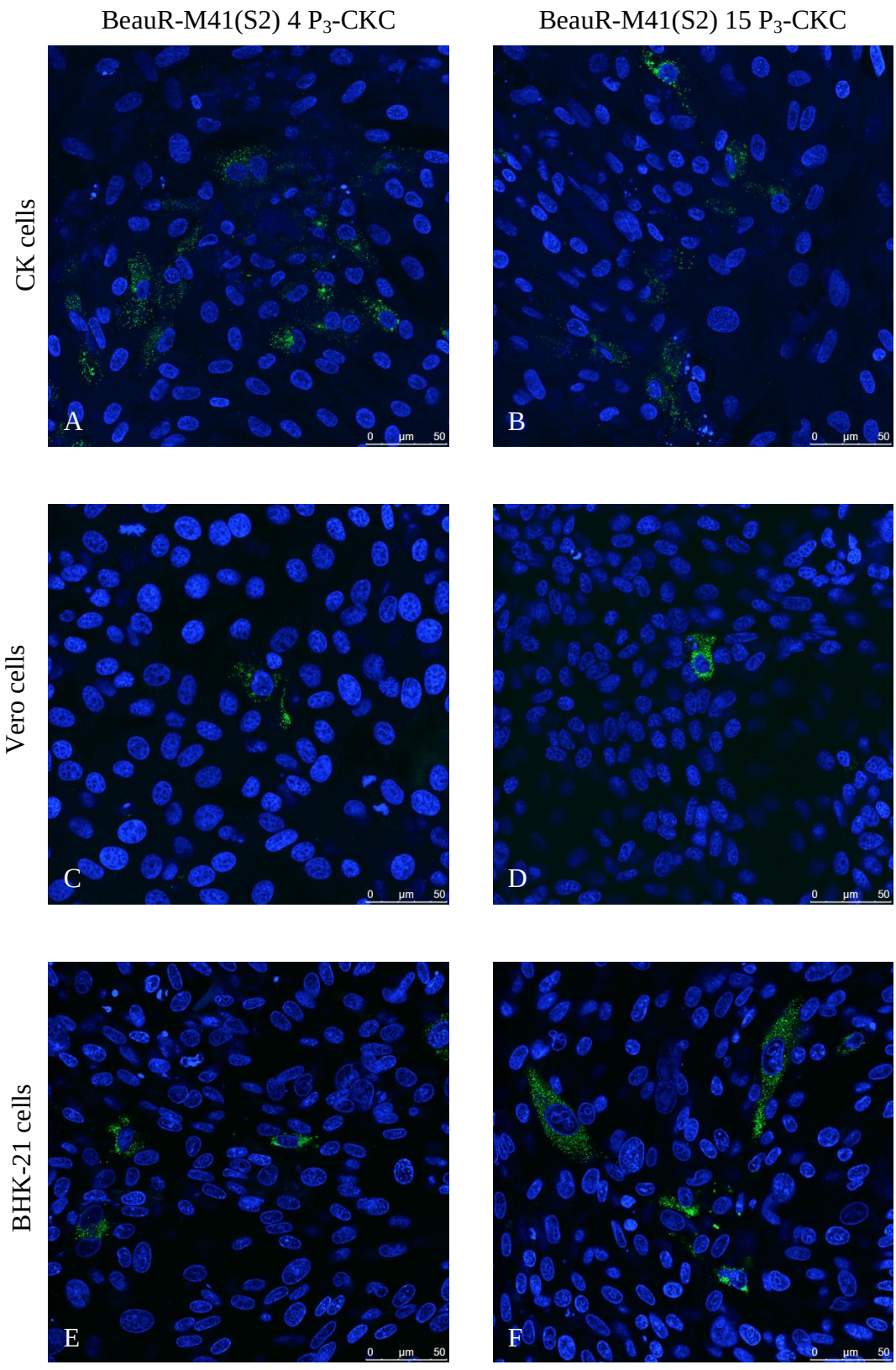
BeauR-M41(S2) 4 P3-CKC
BeauR-M41(S2) 15 P3-CKC
CK cells
Vero cells
BHK-21 cells
A
B
C
D
E
F
0 µm 50

Figure 3.19. Confocal microscopy of rIBV BeauR-M41(S2) P_3-Vero growth on CK, Vero and BHK-21 cells. Chick kidney cells were infected with A. BeauR-M41(S2) 4 P_3-Vero, B. BeauR-M41(S2) 15 P_3-Vero. Vero cells were infected with C. BeauR-M41(S2) 4 P_3-Vero, D. BeauR-M41(S2) 15 P_3-Vero. Baby hamster kidney-21 cells were infected with E. BeauR-M41(S2) 4 P_3-Vero, F. BeauR-M41(S2) 15 P_3-Vero. Infected cells were fixed 24 hours post-infection and immunolabelled with mouse anti-dsRNA, secondary antibody AlexaFluor 488 goat anti-mouse (green, Invitrogen). Nuclei were labelled with DAPI (blue). Images have been brightened for printing.

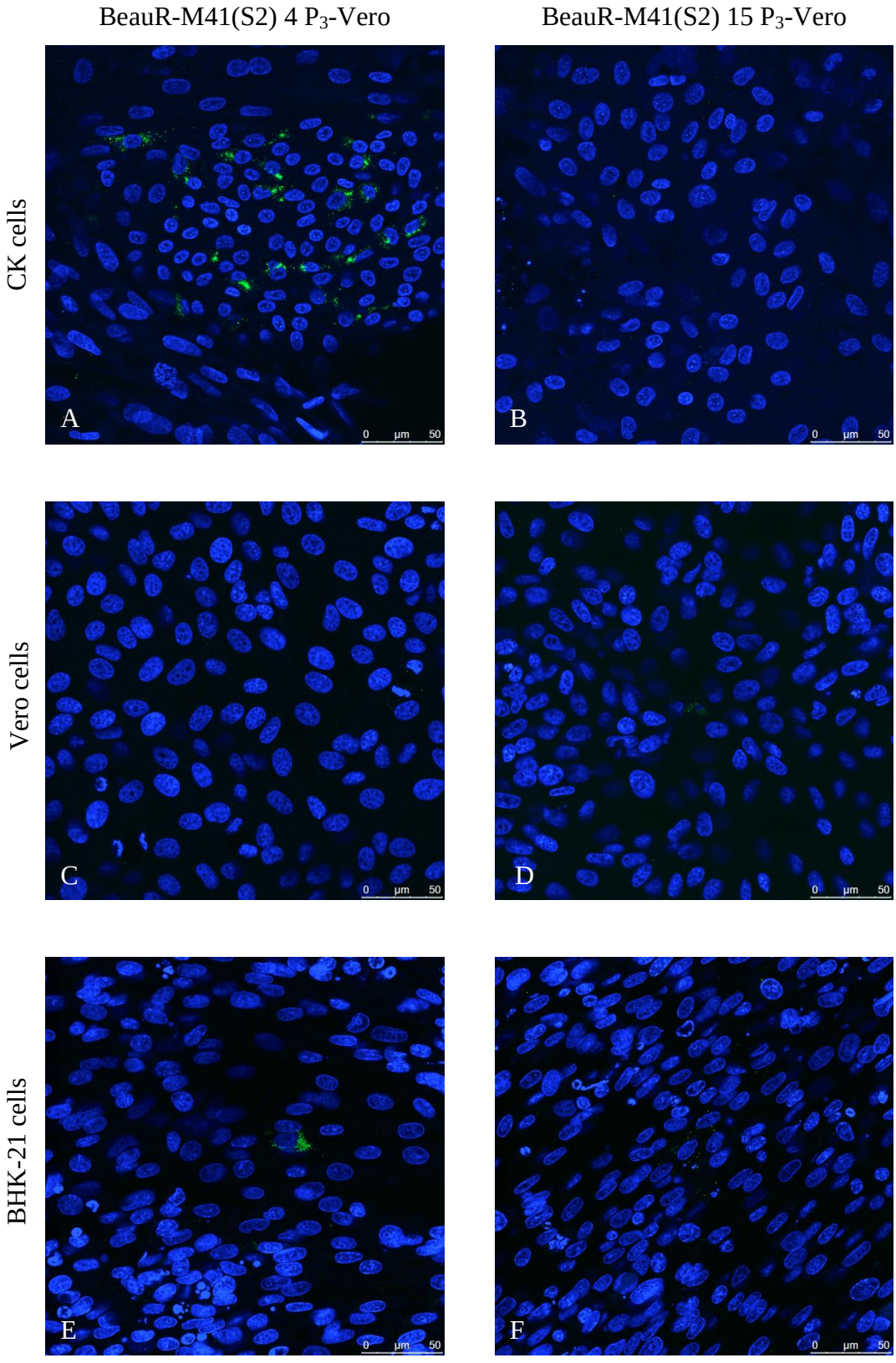
BeauR-M41(S2) 4 P3-Vero
BeauR-M41(S2) 15 P3-Vero
CK cells
Vero cells
BHK-21 cells
A
B
C
D
E
F
0 µm 50

Growth kinetics of rIBVs on CK, Vero and BHK-21 cells

Chick kidney, Vero and BHK-21 cells were infected with Beau-R, M41-CK, BeauR-M41(S), BeauR-M41(S1) 2 P_3-CKC and BeauR-M41(S2) 4 P_3-CKC at a multiplicity of infection of 0.1. Supernatant from the infected cells was harvested at 1, 12, 24, 48 and 72 hours post-infection and titrated on CK cells. Three replicates were performed and the averages taken (Figures 3.20 – 3.22). RNA was extracted from selected samples, RT-PCRs were carried out across the S gene and sequenced to check that the correct virus was present.

All viruses were shown to replicate to a similar titre on CK cells (Figure 3.20). Peak titres for all viruses were observed at 48 hours post-infection. Growth of BeauR-M41(S1) and BeauR-M41(S2) was observed to be slower than the parent viruses between 1 – 24 hours post-infection. At 24 hours post-infection, the titres of the parent virus controls were between 6 x 10^5 pfu/ml (M41-CK) and 7 x 10^7 pfu/ml (Beau-R), whereas the two recombinant virus titres were 1.5 x 10^2 and 5 x 10^2 pfu/ml for BeauR-M41(S1) and BeauR-M41(S2) respectively, a 10^3 – 10^5 fold difference in titre. The recombinant viruses reached similar titres to the parental viruses by 48 hours post-infection with titres for all viruses declining after 48 hours post-infection.

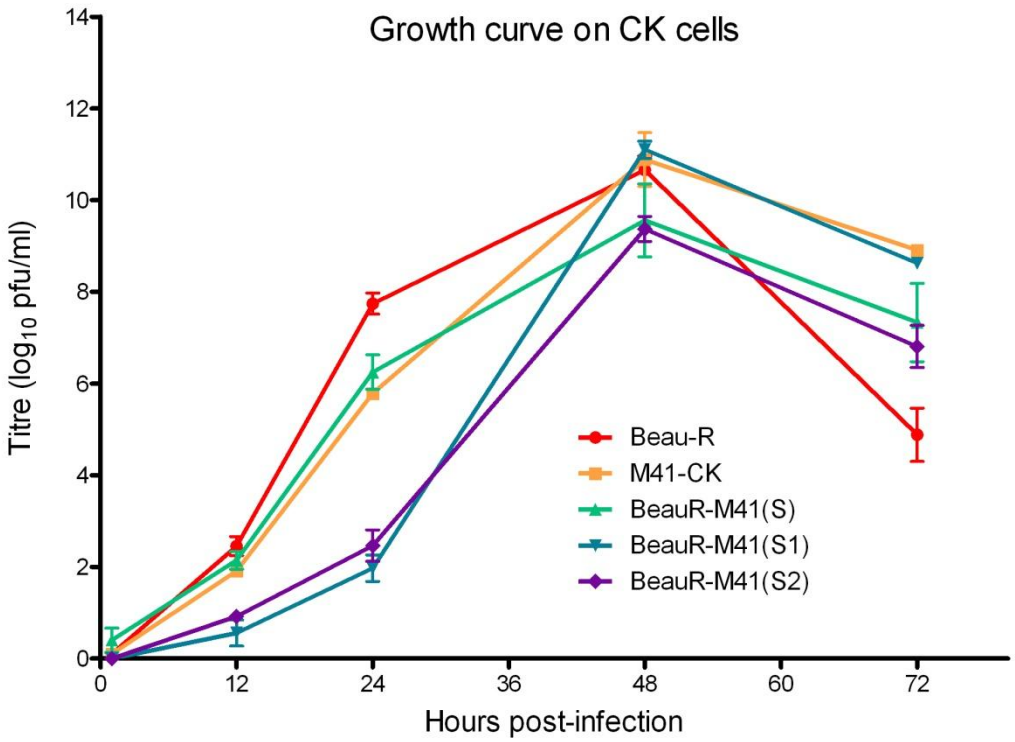

Figure 3.20. Growth kinetics of rIBVs on CK cells. Chick kidney cells were infected with Beau-R, M41-CK, BeauR-M41(S), BeauR-M41(S1) 2 P_3-CKC and BeauR-M41(S2) 4 P_3-CKC at a multiplicity of infection of 0.1. Supernatant was harvested at 1, 12, 24, 48 and 72 hours post-infection and titrated on CK cells. Three replicates were performed and the averages taken. Error bars indicate standard error of the mean.

Beau-R replicated to the highest titre on Vero cells (Figure 3.21). Growth of M41-CK, BeauR-M41(S) and BeauR-M41(S2) did not reach titres greater than 1.5 $\log_{10}$ pfu/ml on Vero cells. BeauR-M41(S1) followed a similar growth curve to Beau-R on Vero cells but final titres of BeauR-M41(S1) were approximately 10^3-fold lower than those of Beau-R. Unlike on CK cells (Figure 3.20), replication of Beau-R and BeauR-M41(S1) did not peak at 48 hours post-infection but rather continued to increase until 72 hours post-infection, the final time point measured.

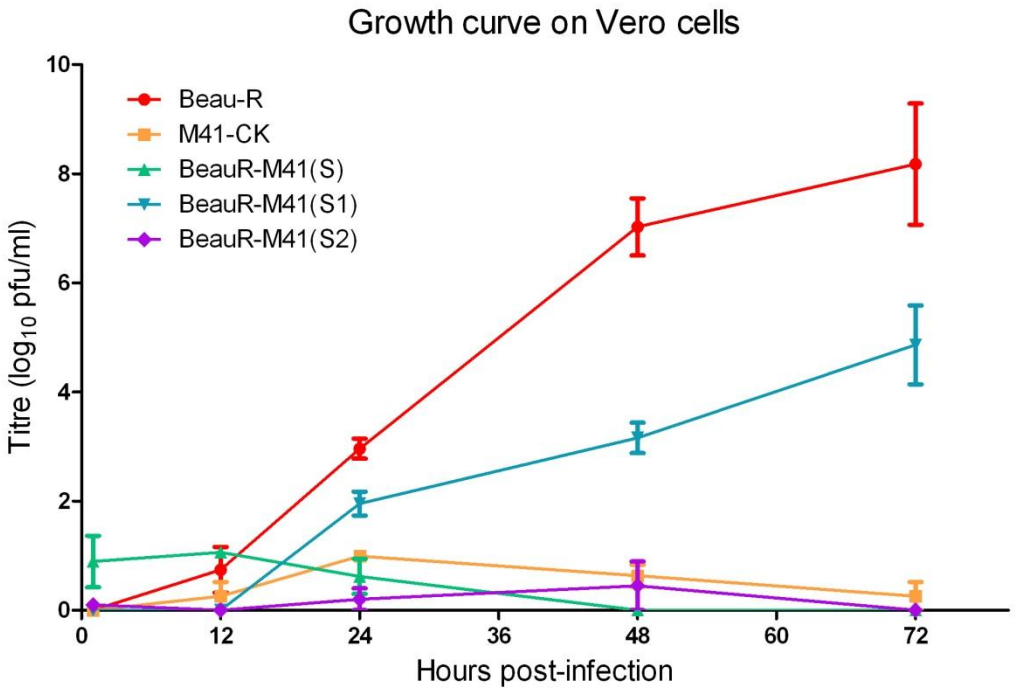

Figure 3.21. Growth kinetics of rIBVs on Vero cells. Vero cells were infected with Beau-R, M41-CK, BeauR-M41(S), BeauR-M41(S1) 2 P_3-CKC and BeauR-M41(S2) 4 P_3-CKC at a multiplicity of infection of 0.1. Supernatant was harvested at 1, 12, 24, 48 and 72 hours post-infection and titrated on CK cells. Three replicates were performed and the averages taken. Error bars indicate standard error of the mean.

Beau-R replicated to the highest titre on BHK-21 cells (Figure 3.22). Unlike on CK cells (Figure 3.20), replication of Beau-R did not peak at 48 hours post-infection but rather continued to increase until 72 hours post-infection, the final time point measured. This followed a similar pattern to growth of Beau-R on Vero cells (Figure 3.21). No growth of M41-CK was observed and BeauR-M41(S) did not reach titres greater than 10 pfu/ml on BHK-21 cells.

BeauR-M41(S1) growth was very low for the first 24 hours post-infection then increased at 48 hours post-infection. Final titres of BeauR-M41(S1) were 8.67×10^4 pfu/ml, approximately 1700-fold lower than those of Beau-R. No growth of BeauR-M41(S2) was observed on BHK-21 cells.

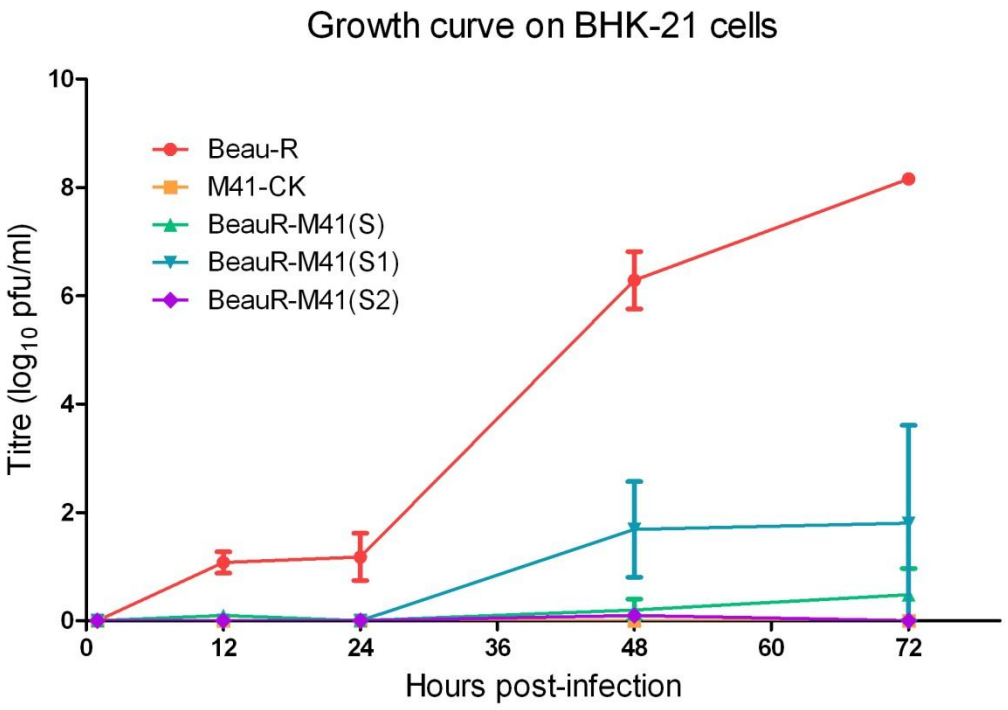

Figure 3.22. Growth kinetics of rIBVs on BHK-21 cells. Baby hamster kidney-21 cells were infected with Beau-R, M41-CK, BeauR-M41(S), BeauR-M41(S1) 2 P_3-CKC and BeauR-M41(S2) 4 P_3-CKC at a multiplicity of infection of 0.1. Supernatant was harvested at 1, 12, 24, 48 and 72 hours post-infection and titrated on CK cells. Three replicates were performed and the averages taken. Error bars indicate standard error of the mean.

Discussion

Two isolates each of the recombinant viruses, BeauR-M41(S1) and BeauR-M41(S2), were successfully rescued and passaged in CK cells, demonstrating that it is possible to generate viable rIBV with chimaeric S glycoproteins. The S gene sequences were verified both prior to rescue and after three passages in CK cells. The P_3-CKC isolates of both BeauR-M41(S1) and BeauR-M41(S2) grew well on CK cells as shown by confocal microscopy (Figures 3.15 and 3.18) and replicated to a similar titre to the parent viruses on CK cells (Figure 3.20).

These are the first rIBVs to have chimaeric S genes with one subunit from a different strain of IBV to the rest of the genome. A previous study replaced the ectodomain of the S glycoprotein of Beaudette with that of M41 within the background of Beau-R, creating BeauR-M41(S) (Casais *et al.,* 2005). This virus exhibited the *in vitro* cellular tropism of M41, however did not replicate as well as M41 in the trachea and nose of infected birds and was apathogenic like Beau-R, not pathogenic like M41 (Hodgson *et al.*, 2004).

The P_3-CKC isolates of BeauR-M41(S1) and BeauR-M41(S2) were passaged on Vero cells. In order to determine whether the rIBVs were able to sustain replication on the mammalian cell line, RNA was extracted from the cell culture supernatant of passages 1 – 3 and RT-PCRs carried out across the end of the S gene (Figure 3.11). The P_3-Vero isolates were titrated on CK cells (Table 3.1). The P_3-Vero isolates were grown on CK, Vero and BHK-21 cells in order to assess their growth

phenotypes by confocal microscopy with indirect immunofluorescence (Figures 3.16 and 3.19).

Growth of BeauR-M41(S2) P_3-CKC isolates on Vero and BHK-21 cells yielded very few infected cells (Figure 3.18) and the rIBVs were unable to sustain replication on Vero cells after three passages. Titres and RT-PCR products were dramatically reduced by P_3-Vero (Table 3.1 and Figure 3.11). Unsurprisingly, when CK, Vero or BHK-21 cells were inoculated with BeauR-M41(S2) P_3-Vero cell culture supernatant, very few infected cells were observed by confocal microscopy with indirect immunofluorescence (Figure 3.19).

BeauR-M41(S1) was found to be able to replicate well on Vero cells and all RT-PCRs were positive for virus presence (Figure 3.11). Infectious centres were formed when BeauR-M41(S1) P_3-CKC and P_3-Vero isolates were grown on CK and Vero cells (Figures 3.15 and 3.16). BeauR-M41(S1) P_3-CKC and P_3-Vero isolates infected BHK-21 cells but did not form infectious centres.

Four further passages of BeauR-M41(S1) P_3-Vero isolates were carried out on Vero cells and virus replication was maintained. The P_7-Vero isolates were also titrated on CK cells (Table 3.1) and their growth phenotypes on CK, Vero and BHK-21 cells were assessed by confocal microscopy with indirect immunofluorescence (Figure 3.17). The growth phenotypes of the P_7-Vero isolates were similar to that of the earlier passages, infectious centres were formed on CK and Vero cells but not BHK-21 cells, although replication still occurred (Figures 3.15 – 3.17).

Titres of the P_3-Vero isolates were lower than the P_3-CKC isolates on CK cells, although these had increased by P_7-Vero (Table 3.1). Additional passages on Vero cells further adapted the BeauR-M41(S1) isolates to growth on Vero cells and the P_5-Vero isolates began to form syncytia, a characteristic maintained at least until P_7 (Figure 3.12). The S genes of the P_7-Vero isolates were sequenced in order to identify any amino acid changes that could be responsible for this change in growth phenotype (Figure 3.13).

Five nucleotide differences were identified between the P_7-Vero isolates and the parent, Beau-R and M41-CK, S gene sequences. These resulted in three amino acid changes, one of which was shared between both isolates. All changes occurred within the S2 subunit of the S glycoprotein. The S2 subunit is responsible for virus-cell and cell-cell fusion (Luo and Weiss, 1998), and it is possible that one or more of these changes could be involved in syncytium formation in Vero cell culture.

A recent study by Yamada *et al.*, (2009) has suggested a number of amino acid substitutions in the S glycoprotein of IBV that may be involved in the acquisition of cell-cell fusion activity *in vitro*, however none of these correspond to the changes identified in the BeauR-M41(S1) P_7-Vero S glycoproteins.

In depth analysis of the growth kinetics of BeauR-M41(S1) and BeauR-M41(S2) P_3-CKC isolates on Vero and BHK-21 cells was carried out by growth curves (Figures 3.21 and 3.22). Unlike on CK cells (Figure 3.20), titres did not peak at 48 hours post-infection, rather continued to increase until the last time point at 72 hours post-infection. Beau-R grew to the highest titre on both Vero and BHK-21 cells, followed

by BeauR-M41(S1). Although the peak titre of BeauR-M41(S1) on Vero cells was lower than that of Beau-R, it must be remembered that this was the first time that the P_3-CKC isolate had been grown on Vero cells. The titres of the P_7-Vero isolates were higher than the titres of the P_3-Vero isolates, and were within one – two $\log_{10}$ of the Beau-R titre on CK cells (Table 3.1). It would be reasonable to suppose that growth curves carried out with a P_7-Vero isolate rather than a P_3-CKC isolate would be closer to those of Beau-R on Vero cells.

As expected from the analysis of the growth phenotypes by confocal microscopy, BeauR-M41(S2) replicated very poorly on Vero and BHK-21 cells and followed a similar growth curve to M41-CK and BeauR-M41(S) on both cell types.

It appears that while BeauR-M41(S1) is able to replicate on Vero cells, BeauR-M41(S2) is not, indicating that it is the S2 subunit of Beau-R that confers the ability to grow on Vero cells.

Although it was not anticipated that the S2 subunit would be the determinant of cellular tropism as it is the S1 subunit that contains the receptor binding domain (Cavanagh *et al.*, 1986), a report by Koch *et al.*, (1990) identified a neutralizing monoclonal antibody (MAb) against part of the IBV S2 subunit, suggesting that this area may be involved in binding or fusion of IBV to host cells.

A study by de Haan *et al.*, (2006) generated several recombinant viruses based on MHV-A59 but with chimaeric S glycoproteins where parts of the spike were derived from cell culture-adapted virus MHV/BHK. It was determined that a combination

of amino acids in the S1 and S2 subunits were responsible for the extended host range of MHV/BHK in cell culture. A previous study exchanging just an amino-terminal section of the MHV-A59 spike for that of MHV/BHK resulted in a virus with the extended host range of MHV/BHK but unable to induce a second round of infection in nonmurine cells (Thackray and Holmes, 2004).

Replication on BHK-21 cells may be controlled by different factors to replication on Vero cells. Whereas BeauR-M41(S1) replicated well on Vero cells, the virus replicated to a much lower titre on BHK-21 cells and BeauR-M41(S2) was unable to replicate on either cell type. Passage of BeauR-M41(S1) on BHK-21 cells may adapt the virus for growth on this cell type.

Chapter 4: Investigation into the role of the Beaudette–specific motif in cellular tropism

Summary

Two recombinant IBVs, with either the Beaudette-specific motif from Beau-R or the corresponding sequence from M41 within the S gene of the other strain and the genomic background of Beaudette, were generated using a vaccinia virus reverse genetics system. The growth characteristics and cellular tropism of the rIBVs were investigated. The Beaudette-specific motif of Beaudette was found to be sufficient to confer the ability to grow on Vero cells to a rIBV with the M41 S glycoprotein. Replacement of the Beaudette-specific motif with the corresponding sequence from M41 in the Beau-R S glycoprotein resulted in loss of ability to grow on Vero cells.

Introduction

Results from Chapter 3 showed that the S2 subunit (Figure 4.1) of the S glycoprotein is responsible for the extended cellular tropism of Beau-R in cell culture. In order to further narrow down the area of the S2 subunit involved in determination of tropism, additional recombinant viruses were created with chimaeric S genes.

A heparan sulphate binding site was identified between amino acid residues 686 – 691 within the S2 subunit of the Beaudette S glycoprotein by Madu *et al.*, (2007). This binding site was not identified in any other strain of IBV investigated. Results

from the work indicate that heparan sulphate might be involved as a cofactor in Beaudette virus entry to host cells.

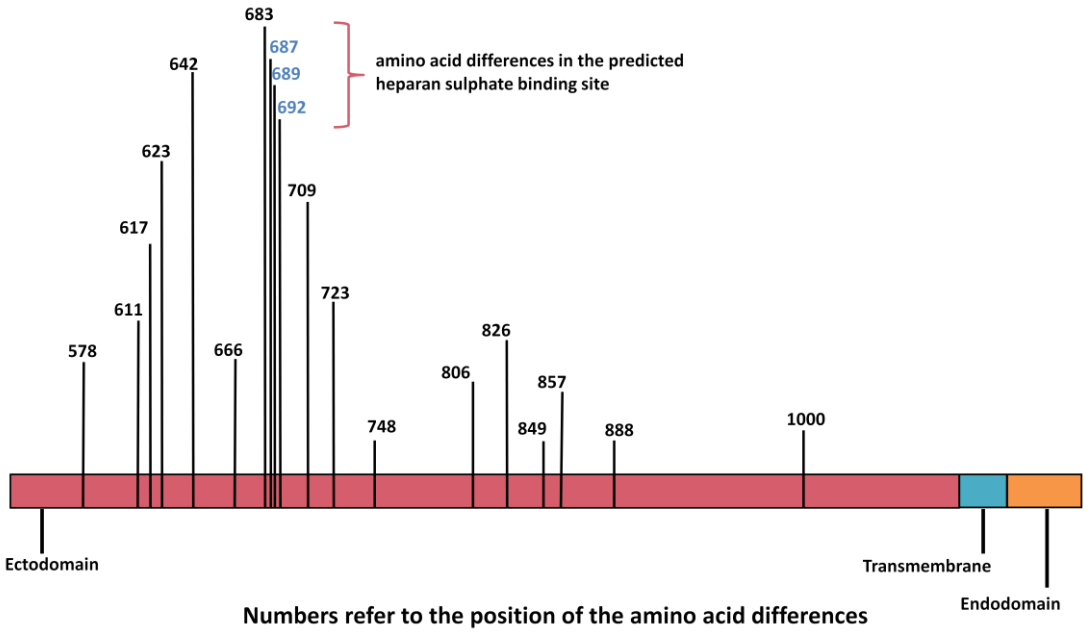

Figure 4.1. Locations of the amino acid differences between Beau-R and M41-CK within the S2 subunit of the S glycoprotein. The S2 subunit contains 19 amino acid differences between Beau-R and M41-CK, three of which comprise a putative heparan sulphate binding site, shown in blue.

Heparan sulphate is a glycosaminoglycan (GAG) found on the surface of mammalian cells (Liu and Thorp, 2002). The consensus sequence for a heparin-binding site is XBBXBX, where B is a basic amino acid and X is a hydropathic amino acid (Cardin and Weintraub, 1989). The sequence identified in the Beaudette S glycoprotein was $_{686}$SRRKRS$_{691}$ or $_{686}$SRRRRS$_{691}$ (Madu *et al.*, 2007). This sequence was not found in the S glycoprotein of any other strains of IBV, which is a possible explanation for the extended host range of Beaudette in comparison to M41. A number of other

viruses are also able to use heparan sulphate as an adhesion receptor, including foot and mouth disease virus and herpes simplex virus (Liu and Thorp, 2002). This Beaudette-specific motif, sequence $RRRR_{690}$/S, was later also identified by Yamada and Liu (2009) as a potential second cleavage site.

Taking into consideration work by Madu *et al.*, (2007) that the Beaudette-specific motif may have a potential role in conferring the ability of Beaudette to grow on Vero cells, the sequences of several IBV strains were compared. Due to the presence of an amino acid change immediately upstream of the motif identified by Madu *et al.*, (2007), we decided to investigate an extended Beaudette-specific motif, $_{686}$SRRKRSLIE$_{694}$.

Two recombinant IBVs were designed to investigate the role of the Beaudette-specific motif on the ability of Beau-R to grow on Vero cells. One virus, rIBV BeauR-S-M41-Hep, has the genomic background and S gene of Beau-R with the Beaudette-specific motif replaced with the corresponding sequence from M41, $_{686}$SPRRRSFIE$_{694}$. The other virus, rIBV M41-S-BeauR-Hep, is based on BeauR-M41(S) and has the S gene from M41 within the genomic background of Beau-R but with the Beaudette-specific motif, sequence $_{686}$SRRKRSLIE$_{694}$, also from Beau-R (Figure 4.2). The growth characteristics of these viruses were determined on various cell types by confocal microscopy and growth curves.

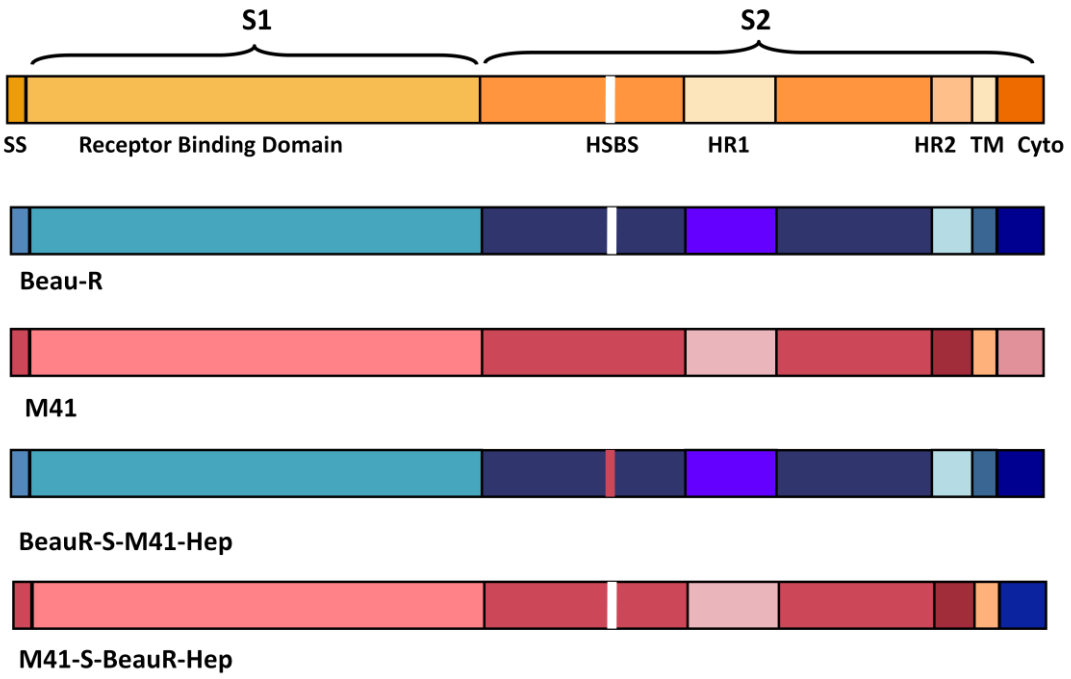

Figure 4.2. Schematic diagram of the S genes of different strains of IBV. The S1 domain contains the receptor binding domain and the cleaved signal sequence (SS). The S2 domain contains two heptad repeats, HR1 and 2, a transmembrane (TM) domain and a cytoplasmic (Cyto) domain. Beau-R also contains a putative heparan sulphate binding sequence (HSBS) not found in M41. The HSBS of Beau-R was introduced into the M41-CK S gene to create M41-S-BeauR-Hep and the equivalent sequence from M41-CK was introduced into the Beau-R S gene to create BeauR-S-M41-Hep.

Methods

Plasmids

Two plasmids were designed, one with a section of the Beau-R S gene with the Beaudette-specific motif, $_{686}$SRRKRSLIE$_{694}$, located within the S2 subunit replaced with the corresponding sequence from M41, $_{686}$SPRRRSFIE$_{694}$, (pGPT-BeauCK-S-M41-Hep). The other plasmid has a section of the M41 S gene with the Beaudette-specific motif, $_{686}$SRRKRSLIE$_{694}$, replacing the corresponding M41 S gene sequence, $_{686}$SPRRRSFIE$_{694}$, (pGPT-M41-S-BeauCK-Hep). These sequences were synthesised by Geneart and cloned into pGPT-NEB193 (Figure 4.3).

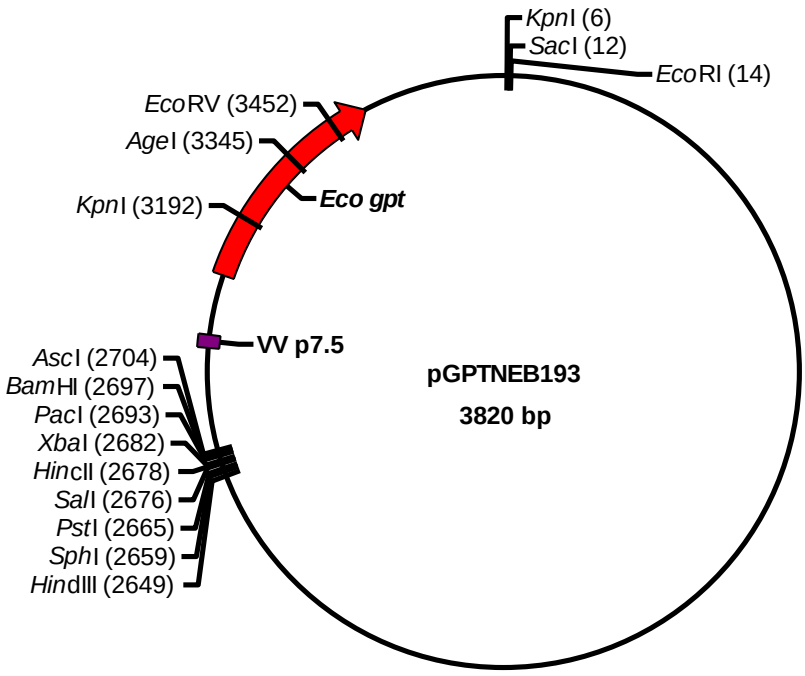

Figure 4.3. Diagram of pGPTNEB193. The modified S genes were cloned into plasmid pGPTNEB193 to create pGPT-M41-S-BeauCK-Hep and pGPT-BeauCK-S-M41-Hep (Figure 4.4).

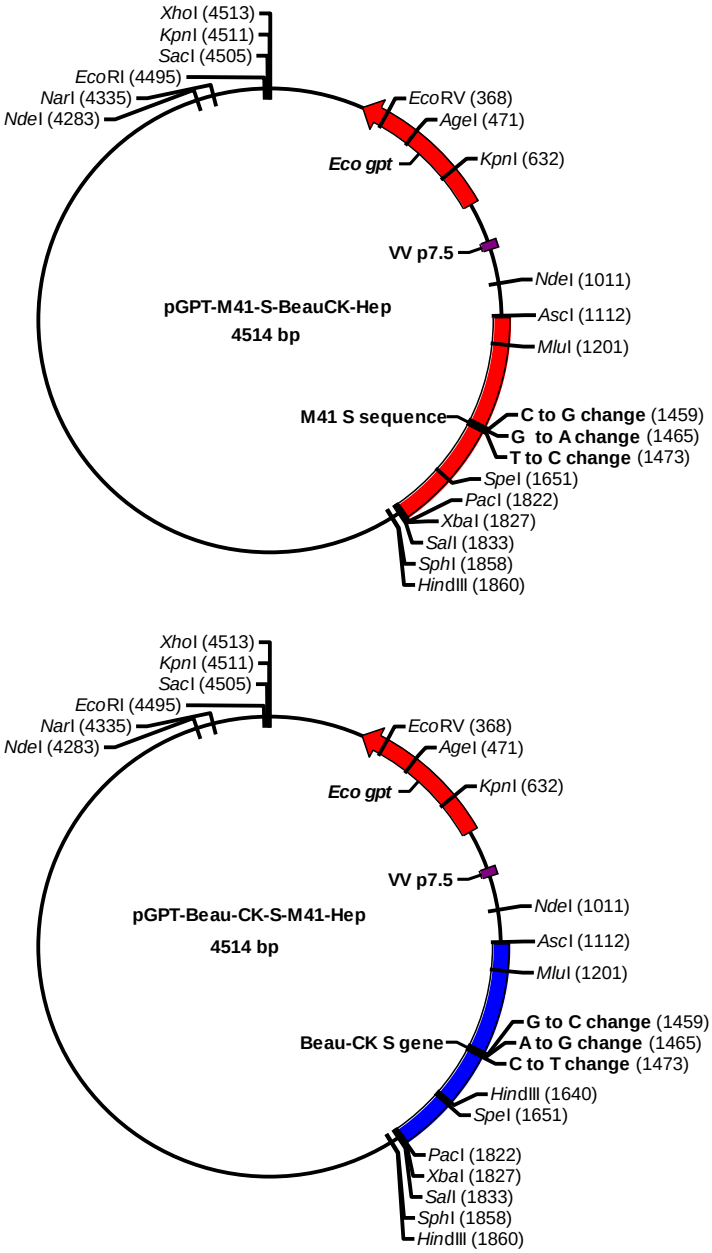

Figure 4.4. Diagrams of pGPT-M41-S-BeauCK-Hep and pGPT-BeauCK-S-M41-Hep. The plasmids pGPT-M41-S-BeauCK-Hep and pGPT-BeauCK-S-M41-Hep were used in the reverse genetics system to alter the sequence of BeauR-M41(S) (red) and Beau-R (blue) respectively.

Reverse genetics system

The plasmids pGPT-M41-S-BeauCK-Hep and pGPT-BeauCK-S-M41-Hep (Figure 4.4) were used to insert the modified S gene sequence into vNotI/IBVfl-M41S, a recombinant vaccinia virus (rVV) containing the full-length IBV Beau-R cDNA genome with the S gene from M41, or vNotI/IBVfl, an rVV containing the full-length IBV Beau-R cDNA genome, respectively. Two rVVs containing the correctly modified S gene sequence for each type were identified for recovery of rIBVs; isolates 7 and 20 of rIBV BeauR-S-M41-Hep and isolates 5 and 26 of rIBV M41-S-BeauR-Hep. These were rescued and passaged three times on CK cells followed by three times on Vero cells.

Results

Recovery and passage of rIBVs

Rescue of rIBV BeauR-S-M41-Hep and M41-S-BeauR-Hep in CK cells

DNA was extracted from two isolates of each rVV containing the rIBV cDNA with modified S gene sequences, digested with SalI and analysed by pulsed field gel electrophoresis to check that the entire rIBV cDNA genome was intact. This is indicated by the presence of a 30kb SalI restriction fragment. An example pulsed field gel is shown in Chapter 3, Figure 3.6. The chimaeric S gene sequences were verified by sequencing then two isolates each of rIBV BeauR-S-M41-Hep, isolates 7 and 20, and M41-S-BeauR-Hep, isolates 5 and 26, were rescued from CK cells.

Sequencing of P_3-CKC rIBVs

The rescued viruses were passaged three times on CK cells. At each passage on CK cells, RNA was extracted from the infected cell supernatant and RT-PCRs were carried out across the end of the S genes to confirm virus presence. The entire S gene sequences of the P_3-CKC viruses were confirmed by sequence analysis (Figures 4.5 and 4.6). The BeauR-S-M41-Hep sequences correspond to that of the Beau-R sequence apart from the Beaudette-specific motif, which matches the M41 sequence. The M41-S-BeauR-Hep sequences correspond to that of the M41 sequence apart from the Beaudette-specific motif, which matches the Beau-R sequence.

Figure 4.5. Sequencing to check the Beaudette-specific motif of BeauR-S-M41-Hep P_3-CKC isolates. Sequence analysis of the BeauR-S-M41-Hep isolates showed that the Beaudette-specific motif in the Beau-R S gene had been changed to the corresponding M41 sequence, G➔C, A➔G and C➔T. The rest of the S gene sequence corresponded to Beau-R. The nucleotide positions are shown above each section of sequencing. Nucleotides corresponding to the consensus sequence are shown by dots, differing nucleotides are shown by letter. The highlighted nucleotide is indicated by a blue line on the sequence trace.

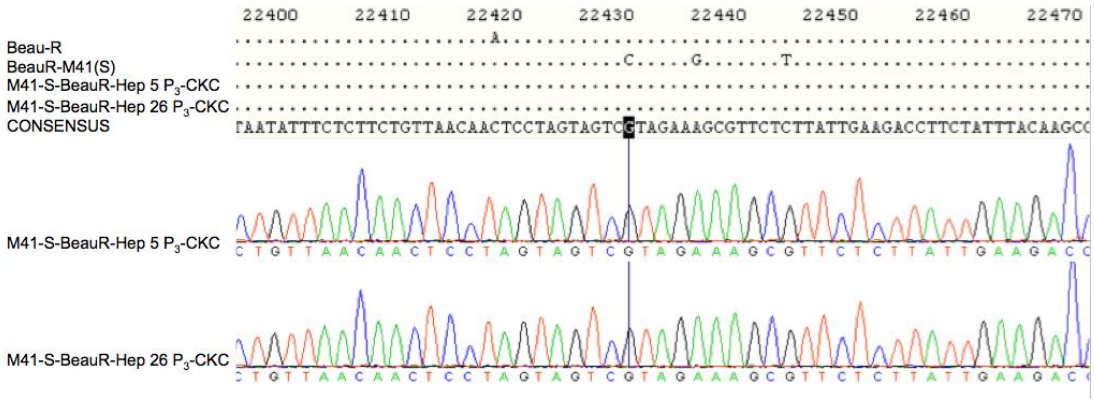

Figure 4.6. Sequencing to check the Beaudette-specific motif of M41-S-BeauR-Hep P_3-CKC isolates. Sequence analysis of the M41-S-BeauR-Hep isolates showed that the Beaudette-specific motif had been introduced into the M41 S gene sequence, C➔G, G➔A and T➔C. The rest of the S gene sequence corresponds to M41-CK. The nucleotide positions are shown above each section of sequencing. Nucleotides corresponding to the consensus sequence are shown by dots, differing nucleotides are shown by letter. The highlighted nucleotide is indicated by a blue line on the sequence trace.

Passage of P_3-CKC rIBVs on Vero cells

The P_3-CKC rIBVs were passaged three times on Vero cells to determine whether virus replication could be maintained on this mammalian cell line. At each passage, RNA was extracted and RT-PCRs were carried out across the end of the S genes to confirm virus presence (Figure 4.7). The RT-PCR results showed that both M41-S-BeauR-Hep isolates grew on Vero cells at each passage. Cytopathic effect in the form of rounded and floating cells were observed from around 24 hours post-infection. The RT-PCRs for the presence of BeauR-S-M41-Hep isolates were negative by passage 3.

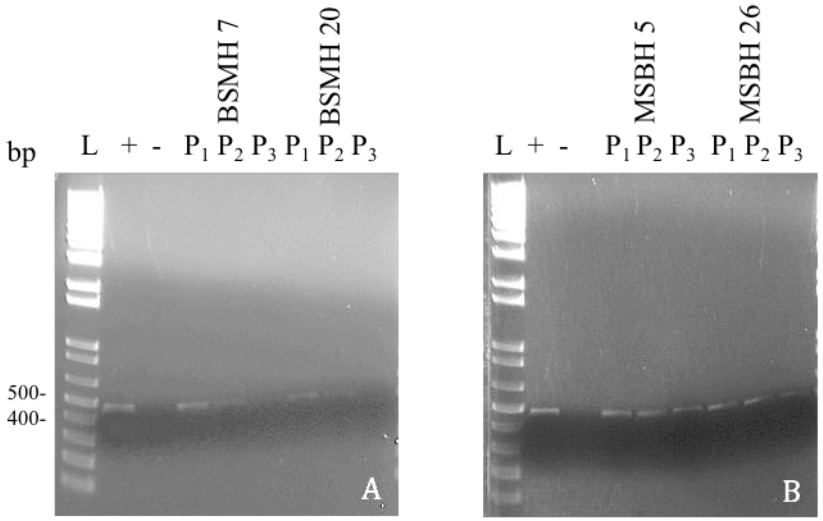

Figure 4.7. Agarose gel analysis of RT-PCR products from rIBV BeauR-S-M41-Hep and M41-S-BeauR-Hep P_{1-3}-Vero isolates. RNA was extracted from Vero cell culture supernatants of (A) BeauR-S-M41-Hep (BSMH) 7 and 20 and (B) M41-S-BeauR-Hep (MSBH) 5 and 26 P_{1-3}-Vero. RT-PCRs were carried out on each. A molecular size ladder (L) is shown to compare the sizes of DNA fragments. The positive control (+) shows a band between 400-500 bp. Negative control (-) shows no band. All passages of M41-S-BeauR-Hep have bands of correct sizes. Band intensity decreases from P_{1-3} of BeauR-S-M41-Hep so that P_3 of both isolates can no longer be seen.

BeauR-S-M41-Hep isolates caused no cpe when grown on Vero cells (Figure 4.8). M41-S-BeauR-Hep P_3-Vero isolates were further passaged on Vero cells to establish whether viral replication could be maintained on this cell type. It was decided to stop passaging at P_7 as M41-S-BeauR-Hep replication appeared to be stable on Vero cells. Typical cpe produced by infection of Vero cells with M41-S-BeauR-Hep P_7-Vero isolates included rounded and floating cells and syncytia formation.

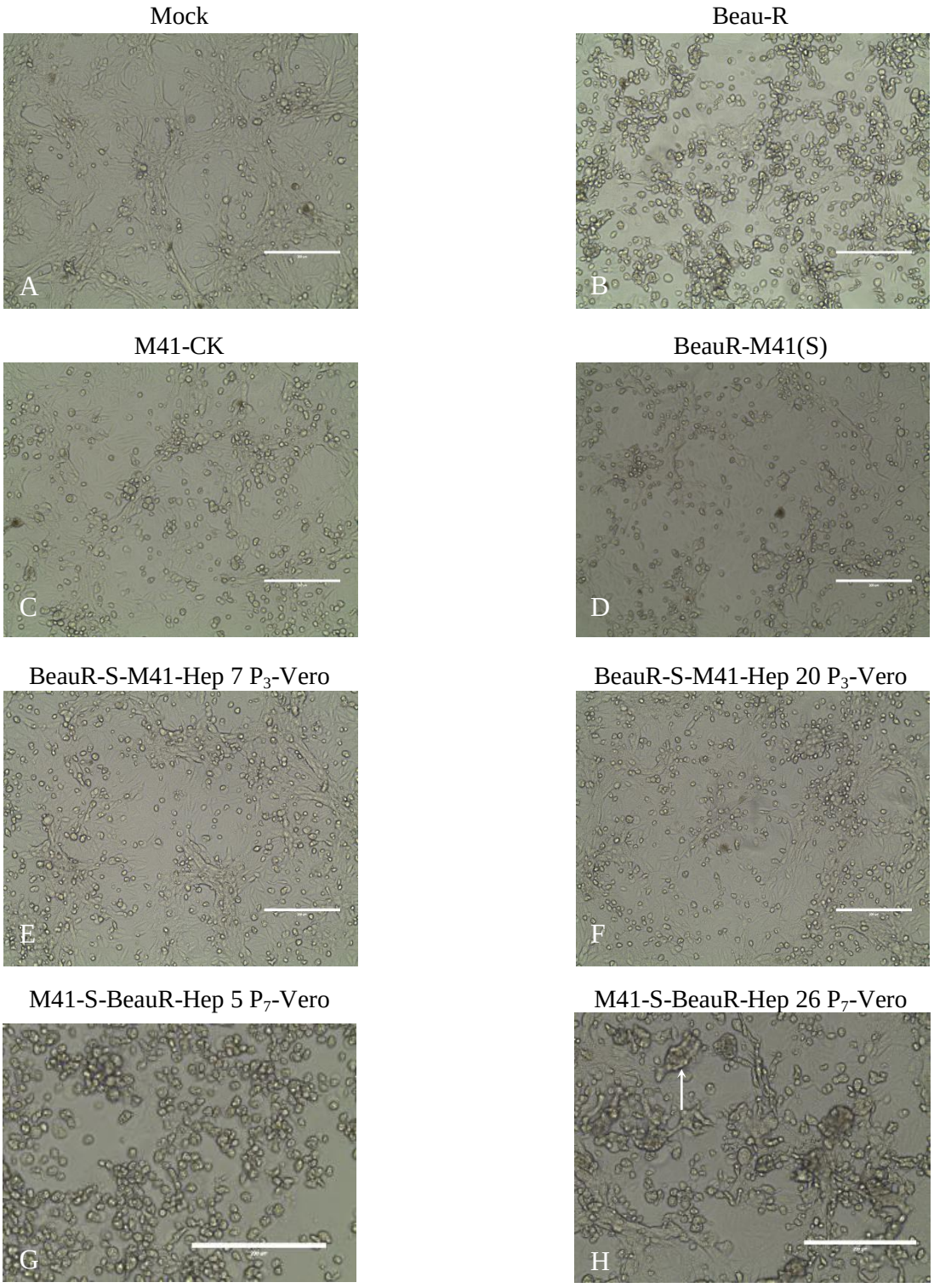

Figure 4.8. Brightfield microscopy of rIBV growth on Vero cells. Vero cells infected with A. mock, B. Beau-R, C. M41-CK, D. BeauR-M41(S), E. BeauR-S-M41-Hep 7 P_3-Vero, F. BeauR-S-M41-Hep 20 P_3-Vero, G. M41-S-BeauR-Hep 5 P_7-Vero, H. M41-S-BeauR-Hep 26 P_7-Vero. Syncytia indicated by arrows. Photographs taken 48 hours post-infection.

Sequencing of M41-S-BeauR-Hep P_7-Vero S genes

RNA was extracted from infected cell supernatant and RT-PCRs were carried out across the S gene. These were then sequenced and compared to Beau-R and BeauR-M41(S) sequences (Figure 4.9). Three nucleotide differences were identified between the M41-S-BeauR-Hep P_7-Vero isolates and the parent viruses, Beau-R and BeauR-M41(S); one is located within the S1 subunit and two are located within the S2 subunit. None of the amino acid changes identified in the M41-S-BeauR-Hep P_7-Vero isolates correspond to those identified in BeauR-M41(S1) P_7-Vero isolates (Chapter 3, Figure 3.13).

The first nucleotide change is located at nucleotide position 21818. Beau-R has an A at this position, M41 and M41-S-BeauR-Hep isolate 26 P_7-Vero have a C at this position and M41-S-BeauR-Hep isolate 5 P_7-Vero has a T (Figure 4.9A). This results in an amino acid change of asparagine (Beau-R)/threonine (M41) to isoleucine.

The second nucleotide change occurs at position 22227 and was identified in isolate 26 only (Figure 4.9B). This results in an amino acid change of aspartic acid to alanine. The third nucleotide change was identified in isolate 5 only and occurs at position 22966, resulting in an amino acid change of glutamine to histidine (Figure 4.9C). It is possible that these changes could contribute to the further adaptation of M41-S-BeauR-Hep to growth on Vero cells.

Figure 4.9. Sequencing of M41-S-BeauR-Hep P_7-Vero S genes. RNA was extracted from M41-S-BeauR-Hep P_7-Vero cell culture supernatant, RT-PCRs were carried out across the S gene, purified and sequenced in positive and negative directions. Three nucleotide differences were observed in the S genes of M41-S-BeauR-Hep P_7-Vero isolates when compared to Beau-R and BeauR-M41(S); one occurred within the S1 subunit and two occurred within the S2 subunit. The sequences of the S genes otherwise corresponded to M41, apart from the Beaudette-specific motif in the S2 subunit. The nucleotide positions are shown above each section of sequencing. Nucleotides corresponding to the consensus sequence are shown by dots, differing nucleotides are shown by letter. The highlighted nucleotide is indicated by a blue line on the sequence trace.

A

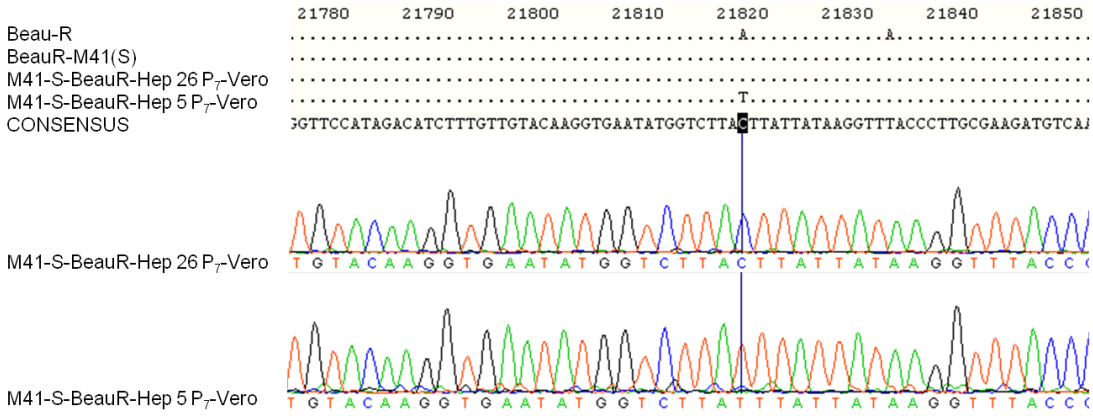
21780
21790
21800
21810
21820
21830
21840
21850
Beau-R
BeauR-M41(S)
M41-S-BeauR-Hep 26 P7-Vero
M41-S-BeauR-Hep 5 P7-Vero
CONSENSUS
M41-S-BeauR-Hep 26 P7-Vero
M41-S-BeauR-Hep 5 P7-Vero

B

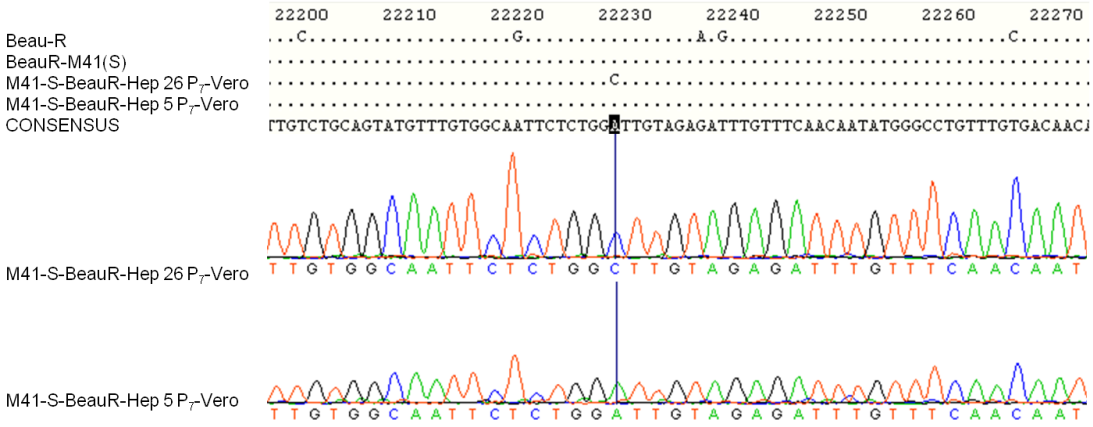
22200
22210
22220
22230
22240
22250
22260
22270
Beau-R
BeauR-M41(S)
M41-S-BeauR-Hep 26 P7-Vero
M41-S-BeauR-Hep 5 P7-Vero
CONSENSUS
M41-S-BeauR-Hep 26 P7-Vero
M41-S-BeauR-Hep 5 P7-Vero

C

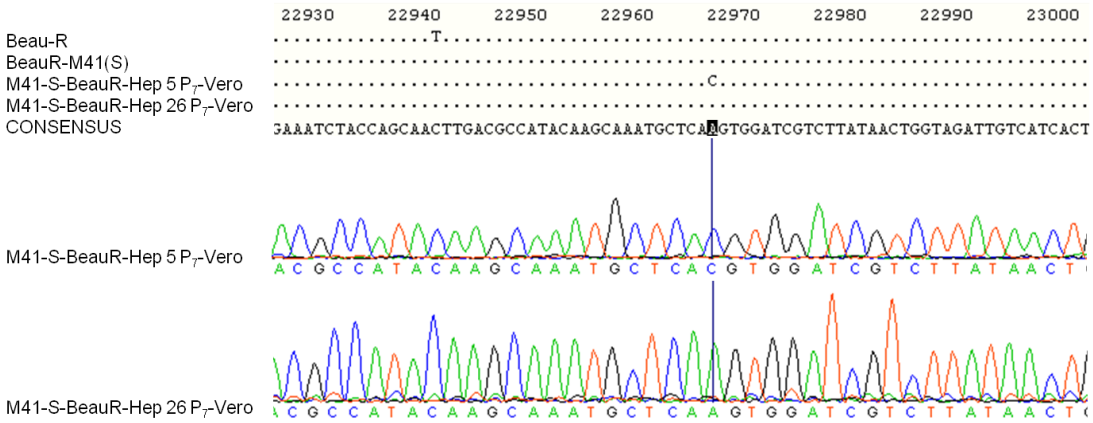
22930
22940
22950
22960
22970
22980
22990
23000
Beau-R
BeauR-M41(S)
M41-S-BeauR-Hep 5 P7-Vero
M41-S-BeauR-Hep 26 P7-Vero
CONSENSUS
M41-S-BeauR-Hep 5 P7-Vero
M41-S-BeauR-Hep 26 P7-Vero

Titration of rIBVs on CK cells

Isolates 7 and 20 of rIBV BeauR-S-M41-Hep P_3-CKC and P_3-Vero and isolates 5 and 26 of rIBV M41-S-BeauR-Hep P_3-CKC, P_3-Vero and P_7-Vero were titrated on CK cells and compared to parent strains of IBV, Beau-R, M41-CK and BeauR-M41(S) (Table 4.1). Beau-R and BeauR-M41(S) are recombinant IBV strains, M41-CK is not. The titres for the P_3-CKC recombinant viruses were comparable to those of laboratory strains Beau-R and M41-CK. No plaques were produced by BeauR-S-M41-Hep P_3-Vero isolates. The titres of the M41-S-BeauR-Hep P_3-Vero isolates were lower than those of the P_3-CKC isolates, indicating that the Beaudette-specific motif alone may not confer the full ability to grow on Vero cells, when compared to the complete Beaudette S2 subunit (Chapter 3). However, further passage of M41-S-BeauR-Hep on Vero cells to P_7 increased the titre to a similar level as the P_3-CKC isolates.

Table 4.1. Comparison of virus titres on CK cells. Virus supernatant was serially diluted 1:10 in cell culture medium. Confluent CK cells in six-well plates were infected with 500 µl diluted supernatant in duplicate and incubated at 37°C for 1 hour. Inoculum was replaced with 3 ml medium containing 1% agar and plates were incubated at 37°C for 48 – 72 hours. Living cells were stained with 0.01% neutral red and plaques counted several hours later. The number of plaque forming units (pfu) per ml was calculated. The titres are an average of three separate experiments.

Virus	**Titre (pfu/ml)**
Beau-R	9×10^9
M41-CK	3×10^9
BeauR-M41(S)	3×10^4
BeauR-S-M41-Hep 7 P_3-CKC	5×10^9
BeauR-S-M41-Hep 7 P_3-Vero	0
BeauR-S-M41-Hep 20 P_3-CKC	3×10^9
BeauR-S-M41-Hep 20 P_3-Vero	0
M41-S-BeauR-Hep 5 P_3-CKC	8×10^9
M41-S-BeauR-Hep 5 P_3-Vero	2×10^5
M41-S-BeauR-Hep 5 P_7-Vero	4×10^9
M41-S-BeauR-Hep 26 P_3-CKC	9×10^9
M41-S-BeauR-Hep 26 P_3-Vero	4×10^5
M41-S-BeauR-Hep 26 P_7-Vero	5×10^8

Analysis of rIBV growth phenotypes by confocal microscopy

Chicken kidney, Vero and BHK-21 cells on coverslips were infected with isolates 7 and 20 of rIBV BeauR-S-M41-Hep P_3-CKC and P_3-Vero and isolates 5 and 26 of rIBV BeauR-M41-S-BeauR-Hep P_3-CKC and P_3-Vero. Cells were also infected with Beau-R, M41-CK and BeauR-M41(S) for comparison (Chapter 3, Figure 3.14). Infected cells were immunolabelled with mouse anti-dsRNA, secondary antibody AlexaFluor 488 goat anti-mouse (green). Nuclei were labelled with DAPI (blue).

The parent virus controls, Beau-R, M41-CK and BeauR-M41(S) all replicated in CK cells, forming infectious centres. Beau-R also replicated and formed infectious centres on Vero cells whereas infected BHK-21 cells were only observed singly. Only small numbers of infected Vero or BHK-21 cells were observed in wells infected with M41-CK or BeauR-M41(S) and no infectious centres were observed (Chapter 3, Figure 3.14).

BeauR-S-M41-Hep P_3-CKC isolates formed infectious centres in CK cells and only a small number of infected Vero cells were observed, none of which formed infectious centres. There appeared to be a greater number of infected BHK-21 cells although these too did not form infectious centres (Figure 4.10). No infected CK or Vero cells and just one infected BHK-21 cell were observed in wells infected with BeauR-S-M41-Hep P_3-Vero isolates (Figure 4.11).

While BeauR-S-M41-Hep P_3-CKC isolates grew well on CK cells and infected small numbers of Vero and BHK-21 cells, P_3-Vero isolates infected very few cells of any

type and formed no infectious centres. This is probably due to the reduction of virus titres to undetectable levels after three passages of BeauR-S-M41-Hep P_3-CKC isolates on Vero cells, as indicated in Figure 4.7 and Table 4.1. This confirms that replacement of the Beaudette-specific motif with the corresponding M41 sequence resulted in the loss of ability of the Beaudette S glycoprotein to confer growth on Vero cells.

BeauR-S-M41-Hep P_3-CKC isolates appeared to be able to infect more BHK-21 cells than Vero cells as there were a greater number of infected BHK-21 cells than Vero cells in separate wells infected with the same amount of virus inoculum. No infectious foci were observed with either cell type.

The BeauR-S-M41-Hep S2 subunit contains other amino acids that are different to M41 (Figure 4.1). It appears that other regions apart from the Beaudette-specific motif may be involved in the ability to grow on BHK-21 cells.

Figure 4.10. Confocal microscopy of rIBV BeauR-S-M41-Hep P_3-CKC growth on CK, Vero and BHK-21 cells. Chick kidney cells were infected with A. BeauR-S-M41-Hep 7 P_3-CKC, B. BeauR-S-M41-Hep 20 P_3-CKC. Vero cells were infected with C. BeauR-S-M41-Hep 7 P_3-CKC, D. BeauR-S-M41-Hep 20 P_3-CKC. Baby hamster kidney-21 cells were infected with E. BeauR-S-M41-Hep 7 P_3-CKC, F. BeauR-S-M41-Hep 20 P_3-CKC. Infected cells were fixed 24 hours post-infection and immunolabelled with anti-dsRNA, secondary antibody AlexaFluor 488 goat anti-mouse (green, Invitrogen). Nuclei were labelled with DAPI (blue). Images have been brightened for printing.

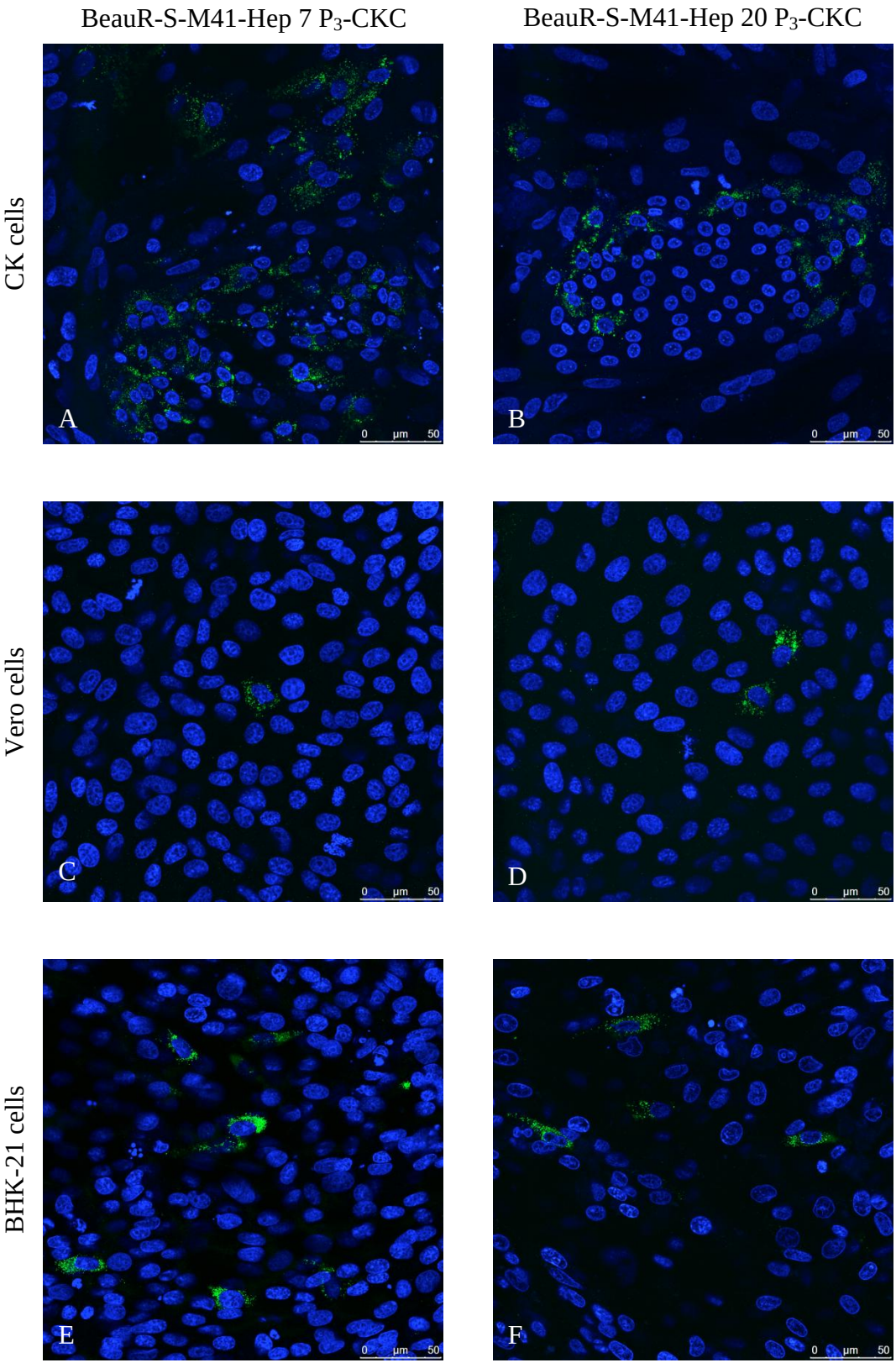
BeauR-S-M41-Hep 7 P3-CKC
BeauR-S-M41-Hep 20 P3-CKC
CK cells
Vero cells
BHK-21 cells
A
B
C
D
E
F
0 µm 50

Figure 4.11. Confocal microscopy of rIBV BeauR-S-M41-Hep P_3-Vero growth on CK, Vero and BHK-21 cells. Chick kidney cells were infected with A. BeauR-S-M41-Hep 7 P_3-Vero, B. BeauR-S-M41-Hep 20 P_3-Vero. Vero cells were infected with C. BeauR-S-M41-Hep 7 P_3-Vero, D. BeauR-S-M41-Hep 20 P_3-Vero. Baby hamster kidney-21 cells were infected with E. BeauR-S-M41-Hep 7 P_3-Vero, F. BeauR-S-M41-Hep 20 P_3-Vero. Infected cells were fixed 24 hours post-infection and immunolabelled with anti-dsRNA, secondary antibody AlexaFluor 488 goat anti-mouse (green, Invitrogen). Nuclei were labelled with DAPI (blue). Images have been brightened for printing.

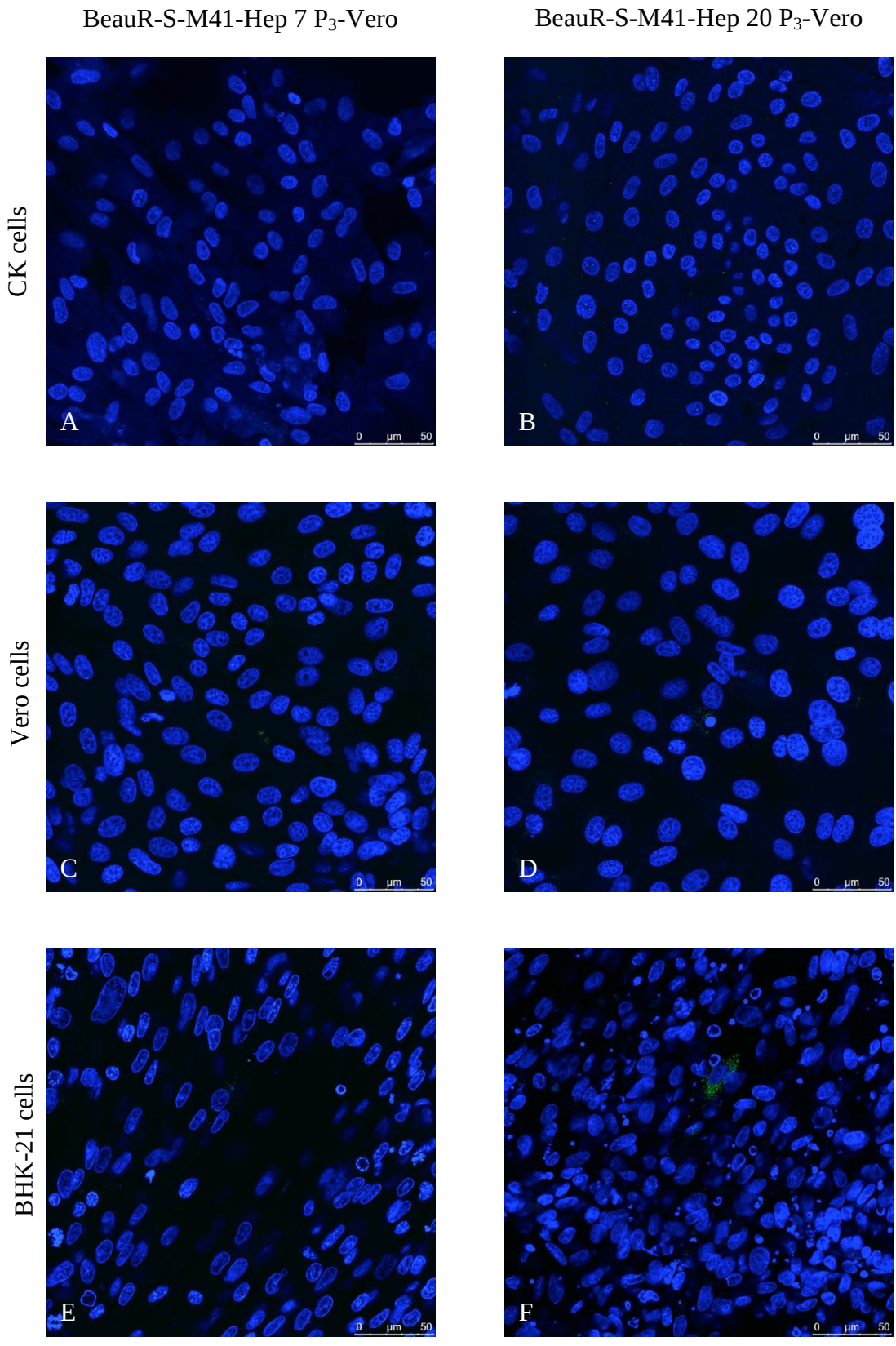
BeauR-S-M41-Hep 7 P3-Vero
BeauR-S-M41-Hep 20 P3-Vero
CK cells
Vero cells
BHK-21 cells
A
B
C
D
E
F
0 µm 50

Infectious centres were observed in CK and Vero cells infected with both M41-S-BeauR-Hep P_3-CKC isolates. A small number of infected BHK-21 cells were observed, however none were in infectious centres (Figure 4.12). Replication of M41-S-BeauR-Hep P_3-Vero isolates resulted in infectious centres in both CK and Vero cells. No infectious centres were formed on BHK-21 cells though some infected cells were observed (Figure 4.13).

There appears to be no difference between the growth phenotypes of the different M41-S-BeauR-Hep isolates on CK, Vero and BHK-21 cells. All isolates grew well on CK and Vero cells, forming infectious centres. The isolates grew less well on BHK-21 cells and infected cells were not observed in infectious foci, rather singly. Progeny virus from BHK-21 cells may be less infectious or less progeny virus may be released from BHK-21 cells.

Figure 4.12. Confocal microscopy of rIBV M41-S-BeauR-Hep P_3-CKC growth on CK, Vero and BHK-21 cells. Chick kidney cells were infected with A. M41-S-BeauR-Hep 5 P_3-CKC, B. M41-S-BeauR-Hep 26 P_3-CKC. Vero cells were infected with C. M41-S-BeauR-Hep 5 P_3-CKC, D. M41-S-BeauR-Hep 26 P_3-CKC. Baby hamster kidney-21 cells were infected with E. M41-S-BeauR-Hep 5 P_3-CKC, F. M41-S-BeauR-Hep 26 P_3-CKC. Infected cells were fixed 24 hours post-infection and immunolabelled with anti-dsRNA, secondary antibody AlexaFluor 488 goat anti-mouse (green, Invitrogen). Nuclei were labelled with DAPI (blue). Images have been brightened for printing.

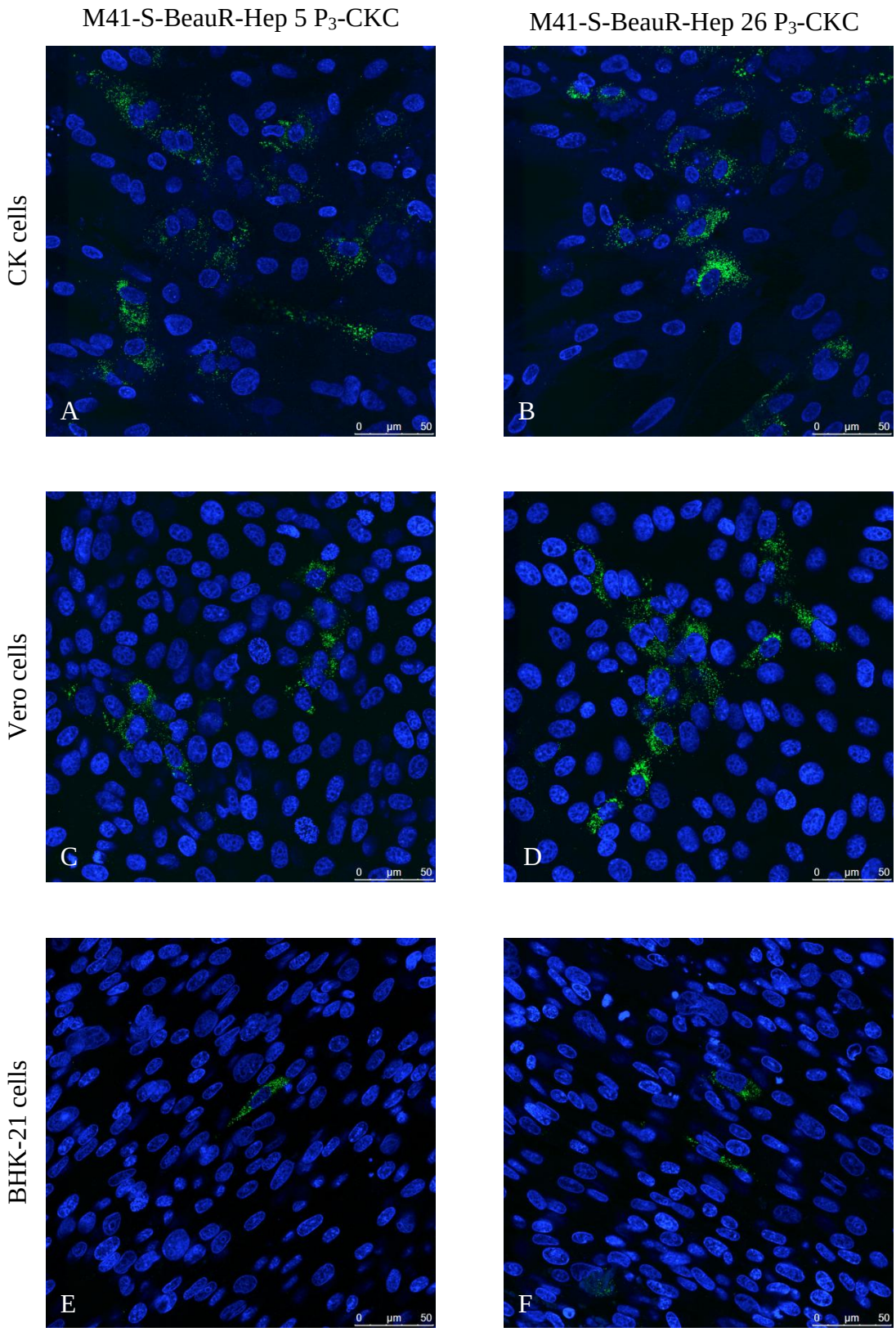
M41-S-BeauR-Hep 5 P3-CKC
M41-S-BeauR-Hep 26 P3-CKC
CK cells
Vero cells
BHK-21 cells
A
B
G
D
E
F
0 µm 50

Figure 4.13. Confocal microscopy of rIBV M41-S-BeauR-Hep P_3-Vero growth on CK, Vero and BHK-21 cells. Chick kidney cells were infected with A. M41-S-BeauR-Hep 5 P_3-Vero, B. M41-S-BeauR-Hep 26 P_3-Vero. Vero cells were infected with C. M41-S-BeauR-Hep 5 P_3-Vero, D. M41-S-BeauR-Hep 26 P_3-Vero. Baby hamster kidney-21 cells were infected with E. M41-S-BeauR-Hep 5 P_3-Vero, F. M41-S-BeauR-Hep 26 P_3-Vero. Infected cells were fixed 24 hours post-infection and immunolabelled with anti-dsRNA, secondary antibody AlexaFluor 488 goat anti-mouse (green, Invitrogen). Nuclei were labelled with DAPI (blue). Images have been brightened for printing.

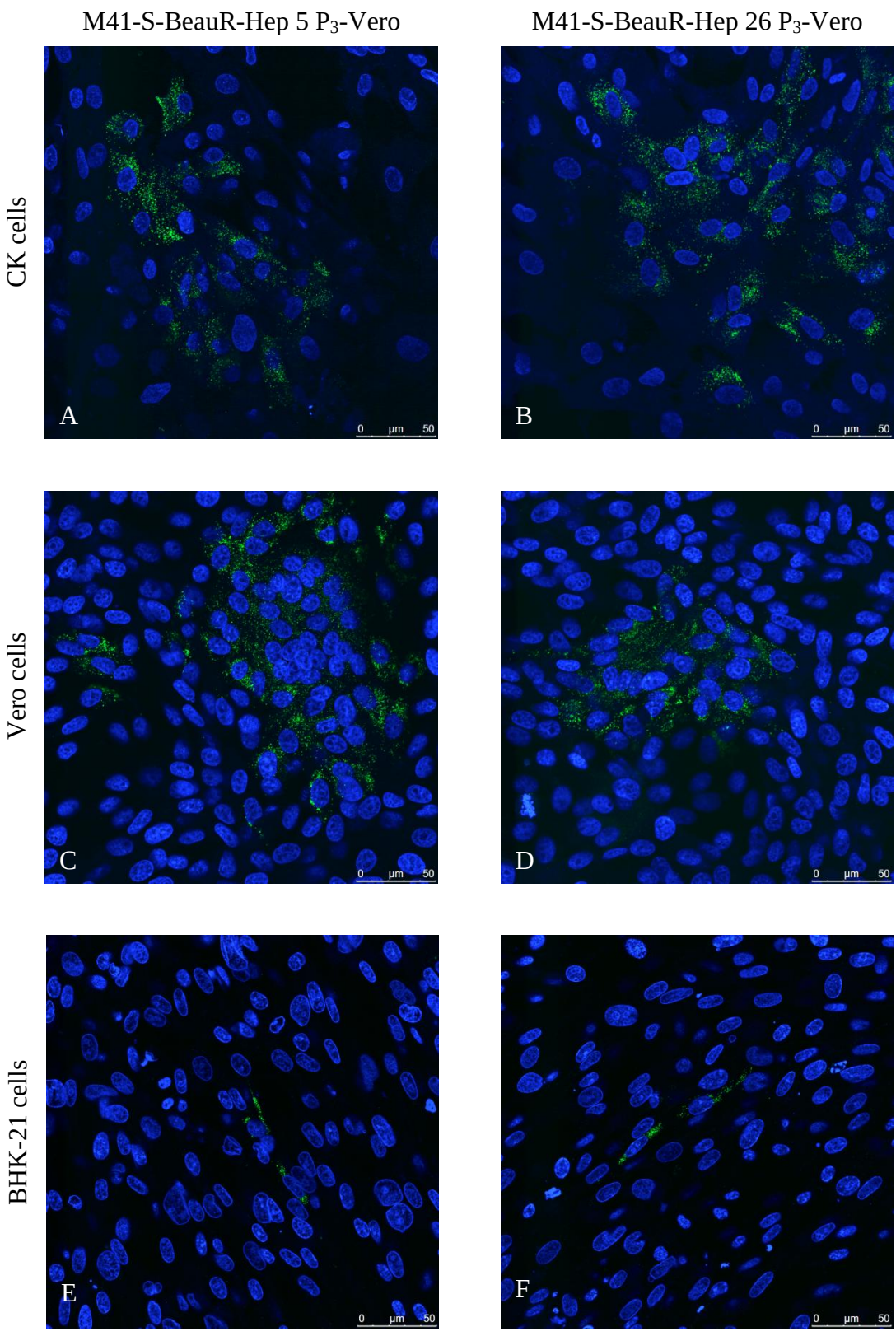
M41-S-BeauR-Hep 5 P3-Vero
M41-S-BeauR-Hep 26 P3-Vero
CK cells
Vero cells
BHK-21 cells
A
B
C
D
E
F
0 µm 50

Growth kinetics of rIBVs on CK, Vero and BHK-21 cells

Chick kidney, Vero and BHK-21 cells were infected with Beau-R, M41-CK, BeauR-M41(S), BeauR-S-M41-Hep 7 P_3-CKC and M41-S-BeauR-Hep 26 P_3-CKC at a multiplicity of infection of 0.1. Supernatant from the infected cells was harvested at 1, 12, 24, 48 and 72 hours post-infection and titrated on CK cells. Three replicates were performed and the averages taken (Figures 4.14 – 4.16). RNA was extracted from selected samples then RT-PCRs were carried out across the S gene and sequenced to check that the correct virus was present.

All viruses were shown to replicate to a similar titre on CK cells (Figure 4.14). Peak titres for all viruses were observed at 48 hours post-infection. Growth of M41-S-BeauR-Hep was seen to be slightly slower than the parent viruses between 1 – 24 hours post-infection but reached as high a titre as the parent viruses by 48 hours post-infection. At 24 hours post-infection, the titres of the parent virus controls were between 6×10^5 pfu/ml (M41-CK) and 7×10^7 pfu/ml (Beau-R), whereas the titre of M41-S-BeauR-Hep was 1×10^4 pfu/ml. This rapidly increased to 9×10^{10} pfu/ml at 48 hours. The titres of the parent virus controls were between 5×10^{10} pfu/ml (BeauR-M41(S)) and 5×10^{11} pfu/ml (M41-CK). BeauR-S-M41-Hep growth followed the same trends as the parent viruses; the titre at 24 hours post-infection was 2×10^7 pfu/ml and 7×10^9 pfu/ml at 48 hours post-infection. Titres for all viruses declined from 48 – 72 hours post-infection.

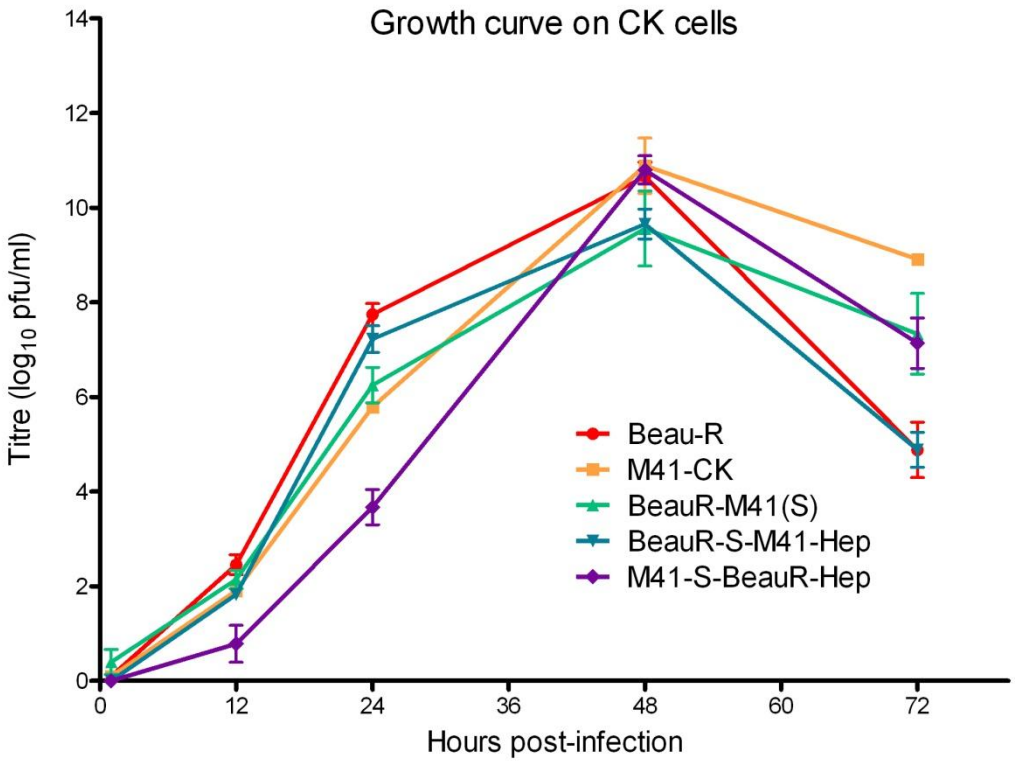

Figure 4.14. Growth kinetics of rIBVs on CK cells. Chick kidney cells were infected with Beau-R, M41-CK, BeauR-M41(S), BeauR-S-M41-Hep 7 P_3-CKC and M41-S-BeauR-Hep 26 P_3-CKC at a multiplicity of infection of 0.1. Supernatant was harvested at 1, 12, 24, 48 and 72 hours post-infection and titrated on CK cells. Three replicates were performed and the averages taken. Error bars indicate standard error of the mean.

Beau-R replicated to the highest titre on Vero cells (Figure 4.15). Growth of M41-CK and BeauR-M41(S) did not reach titres greater than 1.5 $\log_{10}$ pfu/ml on Vero cells. BeauR-S-M41-Hep formed no plaques.

M41-S-BeauR-Hep titre started to increase at 24 hours post-infection and reached a peak at 72 hours post-infection of 1 x 10^2 pfu/ml. Unlike on CK cells (Figure 4.14), replication of Beau-R did not peak at 48 hours post-infection but rather continued to increase until 72 hours post-infection, the final time point measured. This trend was followed by M41-S-BeauR-Hep but final titres were approximately 10^6-fold lower than those of Beau-R.

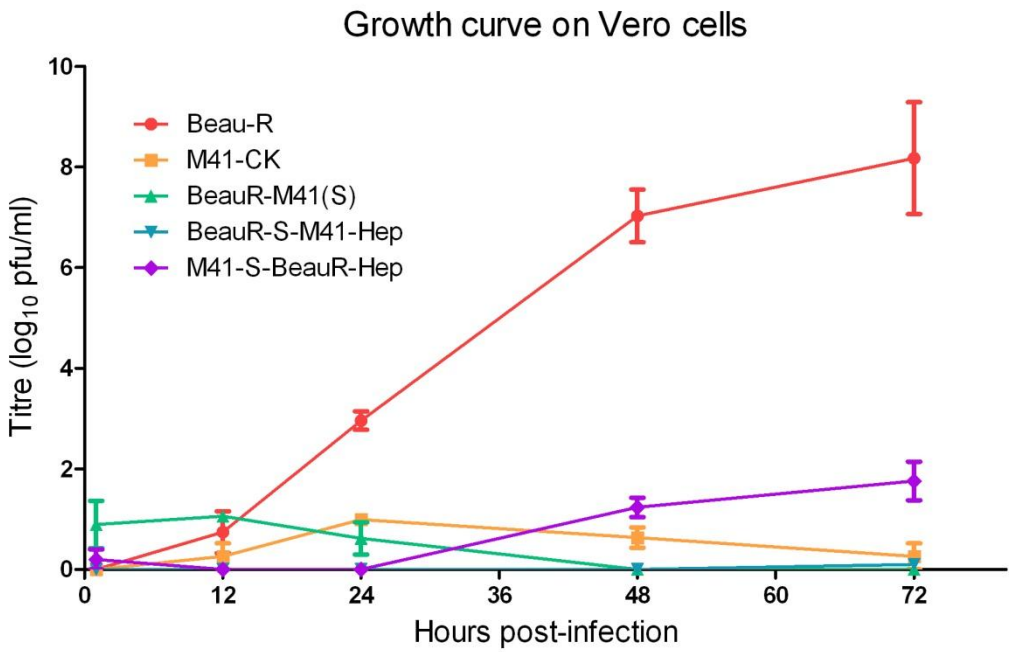

Figure 4.15. Growth kinetics of rIBVs on Vero cells. Vero cells were infected with Beau-R, M41-CK, BeauR-M41(S), BeauR-S-M41-Hep 7 P_3-CKC and M41-S-BeauR-Hep 26 P_3-CKC at a multiplicity of infection of 0.1. Supernatant was harvested at 1, 12, 24, 48 and 72 hours post-infection and titrated on CK cells. Three replicates were performed and the averages taken. Error bars indicate standard error of the mean.

Beau-R replicated to the highest titre on BHK-21 cells (Figure 4.16). Unlike on CK cells (Figure 4.14), replication of Beau-R did not peak at 48 hours post-infection but rather continued to increase until 72 hours post-infection, the final time point measured. No growth of M41-CK was observed and BeauR-M41(S) did not reach titres greater than 10 pfu/ml on BHK-21 cells.

Growth of BeauR-S-M41-Hep began to increase at 24 hours post-infection, reaching a high titre of 2×10^5 pfu/ml at 72 hours post-infection. The growth curve followed the same pattern as Beau-R but the peak titre was approximately 10^3-fold lower than that of Beau-R. Second only to Beau-R, BeauR-S-M41-Hep had the highest peak titre on BHK-21 cells.

M41-S-BeauR-Hep growth also followed a similar pattern to that of Beau-R and BeauR-S-M41-Hep, but titres were much lower. Peak titre at 72 hours post-infection was approximately 10^6-fold lower than that of Beau-R at 3×10^2 pfu/ml but 33 times higher than parent virus, BeauR-M41(S).

These results indicate that other amino acids in addition to the Beaudette-specific region are involved in the ability of Beau-R to grow on BHK-21 cells.

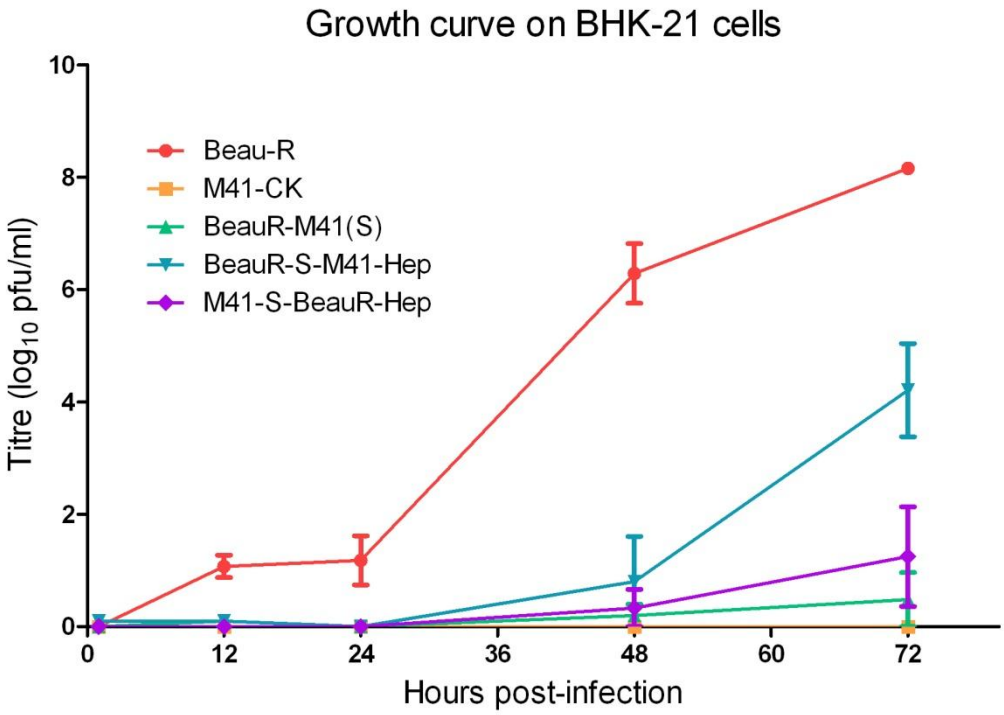

Figure 4.16. Growth kinetics of rIBVs on BHK-21 cells. Baby hamster kidney-21 cells were inoculated with Beau-R, M41-CK, BeauR-M41(S), BeauR-S-M41-Hep 7 P_3-CKC and M41-S-BeauR-Hep 26 P_3-CKC at a multiplicity of infection of 0.1. Supernatant was harvested at 1, 12, 24, 48 and 72 hours post-infection and titrated on CK cells. Three replicates were performed and the averages taken. Error bars indicate standard error of the mean.

Discussion

Two isolates each of the recombinant viruses, BeauR-S-M41-Hep and M41-S-Beau-Hep, were successfully rescued and passaged in CK cells. The S gene sequences were verified both prior to rescue and after three passages in CK cells. The P_3-CKC isolates of both BeauR-S-M41-Hep and M41-S-BeauR-Hep grew on CK cells as shown by confocal microscopy (Figures 4.10 and 4.12) and replicated to a similar titre to the parent viruses on CK cells (Figure 4.14).

Swapping the Beaudette-specific motif between the S glycoproteins of Beau-R and M41-CK has not hindered the replication of either recombinant on CK cells when compared to the growth of the parent viruses, Beau-R and BeauR-M41(S).

The ability of the rIBVs BeauR-S-M41-Hep and M41-S-Beau-Hep to grow on Vero cells was analysed by serial passage of P_3-CKC isolates on the mammalian cell line and virus presence was detected by RT-PCR at each stage (Figure 4.7). The P_3-Vero isolates were titrated on CK cells (Table 4.1) and growth phenotypes on CK, Vero and BHK-21 cells were investigated by confocal microscopy with indirect immunofluorescence (Figures 4.11 and 4.13).

Growth of BeauR-S-M41-Hep P_3-CKC isolates on Vero cells yielded very few infected cells, none in infectious centres (Figure 4.10), and the rIBVs were unable to sustain replication on Vero cells. Titres and RT-PCR products were undetectable by P_3-Vero (Table 4.1 and Figure 4.7). Unsurprisingly, when CK or Vero cells were inoculated with BeauR-S-M41-Hep P_3-Vero cell culture supernatant, no infected

cells were observed by confocal microscopy with indirect immunofluorescence (Figure 4.11).

BeauR-S-M41-Hep P_3-CKC isolates appeared to have a higher tropism for replication on BHK-21 cells than Vero cells, although no infectious centres were formed (Figure 4.10). In fact, the only cell type infected by P_3-Vero isolate 20 was BHK-21 cells (Figure 4.11).

M41-S-BeauR-Hep isolates were found to be able to replicate well when passaged on Vero cells and all RT-PCRs were positive for virus presence (Figure 4.7). Infectious centres were formed when M41-S-BeauR-Hep P_3-CKC and P_3-Vero isolates were grown on Vero cells but not BHK-21 cells (Figures 4.12 and 4.13). Additional passage of M41-S-BeauR-Hep isolates on Vero cells to P_7 increased the virus titre on CK cells (Table 4.1). A number of mutations were identified in the M41-S-BeauR-Hep P_7-Vero S glycoproteins that may play a role in further adapting the virus for growth on Vero cells (Figure 4.9).

The M41-S-BeauR-Hep P_3-Vero and P_7-Vero isolates formed syncytia in Vero cell culture (Figure 4.8). Yamada and Liu, (2009) suggested that the putative HSBS found in the Beau-R S glycoprotein might not be involved in heparan sulphate binding at all; rather this site might be used as a second furin-cleavage site and be concerned with syncytium formation. While this could explain the ability of M41-S-BeauR-Hep to form syncytia in Vero cell culture, it does not explain why Beau-R cannot. It is possible that the M41 S glycoprotein is already fusogenic however, as M41 is unable to grow in Vero cells, this is unknown.

In depth analysis of the growth kinetics of BeauR-S-M41-Hep and M41-S-BeauR-Hep P_3-CKC isolates on Vero and BHK-21 cells was carried out by growth curves (Figures 4.15 and 4.16). Unlike on CK cells (Figure 4.14), titres did not peak at 48 hours post-infection, rather continued to increase until the last time point at 72 hours post-infection. Beau-R grew to the highest titre on Vero cells, followed by M41-S-BeauR-Hep. Although the peak titre of M41-S-BeauR-Hep on Vero cells was lower than that of Beau-R, it must be remembered that this was the first time that the P_3-CKC isolate had been grown on Vero cells. Further passage of M41-S-BeauR-Hep isolates on Vero cells increased their titres to similar levels to that of Beau-R (Table 4.1). It is possible that growth curves carried out with a Vero-passaged isolate rather than a P_3-CKC isolate would be closer to those of Beau-R on Vero cells.

As expected from the analysis of the growth phenotypes by confocal microscopy, BeauR-S-M41-Hep replicated very poorly on Vero cells and followed a similar growth curve to M41-CK and BeauR-M41(S) (Figure 4.15). On BHK-21 cells however, BeauR-S-M41-Hep replicated well and reached a high titre, second only to Beau-R. In contrast to growth on Vero cells, M41-S-BeauR-Hep replicated less well than BeauR-S-M41-Hep on BHK-21 cells. The highest titre of M41-S-BeauR-Hep was not significantly greater than that of BeauR-M41(S) (Figure 4.16).

Removing the Beaudette-specific motif from Beau-R completely eliminated the virus' ability to grow on Vero cells. This result differs from the study by Yamada and Liu, (2009), which claimed that the extended cell-tropism of Beau-R is not due to the HSBS, as a mutant virus with this site removed was still able to grow in Vero cells. In fact, Yamada and Liu, (2009) rule out the possibility that Beau-R may

utilise heparan sulphate as an entry receptor. This is in conflict with work by Madu *et al*., (2007) who used soluble heparin and mutant cell lines with no heparan sulphate expression to show that heparan sulphate is used as an attachment factor for the Beaudette strain of IBV on Vero cells.

While it appears clear that the Beaudette-specific motif plays a role in the ability of Beau-R to grow on Vero cells, it may not be involved in the entire extended host range of Beau-R. Removal of the Beaudette-specific motif from the Beau-R S glycoprotein had a much more subtle effect on the ability to grow on BHK-21 cells. Replication of BeauR-S-M41-Hep on BHK-21 cells was reduced in comparison to Beau-R but not abolished. Introduction of the Beaudette-specific motif from Beau-R into BeauR-M41(S) allowed the virus to grow on Vero cells but did not improve the virus' ability to grow on BHK-21 cells. It would be interesting to passage the recombinant viruses BeauR-S-M41-Hep and M41-S-BeauR-Hep on BHK-21 cells to assess whether virus replication could be maintained.

It seems that additional factors may play a role in the ability of Beau-R to grow on both Vero and BHK-21 cells. There are a total of nineteen amino acid differences in the S2 subunits of Beau-R and M41 (Figure 4.1). Only three of these are included in the Beaudette-specific motif and were swapped between Beau-R and BeauR-M41(S) to create the recombinant viruses BeauR-S-M41-Hep and M41-S-BeauR-Hep. Any of the other amino acid differences may be involved in the ability of Beau-R to grow on Vero cells.

There is one other amino acid change from asparagine to threonine between the M41-CK and Beau-R S glycoproteins located close to the HSBS at position 683 that was not included in the swap to make recombinants BeauR-S-M41-Hep and M41-S-BeauR-Hep. It would be interesting to create two further recombinants including this amino acid change in the Beaudette-specific motif and find out whether this has any impact on the growth phenotype and kinetics of the new viruses when compared to BeauR-S-M41-Hep and M41-S-BeauR-Hep.

Further work would be required in order to investigate the role of the HSBS in the extension of Beau-R cell tropism, whether it is involved in heparan sulphate binding or acts as a furin cleavage site.

Chapter 5: Investigation into cell-to-cell fusion properties of the IBV Beau-R S glycoprotein

Summary

Although Beau-R is able to grow on Vero cells, it does not cause syncytia. Therefore, Beau-R was passaged on Vero cells in order to further adapt the strain for growth on this mammalian cell line. Syncytia started to form after nine passages of Beau-R on Vero cells. This new growth phenotype was initially identified by brightfield microscopy and subsequently by confocal microscopy using indirect immunofluorescence. The P_{10} virus population was sequenced and deep amplicon sequencing was carried out using three Beau-R P_{10} isolates in order to compare the adapted Beau-R S gene sequences to the non-adapted Beau-R S gene sequences with the aim of determining which amino acids of the S glycoprotein are involved in cell-cell fusion. Sequence analysis showed that there were many amino acid differences however, few were shared between isolates. This indicated that syncytia formation results from multiple amino acid changes and that no simple or common changes are responsible for this phenomenon.

Introduction

Syncytia are formed by the fusion of cells to produce multinucleate giant cells. This may be a normal physiological process, such as in placental development (West *et al.*, 1995), or may be caused by certain viral infections e.g. human immunodeficiency virus (HIV; Sodroski *et al.*, 1986) and respiratory syncytia virus, mediated by the F

glycoprotein (Kahn *et al.*, 1999). Viral fusion proteins are transported to the cell surface of infected cells and can bind to receptors on neighbouring cells, fusing the cell membranes to form multinucleate cells. This allows infection of neighbouring cells without the release of infectious virions.

In the case of HIV infection, HIV antigens are processed by infected T cells which insert gp120 into their cell surface. Gp120 is then able to attach to CD4 on uninfected T cells and fuse the cells together to form syncytia. One infected T cell is able to fuse with many uninfected T cells. Fused cells lose immune function and quickly die due to compromised permeability of the plasma membrane or toxicity of viral replication (reviewed by Alimonti *et al.*, 2003).

A strain of IBV, Beau-US, was isolated at the Institute for Animal Health that is able to form syncytia in cell culture (Cavanagh *et al.*, 1986). IBV Beau-US is a Vero-adapted isolate of Beau-CK and causes extensive syncytia. A molecular clone of Beau-CK, Beau-R, is able to grow on Vero cells like Beau-CK but is unable to form syncytia in cell culture (Casais *et al.*, 2001). A comparison of the S gene sequences between Beau-US and Beau-R revealed just eight nucleotide differences, five of which are located in subunit S1 and three in subunit S2. Of these nucleotide changes, six result in a change in amino acid sequence (Table 5.1; Casais *et al.*, 2001).

In order to identify which amino acids on the S glycoprotein are involved in cell-cell fusion, Beau-R was serially passaged on Vero cells until the virus adapted to form

syncytia. The adapted S glycoprotein genes were sequenced and compared to the original S gene sequence to identify amino acid changes.

Table 5.1. Nucleotide substitutions between Beau-R and Beau-US.

Gene	Position (nt)	Nucleotide change	Codon change	Amino acid change
S gene	20421	T – C	GCT – GCC	None
	20480	G – A	AGT – AAT	S – N
	20731	T – A	TTA – ATA	L – I
	21403	T – A	TCA – ACA	S – T
	21711	G – A	GTG – GTA	None
	22252	G – A	GGG – AGG	G – R
	22415	A – C	AAT – ACT	N – T
	22612	T – A	TTG – ATG	L – M
ORF 3a	23906	T – C	TGT – TGC	None
ORF 3c (E)	24501	C – T	CAA – TAA	Q – STOP
M gene	24635	G – C	AGT – ACT	S – T
	24746	C – T	GCA – GTA	A – V
Non-coding region	25227	C – T	NA	NA
ORF 5a	25513	G – T	AGA – ATA	R – I
N gene	27087	A – G	GGA – GGG	None

From Casais *et al.*, (2001).

Methods

Serial passage of Beau-R on Vero cells

Vero cells in six-well plates were infected at ~100% confluency with Beau-R and the supernatant was harvested at 72 and 96 hours post-infection (two wells per time-point, pooled) forming passage 1 (P_1) virus. Supernatant from both time points was used to infect fresh Vero cells and supernatant was harvested at 48 and 72 hours post-infection to form the next passage and repeated until P_4 when the number of virus isolates reached sixteen. From P_5 onwards, supernatant was harvested at 48 hours post-infection only (Figure 5.1).

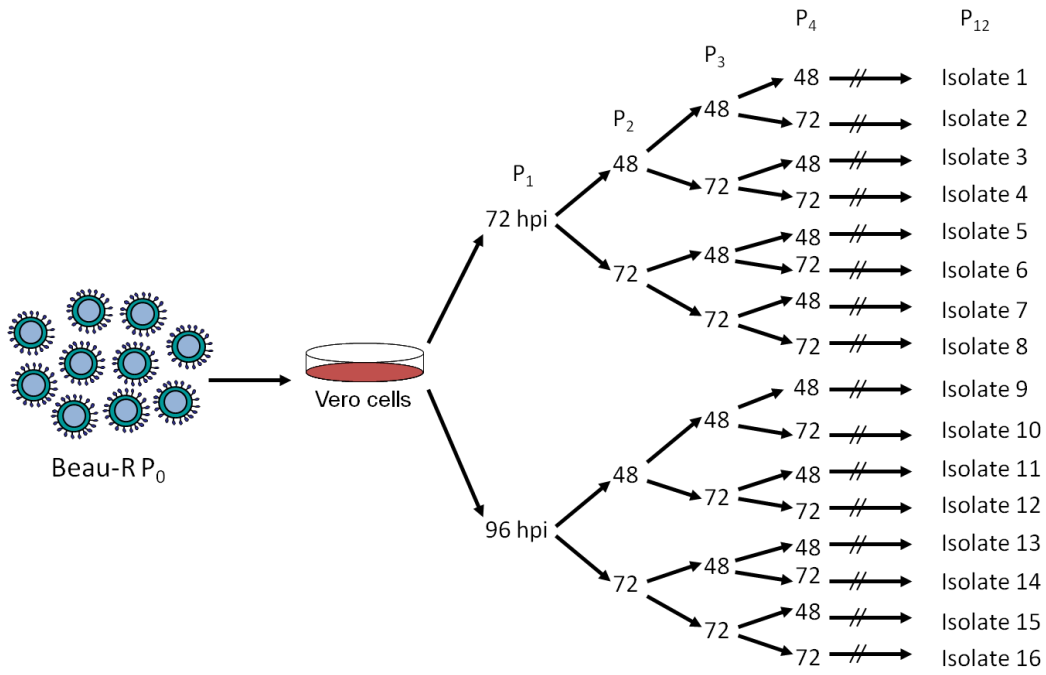

Figure 5.1. The serial passage of Beau-R on Vero cells. Confluent Vero cells in six-well plates were infected with Beau-R P_0 and the supernatant was harvested at 72 and 96 hours post-infection (hpi). The supernatant was used to infect fresh Vero cells and supernatant was harvested at 48 and 72hpi until P_4. After this passage, the 16 isolates were harvested at 48hpi only.

Photographs were taken of Beau-R P_{10}-infected Vero cells by brightfield microscopy and confocal microscopy with indirect immunofluorescence. RNA was extracted from all isolates at P_{10} and the S genes sequenced and compared to the non-adapted Beau-R sequence.

Deep amplicon sequencing

Three isolates of Beau-R P_{10}, P_{10}-4, 9 and 12, were selected for further investigation as they formed large numbers of syncytia in Vero cell culture. Deep amplicon sequencing was carried out to identify changes in the S genes of individual viruses when compared to the parent S gene.

RNA was extracted from each isolate using the Qiagen RNeasy Mini Kit (manufacturer's protocol followed, described in Chapter 2 section: RNA-based methods) and reverse transcribed using Superscript III (Invitrogen, method described in Chapter 2, section: RNA-based methods). Primers produced by Sigma were designed to cover the S gene in three overlapping sections of ~1250 – 1300bp each from nucleotide 20271, 97 bases upstream of the start of the S gene, to nucleotide 23920, 64 bases downstream of the end of the S gene (Table 5.2). The three sections were (1) 20271 – 21518 within the S1 subunit, (2) 21436 – 22700 over the S1/S2 junction and (3) 22625 – 23920 within the S2 subunit. Sections 1 and 2 overlap by 82 nucleotides and sections 2 and 3 overlap by 75 nucleotides (Figure 5.2).

The S gene sections of each isolate were amplified by PCR using *taq* polymerase from Invitrogen to create single deoxyadenosine 3' overhangs (manufacturer's protocol followed, described in Chapter 2, section: DNA-based methods). The PCR

products were cloned into pCR®4-TOPO®, which has single deoxythymidine 3' T overhangs, using the TOPO TA Cloning® Kit for Sequencing (Invitrogen, manufacturer's protocol followed) and 3µl was used to transform One Shot® Max Efficiency DH5α™-T1R competent *E. coli* (Invitrogen, manufacturer's protocol followed). Aliquots of transformation mixture were spread onto LB agar plates containing 100µg/ml ampicillin for selection and incubated overnight at 37°C. Colonies were picked and inoculated into 3ml LB medium containing 100µg/ml ampicillin. Cultures were incubated on a shaker at 37°C overnight then plasmid DNA was extracted using a Qiagen Miniprep DNA extraction kit (manufacturer's protocol followed). Plasmids were digested with EcoR1 (New England Biosciences), restriction sites located either side of the insert, to identify plasmids containing the S gene insert. Samples containing the correct size insert were sequenced by the Sequencing Service at the University of Dundee. Approximately 20 clones of each section of S gene from each isolate were sequenced in positive and negative directions.

Table 5.2. Primers used for deep sequencing of Beau-R P_{10} isolates.

Primer name	Nucleotide position	Nucleotide sequence
DS1	20271 – 20291	TTGAGATTGAAAGCAACGCC
DS2	21498 – 21518	ACACCTTTACACAGCGAAGG
DS3	21436 – 21456	GGTTGCAAGCAATCTGTCTT
DS4	22680 – 22700	TAGCCTGCAGTTGTGTGGCA
DS5	22625 – 22645	CTCTAGTAGCTTCTATGGCT
DS6	23900 – 23920	CTTAGTACAAGTTTACACCA

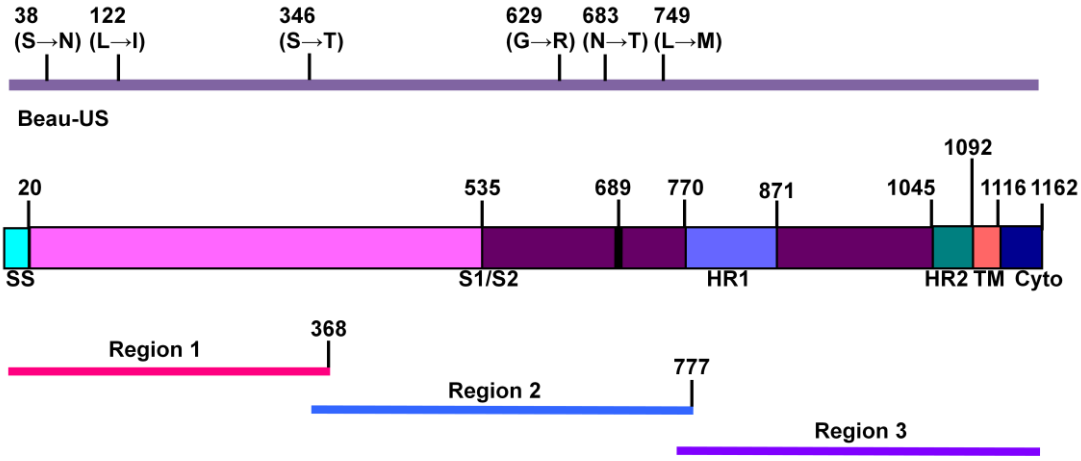

Figure 5.2. Schematic diagram of the Beau-R S gene showing the amino acid differences between the Beau-R and Beau-US S genes (above) and the regions cloned for deep amplicon sequencing (below). There are eight nucleotide differences between the S genes of Beau-R and Beau-US, six of which are coding. Three are located within Region 1 and three are located within Region 2. None are located in Region 3. The numbers refer to the S glycoprotein amino acids with numbers starting from the first amino acid, methionine.

Sequence analysis

Consensus sequences for each of the clones were obtained using the Staden package and these were aligned by ClustalX (Larkin *et al.*, 2007). The aligned consensus sequences were compared using Genedoc (Nicholas *et al.*, 1997) and diagrams showing nucleotide and amino acid differences were generated using Base-by-Base (Brodie *et al.*, 2004).

Results

Adaptation of Beau-R to syncytia formation on Vero cells

Beau-R was successfully adapted to form syncytia in Vero cell culture by serial passage. Twelve passages of Beau-R on Vero cells were carried out (Figure 5.1) and syncytia were observed by light microscopy in several isolates from P_9 onwards.

Brightfield microscopy of cpe caused by Beau-R P_{10}

Vero cells were infected with Beau-R P_{10} and photographs were taken 48 hours post-infection (Figure 5.3). Non-adapted Beau-R causes extensive cpe in Vero cell culture in the form of rounded and floating cells and 'balloon' formation. Selected isolates of Beau-R P_9 started to form syncytia from around 36 hours post-infection.

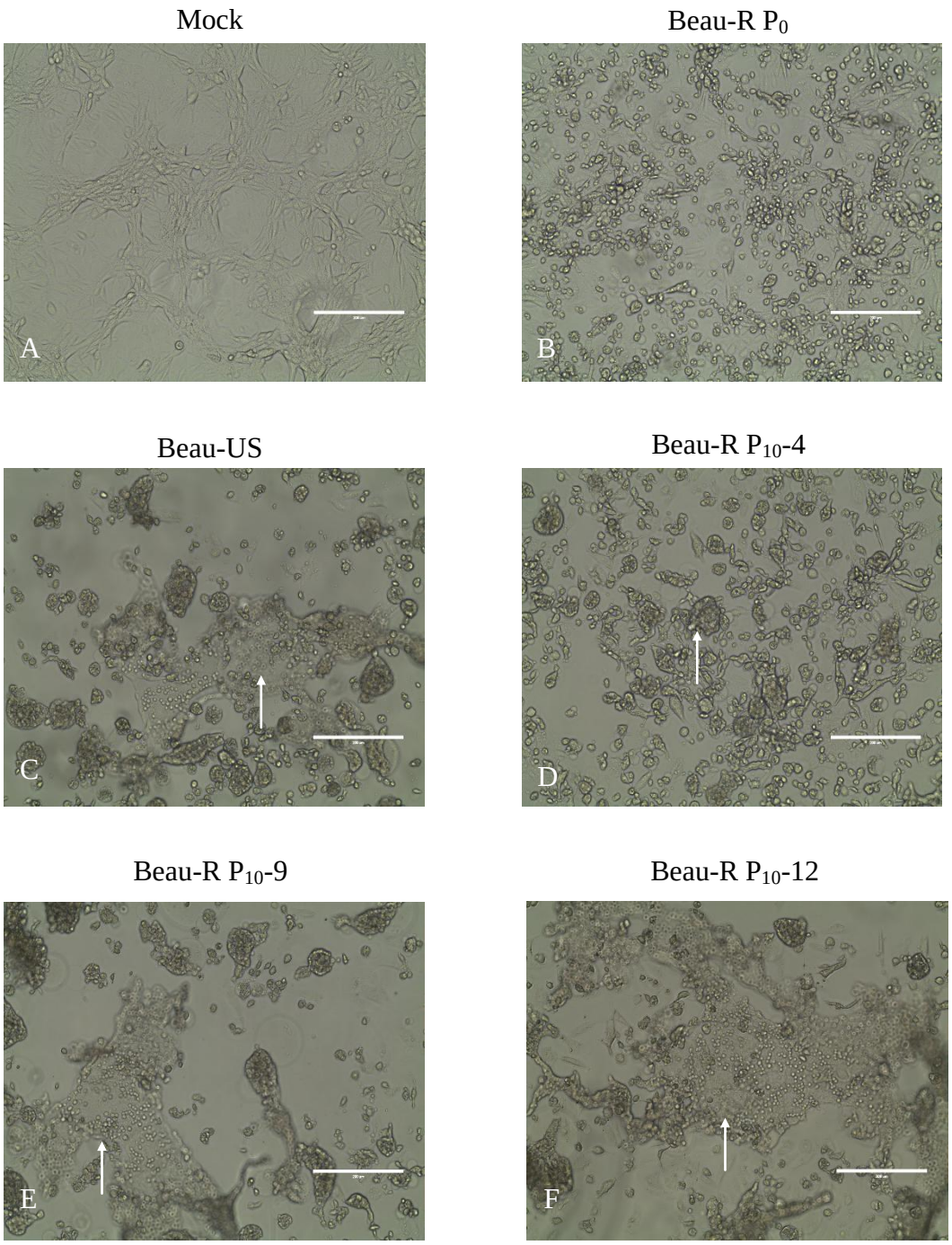

Figure 5.3. Brightfield microscopy of Beau-R P_{10}-infected Vero cells. Vero cells were infected with A. mock, B. Beau-R P_0, C. Beau-US, D. Beau-R P_{10}-4, E. Beau-R P_{10}-9, F. Beau-R P_{10}-12. Cytopathic effect in the form of balloons and rounded cells can be seen in all but the mock-infected cells. Syncytia are indicated by arrows. Photographs were taken 48 hours post-infection at x10 magnification.

Confocal microscopy of Beau-R P_{11}-infected Vero cells

Confocal microscopy with indirect immunofluorescence was used to visualise the syncytia formed by Beau-R in greater detail. All Beau-R P_{11} isolates were grown on Vero cells on coverslips. Non-adapted Beau-R and Beau-US were also grown on Vero cells for comparison (Figure 5.4). Infected cells were immunolabelled with rabbit anti-IBV, secondary antibody AlexaFluor 488 goat anti-rabbit (Invitrogen, green). The endoplasmic reticulum (ER) was labelled with mouse anti-PDI, secondary antibody AlexaFluor 568 goat anti-mouse (Invitrogen, red). Nuclei were labelled with DAPI (blue).

Non-adapted Beau-R infected many Vero cells forming infectious centres, however all cells were separate from each other. Infected cells may be touching but the divisions between them can be clearly seen (Figure 5.5). This is in contrast to the cells infected with Beau-US, most of which have been incorporated to form giant syncytia. There are few uninfected cells. No infected cells were observed in mock-infected samples.

Syncytia were observed in the cell cultures inoculated with Beau-R P_{11} isolates (Figure 5.5) but single infected cells were also seen, indicating the possibility of a mixed population of viruses present in the culture.

Figure 5.4. Confocal microscopy of Beau-R P_{11} growth on Vero cells. Vero cells infected with A. mock, B. Beau-R P_0, C. Beau-US, D. Beau-R P_{11}-4, E. Beau-R P_{11}-9, F. Beau-R P_{11}-12. Infected cells were fixed 24 hours post-infection and immunolabelled with anti-IBV, secondary antibody AlexaFluor 488 goat anti-mouse (green). ER was labelled with mouse anti-PDI, secondary antibody AlexaFluor 568 goat anti-mouse (red). Nuclei were labelled with DAPI (blue). Images have been brightened for printing.

Mock

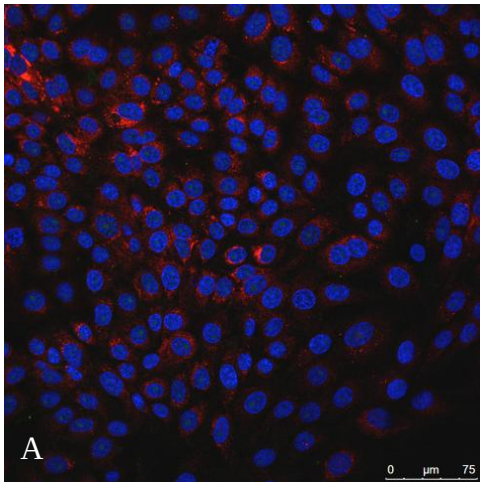

Beau-R P_0

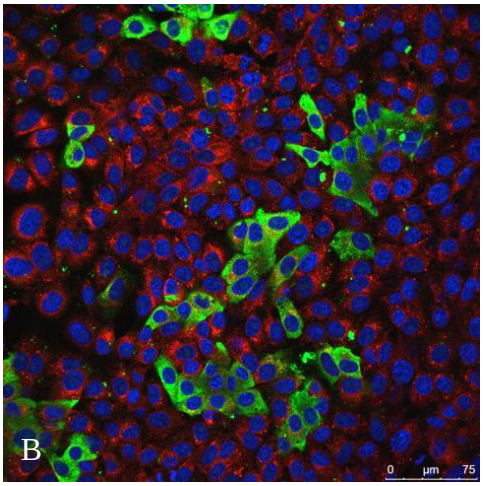

Beau-US

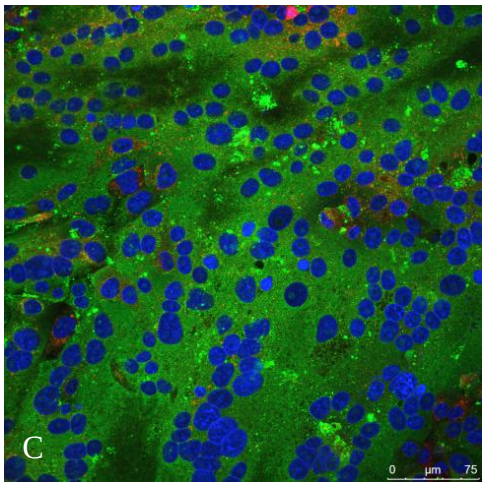

Beau-R P_{11}-4

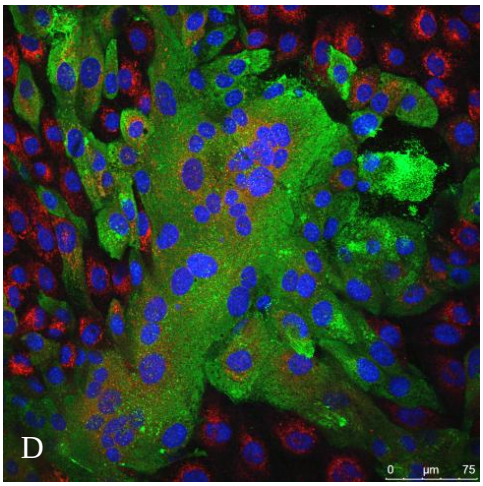

Beau-R P_{11}-9

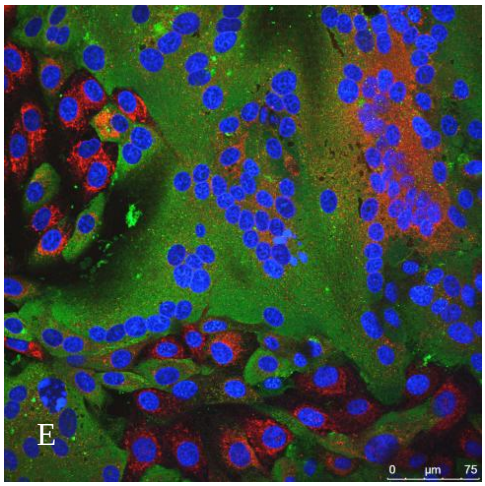

Beau-R P_{11}-12

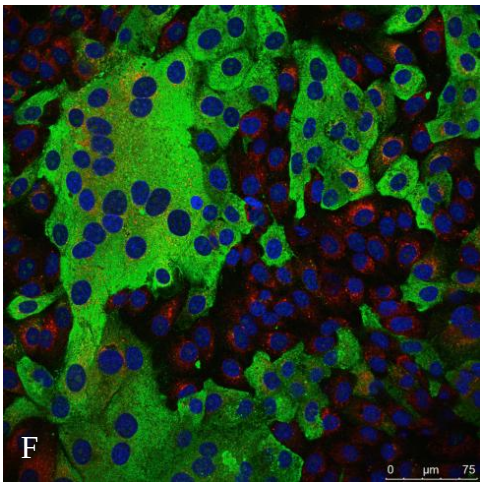

Beau-R P_0 Beau-R P_{11}-12

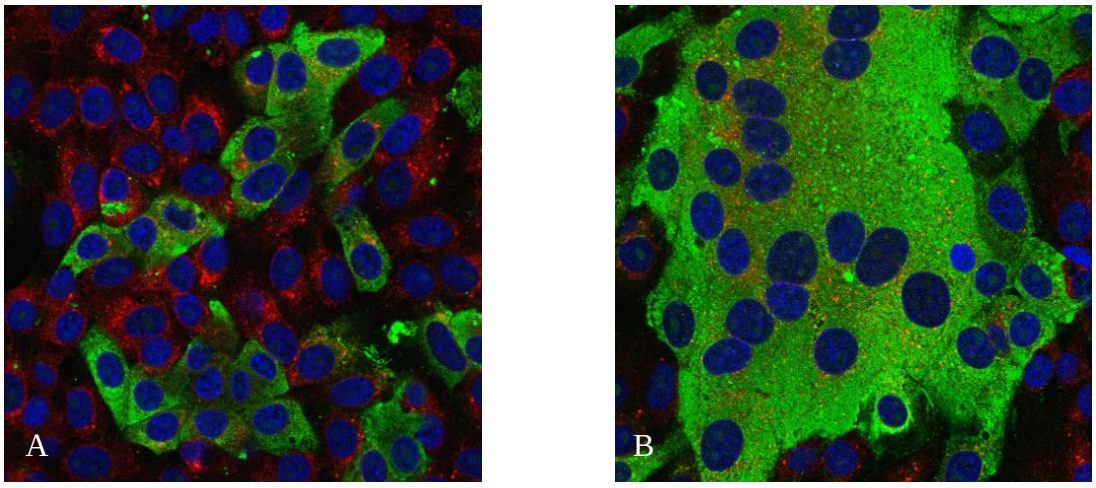

Figure 5.5. Comparison of growth phenotypes of adapted and non-adapted Beau-R on Vero cells. Vero cells infected with A. Beau-R P_0, B. Beau-R P_{11}-12 (magnified from Figure 5.4 B and F). Infected cells were fixed 24 hours post-infection and immunolabelled with anti-IBV, secondary antibody AlexaFluor 488 goat anti-mouse (green). ER was labelled with mouse anti-PDI, secondary antibody AlexaFluor 568 goat anti-mouse (red). Nuclei were labelled with DAPI (blue). Individual cells infected with non-adapted Beau-R can clearly be observed in A, whereas cells infected with adapted Beau-R have fused to form a syncytium in B. Images have been brightened for printing.

Beau-R P_{10} sequence confirmation

In order to confirm that the changes in growth phenotype were due to adaptation of Beau-R to Vero cell culture and not a contaminating virus, RNA was extracted from P_{10} virus supernatant and RT-PCR was carried out on each sample. The region around nucleotide 19666 was amplified and sequenced (Figure 5.6). Beau-R is the only strain of IBV to possess a thymine (T) at nucleotide position 19666 and this is used as a marker in order to identify Beau-R samples by sequencing (Casais *et al.*, 2001). It was found that all Beau-R P_{10} samples also possessed a T at position 19666, confirming that they were derived from Beau-R. This means that any changes in growth phenotype observed, such as syncytia formation, resulted from adaptation of Beau-R.

	19650	19660	19670
Beau-CK	TACACAACTTTGTCAATACCTTTCGAAAACAACAA		
Beau-US	TACACAACTTTGTCAATACCTTTCGAAAACAACAA		
Beau-R	TACACAACTTTGTCAATACCTTTTGAAAACAACAA		
Beau-R P_{10}-1	TACACAACTTTGTCAATACCTTTTGAAAACAACAA		
Beau-R P_{10}-2	TACACAACTTTGTCAATACCTTTTGAAAACAACAA		
Beau-R P_{10}-3	TACACAACTTTGTCAATACCTTTTGAAAACAACAA		
Beau-R P_{10}-4	TACACAACTTTGTCAATACCTTTTGAAAACAACAA		
Beau-R P_{10}-5	TACACAACTTTGTCAATACCTTTTGAAAACAACAA		
Beau-R P_{10}-6	TACACAACTTTGTCAATACCTTTTGAAAACAACAA		
Beau-R P_{10}-7	TACACAACTTTGTCAATACCTTTTGAAAACAACAA		
Beau-R P_{10}-8	TACACAACTTTGTCAATACCTTTTGAAAACAACAA		
Beau-R P_{10}-9	TACACAACTTTGTCAATACCTTTTGAAAACAACAA		
Beau-R P_{10}-10	TACACAACTTTGTCAATACCTTTTGAAAACAACAA		
Beau-R P_{10}-11	TACACAACTTTGTCAATACCTTTTGAAAACAACAA		
Beau-R P_{10}-12	TACACAACTTTGTCAATACCTTTTGAAAACAACAA		
Beau-R P_{10}-13	TACACAACTTTGTCAATACCTTTTGAAAACAACAA		
Beau-R P_{10}-14	TACACAACTTTGTCAATACCTTTTGAAAACAACAA		
Beau-R P_{10}-15	TACACAACTTTGTCAATACCTTTTGAAAACAACAA		
Beau-R P_{10}-16	TACACAACTTTGTCAATACCTTTTGAAAACAACAA		
CONSENSUS	TACACAACTTTGTCAATACCTTTTGAAAACAACAA		

Figure 5.6. Beau-R P_{10} nucleotide sequences from 19641 – 19667. RNA was extracted from Beau-R P_{10} samples and RT-PCR was carried out to amplify the region around the marker nucleotide 19666 (red), which was then sequenced and compared to the parent Beau-R sequence. Beau-R is the only strain of IBV to possess a thymidine (T) at position 19666. As all P_{10} samples also possess a T at 19666, this confirms that they are derived from Beau-R and not contaminated with another strain of IBV. The corresponding region of the Beau-CK, used to generate Beau-R, and Beau-US sequences are included to show that they contain a cytidine (C) residue at position 19666.

Beau-R P_{10} population sequencing

As not all Beau-R P_{11}-infected cells appeared to form syncytia when viewed by brightfield and confocal microscopy with indirect immunofluorescence (Figures 5.3 and 5.4), it was speculated that a mixed population of viruses might be present in the culture. Total cellular RNA was extracted from the cell culture supernatant of each isolate at passage 10 and the S genes of the Beau-R population were sequenced to determine the sequences of the dominant strains present (Table 5.3).

Table 5.3. Location of nucleotide and amino acid differences between Beau-R P_{10} population and non-adapted Beau-R.

Beau-R P_{10} isolate(s)	Nucleotide position	Amino acid position	Non-adapted Beau-R	Beau-R P_{10}	Amino acid change
12	20422	19	G	A	V – I
9	22114	583	A	T	N – Y
7	22822	818	A	T	L – F
7	22862	832	C	T	L – F
11, 14, 15, 16 (10, 12, 13 mixed G/T)	23323	986	G	T	A – S
12	23378	1004	C	T	T – I

Sequence comparison between Beau-R and Beau-US

In order to find out whether any of the amino acid changes identified in the population sequencing corresponded to the Beau-US sequence, a comparison of the S gene sequences of Beau-US and Beau-R, both non-adapted and the P_{10} population, was carried out. None of the amino acid differences between non-adapted Beau-R and Beau-US corresponded to the differences found in the Beau-R P_{10} population sequences (Figure 5.7).

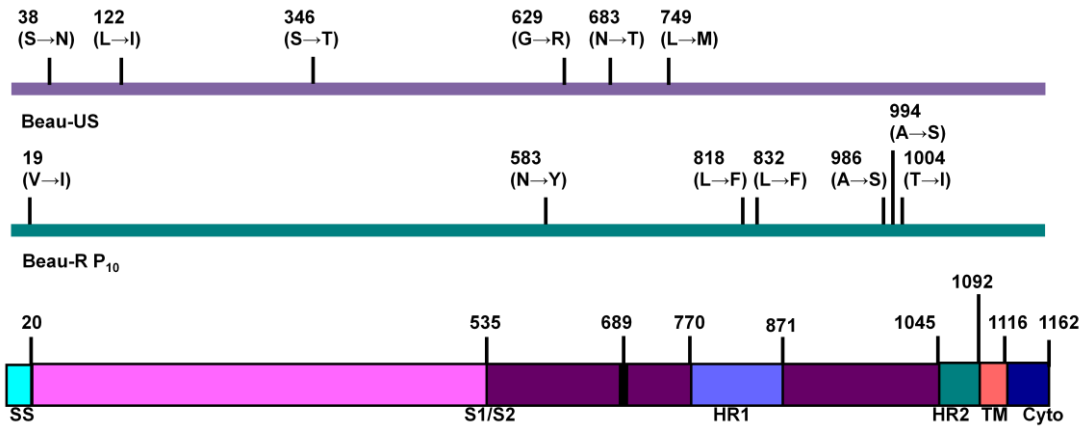

Figure 5.7. Schematic diagram of the Beau-US and Beau-R P_{10} population S genes showing the amino acid differences with Beau-R. There are eight nucleotide differences between the S genes of Beau-R and Beau-US, six of which are coding (top). Three are located in the S1 subunit and three are located in the S2 subunit. There are seven coding nucleotide differences between the Beau-R and the Beau-R P_{10} population S gene sequences (middle). One is located in the S1 subunit and six are located in the S2 subunit. None of the amino acid differences correspond between Beau-US and Beau-R P_{10}. The numbers refer to the S glycoprotein amino acids with numbers starting from the first amino acid, methionine.

Deep amplicon sequencing

Three isolates of Beau-R P_{10} that formed the most syncytia in cell culture were chosen for deep amplicon sequencing in order to determine whether other amino acid changes may be identified that did not predominate in the consensus sequence. Sections of the S genes were amplified by PCR then cloned into TOPO vectors (Invitrogen) and 16 – 21 individual clones of each section were sequenced per isolate and compared to non-adapted Beau-R and Beau-US sequences. Poor quality sequences were discarded. This approach was designed to identify any nucleotide or amino acid changes that occurred in single clones, and to find out if any of these were shared by more than one clone.

Region 1 nucleotide and amino acid changes

Region one comprises the first 368 amino acids of the S1 subunit. The clone numbers used in region 1 do not correspond to clone numbers from the same isolate in regions 2 or 3. The distribution of nucleotide differences between the Beau-R P_{10} isolates and clones is shown in Figure 5.8 and the distribution of amino acid differences is shown in Figure 5.9. All differences appear to be evenly distributed throughout region one.

Region one of Beau-R P_{10}-4 contains 80 nucleotide changes, 44 of which are coding and two result in stop codons (Appendix, Table A.1). There are two deletions, one results in a stop codon and the other results in non-homologous sequence. Two nucleotide substitutions are shared by two different clones each, only one is coding.

Region one of Beau-R P_{10}-9 contains 22 nucleotide changes, 14 of which are coding (Appendix, Table A.2). There are approximately 80 amino acids deleted from the start of isolate 8 in this region due to a mutated start codon at nucleotide position 20370. The protein starts at the second start codon. None of the mutations are shared by more than one clone.

Region one of Beau-R P_{10}-12 contains 41 nucleotide changes, 23 of which are coding (Appendix, Table A.3). There is one deletion resulting in a stop codon. Five nucleotide substitutions are shared by more than one clone, two of which are coding.

There is one nucleotide substitution shared between clones of different isolates. Clone 1 of Beau-R P_{10}-9 and clone 33 of Beau-R P_{10}-4 have a mutation from T – C at nucleotide position 20883, which is not coding.

One nucleotide substitution (G – A) identified in Beau-R P_{10} isolate 12 by population sequencing (Table 5.3) was also identified in Beau-R P_{10}-12 clones 2, 10, 38, 39 and 54 at nucleotide position 20422. This resulted in an amino acid mutation at position 19 of valine to isoleucine. No differences between non-adapted and adapted Beau-R were also shared with Beau-US, although the nucleotide substitution at position 20422 in Beau-R P_{10}-12 isolates 2, 10, 38, 39 and 54 is only one nucleotide downstream of the silent mutation T – C found in Beau-US.

Figure 5.8. Nucleotide differences for all Beau-R P_{10} region 1 isolates and clones and Beau-US, compared to parent Beau-R sequence. A. Beau-R P_{10} isolate 4 clones, B. Beau-R P_{10} isolate 9 clones, C. Beau-R P_{10} isolate 12 clones. Substitutions are shown by a blue line and deletions are shown in red. Nucleotide positions are indicated by numbers underneath. Diagrams were generated using Base-by-base (Brodie *et al.*, 2004) following alignment of individual clone sequences as described in the methods section.

A. Beau-R P_{10}-4 region 1

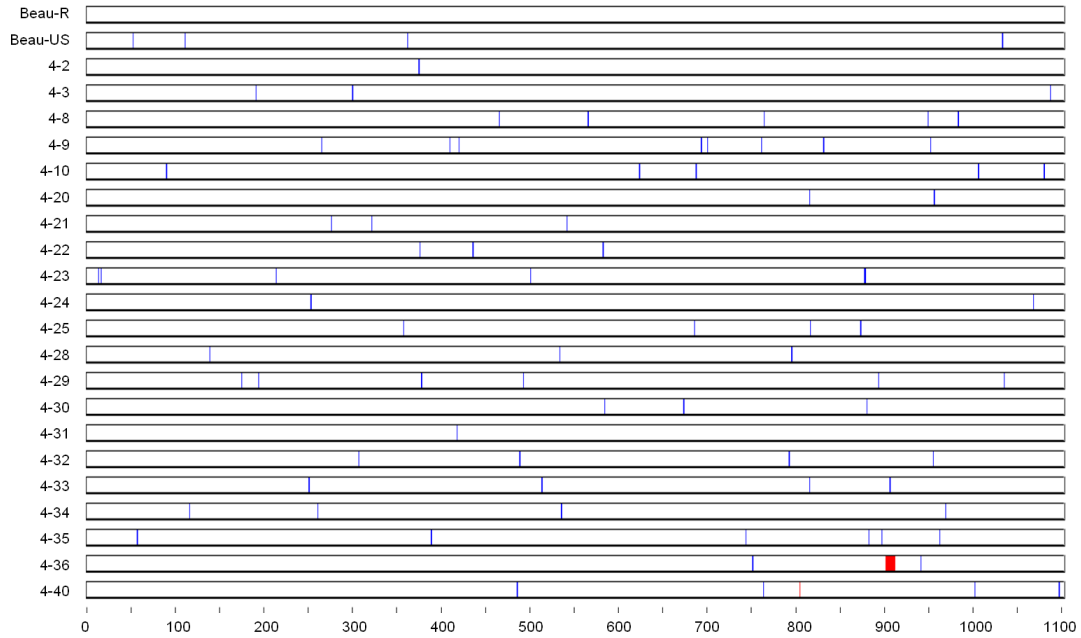

B. Beau-R P_{10}-9 region 1

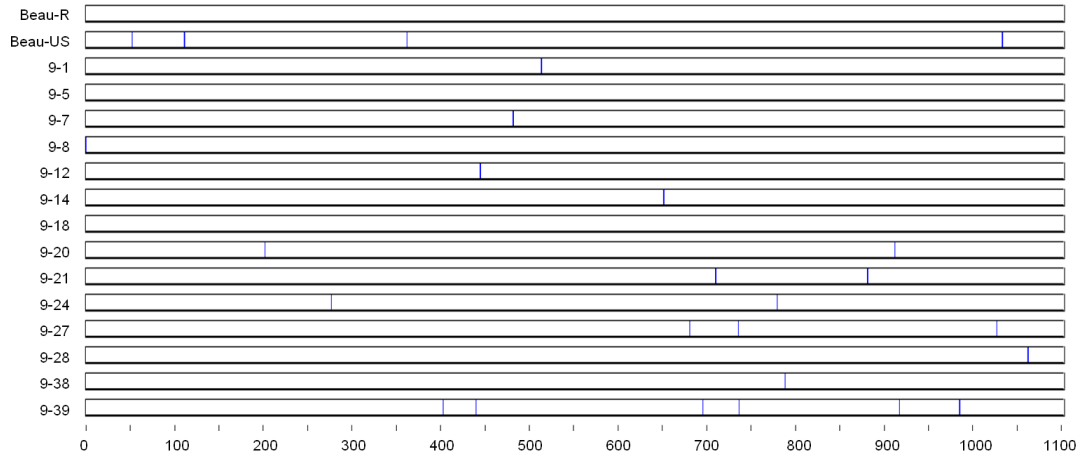

C. Beau-R P_{10}-12 region 1

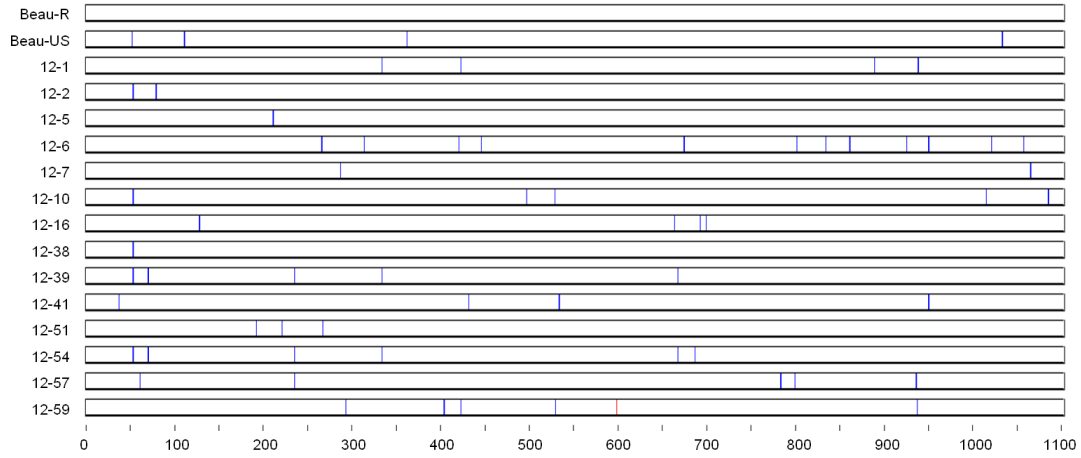

Figure 5.9. Amino acid differences for all Beau-R P_{10} region 1 isolates and clones and Beau-US, compared to parent Beau-R sequence. A. Beau-R P_{10} isolate 4 clones, B. Beau-R P_{10} isolate 9 clones, C. Beau-R P_{10} isolate 12 clones. Substitutions are shown by a blue line and deletions are shown in red. Amino acid positions are indicated by numbers underneath. Deletions indicated here are either due to a nucleotide substitution in the sequence resulting in termination of the amino acid sequence or loss of a nucleotide resulting in loss of the amino acid sequence. The deletions are not large nucleotide deletions, as per Figure 5.8. Diagrams were generated using Base-by-base (Brodie *et al.*, 2004) following alignment of individual clone sequences as described in the methods section.

A. Beau-R P_{10}-4 region 1

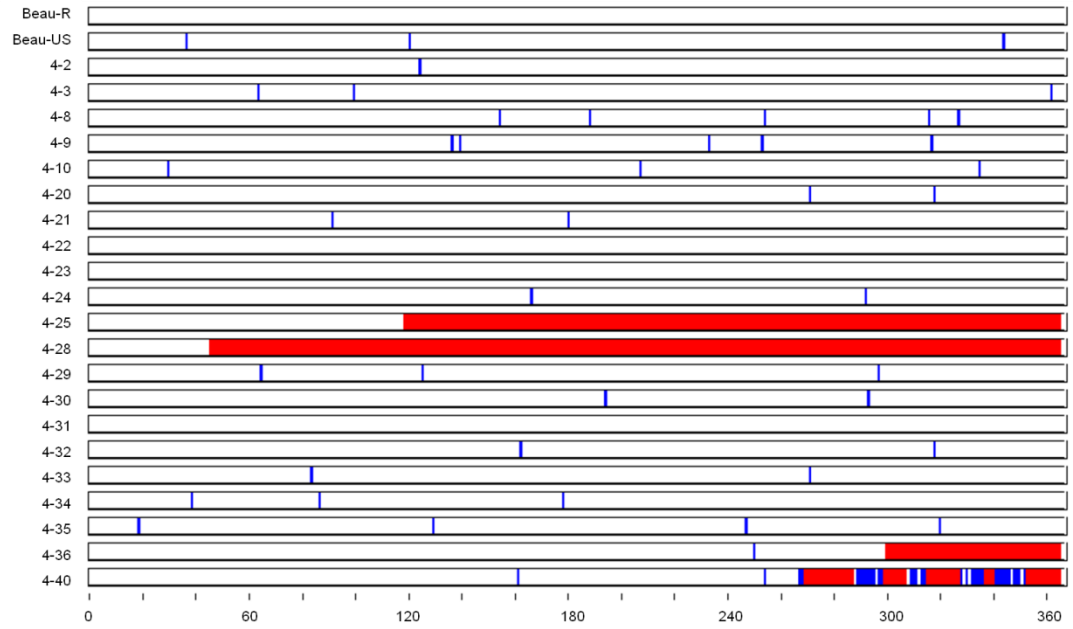

B. Beau-R P_{10}-9 region 1

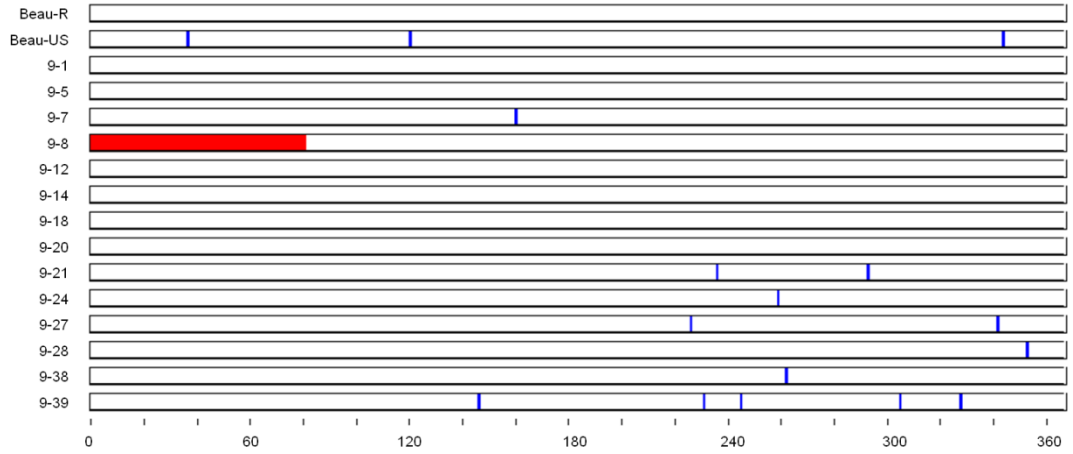

C. Beau-R P_{10}-12 region 1

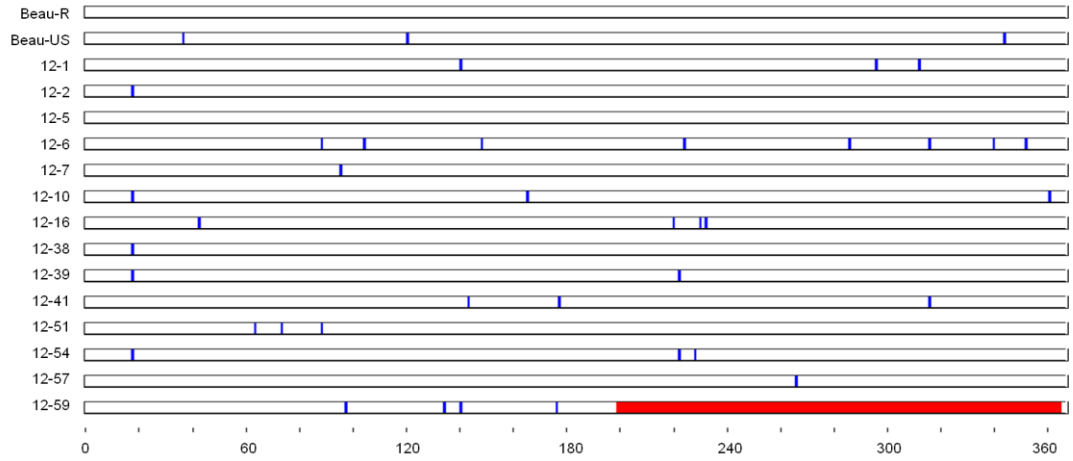

Region 2 nucleotide and amino acid changes

Region two spans the S1/S2 junction and the heparan sulphate binding site (HSBS) of Beau-R (Chapter 4, Figure 4.1) and comprises amino acids 367 – 777. The clone numbers used in region 2 do not correspond to clone numbers from the same isolate in regions 1 or 3. The distribution of nucleotide differences between the Beau-R P_{10} isolates and clones is shown in Figure 5.10 and the distribution of amino acid differences is shown in Figure 5.11.

Region two of Beau-R P_{10}-4 contains eight nucleotide substitutions, none of which are coding (Appendix, Table A.4). There are no deletions. One nucleotide substitution is shared between two clones.

There are ten nucleotide differences in Beau-R P_{10}-9 region two, six of which are coding (Appendix, Table A.5). One nucleotide change A – T identified by population sequencing also occurs in Beau-R P_{10}-9 clones 17, 18, 19 and 20 at nucleotide position 22114. This results in an amino acid change of asparagine – tyrosine at amino acid position 583. There are no deletions.

Beau-R P_{10}-12 region two contains 14 nucleotide differences, six of which result in coding changes (Appendix, Table A.6). One substitution is shared between two clones but is not coding. Three clones share a deletion of three nucleotides resulting in one amino acid change and one deletion, tyrosine-valine – leucine, at postion 613.

No changes are shared between isolates. Mutations appear to be clustered around the centre of the region, the S1/S2 junction (Figures 5.10 and 5.11). No mutations occur in the HSBS although there is a mutation from proline to serine immediately upstream at amino acid position 684 in Beau-R P_{10}-9 clone 17. This is adjacent to a mutation in Beau-US from asparagine to threonine at amino acid position 683.

Figure 5.10. Nucleotide differences for all Beau-R P_{10} region 2 isolates and clones and Beau-US, compared to parent Beau-R sequence. A. Beau-R P_{10} isolate 4 clones, B. Beau-R P_{10} isolate 9 clones, C. Beau-R P_{10} isolate 12 clones. Substitutions are shown by a blue line and deletions are shown in red. Nucleotide positions are indicated by numbers underneath. Diagrams were generated using Base-by-base (Brodie *et al.*, 2004) following alignment of individual clone sequences as described in the methods section.

A. Beau-R P_{10}-4 region 2

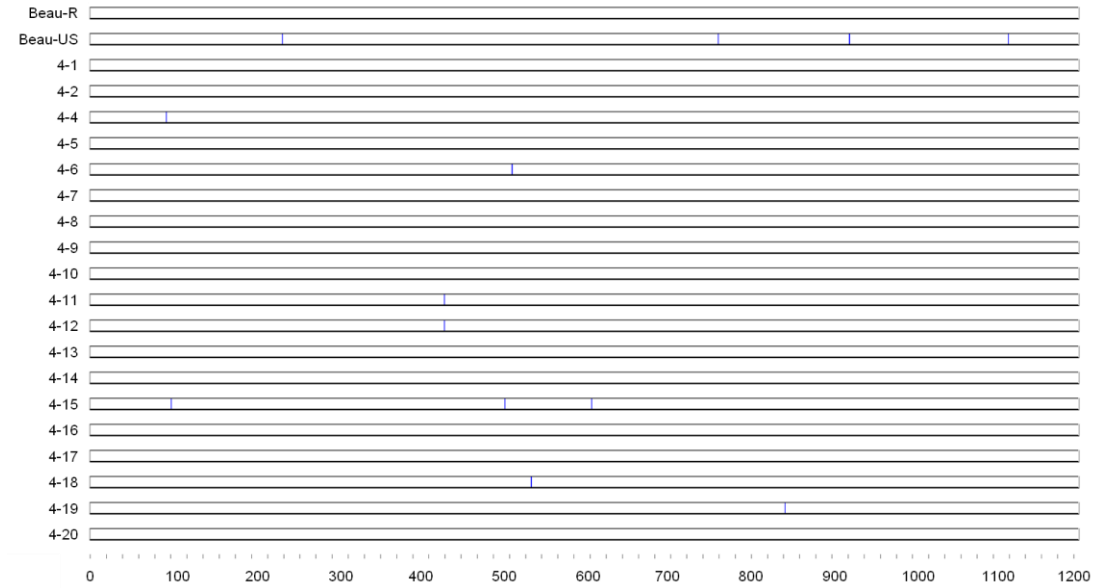

B. Beau-R P_{10}-9 region 2

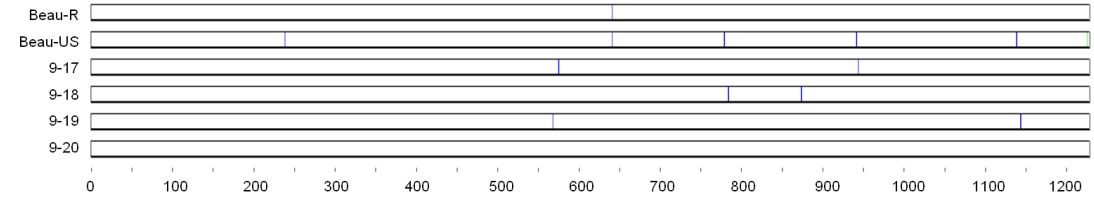

C. Beau-R P_{10}-12 region 2

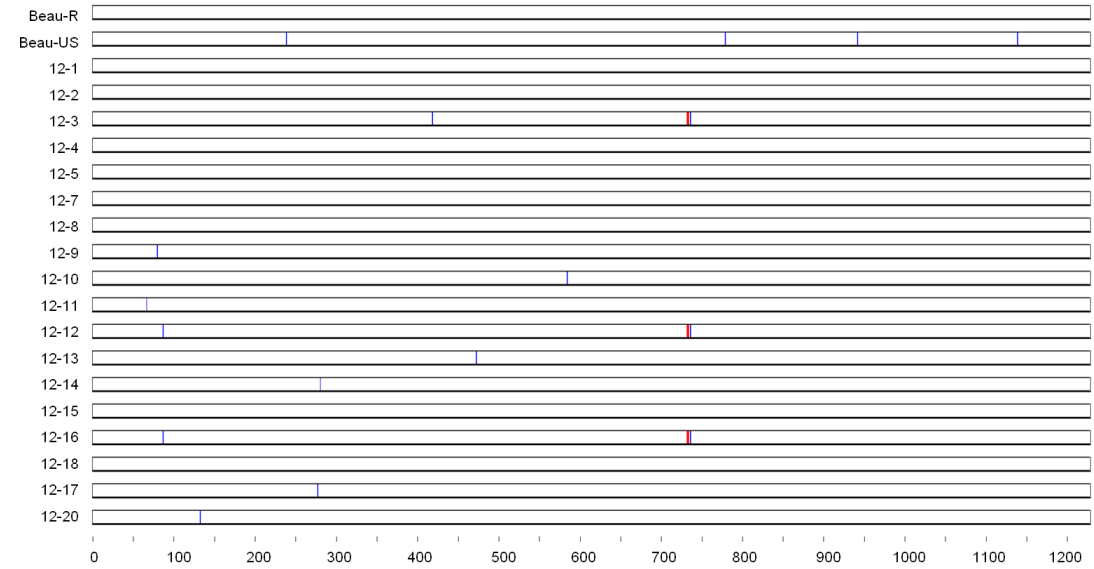

Figure 5.11. Amino acid differences for all Beau-R P_{10} region 2 isolates and clones and Beau-US, compared to parent Beau-R sequence. A. Beau-R P_{10} isolate 4 clones, B. Beau-R P_{10} isolate 9 clones, C. Beau-R P_{10} isolate 12 clones. Substitutions are shown by a blue line and deletions are shown in red. Amino acid positions are indicated by numbers underneath. Diagrams were generated using Base-by-base (Brodie *et al.*, 2004) following alignment of individual clone sequences as described in the methods section.

A. Beau-R P_{10}-4 region 2

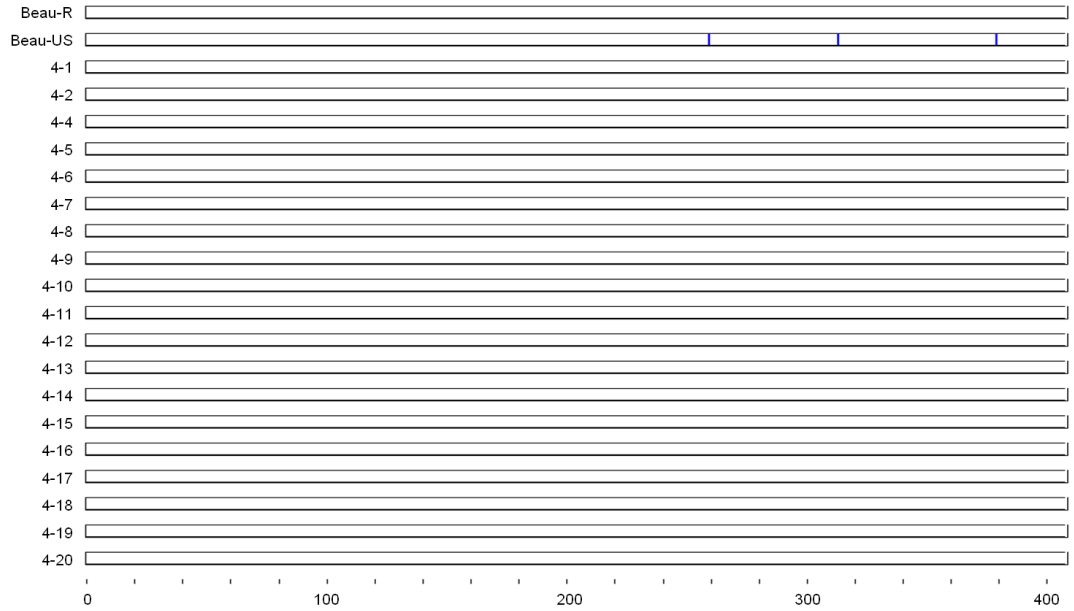

B. Beau-R P_{10}-9 region 2

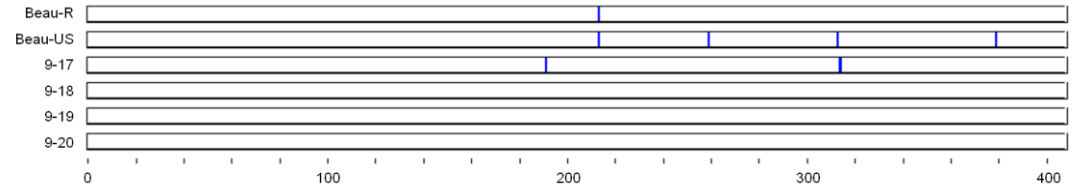

C. Beau-R P_{10}-12 region 2

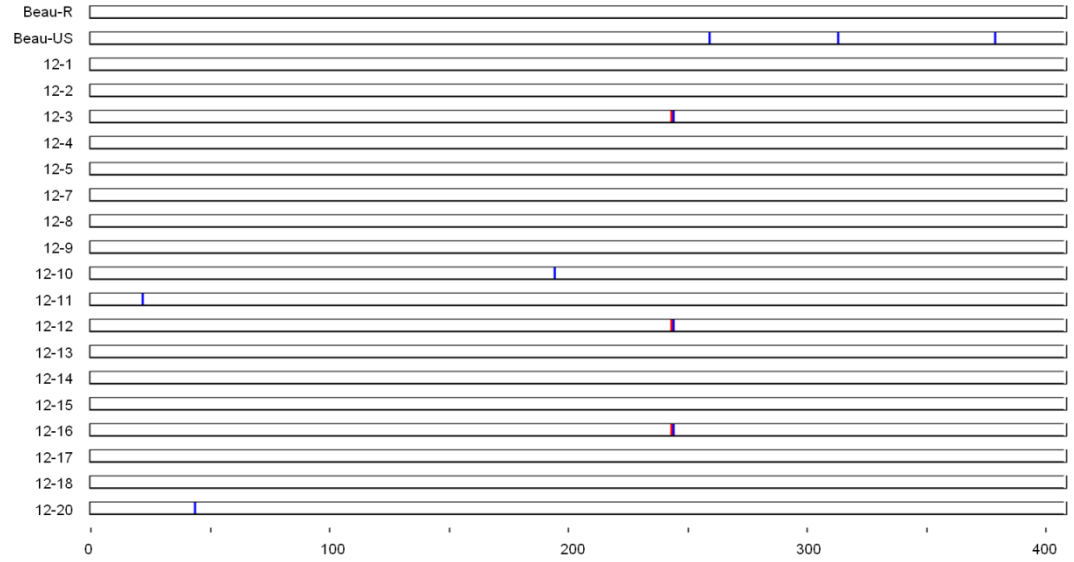

Region 3 nucleotide and amino acid changes

Region three comprises the end of the S2 subunit from amino acid 776. The clone numbers used in region 3 do not correspond to clone numbers from the same isolate in regions 1 or 2. The distribution of nucleotide differences between the Beau-R P_{10} isolates and clones is shown in Figure 5.12 and the distribution of amino acid differences is shown in Figure 5.13. The nucleotide and amino acid differences appear to be evenly spread throughout.

There are 21 nucleotide differences in Beau-R P_{10}-4 region three, 12 of which are coding (Appendix, Table A.7). One nucleotide substitution is shared between two clones, however this is not coding. There are no deletions. One area of nucleotide change results in non-homologous sequence.

Beau-R P_{10}-9 region three contains 30 nucleotide differences, 22 are coding (Appendix, Table A.8). Two result in a stop codon and one results in non-homologous sequence. There are no deletions. One nucleotide substitution at position 23325 is shared by two clones and results in an amino acid change of alanine – serine at position 986.

Region three of Beau-R P_{10}-12 contains 38 nucleotide differences, including three deletions (Appendix, Table A.9). Twenty-four of the nucleotide substitutions are coding and one results in a stop codon. Three substitutions are shared between more than one clone. The first is shared by clones 1 and 12 and results in an amino acid

change of alanine – serine at position 986. The second is shared by nine clones and results in an amino acid change of threonine – isoleucine at position 1004. The last is shared by clones 6 and 7; clone 6 has a nucleotide substitution of T – C and results in an amino acid change of isoleucine – threonine and clone 7 has a nucleotide substitution of T – G and results in an amino acid change of isoleucine – serine, both at position 1090. Clone 3 has a series of nucleotide substitutions and insertions and results in amino acid changes of IRVS – ARKCS from position 889.

Beau-R P_{10}-4 clone 16 and Beau-R P_{10}-9 clone 11 share a nucleotide substitution of C – T resulting in an amino acid change of serine to phenylalanine at position 1005. Beau-R P_{10}-4 clone 1 and Beau-R P_{10}-12 clone 16 share a non-coding nucleotide substitution at amino acid position 922. Clone 16 of Beau-R P_{10}-4 and clone 7 of Beau-R P_{10}-9 share a series of nucleotide substitutions and insertions from amino acid position 962 resulting in non-homologous sequence. Clone 14 of Beau-R P_{10}-9 and clone 7 of Beau-R P_{10}-12 share a nucleotide substitution of T – C that results in an amino acid change of isoleucine – threonine at position 1090. Clone 6 of Beau-R P_{10}-12 also has a nucleotide substitution at this position that results in a serine residue.

A number of differences identified within region three by population sequencing (Table 5.3) were also identified as occurring in at least one clone by deep sequencing. The G – T substitution identified in Beau-R P_{10} isolates 11, 14, 15, 16 and as a mixed population in isolates 10, 12 and 13 was also identified in Beau-R P_{10}--9 clones 11 and 13 and Beau-R P_{10}-12 clones 1 and 12 and resulted in an amino acid

change of alanine – serine at position 986. Nine different clones of Beau-R P_{10}-12 share the nucleotide substitution C – T resulting in a threonine – isoleucine change at position 1004 identified in Beau-R P_{10}-12 by population sequencing.

Figure 5.12. Nucleotide differences for all Beau-R P_{10} region 3 isolates and clones and Beau-US, compared to parent Beau-R sequence. A. Beau-R P_{10} isolate 4 clones, B. Beau-R P_{10} isolate 9 clones, C. Beau-R P_{10} isolate 12 clones. Nucleotide substitutions are shown by a blue line, deletions are shown in red and insertions are shown in green. Nucleotide positions are indicated by numbers underneath. Diagrams were generated using Base-by-base (Brodie *et al.*, 2004) following alignment of individual clone sequences as described in the methods section.

A. Beau-R P_{10}-4 region 3

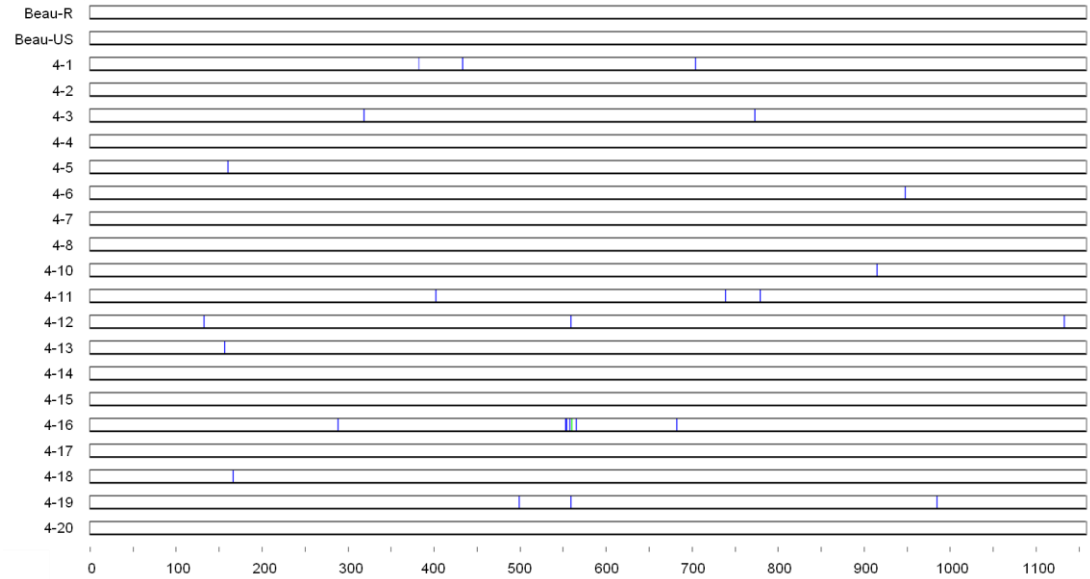

B. Beau-R P_{10}-9 region 3

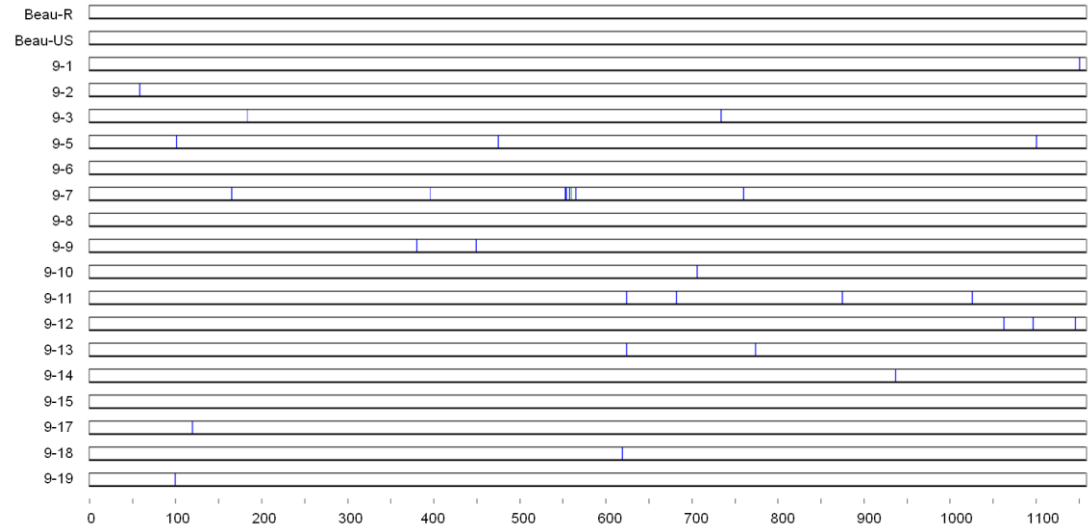

C. Beau-R P_{10}-12 region 3

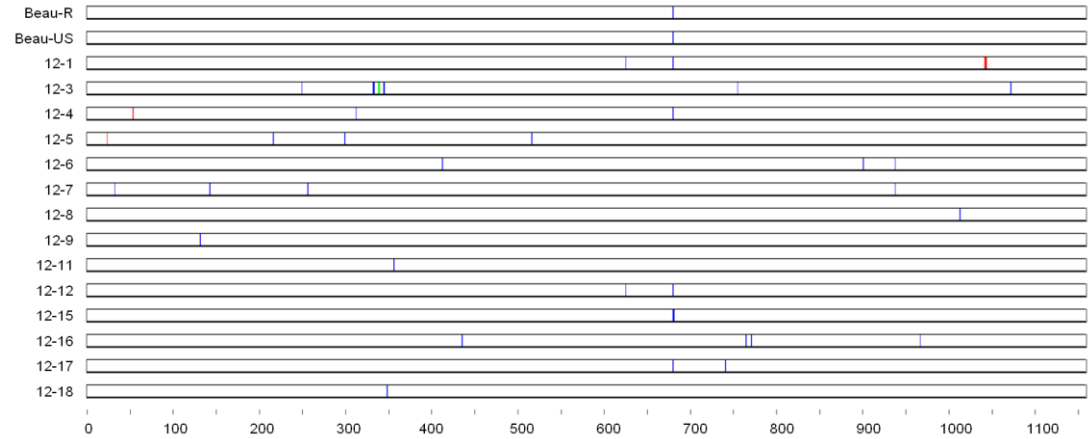

Figure 5.13. Amino acid differences for all Beau-R P_{10} region 3 isolates and clones and Beau-US, compared to parent Beau-R sequence. A. Beau-R P_{10} isolate 4 clones, B. Beau-R P_{10} isolate 9 clones, C. Beau-R P_{10} isolate 12 clones. Nucleotide substitutions are shown by a blue line and deletions are shown in red. Amino acid positions are indicated by numbers underneath. Deletions indicated here are either due to a nucleotide substitution in the sequence resulting in termination of the amino acid sequence or loss of a nucleotide resulting in loss of the amino acid sequence. The deletions are not large nucleotide deletions, as per Figure 5.12. Diagrams were generated using Base-by-base (Brodie *et al.,* 2004) following alignment of individual clone sequences as described in the methods section.

A. Beau-R P_{10}-4 region 3

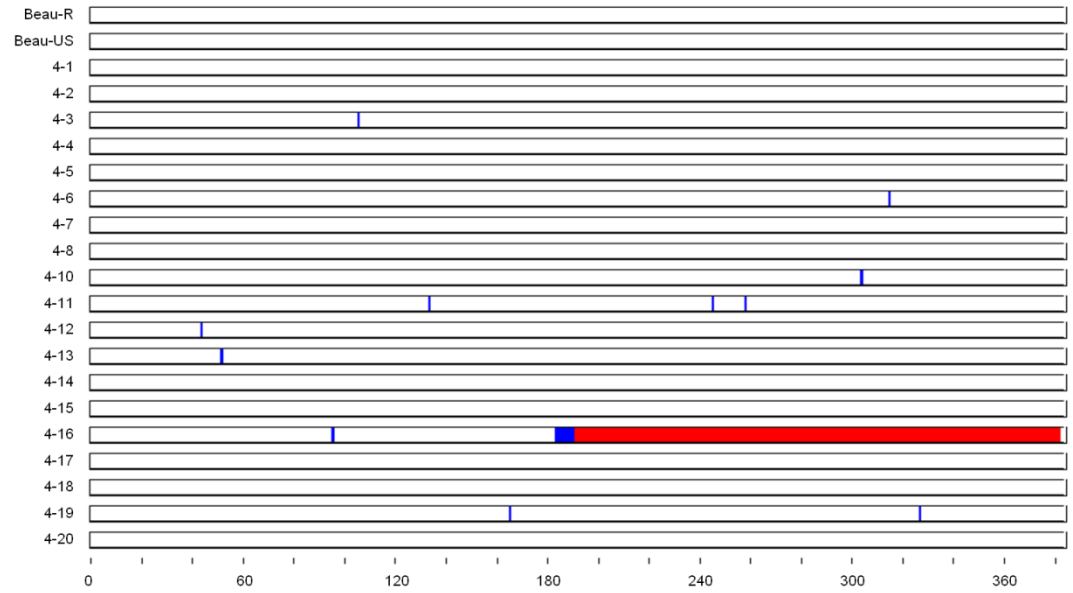

B. Beau-R P_{10}-9 region 3

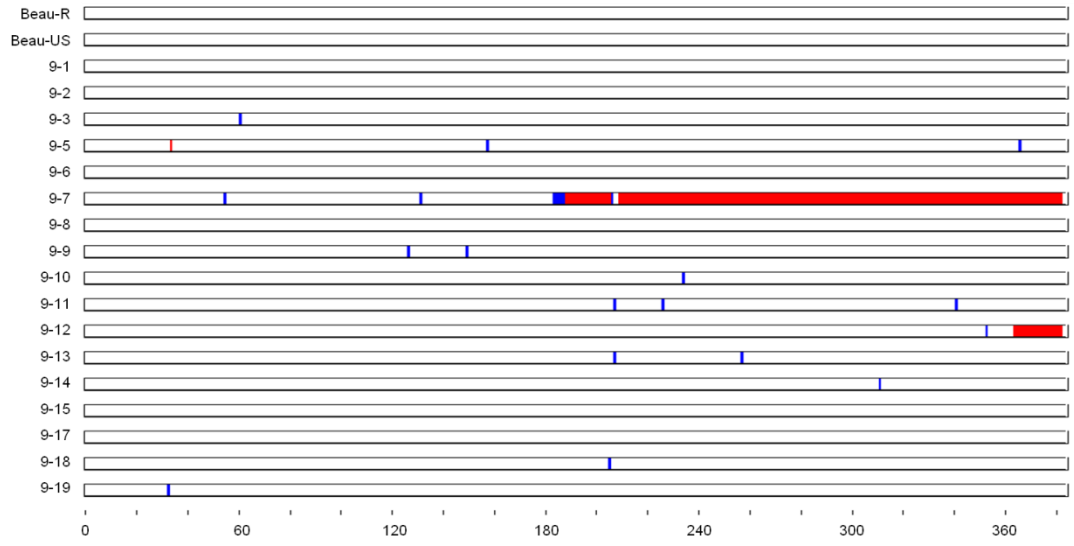

C. Beau-R P_{10}-12 region 3

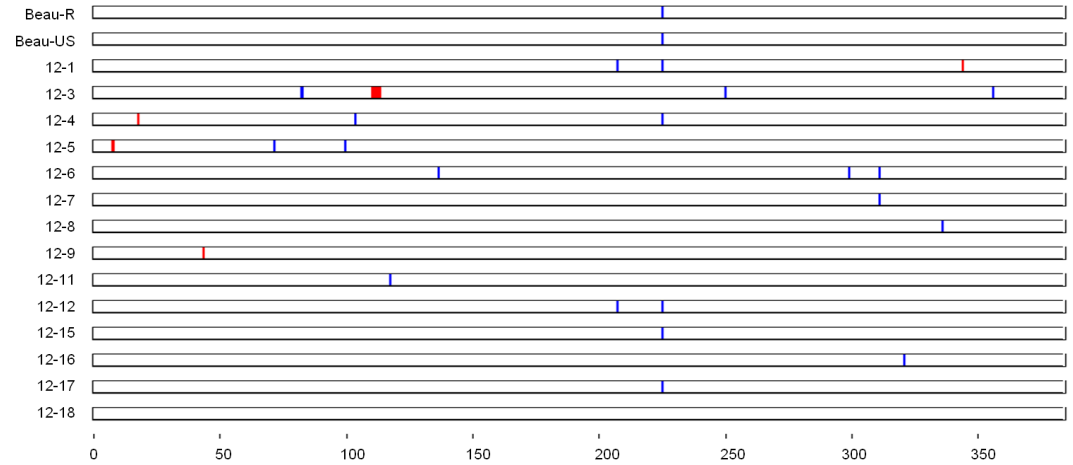

Consensus nucleotide and amino acid sequences

Consensus sequences for each Beau-R P_{10} isolate were constructed using the clone sequences and compared to the non-adapted Beau-R and Beau-US sequences (Figures 5.14 and 5.15). Each Beau-R P_{10} isolate consensus nucleotide sequence has two changes, none are shared between isolates and all are coding. One of the nucleotide differences in the Beau-R P_{10}-12 consensus is adjacent to a silent mutation in the Beau-US sequence, however none of the coding changes are shared between the adapted Beau-R isolates and Beau-US. Only one of the nucleotide and amino acid differences in the adapted Beau-R isolates is located in the S1 subunit. The other nucleotide and amino acid differences are fairly evenly distributed throughout the S2 subunit.

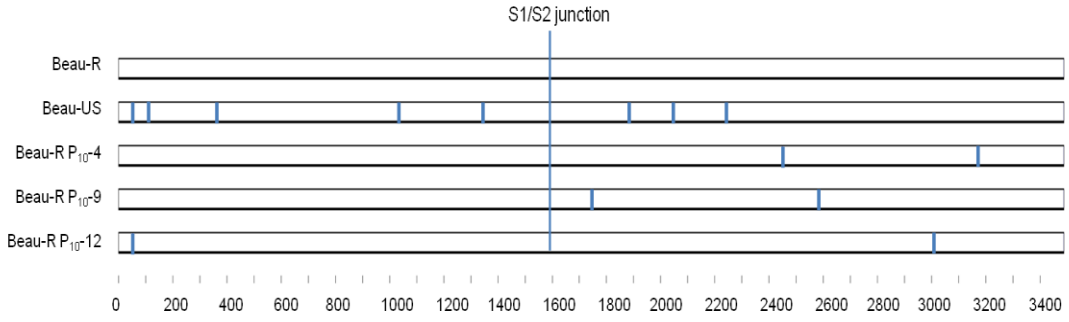

Figure 6.14. Consensus nucleotide sequences for all Beau-R P_{10} isolates, compared to parent Beau-R and Beau-US sequences. Substitutions are shown by a blue line. Nucleotide positions are indicated by numbers underneath. Diagrams were generated using Base-by-base (Brodie *et al.*, 2004) following alignment of individual clone sequences as described in the methods section.

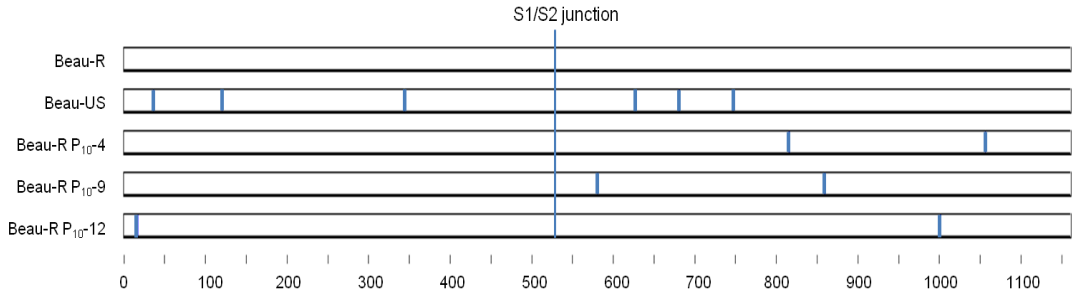

Figure 6.15. Consensus amino acid sequences for all Beau-R P_{10} isolates, compared to parent Beau-R and Beau-US sequences. Substitutions are shown by a blue line. Amino acid positions are indicated by numbers underneath. Diagrams were generated using Base-by-base (Brodie *et al.*, 2004) following alignment of individual clone sequences as described in the methods section.

Discussion

Beau-R was successfully adapted to form syncytia in Vero cell culture after nine passages. The P_{10} virus population was sequenced and seven coding nucleotide substitutions were identified (Table 5.3). One substitution occurred in the S1 subunit and six occurred in the S2 subunit. None corresponded to any of the differences between non-adapted Beau-R and Beau-US. It is likely however, that a mixed population of viruses was present in cell culture as not every infected cell formed syncytia as observed by confocal microscopy with indirect immunofluorescence (Figure 5.4).

Deep amplicon sequencing was carried out on three Beau-R P_{10} isolates, 4, 9 and 12 (Figures 5.8 – 5.13 and Appendix, Tables A.1 – A.9). Of the six differences identified between the Beau-R P_{10} population and non-adapted Beau-R, four were also identified by deep sequencing. The other two differences were identified in Beau-R P_{10}-7, which was not deep sequenced.

A total of 265 nucleotide substitutions were identified across the Beau-R P_{10} S genes by deep sequencing, 79 of which were shared by more than one clone. Only 151 of the substitutions were coding, there were also nine nucleotide deletions and 3 insertions. As it is the S2 subunit that is involved in fusion, it was anticipated that this region might contain the most differences; however, this was not found to be the case. Region two covering the S1/S2 junction had by far the fewest differences with

only twelve coding nucleotide substitutions identified; region one in the S1 subunit had the most with 81, while region three in the S2 subunit had 58.

One amino acid change of interest from proline to serine in Beau-R P_{10}-9 clone 17 region 2 occurs immediately upstream of the HSBS, adjacent to a mutation in Beau-US from asparagine to threonine at amino acid position 683. This amino acid has been previously implicated in syncytium formation by Yamada *et al.,* (2009), however they were unable to prove its involvement. As this mutation is only found in one clone and was not identified in the population sequencing, it is unlikely to be involved in the acquisition of syncytium formation in this case. No other mutations found in Beau-US were identified in Beau-R P_{10}.

A study by Yamada *et al.,* (2009) indicated that a single point mutation from leucine to phenylalanine at amino acid position 857 is responsible for the acquisition of cell-cell fusion activity in the IBV Beaudette spike. Site-directed mutagenesis was used to create S gene constructs containing the L857F mutation and these were expressed in Vero cells. The S glycoprotein containing the L857F mutation was able to induce syncytia formation, whereas the wild-type S glycoprotein could not. A reverse genetics system was used to introduce the L857F mutation into the IBV genome, enabling the recombinant virus to form syncytia. Further point mutations at positions 523 (glutamine – leucine) or 769 (isoleucine – valine) were sufficient to restore the cell-cell fusion activity to an rIBV containing an F857L mutation. Yamada *et al.,* (2009) also identified a further point mutation from glycine to aspartic acid at position 405 that was shown to enhance the cell-cell fusion activity.

Our laboratory isolate of Beaudette contains the phenylalanine at amino acid position 857 identified by Yamada *et al.,* (2009) as being responsible for acquisition of cell-cell fusion, although it does not form syncytia. It is unlikely that this amino acid is involved in syncytium formation by our laboratory isolate of Beaudette according to this study. None of the other amino acids involved in syncytia formation identified by Yamada *et al.,* (2009) have been found to correspond to changes in Beau-R P_{10} in this study.

The adaptation of BeauR-M41(S1) P_7-Vero to syncytia formation on Vero cells is described in Chapter 3 and the S genes of both isolates were sequenced (Figure 3.13). Interestingly, one of the amino acid changes identified in the BeauR-M41(S1) P_7-Vero isolate 2 S glycoprotein sequence corresponds to a change of threonine to isoleucine at position 1004 identified by Beau-R P_{10} population sequencing. This change was also identified by deep sequencing in nine clones of isolate 12 region three (Appendix, Table A.9). None of the amino acid changes identified in the M41-S-BeauR-Hep P_7-Vero isolates correspond to any changes identified in Beau-R P_{10} or BeauR-M41(S1) P_7-Vero isolates.

One limitation of this deep sequencing approach is that the whole S gene from different clones cannot be analysed, as clones from different regions do not correspond to each other. It would be interesting to be able to observe whether any changes in one region of the S gene are concurrent with other changes in different regions. Some nucleotide differences observed may be the result of PCR error,

especially those deletions resulting in non-homologous sequence or stop codons as they are unlikely to encode S glycoproteins present in viable virions.

In order to further investigate the effect of amino acid changes on cell-cell fusion, two approaches could be utilised. Site-directed mutagenesis coupled with the IBV reverse genetics system could be used to construct rIBVs expressing S glycoproteins containing combinations of the amino acid differences identified in this study and the growth phenotypes and kinetics of the resulting viruses could be analysed. Alternatively, modified S glycoproteins could be expressed on the cell-surface of Vero cells in order to observe whether they fuse to form syncytia. One drawback of this method is that the IBV S glycoprotein is not translocated to the cell surface efficiently due to the presence of an ER retention signal (Youn *et al.*, 2005) and transport of spikes not incorporated into virions through the Golgi is very slow (Vennema *et al.*, 1990).

As most of the differences between non-adapted Beau-R and Beau-R P_{10} isolates occur in just one clone and none are shared by more than nine out of a total of 140 clones sequenced, it seems likely that the acquisition of syncytium formation ability is a complex process, possibly involving a range of mutations. The structure of the IBV S glycoprotein is not currently known so it is only possible to speculate as to which areas of the spike might interact. It is feasible that areas involved in cell-cell fusion may be genetically distant from each other.

Chapter 6: General discussion and future work

Discussion

While the IBV strain Beau-R is able to replicate in Vero and BHK-21 cell lines as well as primary chicken cells, the IBV M41 strain is only able to replicate in primary cells. Casais *et al.,* (2003) determined that cellular tropism is conferred by the S glycoprotein by creating an rIBV with the M41 spike in the genomic background of Beau-R that has the cellular tropism of M41. The first objective of this study was to determine which part of the S glycoprotein is responsible for the extended host range of Beau-R.

The first step on the road to achieving this was to passage rIBV BeauR-M41(S) on Vero cells with the intention to adapt the virus to replication on Vero cells and identify any amino acid changes within the S glycoprotein. Despite several attempts, the adaptation of BeauR-M41(S) to growth on Vero cells was unsuccessful.

The second approach was to create two rIBVs with chimaeric S genes in the genomic background of Beau-R with either the S1 or S2 subunit from M41 using the IBV reverse genetics system. This was successful and the two resulting rIBVs, BeauR-M41(S1) and BeauR-M41(S2), were able to replicate as well as the parent viruses on primary chicken cells (Chapter 3, Figure 3.20).

As the S1 subunit is responsible for receptor binding, it was anticipated that this subunit would be responsible for the ability of Beau-R to replicate in Vero and BHK-21 cells rather than the S2 subunit, which is involved in virus-to-cell and cell-to-cell fusion. A previous study has mapped the extended host range of a variant of MHV to the S1 subunit (Schickli *et al.,* 2004). Surprisingly, it was determined that the ability to replicate in Vero and BHK-21 cells was conferred by the Beaudette S2 subunit, not the S1 subunit, although BeauR-M41(S1) did not replicate to as high a titre on Vero or BHK-21 cells as Beau-R (Chapter 3, Figures 3.21 – 22). Seven passages of BeauR-M41(S1) on Vero cells increased the titre (Chapter 3, Table 3.1) and resulted in a number of amino acid changes which may improve growth on the cell line (Chapter 3, Figure 3.13) .

In order to further investigate the role of the S2 subunit in determining cellular tropism, a sequence comparison was carried out between Beau-R and M41 to identify potential amino acid differences within the S2 subunit that could be involved (Chapter 4, Figure 4.1). Three amino acid changes were identified in close proximity to each other and were named the Beaudette-specific motif. Part of this motif has also been noted by other groups as being a putative heparan sulphate binding site (Madu *et al.,* 2007) or a potential furin cleavage site (Yamada and Liu, 2009).

Madu *et al.,* (2007) carried out bioinformatic analysis of the S glycoproteins of different strains of IBV and identified a putative heparan sulphate binding consensus sequence within the S2 subunit of the Beaudette S glycoprotein. This was not present in the thirteen other strains of IBV analysed. Infection of CK and BHK-21 cells by Beaudette was shown to be inhibited by soluble heparin and infection of

heparan sulphate-deficient cells by Beaudette was restricted. M41 infection was unaffected by the presence or absence of heparin, however infection of CK cells by both Beaudette and M41 strains was inhibited by neuraminidase treatment. These results indicate that sialic acid is an attachment factor for both Beaudette and M41 strains of IBV, however only Beaudette is able to utilise heparan sulphate as a selective attachment factor. The putative heparan sulphate binding consensus sequence identified within the S2 subunit of the Beaudette S glycoprotein forms part of the Beaudette-specific motif investigated by this study.

Yamada and Liu, (2009) suggested that a second furin cleavage site may be located within the putative heparan sulphate binding consensus sequence of the IBV Beaudette strain identified by Madu *et al.*, (2007). This XXXR/S motif was shown to be conserved between different coronavirus species. Vero cells were infected with rIBVs with Flag-tagged S glycoproteins to demonstrate that the Beaudette spike is cleaved at two furin sites, the S1/S2 junction and the XXXR/S motif within the S2 subunit. Point mutations introduced into the potential furin cleavage site within the S2 subunit resulted in loss of cleavage and loss of cell-to-cell fusion in the absence of trypsin when the mutated spikes were expressed in HuH-7 and Vero cells respectively. Yamada and Liu, (2009) stated that the extended host range of Beaudette is not due to the presence of the second furin site and that Beaudette does not utilise heparan sulphate as an attachment factor, although no data is shown to support this.

Another coronavirus with extended host range has been identified as using heparan sulphate as an entry receptor (de Haan *et al.*, 2005). The MHV-A59 strain was

serially passaged *in vitro* to produce a new variant, MHV/BHK, which was demonstrated to have an extended host range (Schickli *et al.*, 1997). Comparison of the S gene sequences of MHV-A59 and MHV/BHK revealed that the S gene of MHV/BHK has 56 amino acid substitutions and a seven amino acid insert (Schickli *et al.*, 2004), of which only 22 amino acid substitutions and the seven amino acid insert are required for host range extension (Thackray and Holmes, 2004). The extended host range of the MHV/BHK S glycoprotein was further investigated by de Haan *et al.*, (2005), who identified two putative heparan sulphate binding sites not present in MHV-A59. The predicted furin cleavage site between the S1 and S2 subunits also corresponded to a novel heparan sulphate binding site. This did not interfere with the furin consensus sequence, although the S glycoprotein of MHV/BHK was no longer cleaved at this site. Infectivity of a recombinant MHV expressing the MHV/BHK spike was reduced in the presence of heparin and after heparinase treatment of cells whereas infectivity of a recombinant MHV expressing the A59 spike was unaffected, indicating that heparan sulphate binding is involved in the extended host range of MHV/BHK.

In a study of FCoV strains with varying host range, heparan sulphate binding motifs were also identified at the S1-S2 boundaries (de Haan *et al.*, 2008). Strain UCD of FCoV, which is unable to grow in cell culture, did not bind heparin but was cleaved at the S1/S2 junction. Strain UCD1 of FCoV, which was adapted for cell culture and has an extended host range, did bind heparin but was not cleaved at the S1/S2 junction. Trypsin treatment of the UCD1 spike resulted in cleavage although infectivity was reduced. It appears that the heparan sulphate binding site only

functions as long as the spike is not cleaved and UCD1 has swapped cleavage for the ability to utilise heparan sulphate as an entry receptor.

In order to investigate the role of the Beaudette-specific motif of the Beaudette S2 subunit on the extended cellular tropism of Beau-R, two further rIBVs were created with chimaeric S genes in the genomic background of Beau-R (Chapter 4, Figure 4.2). The first rIBV, BeauR-S-M41-Hep, has the S gene from Beau-R but with the Beaudette-specific motif swapped for the corresponding sequence from M41. The second rIBV, M41-S-BeauR-Hep, has the S glycoprotein from M41 with the Beaudette-specific motif from Beau-R. Both recombinant viruses replicated as well as their parent viruses on CK cells (Chapter 4, Figure 4.14), and the Beaudette-specific motif was found to be sufficient to confer the ability to grow on Vero cells to M41-S-BeauR-Hep (Chapter 4, Figure 4.15). Replacement of the Beaudette-specific motif with the corresponding sequence from M41 in BeauR-S-M41-Hep resulted in the loss of ability to grow on Vero cells. Seven passages of M41-S-BeauR-Hep on Vero cells increased the titre (Chapter 4, Table 4.1) and resulted in a number of amino acid changes which may improve growth on the cell line (Chapter 4, Figure 4.9).

Although there is a clear indication of the involvement of the Beaudette-specific motif in the ability of Beau-R to replicate on Vero cells, it doesn't appear to affect growth on BHK-21 cells in the same way (Chapter 4, Figure 4.16). While M41-S-BeauR-Hep and BeauR-M41(S2) replicated poorly on BHK-21 cells, BeauR-S-M41-Hep replicated well and achieved a peak titre of over two log greater than that of BeauR-M41(S1). This indicates that the Beaudette-specific motif may not be the

only region of the Beau-R S glycoprotein that is responsible for the extended host range of Beau-R in mammalian cells other than Vero cells.

Several other coronaviruses have been studied with an expanded cellular tropism. The ability to infect macrophages is a virulence factor for FCoV pathogenesis. A strain of FCoV unable to infect macrophages causes mild enteritis in cats whereas a strain of FCoV that is able to infect macrophages causes fatal peritonitis. The ability to infect macrophages was mapped to the C-terminal region of the S glycoprotein, suggesting a role for fusion in host range expansion (Rottier *et al.*, 2005).

McRoy and Baric, (2008) studied another strain of MHV, V51, with extended host range and determined that the amino acid changes within the S2 subunit, specifically within and adjacent to the HR1 domain, were exclusively responsible for the determination of cellular tropism. No heparan sulphate binding sites were identified with the MHV-V51 S glycoprotein and the virus infected both cells expressing heparan sulphate and those that did not with a similar infectivity. It was postulated that the extended host range of MHV-V51 may be due to changes in the class I fusion mechanism conferred by the alterations in the S2 subunit.

A similar observation has been made in a study of the tropism of an avian retrovirus (Rainey *et al.*, 2003). Avian sarcoma-leukosis virus (ASLV) has a class I fusion protein with a similar structure to those of the *coronavirinae* with SU and TM subunits corresponding to S1 and S2 subunits. The extended host range of an ASLV strain was mapped to a single amino acid substitution in the HR1 domain. The

involvement of the HR1 domain of ASLV in host range expansion was confirmed by Amberg *et al.,* (2006).

A study by de Haan *et al.,* (2006) discovered that mutations in both the S1 and the S2 subunits are required for the extended host range of the A59 strain of MHV. As the structure of the IBV S glycoprotein has yet to be established, it is possible that regions far apart in the sequence may interact to extend the host range of Beau-R.

The second objective of this study was to identify the regions of the S glycoprotein that are involved in cell-to-cell fusion. In order to achieve this, Beau-R was adapted to form syncytia in Vero cell culture (Chapter 5, Figure 5.1). Beau-R is an rIBV derived from the Beaudette-CK strain of IBV. Beaudette-CK is a virus that has been adapted to grow on CK cells and has the ability, like all Beaudette-derived strains of IBV, to grow on Vero cells but does not cause syncytia formation without further adaptation to replication on Vero cells. Beau-R, like Beaudette-CK, was found to grow on Vero cells but not to cause syncytia (Casais *et al.,* 2001).

The Beau-R P_{10} population S gene was sequenced (Chapter 5, Figure 5.7) and deep amplicon sequencing was used to determine the S gene sequences of individual Beau-R P_{10} clones (Chapter 5, Figures 5.8 – 13). These were compared to the S gene sequences of non-adapted Beau-R and Beau-US, a strain of IBV that already forms syncytia in cell culture. Although numerous amino acid changes were identified, few were shared between Beau-R P_{10} clones and no specific areas appeared to be adapted. It appears that cell-to-cell fusion may be a complex process, possibly involving distinct regions of the IBV S glycoprotein.

Other studies have attempted to elucidate the region of the IBV S glycoprotein involved in cell-to-cell fusion. Yamada *et al.,* (2009) used site-directed mutagenesis to produce S gene constructs to investigate the induction of fusion by different isolates of IBV Beaudette. Beaudette was previously adapted to growth on Vero cells by Fang *et al.,* (2005), resulting in 26 amino acid substitutions in the S glycoprotein. Yamada *et al.,* (2009) cloned the S genes from several isolates of the Vero-adapted Beaudette strain and found upon expression that all except the original egg-derived isolate induced syncytia formation. One point mutation within HR1, L857F, was found to be responsible for the acquisition of cell-to-cell fusion activity in the Vero-adapted isolates. Introduction of the L857F mutation into the spike of the Beaudette egg-derived isolate by site directed mutagenesis conferred fusogenicity and reversion of the mutation (F857L) in a Vero-adapted isolate abolished the fusion activity. Recombinant IBVs were produced using an IBV reverse genetics system and the F857L mutation was introduced to the Vero-adapted isolate. This recombinant was not fusogenic, however, two compensatory mutations, Q523L and I769V, were sufficient for restoration of cell-to-cell fusion to occur. When these mutations were in turn introduced into the spike of the Beaudette egg-derived isolate, both induced cell-to-cell fusion. A further amino acid substitution, G405D, was implicated in enhancement of cell-to-cell fusion; when this mutation was introduced into the spike of the Beaudette egg-derived isolate, syncytia formation was also induced. The study was unable to pinpoint the definitive region of the IBV S glycoprotein that is responsible for the induction of cell-to-cell fusion.

The laboratory isolates of Beaudette utilised by the present study, Beaudette-CK and its derivative Beau-R, contain the L857F mutation identified by Yamada *et al.,*

(2009) as being responsible for syncytia formation; however these isolates are unable to induce cell-to-cell fusion. This supports the conclusion that it is likely that the induction of cell-to-cell fusion by the IBV S glycoprotein is a complex process, possibly involving several different regions of the spike.

The ability to form syncytia by the MHV S glycoprotein has been mapped to several different regions including the transmembrane domain (Bos *et al.,* 1995), the signal peptide and cleavage site (Yamada *et al.,* 1997) and the leucine zipper domain within HR2 (Britton, 1991; Luo *et al.*, 1999). Matsuyama and Taguchi, (2002a) studied the entry of soluble receptor resistant mutants of MHV to BHK cells expressing different MHV receptors, CEACAM1a and 1b. Amino acid substitutions within both the RBD in the S1 subunit and at position 1114 in the S2 subunit were found to be important for efficient fusion activity with cells expressing CEACAM1b.

It might be expected that forming syncytia in cell culture would increase the virus yield, potentially making the ability to form syncytia advantageous for vaccine production. It has been found, however, that a non-fusogenic strain of MHV replicates to a higher titre than a fusogenic strain of MHV in the same cell type (Zhu *et al.,* 2009). The viruses were determined to have similar infectivities; however, the genome of the non-fusogenic strain arrived at the ER earlier than the genome of the fusogenic strain. This indicates a role for the S glycoprotein in viral genome transport from the cell surface to the ER during infection but it is unclear how this is affected by the fusogenicity of the spike.

While it is currently uncertain exactly how the S2 subunit, in particular the Beaudette-specific motif, of Beaudette is involved in extended tropism, this knowledge can be exploited utilising the IBV reverse genetics system to grow IBV vaccine strains on Vero cells.

Future work

This project has revealed a number of areas for further research, which are outlined below, and has been awarded a grant from the BBSRC follow on fund in order to pursue these. In addition to this, rIBV BeauR-M41(S1) will be assessed by Intervet for its ability to grow in cell culture, stability during storage and immunogenicity as an inactivated vaccine formulation.

Extension of the Beaudette-specific motif in rIBV M41-S-BeauR-Hep

Other Beaudette-specific amino acids in addition to the Beaudette-specific motif will be investigated to ascertain whether they are involved in the tropism for Vero cells. A number of other Beaudette-specific amino acids have been identified in the S2 domain, which will be introduced into rIBV M41-S-BeauR-Hep using the IBV reverse genetics system by the replacement of the M41 amino acids with the Beaudette-specific amino acids. The growth phenotype and kinetics of the resulting rIBV on Vero cells will be investigated in comparison with M41-S-BeauR-Hep. Identification of a minimal sequence for the conferment of tropism for Vero cells will be beneficial as this will reduce the possibility of instability of complete S1 and S2 subunits from two different and more distantly related S proteins. The S1 subunits of different IBV isolates can vary by 5 – 50%.

Introduction of different S1 subunits into Beau-R

To develop the principle of using an rIBV with a chimaeric S gene as a vaccine strain, the S1 subunits from a common IBV live attenuated vaccine strain and a virulent field isolate of IBV will be introduced into the Beau-R genome using the IBV reverse genetics system. The resulting rIBVs will be used to confirm that the ability to grow on Vero cells is conferred by the S2 subunit as well as proving that the S1 subunit of an IBV vaccine or field strain can be expressed by an rIBV capable of growth in cell culture rather than embryonated eggs. This will be beneficial as the resulting potential vaccine will not require a lengthy attenuation step, will have a known genetic background and will be able to grow in cell culture rather than being restricted to embryonated eggs.

The role of heparan sulphate in the extended host range of Beau-R

There are a numbers of ways to investigate whether binding to heparan sulphate plays a role in the extended host range of Beau-R. Plaque reduction assays could be carried out in which Beau-R and the two rIBVs, BeauR-M41(S1) and M41-S-BeauR-Hep, are incubated in the presence of soluble heparin sodium salt at various concentrations 0 – 20 mg/ml before being used to carry out plaque assays on CK, Vero or BHK-21 cells. The number of plaques produced would indicate whether the presence of heparin at varying concentrations has any effect on the ability of the viruses to grow on that cell type.

Confocal microscopy with indirect immunofluorescence could be used to observe the effect of heparin on IBV infection by incubating different strains of IBV in the presence of heparin sodium salt at 15 mg/ml and in absence before infecting Vero,

CK and BHK-21 cells. The number of cells infected by viruses that were incubated with heparin can be compared to the number of cells infected by viruses that were incubated without heparin to establish if the degree of infection is affected.

The role of the putative second cleavage site in extended host range of Beau-R

In order to determine whether the Beau-R S glycoprotein is cleaved at the Beaudette-specific motif, the spike could be expressed, purified then run on a SDS PAGE gel to visualise whether it is cleaved at the S1/S2 junction only or also within the S2 subunit.

Further investigation of the amino acid changes in Beau-R P_{10} S glycoproteins that could be involved in syncytia formation

Two approaches could be utilised in order to further investigate the effect of amino acid changes in Beau-R P_{10} on cell-to-cell fusion. The IBV reverse genetics system could be used to construct rIBVs expressing S glycoproteins containing the amino acid differences identified in this study and the growth phenotypes and kinetics of the resulting viruses could be analysed. Alternatively, modified S glycoproteins could be produced using site-directed mutagenesis and expressed on the cell-surface of Vero cells in order to observe whether they fuse to form syncytia.

In order to determine whether the ability to form syncytia in Vero cell culture conveys a replicative advantage to Beau-R P_{10} over non-syncytia-forming isolates, growth curves could be carried out on Vero cells to compare the growth kinetics of Beau-R P_{10} isolates with non-adapted Beau-R.

Appendix

Table A.1. Beau-R P_{10}-4 deep sequencing region 1 nucleotide and amino acid differences. Nucleotide and amino acid differences identified in more than one isolate are shown in red, deletions are indicated by *, non-homologous sequence is indicated by ?.

clone	nucleotide position	adapted nucleotide	original nucleotide	amino acid position	amino acid change
23	20382	C	T	5	P - P
23	20385	C	T	6	L - L
35	20426	C	T	20	L - S
10	20459	T	A	31	Q - L
34	20485	A	T	40	W - R
28	20508	A	T	47	Y - STOP
29	20544	G	A	59	A - A
3	20560	C	T	65	C - R
29	20563	G	A	66	T - A
23	20583	C	T	72	G - G
33	20620	A	G	85	A - T
24	20622	G	A	85	A - A
34	20630	T	C	88	S - L
9	20634	C	T	89	G - G
21	20645	T	C	93	S - F
3	20669	G	A	101	H - R
32	20676	C	T	103	N - N
21	20691	C	A	108	T - T
25	20727	A	T	120	C - STOP
2	20744	C	T	126	L - P
22	20745	C	T	126	L - L
29	20747	G	A	127	Q - R
35	20758	G	A	131	I - V
9	20779	G	A	138	N - D
31	20787	A	G	140	Q - Q
9	20789	C	T	141	L - P
22	20805	T	A	146	T - T
8	20835	C	A	156	R - S
40	20855	G	A	163	N - S
32	20858	C	T	164	L - S
29	20862	T	A	165	T - T
23	20870	G	A	168	Y - C
33	20883	C	T	172	D - D
28	20903	G	A	179	E - G
34	20905	G	A	180	T - A

clone	nucleotide position	adapted nucleotide	original nucleotide	amino acid position	amino acid change
8	20935	C	T	190	F - L
22	20952	G	T	195	P - P
30	20954	C	T	196	I - T
30	21046	C	A	226	R - R
25	21058	A	G	230	A - T
10	21060	G	A	230	A - A
9	21066	A	G	232	Q - Q
9	21073	T	A	235	T - S
36	21124	G	A	252	K - E
9	21134	C	T	255	F - S
40	21136	G	A	256	I - V
8	21137	C	T	256	I - T
32	21165	C	T	265	T - T
28	21168	C	T	266	T - T
40	21177	*	A	269	L - ?
20	21188	C	T	273	I - T
33	21188	C	T	273	I - T
25	21189	C	T	273	I - I
9	21204	A	T	278	T - T
25	21246	A	T	292	T - T
23	21250	TT	CA	294	Q - L
30	21253	C	A	295	T - P
35	21255	G	A	295	T - T
29	21266	G	A	299	Q - R
35	21270	C	T	300	S - S
36	21276	*	T	302	Y - ?
33	21279	C	T	303	Y - Y
36	21314	G	A	315	Y - C
8	21322	C	T	318	S - P
9	21325	G	A	319	N - D
32	21328	C	T	320	F - L
20	21329	C	T	320	F - S
35	21335	G	A	322	Y - C
34	21342	C	T	324	S - S
8	21356	A	G	329	C - Y
40	21375	C	T	335	T - T
10	21379	G	A	337	N - D
29	21408	T	A	346	S - S
24	21441	C	T	357	G - G
10	21453	A	T	361	S - S
3	21460	G	A	364	K - E
40	21470	T	C	367	A - V
35	21493	A	T	375	Y - N
32	21501	C	T	377	G - G
3	21501	C	T	377	G - G

Table A.2. Beau-R P_{10}-9 deep sequencing region 1 nucleotide and amino acid differences. Nucleotide deletions are indicated by *, non-homologous sequence is indicated by ?.

clone	nucleotide position	adapted nucleotide	original nucleotide	amino acid position	amino acid change
8	20370	A	T	1	M - K
20	20572	C	T	68	G - G
39	20773	C	T	135	A - A
39	20810	G	A	148	S - G
12	20815	G	A	149	V - V
7	20852	G	A	162	N - D
1	20884	C	T	172	D - D
14	21021	C	T	218	V - V
27	21051	C	T	228	L - S
39	21066	T	A	233	Y - F
21	21080	CC	TT	238	F - P
27	21106	A	T	246	T - T
39	21107	G	A	247	N - D
24	21146	G	A	260	N - S
38	21159	G	A	264	N - S
21	21252	T	C	295	T - I
20	21283	C	T	305	F - F
39	21288	C	T	307	F - S
39	21356	G	A	330	K - E
27	21398	C	T	344	S - P
28	21433	T	A	355	Q - H
20	21499	C	T	377	G -G

Table A.3. Beau-R P_{10}-12 deep sequencing region 1 nucleotide and amino acid differences. Nucleotide and amino acid differences identified in more than one isolate are shown in red, deletions are indicated by *, non-homologous sequence is indicated by ?.

clone	nucleotide position	adapted nucleotide	original nucleotide	amino acid position	amino acid change
41	20406	C	T	13	C - C
10	20422	A	G	19	V - I
38	20422	A	G	19	V - I
2	20422	A	G	19	V - I
39	20422	A	G	19	V - I
54	20422	A	G	19	V - I
57	20430	C	T	21	Y - Y
39	20439	C	T	24	S - S
54	20439	C	T	24	S - S
2	20448	C	T	27	V - V
16	20497	A	G	43	G - R
51	20561	T	G	65	C - F
5	20580	C	T	71	H -H
51	20590	A	G	75	V - I
57	20604	C	T	79	S - S
39	20604	C	T	79	S - S
54	20604	C	T	79	S - S
6	20635	G	A	90	M - V
51	20636	C	T	90	M - T
1	20704	G	A	112	T - T
39	20704	G	A	112	T - T
54	20704	G	A	112	T - T
59	20774	G	A	136	M - V
6	20791	C	T	141	L - L
1	20793	C	T	142	F - S
59	20793	C	T	142	F - S
41	20802	C	T	145	L - S
59	20900	G	A	178	N - D
41	20904	G	A	179	E - G
59	20970	*	A	201	M - ?
39	21038	C	T	224	S - P
54	21038	C	T	224	S - P
57	21156	C	T	262	S - S
57	21172	G	A	268	T - A
1	21262	C	G	298	A - P
57	21309	C	T	313	F - F
59	21310	A	G	314	V - I
1	21311	C	T	314	V - A
10	21388	C	T	340	L - L
7	21438	C	T	356	G - G

Table A.4. Beau-R P_{10}-4 deep sequencing region 2 nucleotide and amino acid changes. Nucleotide and amino acid differences identified in more than one isolate are shown in red.

clone	nucleotide position	adapted nucleotide	original nucleotide	amino acid position	amino acid change
4	21567	C	T	400	Y -Y
15	21573	C	T	402	T - T
11	21912	C	T	515	T - T
12	21912	C	T	515	T - T
15	21987	C	T	540	T - T
6	21996	C	T	543	V - V
18	22020	C	T	551	Y -Y
19	22335	C	T	656	S - S

Table A.5. Beau-R P_{10}-9 deep sequencing region 2 nucleotide and amino acid changes. Nucleotide and amino acid differences identified in more than one isolate are shown in red.

clone	nucleotide position	adapted nucleotide	original nucleotide	amino acid position	amino acid change
19	22041	C	T	558	P - P
17	22048	C	T	561	S - P
17	22114	T	A	583	N - Y
18	22114	T	A	583	N - Y
20	22114	T	A	583	N - Y
19	22114	T	A	583	N - Y
18	22258	C	T	630	P - P
18	22348	C	T	660	A - A
17	22418	T	C	684	P - S
19	22618	C	T	750	Y - Y

Table A.6. Beau-R P_{10}-12 deep sequencing region 2 nucleotide and amino acid changes. Nucleotide differences identified in more than one isolate are shown in red, deletions are indicated by *.

clone	nucleotide position	adapted nucleotide	original nucleotide	amino acid position	amino acid change
11	21541	G	A	391	H - R
9	21554	C	T	395	C - C
16	21561	C	T	398	L - L
12	21561	C	T	398	L - L
20	21607	T	C	413	T - I
17	21752	G	A	461	A - A
14	21755	C	T	463	G - G
3	21893	C	T	508	I - I
8	21899	C	T	510	T - T
13	21948	T	C	526	I - I
10	22061	G	A	564	T - A
16	22209	T*TG**TG	TATGTTTG	613	YV – L*
12	22209	T*TG**TG	TATGTTTG	613	YV – L*
3	22209	T*TG**TG	TATGTTTG	613	YV – L*

Table A.7. Beau-R P_{10}-4 deep sequencing region 3 nucleotide and amino acid changes. Nucleotide and amino acid differences identified in more than one isolate are shown in red, deletions are indicated by *, non-homologous sequence is indicated by ?.

clone	nucleotide position	adapted nucleotide	original nucleotide	amino acid postion	amino acid change
12	22832	G	A	822	Q - R
13	22856	T	C	830	A - V
5	22860	A	T	831	I - I
18	22866	A	T	833	T - T
16	22988	C	T	874	L - S
3	23019	T	A	884	K - M
1	23082	C	T	905	C - C
11	23102	A	G	912	R - K
1	23133	C	T	922	V - V
19	23199	G	T	944	S - R
16	23252	*	A	962	S - ?
12	23259	C	T	964	Y - Y
19	23259	C	T	964	Y - Y
16	23381	T	C	1005	S - F
1	23403	C	T	1012	S - S
11	23438	G	A	1024	N - S
3	23472	G	A	1035	K - K
11	23478	T	G	1037	W - C
6	23647	C	T	1094	W - R
19	23684	C	T	1106	I - T
12	23832	G	A	1155	Q - Q

Table A.8. Beau-R P_{10}-9 deep sequencing region 3 nucleotide and amino acid changes. Nucleotide and amino acid differences identified in more than one isolate are shown in red, deletions are indicated by *, non-homologous sequence is indicated by ?.

clone	nucleotide position	adapted nucleotide	original nucleotide	amino acid position	amino acid change
6	22675	T	C	770	P - S
7	22694	G	A	776	Q - R
2	22758	A	T	797	A - A
9	22765	C	T	800	F - L
19	22799	C	T	811	F - S
5	22801	T	A	812	R - *
17	22819	C	T	818	L - L
7	22865	T	C	833	T - I
3	22883	A	T	839	L - H
9	23081	C	T	905	C - R
7	23096	T	C	910	S - F
9	23151	G	A	928	N - D
5	23177	G	A	936	I - M
7	23254	*	A	962	S - ?
18	23320	C	T	984	I - T
11	23325	T	G	986	A - S
13	23325	T	G	986	A - S
11	23383	T	C	1005	S - F
10	23407	C	T	1013	V - A
3	23435	G	A	1022	V - V
7	23461	G	A	1031	D - G
13	23475	A	T	1036	W - R
11	23576	C	T	1069	V - V
14	23638	C	T	1090	I - T
11	23727	G	T	1120	C - G
12	23764	T	C	1132	P - L
12	23798	A	T	1143	Y - STOP
5	23802	G	A	1145	T - A
12	23847	G	A	1160	K - E
1	23852	C	T	1161	S - S

Table A.9. Beau-R P_{10}-12 deep sequencing region 3 nucleotide and amino acid changes. Nucleotide and amino acid differences identified in more than one isolate are shown in red, deletions are indicated by *.

clone	nucleotide position	adapted nucleotide	original nucleotide	amino acid position	amino acid change
5	22722	*	C	785	T - *
7	22733	C	T	790	L – L
4	22749	*	A	794	E - *
9	22832	T	C	822	Q - *
7	22843	C	T	825	V - V
5	22917	C	T	850	I - T
3	22950	T	A	861	Q - L
7	22957	C	T	863	N - N
5	23000	C	T	878	S - P
3	23033	GCTAGAAAGTGTAG	ATTAG**AGTGTCA	889	IRVS - ARKCS
18	23047	G	A	893	Q - Q
11	23055	C	A	896	E - A
16	23134	C	T	922	V - V
5	23215	C	T	949	T - T
12	23324	T	G	986	A - S
1	23324	T	G	986	A - S
16	23379	T	C	1004	T - I
7	23379	T	C	1004	T - I
5	23379	T	C	1004	T - I
3	23379	T	C	1004	T - I
18	23379	T	C	1004	T - I
8	23379	T	C	1004	T - I
6	23379	T	C	1004	T - I
9	23379	T	C	1004	T - I
11	23379	T	C	1004	T - I
15	23380	C	T	1004	T - T
17	23440	C	T	1024	N - N
3	23454	C	T	1029	F - S
16	23464	G	A	1032	E - E
16	23470	T	A	1034	S - S
6	23600	T	A	1078	I - L
7	23637	C	T	1090	I - T
6	23637	G	T	1090	I - S
16	23666	G	A	1100	I - V
8	23712	C	T	1115	F - S
1	23741	***	GTT	1125	GC – G*
3	23771	G	A	1135	S - G

Bibliography

Alimonti, J., Ball T. and Fowke, K. (2003). Mechanisms of CD4+ T lymphocyte cell death in human immunodeficiency virus infection and AIDS. *J. Gen. Virol.* **84**: 1649 – 1661.

Ambali, A. and Jones, R. (1990). Early pathogenesis in chicks of infection with an enterotropic strain of infectious bronchitis virus. *Avian Dis.* **34:** 809 – 817.

Amberg, S., Netter, R., Simmons, G. and Bates, P. (2006). Expanded tropism and altered activation of a retroviral glycoprotein resistant to an entry inhibitor peptide. *J. Virol.* **80**: 353 – 359.

Armesto, M., Cavanagh, D. and Britton, P. (2009). The replicase gene of avian coronavirus infectious bronchitis virus is a determinant of pathogenicity. *PLoS One* **4**: e7384.

Babcock, G., Esshaki, D., Thomas, W. and Ambrosino, D. (2004). Amino acids 270 to 510 of the severe acute respiratory syndrome coronavirus spike protein are required for interaction with receptor. *J. Virol.* **78:** 4552 – 4560.

Baudoux, P., Carrat, C., Besnardeau, L., Charley, B. and Laude, H. (1998). Coronavirus pseudoparticles formed with recombinant M and E proteins induce alpha interferon synthesis by leukocytes. *J. Virol*. **72:** 8636 – 8643.

Bonavia, A., Zelus, B., Wentworth, D., Talbot, P. and Holmes, K. (2003). Identification of a Receptor-Binding Domain of the Spike Glycoprotein of Human Coronavirus HCoV-229E. *J. Virol.* **77:** 2530 – 2538.

Bos, E., Heijnen, L., Luytjes, W. and Spaan, W. (1995). Mutational analysis of the murine coronavirus spike protein: effect on cell-to-cell fusion. *Virology* **214**: 453 – 463.

Bos, E., Luytjes, W. and Spaan, W. (1997). The function of the spike protein of mouse hepatitis virus strain A59 can be studied on virus-like particles: cleavage is not required for infectivity. *J. Virol.* **71:** 9427 – 9433.

Bosch, J., van der Zee, R., de Haan, C. and Rottier, P. (2003). The coronavirus spike protein is a class I virus fusion protein: Structural and functional characterization of the fusion core complex. *J. Virol.* **77:** 8801 – 8811.

Boursnell, M., Brown, T., Foulds, I., Green, P., Tomley, F. and Binns, M. (1987). Completion of the sequence of the genome of the coronavirus avian infectious bronchitis virus. *J. Gen. Virol.* **68:** 57 – 77.

Brierley, I., Boursnell, M., Binns, M., Bilimoria, B., Blok, V., Brown, T. and Inglis, S. (1987). An efficient ribosomal frame-shifting signal in the polymerase-encoding region of the coronavirus IBV. *EMBO J.* **6:** 3379 – 3785.

Britton, P. (1991). Coronavirus motif. *Nature* **353**: 394.

Britton, P., Evans, S., Dove, B., Davies, M., Casais, R. and Cavanagh, D. (2005). Generation of a recombinant avian coronavirus infectious bronchitis virus using transient dominant selection. *J. Virol. Methods* **123**: 203 – 211.

Brodie, R., Smith, A., Roper, R., Tcherepanov, V. and Upton, C. (2004). Base-By-Base: Single nucleotide-level analysis of whole viral genome alignments. *BMC Bioinformatics* **5**: 96.

Cardin, A. and Weintraub, H. (1989). Molecular modeling of proteinglycosaminoglycan interactions. *Arteriosclerosis* **9:** 21 – 32.

Carstens, E. (2010). Ratification vote on taxonomic proposals to the International Committee on Taxonomy of Viruses (2009). *Arch. Virol.* **155**: 133 – 146.

Casais, R., Davies, M., Cavanagh, D. and Britton, P. (2005)**.** Gene 5 of the avian coronavirus infectious bronchitis virus is not essential for replication. *J. Virol.* **79:** 8065 – 8078.

Casais, R., Dove, B., Cavanagh, D. and Britton, P. (2003). Recombinant avian infectious bronchitis virus expressing a heterologous spike gene demonstrates that the spike protein is a determinant of cell tropism. *J. Virol.* **77:** 9084 – 9089.

Casais, R., Thiel, V., Siddell, S., Cavanagh, D. and Britton, P. (2001). Reverse genetics system for the avian coronavirus infectious bronchitis virus. *J. Virol.* **75:** 12359 – 12369.

Cavanagh, D. (2007). Coronavirus avian infectious bronchitis virus. *Vet. Res.* **38**: 281 – 297.

Cavanagh, D. (1983). Coronavirus IBV glycopolypeptides: Size of their polypeptide moieties and nature of their oligosaccharides. *J. Gen. Virol.* **64:** 1187 – 1191.

Cavanagh, D., Davis, P., Pappin, D., Binns, M., Boursnell, M. and Brown, T. (1986). Coronavirus IBV: partial amino terminal sequencing of spike polypeptide S2 identifies the sequence Arg-Arg-Phe-Arg-Arg at the cleavage site of the spike precursor polypeptide of IBV strains Beaudette and M41. *Virus Res.* **4**: 133 – 143.

Centres for disease control and prevention (2010). Public health image library, image number 4814. http://phil.cdc.gov/phil/home.asp

Chambers, P., Pringle, C. and Easton, A. (1990). Heptad repeat sequences are located adjacent to hydrophobic regions in several types of virus fusion glycoproteins. *J. Gen. Virol.* **71:** 3075 – 3080.

Chan, D., and Kim, D. (1998). HIV entry and its inhibition. *Cell* **93:** 681 – 684.

Chan, C., Lau, S., Woo, P., Tse, H., Zheng, B., Chen, L., Huang, J. and Yuen, K. (2009). Identification of major histocompatibility complex class I C molecule as an attachment factor that facilitates coronavirus HKU1 spike-mediated infection. *J. Virol.* **83:** 1026 – 1035.

Chandran, K., Sullivan, N., Felbor, U., Whelan, S. and Cunningham, J. (2005). Endosomal proteolysis of the Ebola virus glycoprotein is necessary for infection. *Science* **308:** 1643 – 1645.

Chu, V., McElroy, L., Chu, V., Bauman, B. and Whittaker, G. (2006). The avian coronavirus infectious bronchitis virus undergoes direct low-pH-dependent fusion activation during entry into host cells. *J. Virol.* **80:** 3180 – 3188.

Chu, V., McElroy, L., Aronson, J., Oura, T., Harbison, C., Bauman B. and Whittaker, G. (2007). Feline aminopeptidase N is not a functional receptor for avian infectious bronchitis virus. *Virology J.* **4**: 20.

Cook, J., Chesher, J., Baxendale, W., Greenwood, N., Huggins, M., and Orbell, S. (2001). Protection of chickens against renal damage caused by a nephropathogenic infectious bronchitis virus. *Avian Pathol.* **30:** 423 – 426.

Corse, E. and Machamer, C. (2003). The cytoplasmic tails of infectious bronchitis virus E and M proteins mediate their interaction. *Virology* **312**: 25 – 34.

DEFRA (2005). Economic assessment of livestock diseases in Great Britain, 2000 – 2002.
http://www.defra.gov.uk/science/Project_Data/DocumentLibrary/ZZ0102/ZZ0102_1215_FRP.doc

de Haan, C., Haijema, B., Schellen, P., Wichgers Schreur, P., te Lintelo, E., Vennema, H. and Rottier, P. (2008). Cleavage of group 1 coronavirus spike proteins: How furin cleavage is traded off against heparan sulfate binding upon cell culture adaptation. *J. Virol.* **82:** 6078 – 6083.

de Haan, C., Li, Z., Lintelo, E., Bosch, B., Haijema, B. and Rottier, P. (2005). Murine coronavirus with an extended host range uses heparan sulfate as an entry receptor. *J. Virol.* **79:** 14451 – 14456.

de Haan, C., Masters, P., Shen, X., Weiss, S. and Rottier, P. (2002). The group-specific murine coronavirus genes are not essential, but their deletion, by reverse genetics, is attenuating in the natural host. *Virology* **296:** 177 – 189.

de Haan, C., Smeets, M., Vernooij, F., Vennema, H. and Rottier, P. (1999). Mapping of the coronavirus membrane protein domains involved in interaction with the spike protein. *J. Virol.* **73**: 7441 – 7452.

de Haan, C., Stadler, K., Godeke, G., Bosch, B. and Rottier, P. (2004). Cleavage inhibition of the murine coronavirus spike protein by a furin-like enzyme affects cell-cell but not virus-cell fusion. *J. Virol*. **78:** 6048 – 6054.

de Haan, C., te Lintelo, E., Li, Z., Raaben, M., Wurdinger, T., Bosch, B. and Rottier, P. (2006). Cooperative involvement of the S1 and S2 subunits of the murine coronavirus spike protein in receptor binding and extended host range. *J. Virol.* **80:** 10909 – 10918.

Delmas, B., Gelfi, J., Haridon, R., Vogel, L., Sjostrom, H., Noren, O. and Laude, H. (1992). Aminopeptidase N is a major receptor for the entero-pathogenic coronavirus TGEV. *Nature* **357**: 417 – 420.

Delmas, B. and Laude, H. (1990). Assembly of coronavirus spike protein and its role in epitope expression. *J. Virol.* **64:** 5367 – 5375.

Donaldson, E., Sims, A., Deming, D. and Baric, R. (2006). Mutational analysis of MHV-A59 replicase protein nsp10. In Perlman, S. and Holmes, K. (Eds), The Nidoviruses: toward control of SARS and other Nidovirus diseases. Advances in experimental medicine and biology **581:** 61 – 66 *Springer.*

Eckerle, L., Brockway, S., Sperry, S., Lu, X. and Denison, M. (2006). Effects of mutagenesis of murine hepatitis virus nsp1 and nsp14 on replication in culture. In Perlman, S. and Holmes, K. (Eds), The Nidoviruses: toward control of SARS and other Nidovirus diseases. Advances in experimental medicine and biology **581:** 55 – 60 *Springer.*

Egloff, M., Ferron, F., Campanacci, V., Longhi, S., Rancurel, C., Dutartre, H., Snijder, E., Gorbalenya, A., Cambillau, C. and Canard, B. (2004). The severe acute respiratory syndrome-coronavirus replicative protein nsp9 is a single-stranded RNA-binding subunit unique in the RNA virus world. *Proc. Natl. Acad. Sci. USA* **101:** 3792 – 3796.

Eifart, P., Ludwig, K., Bottcher, C., de Haan, C., Rottier, P., Korte, T., and Herrmann, A. (2007). Role of endocytosis and low pH in murine hepatitis virus strain A59 cell entry. *J. Virol.* **81**: 10758 – 10768.

Fang, S., Shen, S., Tay, F. and Liu, D. (2005). Selection of and recombination between minor variants lead to the adaptation of an avian coronavirus to primate cells. *Biochem. Biophys. Res. Comm.* **336**: 417 – 423.

Fischer, F., Stegen, C., Masters, P. and Samsonoff, W. (1998). Analysis of constructed E gene mutants of mouse hepatitis virus confirms a pivotal role for E protein in coronavirus assembly. *J. Virol.* **72**: 7885 – 7894.

Fischer, F., Peng, D., Hingley, S., Weiss, S. and Masters, P. (1997). The internal open reading frame within the nucleocapsid gene of mouse hepatitis virus encodes a structural protein that is not essential for viral replication. *J. Virol*. **71**: 996 – 1003.

Follis, K., York, J. and Nunberg, J. (2006). Furin cleavage of the SARS coronavirus spike glycoprotein enhances cell-cell fusion but does not affect virion entry. *Virology* **350**: 358 – 369.

Frana, M., Behnke, J., Sturman, L. and Holmes, K. (1985). Proteolytic cleavage of the E2 glycoprotein of murine coronavirus: host-dependent differences in proteolytic cleavage and cell fusion. *J. Virol.* **56:** 912 – 920.

Frazatti-Gallina, N., Mourao-Fuches, R., Paoli, R., Silva, M., Miyaki, C. and Valentini, E. (2004). Vero-cell rabies vaccine produced using serum-free medium. *Vaccine* **23**: 511 – 517.

Gamblin, S., Haire, L., Russell, R., Stevens, D., Xiao, B., Ha, Y., Vasisht, N., Steinhauer, D., Daniels, R., Elliot, A., Wiley, D. and Skehel, J. (2004). The structure and receptor binding properties of the 1918 influenza hemagglutinin. *Science* **303**: 1838 – 1842.

Garry, R. and Dash, S. (2003). Proteomics computational analyses suggest that hepatitis C virus E1 and pestivirus E2 envelope glycoproteins are truncated class II fusion proteins. *Virology* **307**: 255 – 265.

Godeke, G., de Haan, C., Rossen, J., Vennema, H. and Rottier, P. (2000). Assembly of spikes into coronavirus particles is mediated by the carboxy-terminal domain of the spike protein. *J. Virol.* **74:** 1566 – 1571.

Gosert, R., Kanjanahaluethai, A., Egger, D., Bienz, K. and Baker, S. (2002). RNA replication of mouse hepatitis virus takes place at double-membrane vesicles. *J. Virol.* **76:** 3697 – 3708.

Gorbalenya, A., Enjuanes, L., Ziebuhr, J. and Snijder, E. (2006). Nidovirales: Evolving the largest RNA virus genome. *Virus Research* **117:** 17 – 37.

Gorbalenya, A., Koonin, E., Donchenko, A. and Blinov, V. (1989). Coronavirus genome: prediction of putative functional domains in the non-structural polyprotein by comparative amino acid sequence analysis. *Nucl. Acids Res.* **17:** 4847 – 4861.

Govorkova, E., Murti, G., Meignier, B., de Taisne, C. and Webster, R. (1996). African green monkey kidney (Vero) cells provide an alternative host cell system for influenza A and B viruses. *J. Virol.* **70:** 5519 – 5524.

Graham, R. and Denison, M. (2006). Replication of murine hepatitis virus is regulated by papain-like proteinase 1 processing of nonstructural proteins 1, 2, and 3. *J. Virol.* **80:** 11610 – 11620.

Guo, Y., Tisoncik, J., McReynolds, S., Farzan, M., Prabhakar, B., Gallagher, T., Rong, L. and Caffrey, M. (2009). Identification of a new region of SARS-CoV S protein critical for viral entry. *J. Mol. Biol.* **394:** 600 – 605.

Hagemeijer, M., Verheije, M., Ulasli, M., Shaltie, I., de Vries, L., Reggiori, F., Rottier, P. and de Haan, C. (2010). Dynamics of coronavirus replication-transcription complexes. *J. Virol.* **84:** 2134 – 2149.

Han, D., Lohani, M. and Cho, M. (2007). Specific asparagine-linked glycosylation sites are critical for DC-SIGN- and L-SIGN-mediated severe acute respiratory syndrome coronavirus entry. *J. Virol.* **81:** 12029 – 12039.

Harris, R., Dougherty, R., Biggs, P., Payne, L., Goffe, A., Churchill, A. and Mortimer, R. (1966). Contaminant viruses in two live virus vaccines produced in chick cells. *J. Hyg.* **64**: 1 – 7.

Hodgson, T., Casais, R., Dove, B., Britton, P. and Cavanagh, D. (2004). Recombinant infectious bronchitis coronavirus Beaudette with the spike protein gene of the pathogenic M41 strain remains attenuated but induces protective immunity. *J. Virol.* **78:** 13804 – 13811.

Hodgson, T., Britton, P. and Cavanagh, D. (2006). Neither the RNA nor the proteins of open reading frames 3a and 3b of the coronavirus infectious bronchitis virus are essential for replication. *J. Virol.* **80:** 296 – 305.

Huang, Y. and Wang, C. (2007). Sequence changes of infectious bronchitis virus isolates in the 3' 7.3 kb of the genome after attenuating passage in embryonated eggs. *Avian Pathology* **36**: 59 – 67.

Hurst, K., Kuo, L., Koetzner, C., Ye, R., Hsue, B. and Masters, P. (2005). A major determinant for membrane protein interaction localizes to the carboxy-terminal domain of the mouse coronavirus nucleocapsid protein. *J. Virol.* **79**: 13285 – 13297.

Inoue, Y., Tanaka, N., Tanaka, Y., Inoue, S., Morita, K., Zhuang, M., Hattori, T. and Sugamura, K. (2007). Clathrin-dependent entry of severe acute respiratory syndrome coronavirus into target cells expressing ACE2 with the cytoplasmic tail deleted. *J. Virol.* **81**: 8722 – 8729.

International Committee on Taxonomy of Viruses, Index of Viruses - Coronaviridae (2008). In: ICTVdB - The Universal Virus Database, version 4. Büchen-Osmond, C (Ed), Columbia University, New York, USA.

Jeffers, S., Tusell, S., Gillim-Ross, L., Hemmila, E., Achenbach, J., Babcock, G., Thomas, W., Thackray, L., Young, M., Mason, R., Ambrosino, D., Wentworth, D., DeMartini, J. and Holmes, K. (2004). CD209L (L-SIGN) is a receptor for severe acute respiratory syndrome coronavirus. *Proc. Natl. Acad. Sci. USA* **101:** 15748 – 15753.

Jia, W., and Naqi, S. (1997). Sequence analysis of gene 3, gene 4 and gene 5 of avian infectious bronchitis virus strain CU-T2. *Gene* **189:** 189 – 193.

Kahn, J., Schnell, M., Buonocore, L. and Rose, J. (1999). Recombinant vesicular stomatitis virus expressing respiratory syncytial virus (RSV) glycoproteins: RSV fusion protein can mediate infection and cell fusion. *Virology* **254:** 81 – 91.

Kam, Y., Okumura, Y., Kido, H., Ng, L., Bruzzone, R. and Altmeyer, R. (2009). Cleavage of the SARS coronavirus spike glycoprotein by airway proteases enhances virus entry into human bronchial epithelial cells *in vitro*. *PLoS One* **4:** e7870.

Kamitani, W., Narayanan, K., Huang, C., Lokugamage, K., Ikegami, T., Ito, N., Kubo, H. and Makino, S. (2006). Severe acute respiratory syndrome coronavirus nsp1 protein suppresses host gene expression by promoting host mRNA degradation. *Proc. Natl. Acad. Sci. USA* **103:** 12885 – 12890.

Kawase, M., Shirato, K., Matsuyama, S. and Taguchi, F. (2009)**.** Protease-mediated entry via the endosome of human coronavirus 229E. *J. Virol.* **83:** 712 – 721.

Kistner, O., Barrett, P., Mundt, W., Reiter, M., Schober-Bendixen, S. and Dorner, F. (1998). Development of a mammalian cell (Vero) derived candidate influenza virus vaccine. *Vaccine* **16:** 960 – 968.

Klumperman, J., Locker, J., Meijer, A., Horzinek, M., Geuze, H. and Rottier, P. (1994). Coronavirus M proteins accumulate in the golgi complex beyond the site of virion budding. *J. Virol.* **68:** 6523 – 6534.

Knoops, K., Kikkert, M., Worm, S., Zevenhoven-Dobbe, J., van der Meer, Y., Koster, A., Mommaas, A. and Snijder, E. (2008). SARS- coronavirus replication is supported by a reticulovesicular network of modified endoplasmic reticulum. *PLoS Biol.* **6**: e226.

Koch, G., Hartog, L., Kant, A. and van Roozelaar, D. (1990). Antigenic domains on the peplomer protein of avian infectious bronchitis virus: correlation with biological functions. *J. Gen. Virol.* **71:** 1929 – 1935.

Koetzner, C., Kuo, L., Goebel, S., Dean, A., Parker, M. and Masters, P. (2010). Accessory protein 5a is a major antagonist of the antiviral action of interferon against murine coronavirus. *J. Virol.* **84:** 8262 – 8274.

Kozak, M. (1981). Possible role of flanking nucleotides in recognition of the AUG initiator codon by eukaryotic ribosomes. *Nucleic Acids Res.* **9**: 5233 – 5252.

Kubo, H., Yamada, Y. and Taguchi, F. (1994). Localization of neutralizing epitopes and the receptor-binding site within the amino-terminal 330 amino acids of the murine coronavirus spike protein. *J. Virol.* **68:** 5403 – 5410.

Lai, M., Patton, C., Baric, R. and Stohlman, S. (1983). Presence of leader sequences in the mRNA of mouse hepatitis virus. *J. Virol.* **46:** 1027 – 1033.

Langereis, M., van Vliet, A., Boot, W. and de Groot, R. (2010). Attachment of mouse hepatitis virus to O-acetylated sialic acid is mediated by hemagglutinin-esterase and not by the spike protein**.** *J. Virol.* **84**: 8970 – 8974.

Larkin, M., Blackshields, G., Brown, N., Chenna, R., McGettigan, P., McWilliam, H., Valentin, F., Wallace, I., Wilm, A., Lopez, R., Thompson, J., Gibson T. and Higgins, D. (2007). Clustal W and Clustal X version 2.0. *Bioinformatics* **23:** 2947 – 2948.

Le, S., Sonenberg, N. and Maizel, J. (1994). Distinct structural elements and internal entry of ribosomes in mRNA3 encoded by infectious bronchitis virus. *Virology* **198:** 405 – 411.

Li, W., Moore, M., Vasilieva, N., Sui, J., Wong, S., Berne, M., Somasundaran, M., Sullivan, J., Luzuriaga, K., Greenough, T., Choe, H. and M. Farzan (2003). Angiotensin-converting enzyme 2 is a functional receptor for the SARS coronavirus. *Nature* **426:**450 – 454.

Lim, K. and Liu, D. (2001). The missing link in coronavirus assembly: retention of the avian coronavirus infectious bronchitis virus envelope protein in the pre-golgi compartments and physical interaction between the envelope and membrane proteins. *J. Biol. Chem.* **276:** 17515 – 17523.

Liu, D. and Inglis, S. (1992). Internal entry of ribosomes on a tricistronic mRNA encoded by infectious bronchitis virus. *Virology* **66:** 6143 – 6154.

Liu, J. and Thorp, S. (2002). Cell surface heparan sulfate and its roles in assisting viral infections. *Med. Res. Rev*. **22:** 1 – 25.

Lontok, E., Corse, E. and Machamer, C. (2004). Intracellular targeting signals contribute to localization of coronavirus spike proteins near the virus assembly site. *J Virol* **78:** 5913 – 5922.

Lu, X., Lu, Y. and Denison, M. (1996). Intracellular and *in vitro*-translated 27-kDa proteins contain the 3C-like proteinase activity of the coronavirus MHV-A59. *Virology* **222:** 375 – 382.

Luo, Z., Matthews, A. and Weiss, S. (1999). Amino acid substitutions within the leucine zipper domain of the murine coronavirus spike protein cause defects in oligomerization and the ability to induce cell-to-cell fusion. *J. Virol.* **73**: 8152 – 8159.

Luo, Z. and Weiss, S. (1998). Roles in cell-to-cell fusion of two conserved hydrophobic regions in the murine coronavirus spike protein. *Virology* **244:** 483 – 494.

Machamer, C., Mentonet, S., Rose, J. and Farquhart, M. (1990). The El glycoprotein of an avian coronavirus is targeted to the cis Golgi complex. *Proc. Nat. Acad. Sci. USA* **87**: 6944 – 6948.

Madu, I., Chu, V., Lee, H., Regan, A., Bauman, B. and Whittaker, G. (2007). Heparan sulfate is a selective attachment factor for the avian coronavirus infectious bronchitis virus Beaudette. *Avian Diseases* **51:** 45 – 51.

Madu, I., Roth, S., Belouzard, S. and Whittaker, G. (2009). Characterization of a highly conserved domain within the severe acute respiratory syndrome coronavirus spike protein S2 domain with characteristics of a viral fusion peptide. *J. Virol.* **83**: 7411 – 7421.

Maeda, N., Fan, H. and Yoshikai, Y. (2008). Oncogenesis by retroviruses: old and new paradigms. *Rev. Med. Virol.* **18**: 387 – 405.

Matsuyama, S., Nagata, N., Shirato, K., Kawase, M., Takeda, M. and Taguchi, F. (2010). Efficient activation of the severe acute respiratory syndrome coronavirus spike protein by the transmembrane protease TMPRSS2._ *J. Virol.* **84:** 12658 – 12664.

Matsuyama, S. and Taguchi, F. (2002a). Communication between S1N330 and a region in S2 of murine coronavirus spike protein is important for virus entry into cells expressing CEACAM1b receptor. *Virology* **295:** 160 – 171.

Matsuyama, S. and Taguchi, F. (2002b). Receptor-induced conformational changes of murine coronavirus spike protein. *J. Virol.* **76:** 11819 – 11826.

Matthijs, M., van Eck, J., Landman, W., and Stegeman, J. (2003). Ability of Massachusetts-type infectious bronchitis virus to increase colibacillosis susceptibility in commercial broilers: a comparison between vaccine and virulent field virus. *Avian Pathol*. **32**: 473 – 481.

McBride, C., Li, J. and Machamer, C. (2007). The cytoplasmic tail of the severe acute respiratory syndrome coronavirus spike protein contains a novel endoplasmic reticulum retrieval signal that binds COPI and promotes interaction with membrane protein. *J. Virol.* **81**: 2418 – 2428.

McBride, C. and Machamer, C. (2010). Palmitoylation of SARS-CoV S protein is necessary for partitioning into detergent-resistant membranes and cell–cell fusion but not interaction with M protein. *Virology* **405**: 139 – 148.

McRoy, W. and Baric, R. (2008). Amino acid substitutions in the S2 subunit of mouse hepatitis virus variant V51 encode determinants of host range expansion. *J. Virol.* **82:** 1414 – 1424.

Melikyan, G., White, J. and Cohen, F. (1995). GPI-anchored influenza hemagglutinin induces hemifusion to both red blood cell and planar bilayer membranes. *J. Cell Biol.* **131:** 679 – 691.

Miguel, B., Pharr, G. and Wang, C. (2002). The role of feline aminopeptidase N as a receptor for infectious bronchitis virus. *Arch. Virol.* **147**: 2047 – 2056.

Montagnon, B., Fanget, B. and Nicolas, A. (1981). The large-scale cultivation of Vero cells in microcarrier culture for virus vaccine production. Preliminary results for killed poliovirus vaccine. *Dev. Biol. Stand.* **47:** 55 – 64.

Mulligan, R. and Berg, P. (1981). Selection for animal cells that express the *Escherichia coli* gene coding for xanthine-guanine phosphoribosyltransferase. *Proc. Nat. Acad. Sci. USA* **78**: 2072 – 2076.

Narayanan, K., Chen, C., Maeda, J. and Makino, S. (2003). Nucleocapsid-independent specific viral RNA packaging via viral envelope protein and viral RNA signal. *J. Virol.* **77**: 2922 – 2927.

Nash, T. and Buchmeier, M. (1997). Entry of mouse hepatitis virus into cells by endosomal and nonendosomal pathways. *Virology* **233:** 1 – 8.

Nicholas, K., Nicholas H. and Deerfield, D. (1997). GeneDoc: analysis and visualization of genetic variation. *EMBNEW.NEWS* **4**: 14.

Oostra, M., te Lintelo, E., Deijs, M., Verheije, M., Rottier, P. and de Haan, C. (2007). Localization and membrane topology of coronavirus nonstructural protein 4: involvement of the early secretory pathway in replication. *J. Virol.* **81:** 12323 – 12336.

Oostra, M., Hagemeijer, M., van Gent, M., Bekker, C., te Lintelo, E., Rottier, P. and de Haan, C. (2008). Topology and membrane anchoring of the coronavirus replication complex: not all hydrophobic domains of nsp3 and nsp6 are membrane spanning. *J. Virol.* **82:** 12392 – 12405.

Opstelten, D., Raamsman, M., Wolfs, K., Horzinek, M. and Rottier, P. (1995). Envelope glycoprotein interactions in coronavirus assembly. *J. Cell Biol.* **131:** 339 – 349.

Otsuki, K., Noro, K., Yamamoto, H. and Tsubokura, M. (1979). Studies on avian infectious bronchitis virus (IBV) II. Propagation of IBV in several cultured cells. *Arch. Virol.* **60:** 115 – 122.

Petit, C., Melancon, J., Chouljenko, V., Colgrove, R., Farzan, M., Knipe, D. and Kousoulas, K. (2005). Genetic analysis of the SARS-coronavirus spike glycoprotein functional domains involved in cell-surface expression and cell-to-cell fusion. *Virology* **341**: 215 – 230.

Ponnusamy, R., Mesters, J., Ziebuhr, J., Moll, R. and Hilgenfeld, R. (2006). Non structural proteins 8 and 9 of human coronavirus 229E. In Perlman, S. and Holmes, K. (Eds), The Nidoviruses: toward control of SARS and other Nidovirus diseases. Advances in experimental medicine and biology **581:** 49 – 54 *Springer.*

Prentice, E., Jerome, W., Yoshimori, T., Mizushima, N. and Denison, M. (2004). Coronavirus replication complex formation utilizes components of cellular autophagy. *J. Biol. Chem.* **279**: 10136 – 10141.

Rainey, G., Natonson, A., Maxfield, L. and Coffing, J. (2003). Mechanisms of avian retroviral host range expansion. *J. Virol.* **77:** 6709 – 6719.

Risco, C., Anton, I., Enjuanes, L. and Carrascosa, J. (1996). The transmissible gastroenteritis coronavirus contains a spherical core shell consisting of M and N proteins. *J. Virol.* **70:** 4773 – 4777.

Rota, P., Oberste, M., Monroe, S., Nix, W., Campagnoli, R., Icenogle, J., Penaranda, S., Bankamp, B., Maher, K., Chen, M., Tong, S., Tamin, A., Lowe, L., Frace, M., DeRisi, J., Chen, Q., Wang, D., Erdman, D., Peret, T., Burns, C., Ksiazek, T., Rollin, P., Sanchez, A., Liffick, S., Holloway, B., Limor, J., McCaustland, K., Olsen-Rasmussen, M., Fouchier, R., Gunther, S., Osterhaus, A., Drosten, C., Pallansch, M., Anderson, L. and Bellini, W. (2003). Characterization of a novel coronavirus associated with severe acute respiratory syndrome. *Science* **300:** 1394 – 1399.

Rottier, P., Horzinek, M. and van der Zeijst, B. (1981). Viral protein synthesis in mouse hepatitis virus strain A59-infected cells: effect of tunicamycin. *J. Virol.* **40:** 350 – 357.

Rottier, P., Nakamura, K., Schellen, P., Volders, H. and Haijema, B. (2005). Acquisition of macrophage tropism during the pathogenesis of feline infectious peritonitis is determined by mutations in the feline coronavirus spike protein. *J. Virol.* **79**: 14122 – 14130.

Sainz, B., Rausch, J., Gallaher, W., Garry, R. and Wimley, W. (2005). The aromatic domain of the coronavirus class I viral fusion protein induces membrane permeabilization: putative role during viral entry. *Biochemistry* **44:** 947 – 958.

Sanchez, C., Izeta, A., Sanchez-Morgado, J., Alonso, S., Sola, I., Balasch, M., Plana-Duran, J. and Enjuanes, L. (1999). Targeted recombination demonstrates that the spike gene of transmissible gastroenteritis coronavirus is a determinant of its enteric tropism and virulence. *J. Virol.* **73:** 7607 – 7618.

Sawicki, S. and Sawicki, D. (1995). Coronaviruses use discontinuous extension for synthesis of subgenome-length negative strands. *Advan. Expt. Biol. Med.* **380**: 499 – 506.

Sawicki, S., Sawicki, D. and Siddell, S. (2007). A contemporary view of coronavirus transcription. *J. Virol.* **81**: 20 – 29.

Schickli, J., Thackray, L., Sawicki, S. and Holmes, K. (2004). The N-terminal region of the murine coronavirus spike glycoprotein is associated with the extended host range of viruses from persistently infected murine cells. *J. Virol.* **78:** 9073 – 9083.

Schickli, J., Zelus, B., Wentworth, D., Sawicki, S. and Holmes, K. (1997). The murine coronavirus mouse hepatitis virus strain A59 from persistently infected murine cells exhibits an extended host range. *J. Virol.* **71:** 9499 – 9507.

Schultze, B. and Herrler, G. (1992). Bovine coronavirus uses *N*-acetyl-9-O-acetylneuraminic acid as a receptor determinant to initiate the infection of cultured cells. *J. Gen. Virol.* **73**: 901 – 906.

Schwegmann-Wessels, C., Zimmer, G., Laude, H., Enjuanes, L. and Herrler, G. (2002). Binding of transmissible gastroenteritis coronavirus to cell surface sialoglycoproteins. *J. Virol.* **76**: 6037 – 6043.

Senanayake, S. and Brian, D. (1999). Translation from the 5' untranslated region (UTR) of mRNA 1 is repressed, but that from the 5' UTR of mRNA 7 is stimulated in coronavirus-infected cells. *J. Virol.* **73**: 8003 – 8009.

Simmons, G., Gosalia, D., Rennekamp, A., Reeves, J., Diamond, S. and P. Bates (2005). Inhibitors of cathepsin L prevent severe acute respiratory syndrome coronavirus entry. *Proc. Natl. Acad. Sci. USA* **102**: 11876 – 11881.

Sims, A., Ostermann, J. and Denison, M. (2000). Mouse hepatitis virus replicase proteins associate with two distinct populations of intracellular membranes. *J. Virol.* **74:** 5647 – 5654.

Smith, A., Boursnell, M., Binns, M., Brown, T. and Inglis, S. (1990). Identification of a new membrane-associated polypeptide specified by the coronavirus infectious bronchitis virus. *J. Gen. Virol.* **71:** 3 – 11.

Sodroski, J., Goh, W., Rosen, C., Campbell, K. and Haseltine, W. (1986). Role of the HTLV-III:LAV envelope in syncytium formation and cytopathicity. *Nature* **322:** 470 – 474.

Sturman, L., Holmes, K. and Behnke, J. (1980). Isolation of coronavirus envelope glycoproteins and interaction with the viral nucleocapsid. *J. Virol.* **33:** 449 – 462.

Sutton, G., Fry, E., Carter, L., Sainsbury, S., Walter, T., Nettleship, J., Berrow, N., Owens, R., Gilbert, R., Davidson, A., Siddell, S., Poon, L., Diprose, J., Alderton, D., Walsh, M., Grimes, J. and Stuart, D. (2004). The nsp9 replicase protein of SARS-coronavirus, structure and functional insights. *Structure* **12:** 341 – 353.

Tekes, G., Hofmann-Lehmann, R., Bank-Wolf, B., Maier, R., Thiel, H. and Thiel, V. (2010). Chimeric feline coronaviruses that encode type II spike protein on type I genetic background display accelerated viral growth and altered receptor usage. *J. Virol.* **84:** 1326 – 1333.

Thackray, L. and Holmes, K. (2004). Amino acid substitutions and an insertion in the spike glycoprotein extend the host range of the murine coronavirus MHV-A59. *Virology* **324**: 510 – 524.

Thiel, V. and Siddell, S. (1994). Internal ribosome entry in the coding region of murine hepatitis virus mRNA 5. *J. Gen. Virol.* **75:** 3041 – 3046.

Tomley, F., Mockett, A., Boursnell, M., Binns, M., Cook, J., Brown, D. and Smith, G. (1987). Expression of the infectious bronchitis virus spike protein by recombinant vaccinia virus and induction of neutralizing antibodies in vaccinated mice. *J. Gen. Virol.* **68:** 2291 – 2298.

Tooze, J., Tooze, S. and Fuller, S. (1987). Sorting of progeny coronavirus from condensed secretory proteins at the exit from the trans-Golgi network of AtT20 cells. *J. Cell. Biol.* **105:** 1215 – 1226.

Tseng, Y., Wang, S., Huang, K., Lee, A., Chiang, C. and Wang, C. (2010). Self-assembly of severe acute respiratory syndrome coronavirus membrane protein. *J. Biol. Chem.* **285**: 12862 – 12872.

Tynell (1968). Virology: Coronaviruses. *Nature* **220**: 650.

van der Meer, Y., Snijder, E., Dobbe, J., Schleich, S., Denison, M., Spaan, W. and Locker, J. (1999). Localization of mouse hepatitis virus nonstructural proteins and RNA synthesis indicates a role for late endosomes in viral replication. *J. Virol.* **73:** 7641 – 7657.

van Hemert, M., van den Worm, S., Knoops, K., Mommaas, A., Gorbalenya, A. and Snijder, E. (2008). SARS-coronavirus replication/transcription complexes are membrane-protected and need a host factor for activity *in vitro*. *PLoS Pathog.* **4**: e1000054.

Vennema, H., Heijnen, L., Zijderveld, A., Horzinek, M. and Spaan, W. (1990). Intracellular transport of recombinant coronavirus spike proteins: implications for virus assembly. *J. Virol.* **64:** 339 – 346.

Verheije, M., Hagemeijer, M., Ulasli, M., Reggiori, F., Rottier, P., Masters, P. and de Haan, C. (2010). The coronavirus nucleocapsid protein is dynamically associated with the replication-transcription complexes. *J. Virol.* published ahead of print.

ViralZone (2010). Swiss Institute of Bioinformatics. www.expasy.org/viralzone

West, J., Flockhart, J. and Keighren, M. (1995). Biochemical evidence for cell fusion in placentas of mouse aggregation chimeras. *Dev. Biol.* **168:** 76 – 85.

Williams, R., Jiang, G. and Holmes, K. (1991). Receptor for mouse hepatitis virus is a member of the carcinoembryonic antigen family of glycoproteins. *Proc. Nat. Acad. Sci. USA* **88**: 5533 – 5536.

Wilson, L., McKinlay, C., Gage, P. and Ewart, G. (2004). SARS coronavirus E protein forms cation-selective ion channels. *Virology* **330:** 322 – 331.

Winter, C., Herrler, G. and Neumann, U. (2008)**.** Infection of the tracheal epithelium by infectious bronchitis virus is sialic acid dependent. *Microbes Infect.* **10:** 367 – 373.

Winter, C., Schwegmann-Wessels, C., Cavanagh, D., Neumann, U. and Herrler, G. (2006). Sialic acid is a receptor determinant for infection of cells by avian Infectious bronchitis virus. *J. Gen. Virol.* **87:** 1209 – 1216.

Xu, Y., Liu, Y., Lou, Z., Qin, L., Li, X., Bai, Z., Pang, H., Tien, P., Gao, G. and Rao, Z. (2004). Crystal structure of mouse hepatitis virus spike protein fusion core. Structural basis for coronavirus-mediated membrane fusion. *J. Biol. Chem.* **279**: 30514 – 30522.

Yamada, Y. and Liu, D. (2009). Proteolytic activation of the spike protein at a novel RRRR/S motif is implicated in furin-dependent entry, syncytium formation, and infectivity of coronavirus infectious bronchitis virus in cultured cells. *J. Virol.* **83**: 8744 – 8758.

Yamada, Y., Liu, B., Fang, S., Tay, F. and Liu, D. (2009). Acquisition of cell-cell fusion activity by amino acid substitutions in spike protein determines the infectivity of a coronavirus in cultured cells. *PLoS One* **4:** e6130.

Yamada, Y., Takimoto, K., Yabe, M. and Taguchi, F. (1997). Acquired fusion activity of a murine coronavirus MHV-2 variant with mutations in the proteolytic cleavage site and the signal sequence of the S protein. *Virology* **227**: 215 – 219.

Yang, Z., Huang, Y., Ganesh, L., Leung, K., Kong, W., Schwartz, O., Subbarao, K. and Nabel, G. (2004). pH-dependent entry of severe acute respiratory syndrome coronavirus is mediated by the spike glycoprotein and enhanced by dendritic cell transfer through DC-SIGN. *J. Virol.* **78:** 5642 – 5650.

Yeager, C., Ashmun, R., Williams, R., Cardellichio, C., Shapiro, L., Look, A. and Holmes, K. (1992). Human aminopeptidase N is a receptor for human coronavirus 229E. *Nature* **357**: 420 – 422.

Yin, H., Wen, X., Paterson, R., Lamb, R. and Jardetzky, T. (2006). Structure of the parainfluenza virus 5 F protein in its metastable, prefusion conformation. *Nature* **439**: 38 – 44.

Youn, S., Collisson, E. and Machamer, C. (2005)**.** Contribution of trafficking signals in the cytoplasmic tail of the infectious bronchitis virus spike protein to virus infection. *J. Virol.* **79:** 13209 – 13217.

Zelus, B., Schickli, J., Blau, D., Weiss, S. and Holmes, K. (2003). Conformational changes in the spike glycoprotein of murine coronavirus are induced at 37°C either by soluble murine CEACAM1 receptors or by pH 8. *J. Virol.* **77:** 830 – 840.

Ziebuhr, J., Snijder E. and Gorbalenya, A. (2000). Virus-encoded proteinases and proteolytic processing in the *Nidovirales. J. Gen. Virol.* **81:** 853 – 879.

Zhai, Y., Sun, F., Li, X., Pang, H., Xu, X., Bartlam, M. and Rao, Z. (2005). Insights into SARS-CoV transcription and replication from the structure of the nsp7-nsp8 hexadecamer. *Nat. Struct. Mol. Biol.* **12:** 980 – 986.

Zhou, Y., Lu, K., Pfefferle, S., Bertram, S., Glowacka, I., Drosten, C., Pöhlmann, S. and Simmons, G. (2010). A single asparagine-linked glycosylation site of the SARS-coronavirus spike glycoprotein facilitates inhibition by mannose-binding lectin through multiple mechanisms. *J. Virol.* **84:** 8753 – 8764.

Zhu, H., Yu, D. and Zhang, X. (2009). The spike protein of murine coronavirus regulates viral genome transport from the cell surface to the endoplasmic reticulum during infection. *J. Virol.* **83:** 10653 – 10663.